UV AND NMR STUDIES OF

TANNIN COMPLEXATION

by

Md. Lokman Khan

A thesis submitted for the degree

of Doctor of Philosophy

Department of Chemistry

University of Sheffield

March 1996

To the memory of my

grandfather

ACKNOWLEDGEMENTS

UV AND NMR STUDIES OF TANNIN COMPLEXATION

Md. Lokman Khan

SUMMARY

Vegetable tannins or plant polyphenols constitute a distinctive and large family of higher plants. Tannins have affinity for many biological molecules, of which proteins and peptides are probably the most important ones. Due to their physiological and industrial importance, tannins have attracted increasing scientific attention.

The principal goal of the work described in this thesis was to have a better understanding of tannin complexation. The secondary aim was to investigate medicinal implications of a few tannins.

A number of tannins were isolated, purified and characterised by mainly spectroscopic means. A model condensed tannin (procyanidin B-2) was targetted for multi-dimensional ^{1}H & ^{13}C NMR studies coupled with molecular mechanics calculations. The complexation of various tannins with proteins and caffeine was studied by UV and ^{1}H NMR spectroscopy. Effect of solvent composition on caffeine-tannin complexation was examined. Caffeine was used as a model for proline as well as being a physiologically significant compound. A complementary caffeine-calixarene complexation was also studied. Association constants were obtained from chemical shift changes for the caffeine-tannin/calixarene interactions .

The complexation of tannins with the physiologically significant hormone peptide bradykinin was investigated by ^{1}H NMR spectroscopy. Tannins were found to effectively complex with bradykinin and ultimately precipitate from aqueous media. The peptide was found to remain extended or unstructured during the complexation with tannins. Association constants for the interactions were obtained from chemical shift changes.

Hydrophobic interactions have been confirmed to be the principal binding force in complexation and precipitation of substrates by tannin; hydrogen bonding probably acts as secondary stabilisation factor.

CONTENTS

Chapter 1 Introduction

Chapter 2 Experimental procedure

Chapter 3 NMR studies of procyanidin B-2

Chapter 4 Tannin-protein precipitation

Chapter 5 A study of the interaction of caffeine with

tannins

Chapter 6: A study of the molecular-recognition of caffeine and a proline-peptide by calixarenes

Chapter 7 An investigation into the binding of bradykinin and its analogues with tannins

Chapter 8 Concluding remarks

Appendices

LIST OF ABBREVIATIONS

A-2	proanthocyanidin A-2
B-2	procyanidin B-2
B-3	procyanidin B-3
B-4	procyanidin B-4
δ	chemical shift
δ_b	chemical shift of bound species
δ_{calc}	calculated chemical shift
δ_{max}	maximum chemical shift
δ_{obs}	observed chemical shift
DGG	2,6-digalloyl-D-glucopyranose
DGAG	2,6-di-O-galloyl-1,5-anhydro-D-glucitol
$\Delta\delta_{max}$	maximum change in chemical shift
$\Delta\delta/\Delta T$	chemical shift temperature coefficient
EC	(-)epicatechin
EGCG	(-)epigallocatechingallate
HMQC	two-dimensional heteronuclear multiple quantum coherence spectroscopy
HMBC	two-dimensional heteronuclear multiple bond correlation spectroscopy
HSQC	two-dimensional heteronuclear single quantum coherence spectroscopy
^2J	two bond geminal coupling constant
^3J	three bond vicinal coupling constant
$^3J_{HN\alpha}$	three bond coupling constant between NH and CαH
K_a	association constant
NMR	nuclear magnetic resonance
NOE	nuclear Overhauser effect
PGG	β-1,2,3,4,6-penta-O-galloyl-D-glucopyranose

viii

ROE	rotating frame Overhauser effect
ROESY	two-dimensional rotating frame nuclear Overhauser effect spectroscopy
TeGG	β-1,2,3,6-tetra-O-galloyl-D-glucopyranose
TGG	β-1,3,6-tri-O-galloyl-D-glucopyranose
TOCSY	two-dimensional total correlation spectroscopy
TSP	sodium salt of 3-trimethylsilyl (2,2,3,3-D$_4$) propionate

CHAPTER ONE

INTRODUCTION

1.1 Plant polyphenols - vegetable tannins

Vegetable tannins, today probably more appropriately called plant polyphenols, constitute a distinctive family of higher plant secondary metabolites. Bate-Smith and Swain [1] defined this class of compound as 'water soluble phenolic compounds having molecular weights between 500 and 3000 and, besides giving usual phenolic reactions, they have special properties such as the ability to precipitate alkaloids, gelatine and other proteins'. To a leather chemist or a tanner vegetable tannins are a mixture of compounds, obtained from certain parts of particular species of higher plants by aqueous infusion, which can convert or 'tan' putrescible hides and skins into non-putrescible leather. Tannins however have much wider implications which encompass a variety of physiological activities such as medicinal and dietary and industrial applications such as vegetable tannage of skins or hides to give leather, astringency in beverages, etc. Throughout this thesis tannins will be used to signify vegetable tannins, plant polyphenols or polyphenols.

1.2 Metabolism and metabolites

Metabolism [2] is defined as processes carried out by an integrated network of chemical reactions in living organisms. Two principal types of reactions occur: synthesis or anabolism and breakdown or catabolism. The compounds that take part or are produced by these reactions are called metabolites. Metabolites are broadly divisible into two principal groups: primary and secondary. Primary metabolites are by definition vital for the

1

existence and development of living organisms. They include amino acids, proteins, fats, nucleic acids and polysaccharides. On the other hand a large group of compounds, that are produced by metabolism, have a secondary role in the development of the organism (plants and micro-organism) and are called secondary metabolites and hence the processes by which they are formed as secondary metabolism. Specific examples include alkaloids, mycotoxins, phenols, polyenes, polyacetylenes, terpenes, etc.

1.3 Secondary metabolites

Secondary metabolites are sometimes collectively called 'natural products' and are irregularly distributed throughout nature. They are numbered in tens of thousands. Their role in the economy of living matter is often not clearly defined. Although they are diverse in nature, still they are broadly classifiable into several well established families on the basis of their common chemical & structural features and routes of biosynthesis, e.g., alkaloids, terpenes. The family of compounds we are concerned with, plant polyphenols or vegetable tannins, are secondary metabolites. They have one unique structural feature, i.e., a large number of phenolic groups present within the molecular structure.

1.4 Classification of tannins

On the basis of their structural features and chemical behaviour they are broadly divisible into three main groups [3]:

(a) the proanthocyanidins (**1**) or condensed tannins;

(b) the polyesters (**2**) of gallic (**3**) and/or hexahydroxydiphenic acid (**4**) or hydrolysable tannins; and

(c) complex polyphenols.

2
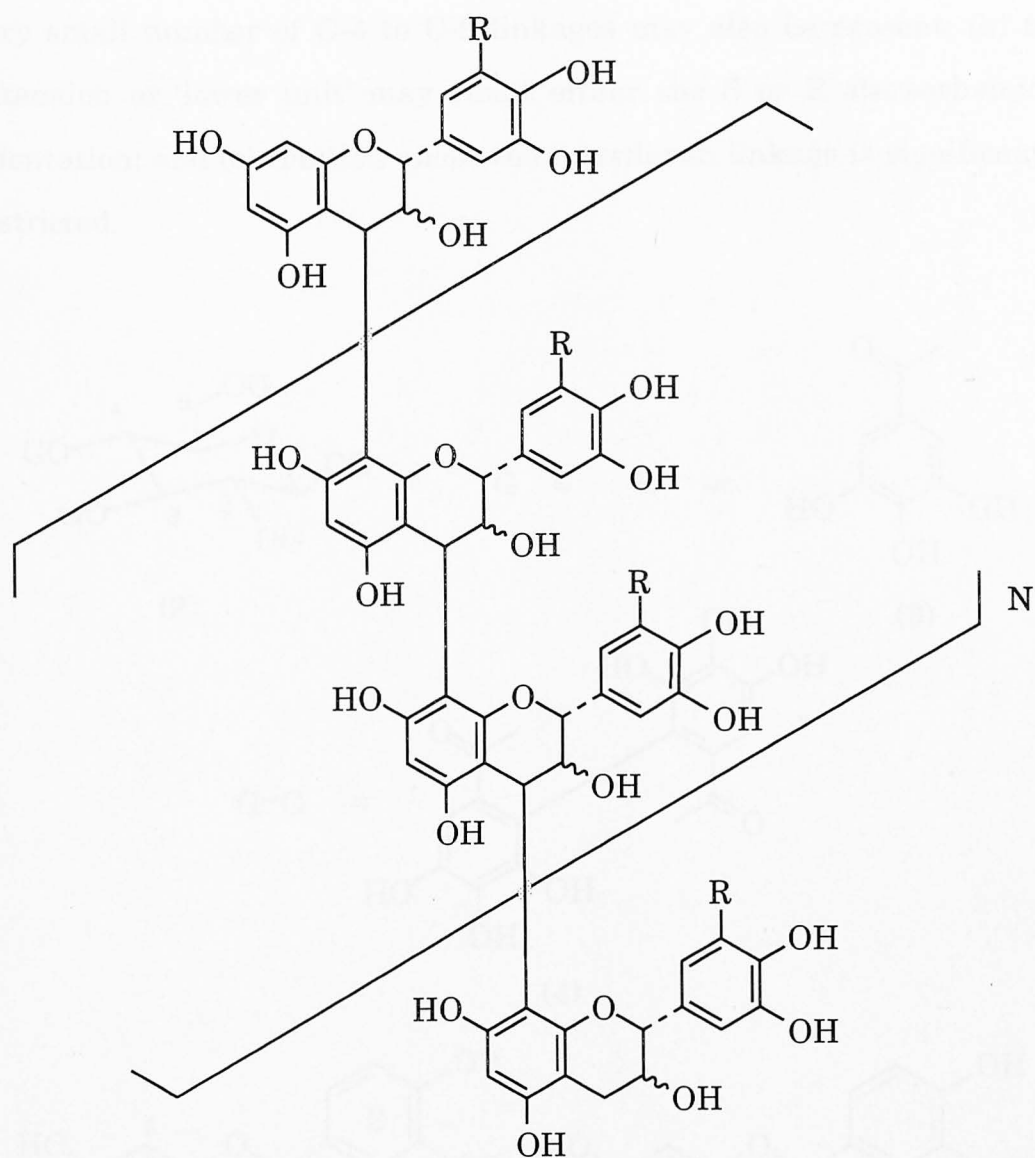
N = 0,1,2, etc.
R = H or OH

(1)

1.4.1 Proanthocyanidins or condensed tannins

Proanthocyanidins have a general structure (1) with a building block of flavan-3-ol units, such as epicatechin (5), catechin (6) gallocatechin (7), epigallocatechin (8), afzelechin (9), epiafzelechin (10), etc. Proantho-cyanidins are generally monomers, dimers, trimers or polymers of flavan-3-ol units with a variety of structural features: (a) monomeric units are usually linked via C-4 of 'upper unit' to C-8 of next or 'lower unit'; but a

3

very small number of C-4 to C-6 linkages may also be present; (b) the extension or 'lower unit' may adopt either the S or R stereochemical orientation; and (c) rotation about the interflavan linkage is significantly restricted.

(2)

G = H or

(3)

G–G =
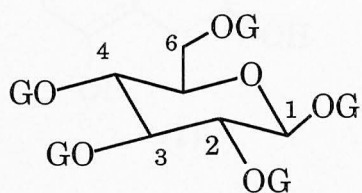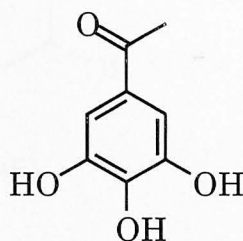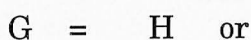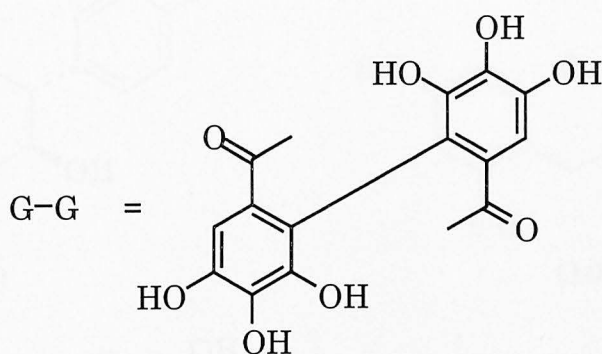
(4)
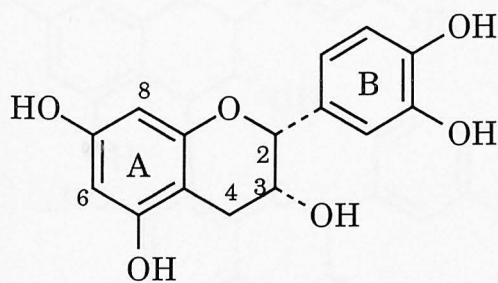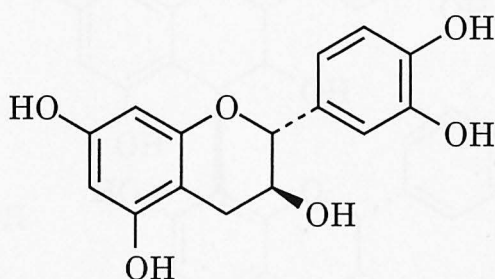
(5)   (6)

Of the two major types of proanthocyanidins, procyanidins (**1, R=H**) and prodelphinidins (**1, R=OH**), the former is the most commonly found group in nature. Major naturally occurring dimeric procyanidins include B-1 (**11**), B-2 (**12**), B-3 (**13**) and B-4 (**14**). They are frequently found in fruits, fruit pods, barks, seeds, and seed shells of a wide range of plants. The properties and structures of these common procyanidins have been

systematically studied and completely elucidated by the Sheffield group [3] and others [4-6].
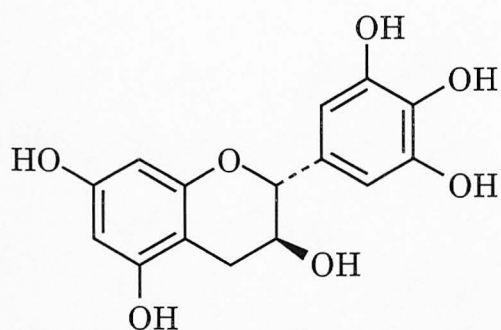
(7)
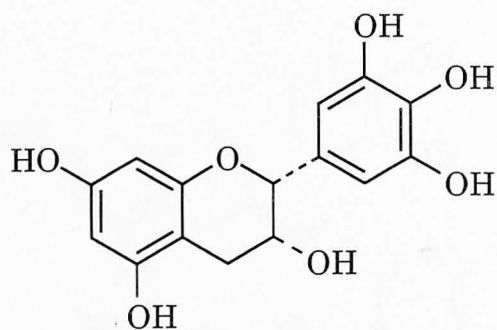
(8)
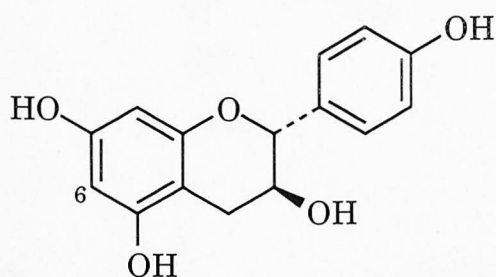
(9)
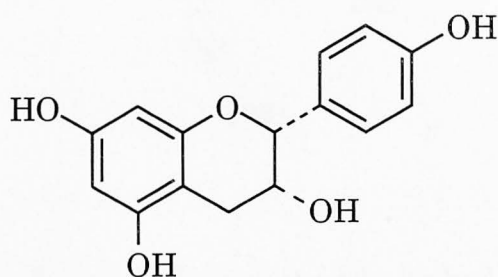
(10)
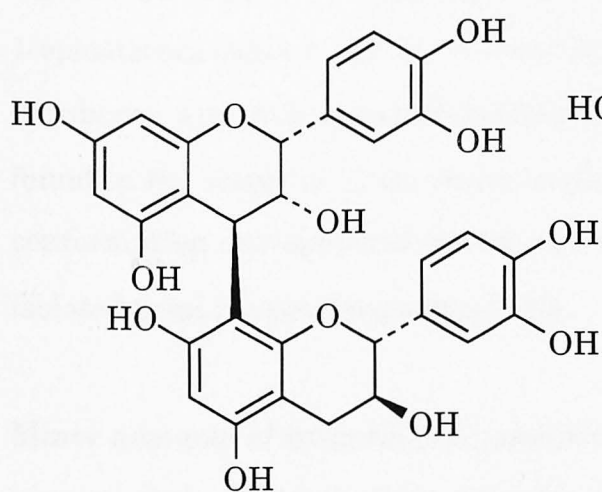
(11)
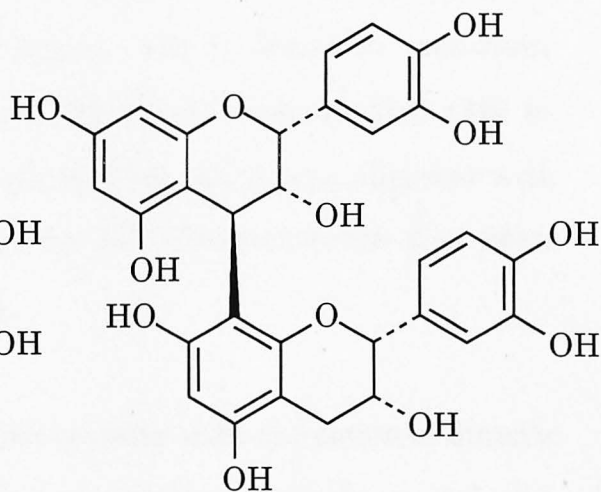
(12)

Some minor dimeric procyanidins are found to co-occur with the major dimers. Thus B-5 (two (-)epicatechins C-4 to C-6 linked) co-occurs with B-2 (12), B-6 (two (+)catechin units C-4 to C-6 linked) with B-3 (13),

B-7 ((-)epicatechin and (+)catechin C-4 to C-6 linked) with B-1 **(11)** and B-8 ((+)catechin and (-)epicatechin C-4 to C-6 linked) with B-4 **(14)** [3].

(13)   **(14)**
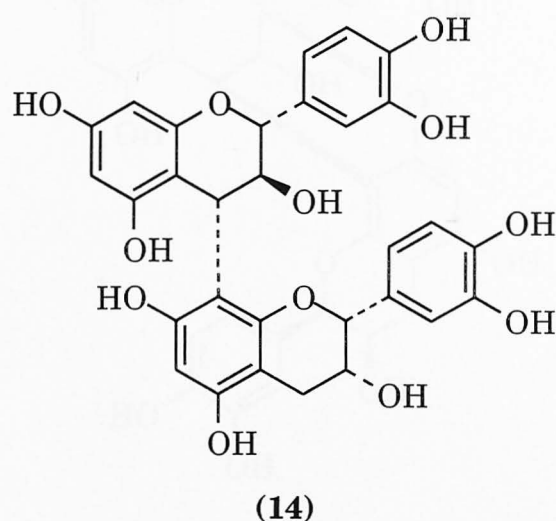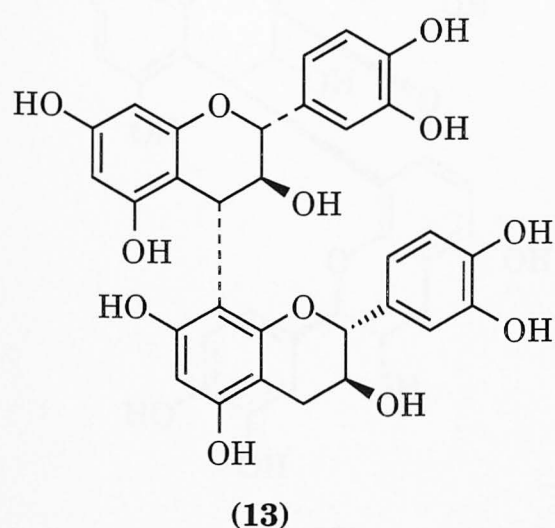
There are other types of dimers where flavan-3-ols are doubly linked. These are called A type proanthocyanidins. Proanthocyanidin A-1(epicatechin-(4β→8, 2β→O→7)-catechin) **(15)** is found in mountain cranberry and A-2(epicatechin-(4β→8, 2β→O→7)-epicatechin) **(16)** is found in the shells of horse chestnut seeds [7-9]. An A type oligomer with conformation ent-epicatechin-(4α→8, 2α→O→7)-epicatechin has been isolated from *Prunus jacquemonti* [9].

Minor amounts of trimeric procyanidins co-occur with the common dimeric procyanidins. Four distinct trimeric procyanidins have been isolated, characterised and their structures elucidated [10]. Trimeric oligomers are called C type proanthocyanidins. Thus C-1 **(18)** and C-2 **(19)** are trimers of (-)epicatechin and (+)catechins, respectively. Other trimers have a mixed composition. A tetrameric proanthocyanidin with the structure epicatechin-(4β→6)-epicatechin-(4β→8)-epicatechin-(4β→6)-epicatechin has been isolated from *Davallia-mariesii* (moore) together with other

6
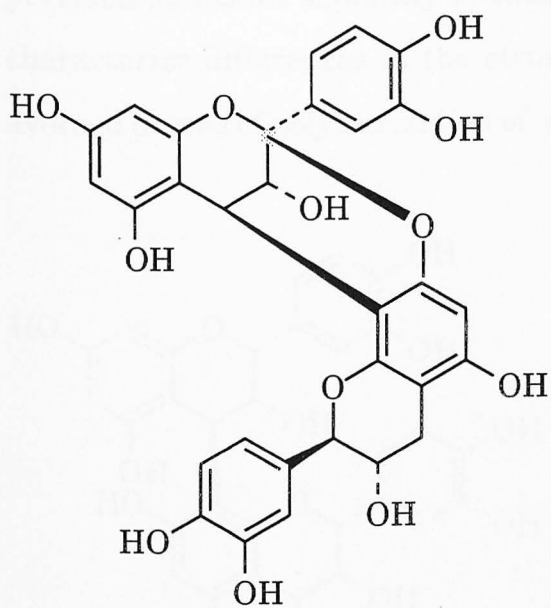
(15)
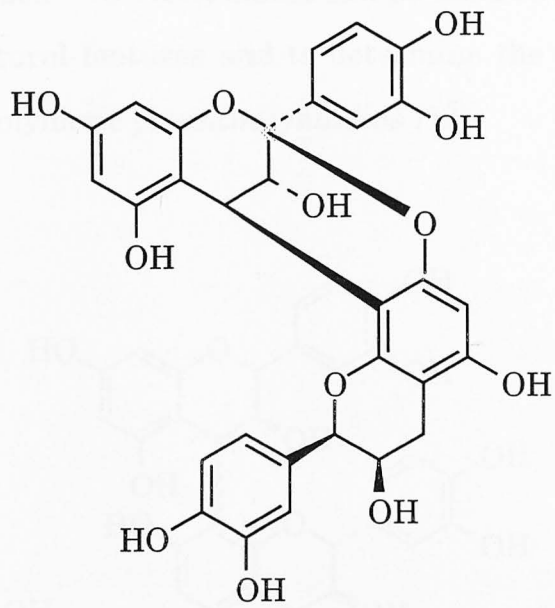
(16)
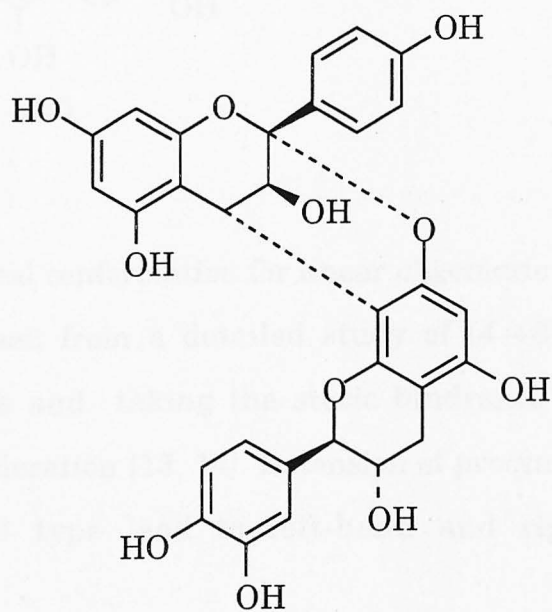
(17)

dimeric (B-5) and trimeric procyanidins and characterised by ^{1}H & ^{13}C NMR spectroscopy [11]. Lack of solubility or poor solubility in suitable solvents has hampered the systematic study of polymeric proanthocyanidins and much is still to be learnt about them. However,

provided sufficient solubility is obtained ^{13}C NMR bands can be used to characterize differences in the structural features and to determine the average degree of polymerization of polymeric proanthocyanidins [12].

(18)   (19)
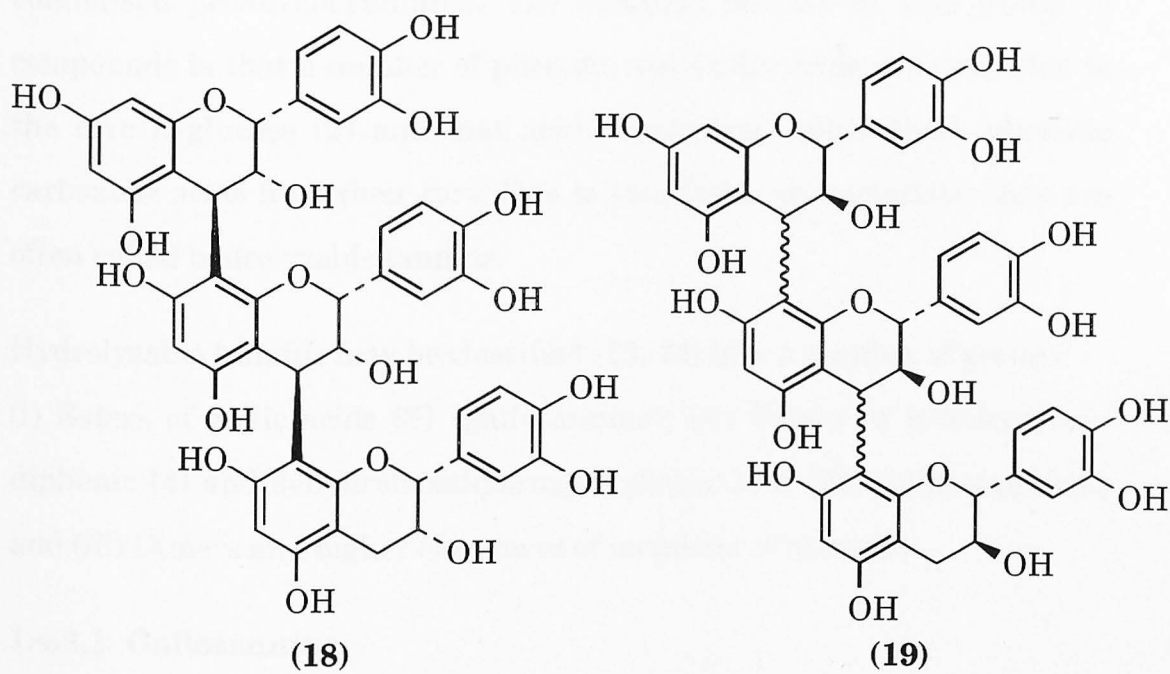
Two different helical conformation for linear oligomeric proanthocyanidins have been proposed from a detailed study of (4→8) type substituted proanthocyanidins and taking the steric hindrance about interflavan linkage into consideration [13, 14]. Extension of procyanidin B-2 type and procyanidins B-3 type lead to left-hand and right-hand helices, respectively.

One common and characteristic property of condensed proantho-cyanidins is their degradation to produce coloured anthocyanidins in acidic media.

1.4.2 Galloyl polyesters

The occurence of galloyl polyesters is limited to a few plant families compared to the relatively widespread occurence in the plant kingdom of condensed proanthocyanidins. The common feature of this group of compounds is that a number of phenolic carboxylic acids are esterified to the core D-glucose (2) and that acidic hydrolysis splits these phenolic carboxylic acids from their core. Due to this latter characteristic they are often called hydrolysable tannins.

Hydrolysable tannins may be classified [13, 14] into a number of groups:
(i) Esters of gallic acids (3) (gallotannins); (ii) Esters of hexahydroxy-diphenic (4) and dehydrohexahydroxy-diphenic acid (20) (ellagitannins); and (iii) Dimers and higher ologomers of members of class (ii).

1.4.2.1 Gallotannins

Gallotannins are the simplest form of hydrolysable tannins. Depending on the number of galloyl groups esterified to the D-glucose core, they may be mono, di, tri, tetra or penta galloyl glucose. Specific examples are β-D-glucogallin (21), β-2,6,-di galloyl-D-glucopyranose or (22), β-1,3,6-tri galloyl -D-glucopyranose (23), β-1,2,3,6-tetra galloyl-D-glucopyranose (24), β-1,2,3,4,6-penta galloyl-D-glucopyranose(PGG) (2, G=galloyl), etc.
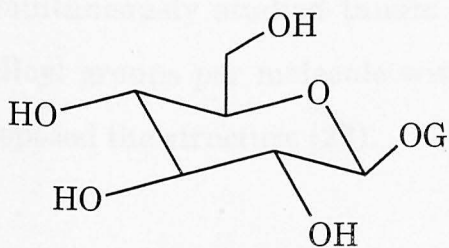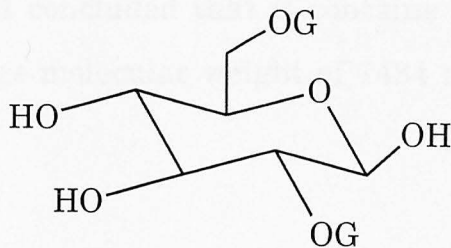
(21, G = (3))   (22, G = (3))
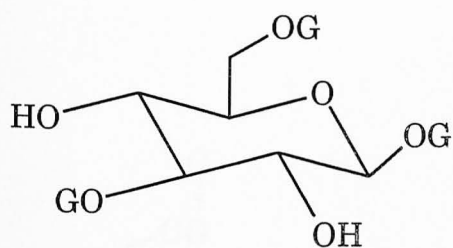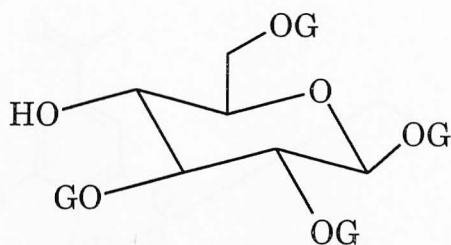
(23, G = (3))   (24, G = (3))

Chinese gallotannin or tannic acid (25) is probably the first commercially important hydrolysable tannin that drew attention of chemists in the early days of the development of the science of vegetable tannins. Fischer [15] and Freudenberg [16] studied chinese gallotannin (from twig galls of *Rhus semialata* L.) systematically and reported it to be a mixture of polygalloylglucoses with depsidically linked galloyl groups, although its structure and composition were not clearly indicated. Haslam etal. [13, 14, 17-22] advanced the chemistry of tannic acid using conventional chemical methods as well as spectroscopy (mainly NMR) providing conclusive evidence on its composition and structure. They concluded that tannic acid has an overall composition of a hepta to octagalloyl-β-D-glucose and on average, two to three extra galloyl groups are depsidically linked to the pre-existing β-1,2,3,4,6-pentagalloyl-D-glucose core and established the structure of tannic acid as (25). ^{13}C NMR Data facilitates the determination of the position of the additional depside residues to be predominantly at C-2 or C-3, C-4 and C-6. However Nishioka et al. [23] simultaneously studied tannic acid and concluded that it contains 8.3 galloyl groups per molecule with average molecular weight of 1434 and proposed the structure (27).
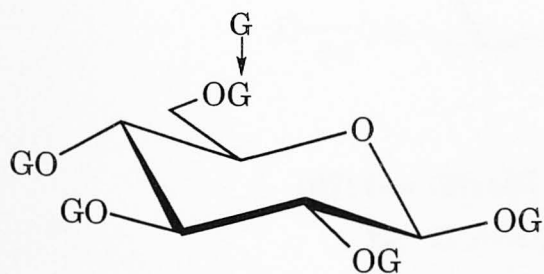
25, G = (3) and G→G = (26)
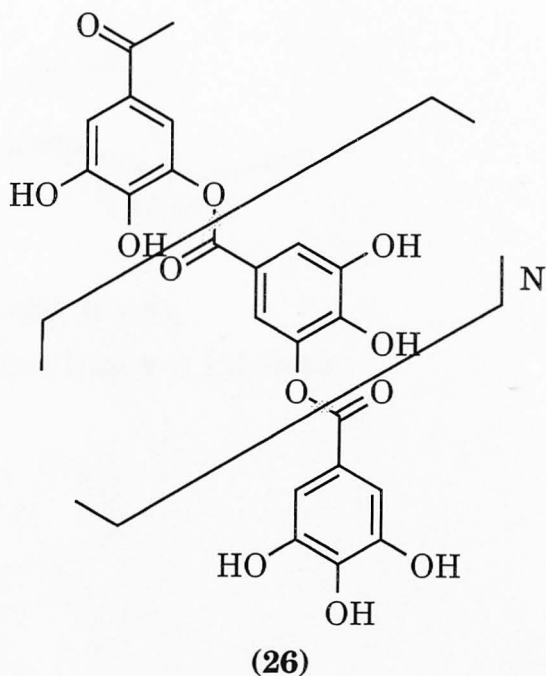
(26)

1.4.2.2 Ellagitannins

The name ellagitannin indicates the presence of hexahydroxydiphenic acid (4) within the parent polyphenol. The first isolated and characterised compound of this group was corilagin (28) [24]. It is believed, following the Schmidt and Mayer hypothesis [25, 26], that oxidative coupling of vicinal galloyl esters leads to the formation of hexahydroxydiphenoyl esters and their derivatives (with the formation of C-C and C-O bonds) (29). A range of compounds of this category occurs in nature, particularly important examples of which are davidiin (30), tellimagrandin I (31) and II (32), pedunculagin (33), casuarictiin (34), etc. Geraniin (35) is a representative example of an ellagitannin having a dehydrohexa-hydroxydiphenoyl ester group in the molecule and was isolated from *Geranium thunbergii* [27, 28].
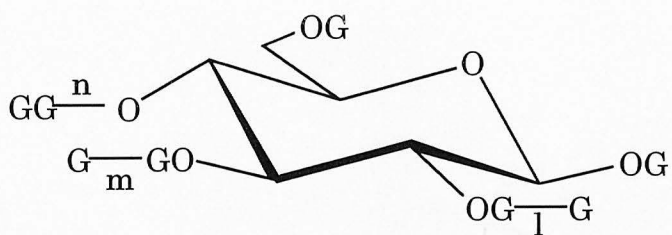
(27: G = (3); GG = (26, N = 0);
G—G = (4); and l, m, n = 1,2, etc.)

(28)

G   +   G   G—G

(29)

(30)

(31, R = OH)
(32, R = β - OG)

12
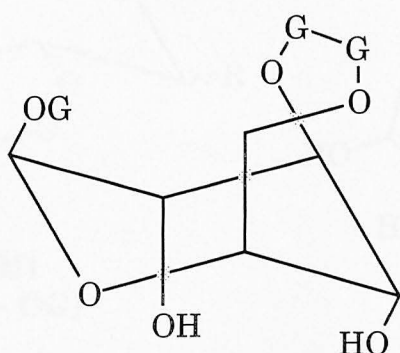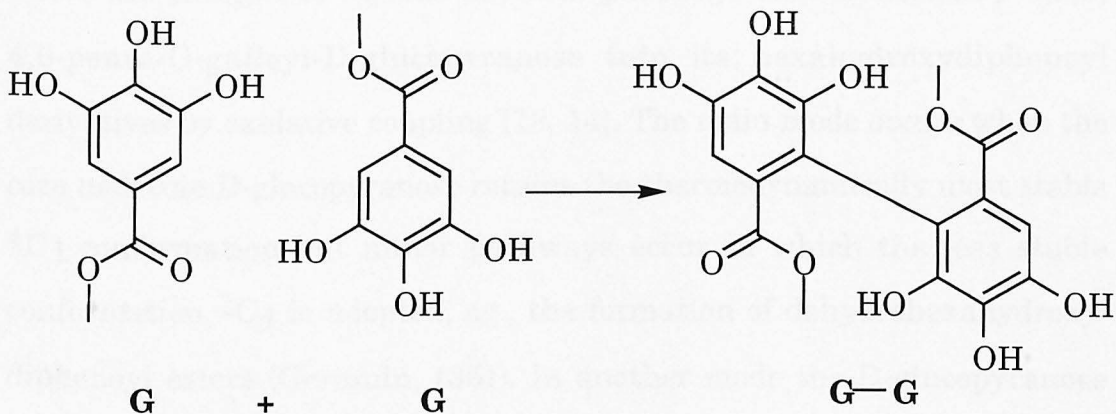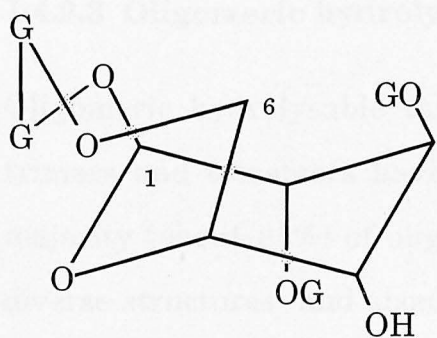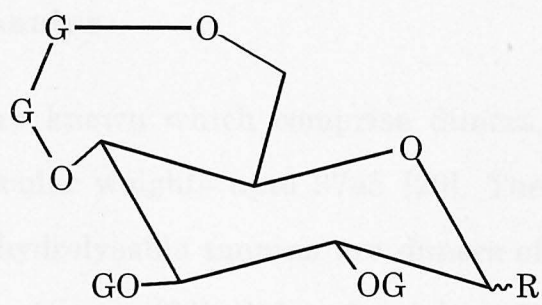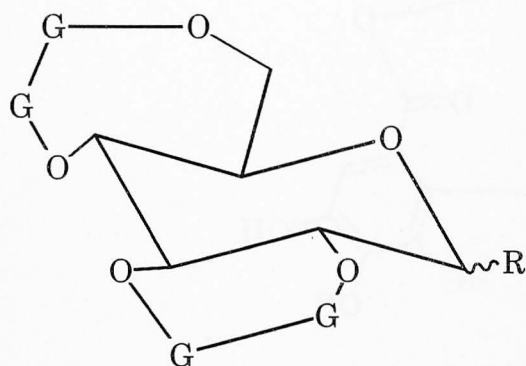
(33, R = OH)
(34, R = β - OG)
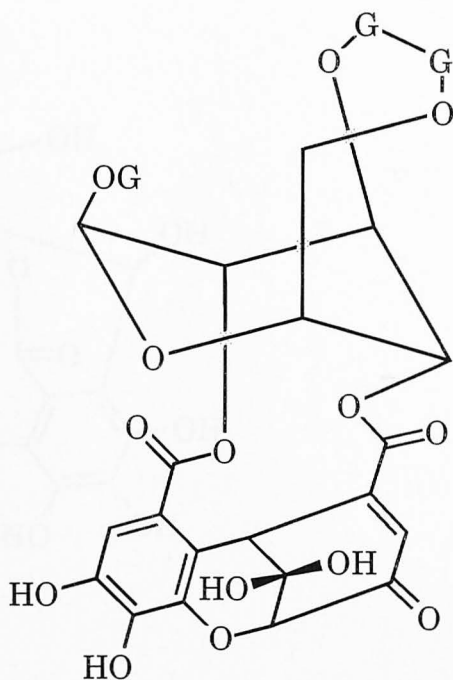
(35)

There are thought to be four different pathways that transform β-1,2,3, 4,6-penta-O-galloyl-D-glucopyranose into its hexahydroxydiphenoyl derivatives by oxidative coupling [13, 14]. The main mode occurs when the core molecule D-glucopyranose retains the thermodynamically most stable $^4C_1$ conformation but minor pathways occur in which the less stable conformation $^1C_4$ is adopted, eg., the formation of dehydrohexahydroxy-diphenoyl esters (Geraniin, (35)). In another mode the D-glucopyranose may be cleaved to form open chain derivatives, eg., casuariin (36).

1.4.2.3 Oligomeric hydrolysable tannins

Oligomeric hydrolysable tannins are known which comprise dimers, trimers and tetramers having molecular weights upto 3745 [29]. The majority (about 85%) of oligomeric hydrolysable tannins are dimers of diverse structures and about 10% are trimers [30]. Only a few (about 5) tetrameric hydrolysable tannins are known so far. It is believed that

13
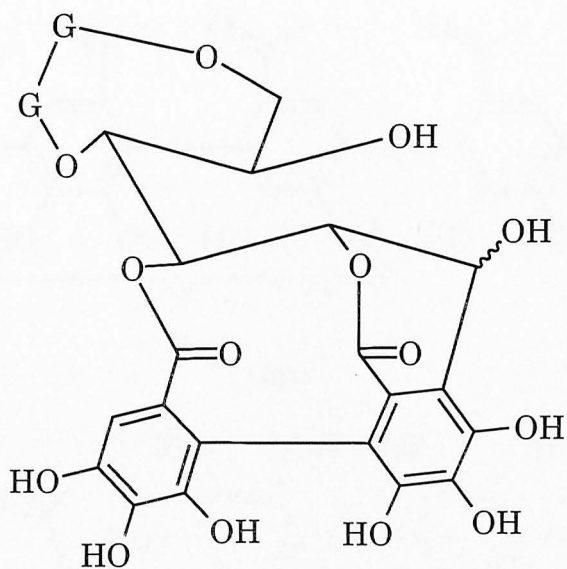
(36)

oligomers are formed via intermolecular oxidative coupling between a hexahydroxydiphenoyl ester group of one tannin molecule with a galloyl ester group of another. Okuda et al. [30] have recently carried out a comprehensive survey of oligomeric hydrolysable tannins and classified them into five distinct types depending on the structures of monomeric units. They have identified five distinctive types of linking units and conveniently abbreviated them as (i) GOG and GOGOG **(37)**, (ii) DOG **(38)**, (iii) GOD **(39)**, (iv) D(OG)$_2$ **(40)** and (v) CD **(41)**, (where G = galloyl **(3)** and D = hexahydroxydiphenyl **(4)**).

(37)

D

(38)

D

(39)

(40)

C

D

(41)

15
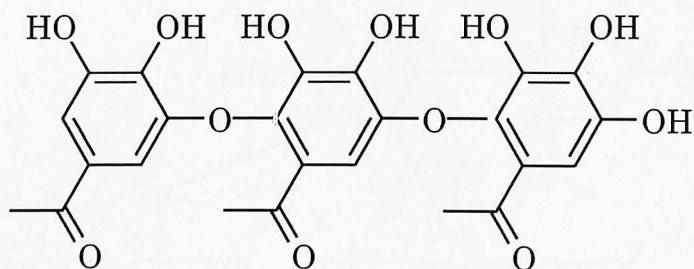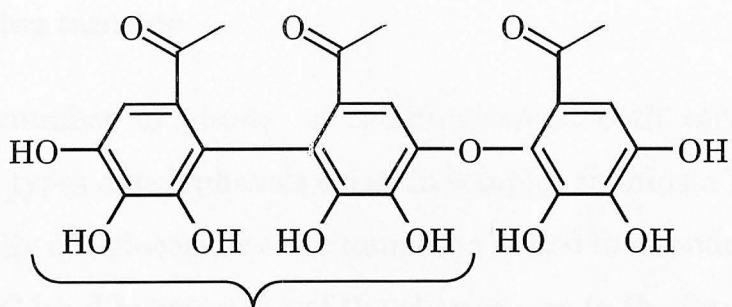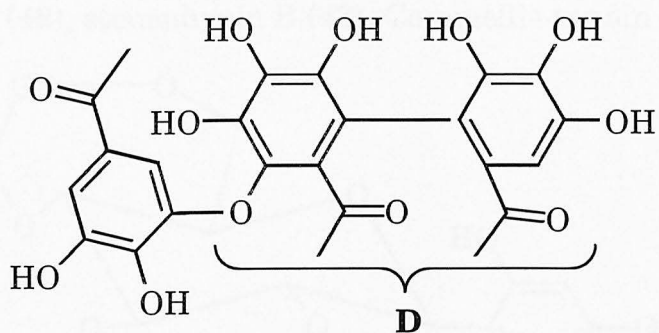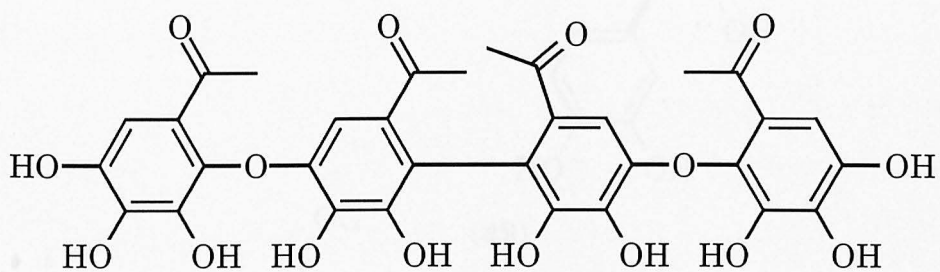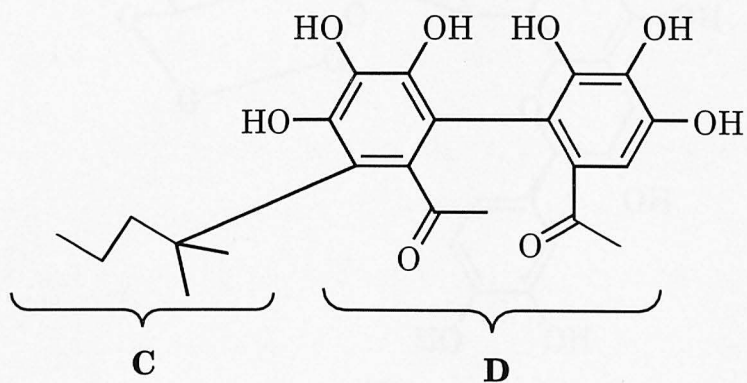
1.4.3 Complex tannins

In a small number of plants a combination of both condensed and hydrolysable types of polyphenols exist. In complex tannins a hydrolysable tannin (usually a C-glucosidic ellagitannin) is linked to a condensed tannin through a C-C bond between C-1 of the glucose core in the former unit and C-8 or C-6 of a flavan-3-ol unit [31]. Representatives of this class are stenophynin A (42), stenophynin B (43), Cammellia tannin B (44), etc.
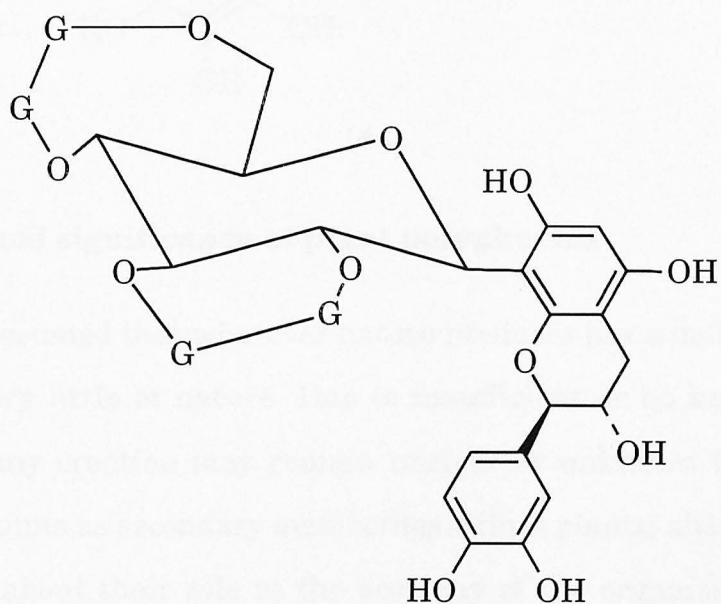
(42)
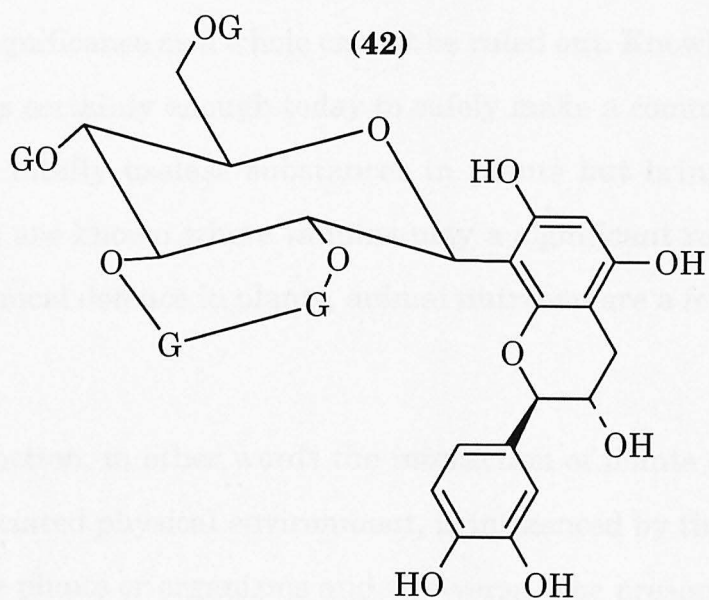
(43)
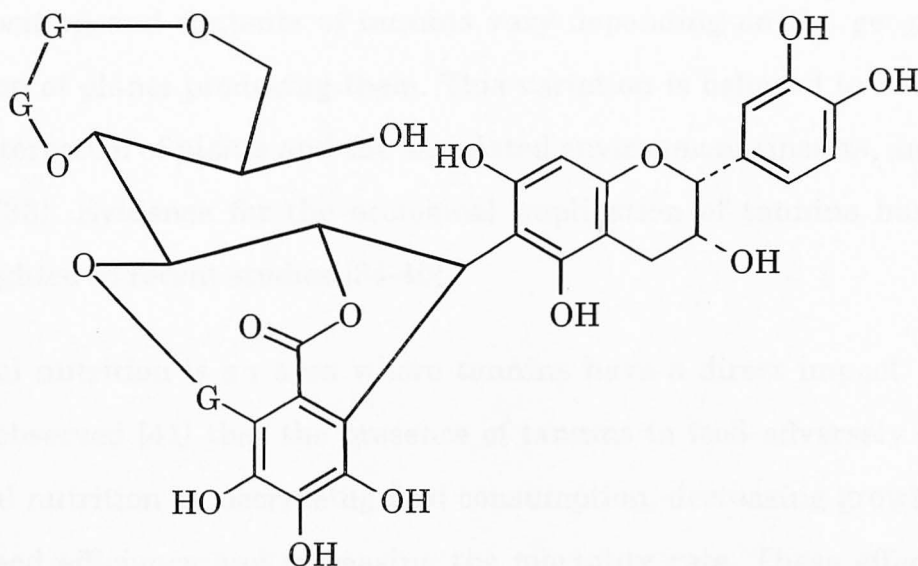
(44)

1.5 Biological significance of plant polyphenols

It is often presumed that whatever nature produces has a definite purpose. We know very little of nature. Due to insufficient or no knowledge, the purpose of any creation may remain unclear or unknown to us. Nature produces tannins as secondary metabolites within plants; although there is controversy about their role in the economy of the organisms producing them, their significance as a whole cannot be ruled out. Knowledge of plant polyphenols is certainly enough today to safely make a comment [32] that they are not totally useless substances in plants but bring benefits to plants. Areas are known where tannins play a significant role; ecological function, chemical defence in plants, animal nutrition are a few which may be mentioned.

Ecological function, in other words the interaction of plants or organisms with the associated physical environment, is influenced by the presence of tannins in the plants or organisms and vice-versa. The presence of tannins in plants and their retention or release into the environment greatly influence the nutrient cycle. It has been found that the characteristics,

17

composition and contents of tannins vary depending on the geographic location of plants producing them. This variation is believed to be due to the interaction of plants and the associated environment (insects, animals, etc.) [33]. Evidence for the ecological implication of tannins has been highlighted in recent studies [34-40].

Animal nutrition is an area where tannins have a direct impact. It has been observed [41] that the presence of tannins in food adversely affects animal nutrition by decreasing food consumption, decreasing growth rate and feed efficiency and increasing the mortality rate. These effects are probably caused by poor digestibility and systemic metabolic effects. The reverse effects have also been seen on herbivores by supplementation with tannin-binding agents, removal of tannins by dehulling, reducing tannin levels by cooking or chemical detoxification. In a more recent investigation [42] the toxic effects of hydrolysable tannins on ruminants has been re-investigated and at the same time the non-toxicity of condensed tannins in forage legumes has been explained to be due to microbial protein synthesis, increased use of endogeneous nitrogen in the rumen, and increased secretion of salivary glycoprotein. In another study [43] it has been found that diets containing crude quebracho tannin (2.9%) have no effect on growth or survival of meadow voles and they can accomodate a higher content of the same tannin (6%) in the diet with an initial loss of body mass, higher mortality rate and decreasing food consumption.

There may be some doubt [44] about the role of tannins as agents of chemical defence against environmental stresses but they are generally recognized as deterrents to herbivory. Astringency is an intrinsic property of tannins that is recognized. It produces in the palate a feeling of tightness, roughness and dryness. One of the causes for the nutritional deprivation or the deterrence of herbivory by tannins is believed to be

astringency and the other is thought to be the reduced digestibility of dietary proteins due to their complex formation with tannins [45]. According to Bate-Smith [46] "From the biological point of view the importance of tannins in plants lies in their effectiveness as repellents to predators, whether animal or microbial. In either case the relevant property is astringency rendering the tissues unpalatable by precipitating proteins or by immobilizing enzymes, impeding invasion of the host by the parasite."

1.6 The benefits of tannins to man

Plant polyphenols have a wide range of uses to man. Recognized uses include tanning agents in leather making, specialty chemicals, herbal medicine, biocides, etc.

1.6.1 Tannins in leather making

The use of tannins to convert animal hides and skins into leather is one of the earliest uses of tannins and has a recorded history of some 3,000 years. Throughout ancient times to the middle of the 19th century [47] man used aqueous infusions of a mixture of crushed or chopped raw materials such as barks, woods, dried fruits and leaves to tan hides and skins. These infusions are rich in tannins and during the tanning process hides and skins absorb tannins. Towards the end of 19th century the idea of extracting tanning materials emerged. Nowadays spray dried powder with a certain moisture content is used and the extraction process may be controlled by computers [47]. A huge variety of leathers are made from vegetable tannins. The use of synthetic tannins or metallic salts with natural tannins is gaining popularity due to the better control of the tanning process and the fact that this produces finer quality leathers.

19

Vegetable tanning is considered one of the most ecofriendly options of the leather making processes.

The principal protein of the hides and skins is collagen - a proline rich fibrous protein. During the tanning process tannins are absorbed by collagen and subsequently tannin molecules bind and cross-link adjacent protein fibres.

1.6.2 Tannins as specialty chemicals

Apart from their traditional use for leather making, tannins have other successful applications as adhesives, biocides, etc. The reactivity to formaldehyde has made tannins useful raw materials for producing adhesives [48]. Tannin-based cold-setting adhesives have been introduced and developed by Pizzi etal. [49] that are applied to end-joints. A great number of workers [50-57] have studied the utility of tannin-formaldehyde types of resins in both interior and exterior particle boards.

Anti-microbial and antivirial activities of tannins are now well established. Tannins have been successfully used to preserve food, wood, etc. The copper(II)-tannin complex (45) is an environmentally harmless fungicide [58]. The use of tannins as antiplaque agents for prevention of dental caries has also been reported [59]. A recent study [60] shows that oolong tea extract reduces dental plaque deposition in humans.

(45)

20
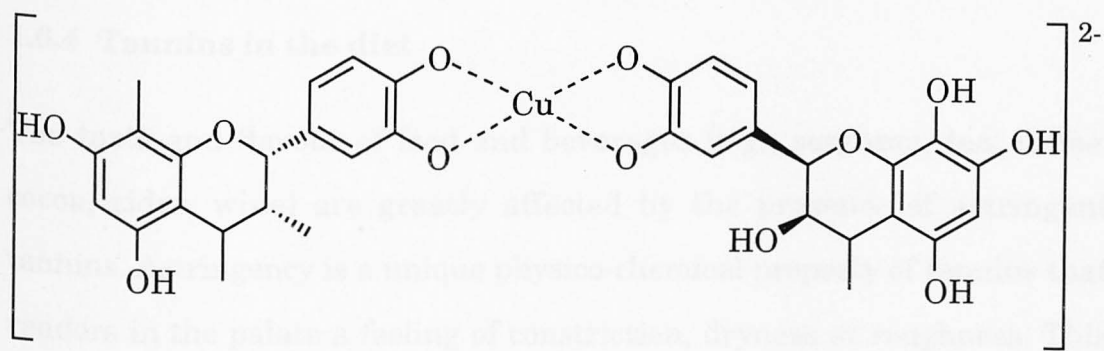
1.6.3 Tannins in medicines

The curative effects of tannins in the treatment of diseases and illnesses has long been known. The early uses of tannins in the treatment of dysentery, diarrhoea, cholera and gonnorrhea have been reported. A comprehensive survey of medicinal plants rich in tannins has been made by Haslam [3]. Typical examples include: (a) Bearberry (*Arctostaphylos uva-ursi*) used as infusion in the treatment of kidney diseases, inflammatory disorders of the urinary tract, etc.; (b) Agrimony (*Agrimonia* sp) used as infusion to treat diarrhoea, as tonic, as ointment to treat wounds; (c) Geranii Herba (*Geranium maculatum*, G. thunbergii) used as decoction to treat haemorrhage, inflammation, skin lesions and stomach ulcers; (d) Oak (*Quercus robus*) used as infusion in the treatment of agues, haemorrhages, chronic diarrhoea and dysentery, also acts as antiseptic; (e) Hawthorn (*Crataegus* sp.) used as an infution in the treatment of high blood pressure and anigma; (f) Meadowsweet (*Filipendula ulmaria*) as tonic and digestive remedies; (g) Raspberry (*Rubus idaeus*) used as gargle, for wounds and ulcers and for children's stomach disorders. Recently it has been reported [61] that ellagic acid and its analogues act as chemopreventive agents against lung tumorigenesis. There are some plants that have a reputation as agents to be used in the case of snakebites such as persimmon tannin from *Diospyros kaki* [62].

1.6.4 Tannins in the diet

The taste and flavour of food and beverages (e.g., sorghum, tea, coffee, cocoa, cider, wine) are greatly affected by the presence of astringent tannins. Astringency is a unique physico-chemical property of tannins that renders in the palate a feeling of constriction, dryness or roughness. This feeling of extreme dryness and puckeriness is not restricted to a particular region of the mouth or tongue, but is experienced as a diffuse stimulas.

21

The mechanism of astringency has been believed to be the cross-linking and precipitation of proteins and mucopolysaccharides in the mucous secretion by tannins [63-65]. Tannins also may make irreversible complexes with the digestive enzymes and dietary proteins; foods that are rich in tannins generally lead to poor nutritional quality. There is evidence that some tannins can indirectly cause oesophegeal cancer and frequent consumption of tannin-rich beverages makes the oesophageal epithelium increasingly vulnerable to carcinogens.

1.7 Tannin interactions

Tannins form complexes with a wide variety of species, ranging in size from divalent and trivalent metal ions to macromolecules. The later may either be naturally occuring or synthetic. Specific examples include proteins and peptides of various sizes, carbohydrates, chromium, zirconium or copper ions, etc. Amongst these substrates, tannin/protein, tannin/peptide and tannin/carbohydrate systems have attracted much attention and have been extensively studied.

The principal forces that take part in the tannin/substrate interactions are believed to be (a) hydrophobic effects and (b) hydrogen bonding, along with other physical influences. The ideas of hydrophobic effects and hydrogen bonding have been adopted from earlier studies [66-74]. Tannin/substrate complexation processes may be reversible or irreversible. From experimental evidence Haslam etal., [63] summarized the dominant aspects that influence reversible tannin-substrate complexation as: (a) solubility, solvation and desolvation; (b) molecular size and conformational flexibility; (c) hydrophobic effects; (d) hydrogen bonding via phenolic groups; (e) the presence of tertiary amide group in the co-substrate; (f) general salt and specific metal ion (eg., Ca^{2+}, Al^{3+}) effects; and suggested a two stage equilibrium with soluble complexes (Fig. 1.1).

22

$$\text{Tannin} + \text{Substrate} + H_2O$$

$$K \quad \downarrow\uparrow \qquad \text{Soluble complexes}$$

$$[\text{Tannin}]_n \cdot [\text{Substrate}]_m + H_2O$$

$$\Uparrow$$

$$\text{Precipitation}$$

$$[\text{Tannin}]_a \cdot [\text{Substrate}]_b + H_2O$$
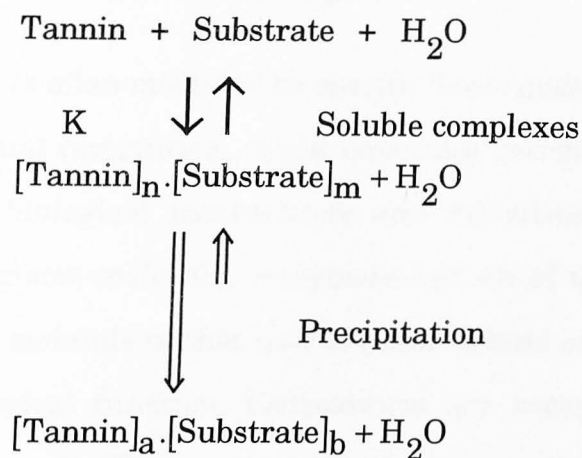
Fig. 1.1 (Figure taken from reference [63])

There are instances where the reversible processes become irreversible (Fig. 1.2) such as: (a) enzymic and non-enzymic browning of fruits and fruit juices; (b) 'fixed tannage' in leather manufacture, etc. The principal cause of irreversibility is the oxidation of the tannin molecule - under the influence of autocatalysis in mild basic media - to produce ortho-quinones which finally form covalent linkages with co-substrate(s).

$$\text{Tannin} + \text{Substrate} + H_2O$$

$$K \quad \downarrow\uparrow \qquad \text{Soluble complexes}$$

$$[\text{Tannin}]_n \cdot [\text{Substrate}]_m + H_2O$$

$$\text{Precipitation}$$

New Products $\qquad\qquad [\text{Tannin}]_x \cdot [\text{Substrate}]_y + H_2O$
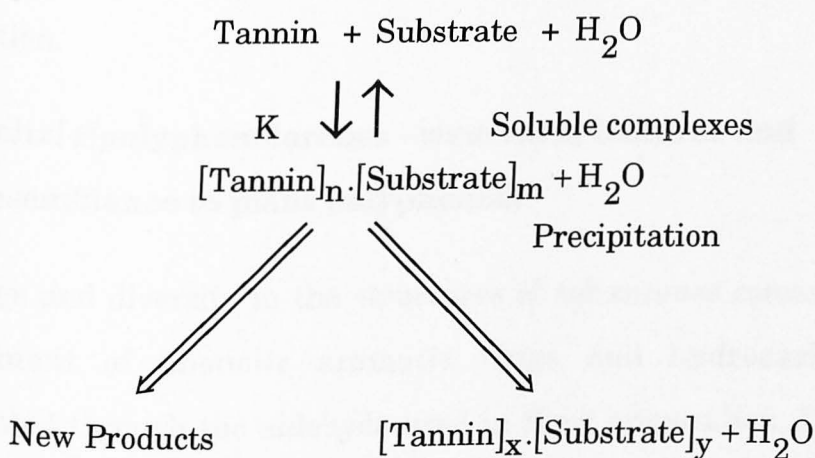
Fig. 1.2 (Figure taken from reference [63])

1.8 Calixarenes - model synthetic polyphenols

Biological processes are often mediated by specific 'host'/'guest' interactions which occur via mutual recognition, called molecular recognition. This is the basis of many biological interactions and activities. The 'host', generally a natural macro-molecule, recognises certain of the structural features of the 'guest' molecule so that they are able to bind each other and thus trigger a biological function. Calixarenes are recognized to be synthetic 'host' compounds. Their compatriot guest compounds are ideally metal ions but complexation with ionic or neutral molecules has been reported [75]. As their name indicates (Greek *calix* meaning vase), they are basket or bowl like molecules and can accomodate and 'deliver' small molecules.

Calixarenes can be made with 4 to 8 aromatic units [76] but 4, 6 or 8 are the most synthetically viable. The most widely studied calixarenes are calix[4]arenes. Examples of calix[4]arenes are calix[4]pyrogallolarene (**46a**), calix[4]resorcinarene (**46b**), etc. Acid catalysed condensation of phenols with aldehydes is one of the most popular methods of calixarene preparation.

1.8.1 Calix[4]polyphenolarenes - structural features and resemblance to plant polyphenols

The range and diversity in the structures of calixarenes comes from the arrangement of phenolic aromatic rings and hydrocarbon tails incorporated through the aldehyde used in their preparation. Depending on the upward or downward facing of the aromatic rings and *cis* or *trans* configuration of the methylene tails, a large number of diastereoisomers are possible. However, the presence of 2(resorcinol) or 3(pyrogallol)
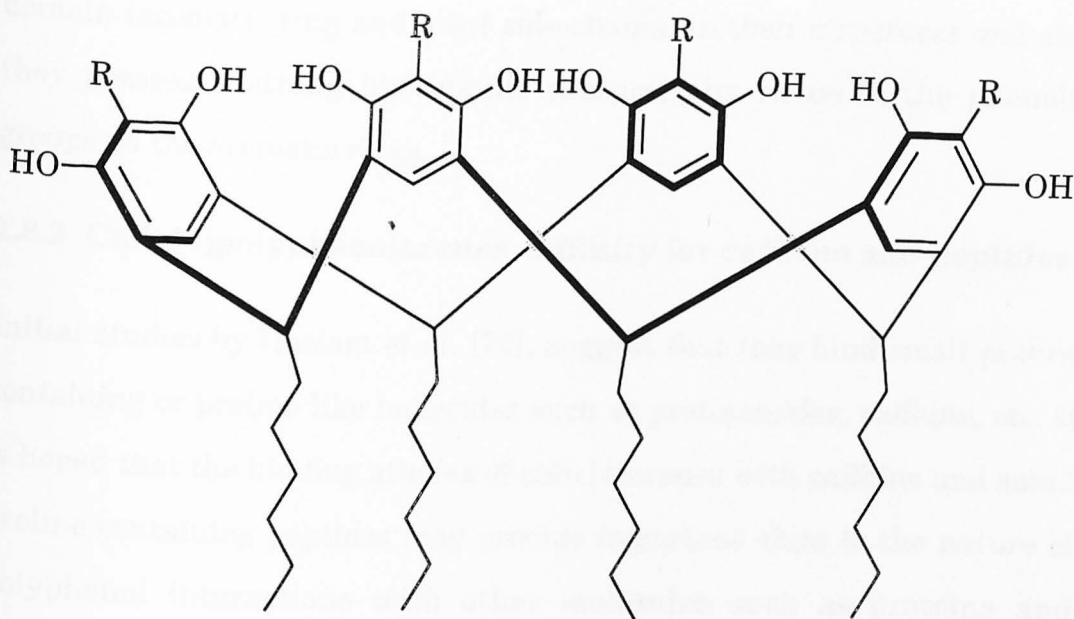
(46a, R = OH)
(46b, R = H)

hydroxyl groups and long hydrocarbon side chain restrict the conformational flexibility of calix[4]arenes. From a close inspection of the molecular models of heptanal derived calix[4]pyrogallolarene or calix[4]resorcenarene, the most likely conformation appears to be a 'crown' **(46)** conformation having all the methylene tails extended with cis or pseudo-cis configuration. Solution NMR [77] and X-ray crystallographic [78] studies of calix[4]resorcinarene have supported the above conformation and it has been highlighted that the aromatic rings are arranged in an all-cis structure and the alkyl side-chains are parallel. It also has been suggested that calix[4]resorcinarene pack in a bowl-to-bowl fashion and alkyl side-chains interdigitate with those of the adjacent calix[4]resorcinarene.

Calix[4]pyrogallolarene and calix[4]resocinarenes are essentially synthetic polyphenols which have some resemblance to plant polyphenols with respect to their physical features. Thus they have a strong hydrophobic

25

domain (aromatic ring and alkyl side-chains) in their structures and also they possess a strong hydrophilic character by virtue of the phenolic groups on the aromatic rings.

1.8.2 Calix[4]polyphenolarenes - affinity for caffeine and peptides

Initial studies by Haslam et al. [79], suggest that they bind small proline containing or proline like molecules such as prolinamides, caffeine, etc. It is hoped that the binding studies of calix[4]arenes with caffeine and small proline containing peptides may provide important clues to the nature of polyphenol interactions with other molecules such as proteins and alkaloids.

1.9 An introduction to the present research

The subject of Vegetable Tannins or Plant Polyphenols has arrived at a more disciplined stage. Incredible number of tannins, their characteristics and significance in nature, are known today.

Tannins have affinity for many biological molecules, of which protein is probably the most important one. Many workers, at Sheffield and elsewhere in the world, have studied tannin-protein complexation process in great detail from different perspectives. Much of the information obtained from those studies has passed the test of time but still many things remain obscure. The aim of this research was to have a better understanding of polyphenol complexation.

There were some secondary but not less important goals. Tannin rich extracts of many plants, such as hawthorn and meadowsweet, are widely used as herbal medicines today. Bradykinin is a well known hormone that has enormous physiological significance in the human body. *In-vitro*

experiments of this hormone were conducted with few tannins with a vew to test the propensity of mutual recognition processes, if any.

Caffeine is another biologically significant compound. A great deal of knowledge is already available on caffeine-tannin complexation. Many workers have exploited this compound as functional model peptides. One of the goals of the present research was to understand the effect of solvent on tannin-caffeine complexation.

A range of tannins were prepared from various plant sources. Many of these tannins has been characterised by previous workers, mainly by NMR spectroscopy. The present work targetted Procyanidin B-2 for multi-dimensional NMR study.

Indeed modern NMR spectrosccopy was extensively exploited throughout this work.

References

1. Bate-smith, E. C. and Swain, T., in *Comprehensive Biochemistry,* H. S. Mason and A. M. Forkin, Editors, 1962, Academic Press, New York, p. 764.

2. Stryer, L., *Biochemistry.* 1995, W. H. Freeman and Company, New York.

3. Haslam, E., *Plant Polyphenols - Vegetable Tannins Revisited.* 1989, Cambridge, Cambridge University Press.

4. Weinges, K., Kaltenhauser, W., Marx, H.-D., Nader, E., Nader, F., Perner, J. and Seiler, D., *Liebigs Ann. Chem.*, 1968, **711**, 184.

5.   Hemingway, R. W. and Foo, L. Y., *J. Chem. Soc. Chem. Commun.*, 1983, 1035.

6.   Porter, L. J., Hirstich, L. N. and Chan, B. G., *Phytochemistry*, 1986, **25**, 223.

7.   Mayer, W., Goll, L., Arnolt, E. V. and Mannschreck, A., *Tetrahedron Letters*, 1966, 429.

8.   Jacques, D., Haslam, E., Bedford, G. R. and Greatbanks, D., *J. Chem. Soc. Perkin Trans. 1*, 1974, 2663.

9.   Pant, G., Nautiyal, A. K., Rawat, S. M., Sutherland, J. K. and Morris, G., *Mag. Res. Chem.*, 1992, **30**, S142.

10.   Hemingway, R. W., Foo, L. Y. and Poeter, L. J., *J. Chem. Soc. Perkin Trans. 1*, 1982, 1209.

11.   Cui, C. B., Tezuke, Y., Kikuka, I., Nakano, H., Tamaoki, T. and Park, J. H., *Chem. Pharm. Bull.*, 1992, **40**, 889.

12.   Thompson, D. and Pizzi, A., *J. Appl. Pol. Sci.*, 1995, **55**, 107.

13.   Haslam, E., *Phytochemistry*, 1977, **16**, 1625.

14.   Haslam, E. and Cai, Y., *Nat. Prod. Reports*, 1994, 41.

15.   Fischer, E., *Chem. Ber.*, 1919, **52**, 809.

16.   Freudenberg, K., *Die Chemie der Naturlichen Gerbstoffe.* 1920, Berlin, Springer-Verlag,

17.   Haslam, E., Haworth, R. D., Jones, K. and Rogers, J., *J. Chem. Soc.*, 1961, 1829.

18. Haslam, E., Haworth, R. D., Mills, S. D., Rogers, H. J., Armitage, R. and Searle, T., *J. Chem. Soc.*, 1961, 1836.

19. Armitage, R., Bayliss, G. S., Gramshaw, J. W., Haslam, E., haworth, R. D., Jones, K., Rogers, H. J. and Searle, T., *J. Chem. Soc.*, 1961, 1842.

20. Britton, G., Crabtrill, P. W., Haslam, E. and Slangroom, J. E., *J. Chem. Soc. C.*, 1966, 783.

21. Haslam, E., *J. Chem. Soc. C.*, 1967, 1734.

22. Haddock, E. A., Gupta, R. K., Al-Shafi, S. M. and Haslam, E., *J. Chem. Soc. Perkin Trans. 1*, 1982, 2515.

23. Nishizawa, M., Yamagishi, T., Nonaka, G. I. and Nishioka, I., *J. Chem. Soc. Perkin Trans. 1*, 1982, 2963.

24. Schmidt, O. T., Schmidt, D. M. and Herok, J., *Liebigs Ann.*, 1954, **587**, 67.

25. Schmidt, O. T. and Mayer, W., *Angew. Chem.*, 1956, **68**, 103.

26. Grimshaw, J., , in *Rodd's Chemistry of Carbon Compounds*, S. Coffey, Editor, 1976, Elsever: Amserdam-Oxford-New York, p. 203.

27. Okuda, T., Yoshida, T. and Nayeshiro, H., *Tetrahedron Letters*, 1976, 3721.

28. Okuda, T., Yoshida, T. and Hatano, T., *J. Chem. Soc. Perkin Trans. 1*, 1982, 9.

29. Okuda, T., Yoshida, T. and Hatano, T., *Heterocycles*, 1990, **30**, 1195.

30. Okuda, T., Yoshida, T. and Hatano, T., *Phytochemistry*, 1993, **32**, 507.

31. Okuda, T., Yoshida, T., Hatano, T., Yazaki, K., Ikegami, Y. and Shingu, T., *Chem. Pharm. Bull.*, 1987, **35**, 443.

32. Galloway, D. F., in *Chemistry and significance of Condensed Tannins*, R. W. Hemingway and J. J. Karchesy, Editors, 1989, Plenum Publishers: p. 447.

33. Tiarks, A. E., Bridges, J. R., Hemingway, R. W. and Shoulders, E., , in *Chemistry and significance of Condensed Tannins*, R. W. Hemingway and J. J. Karchesy, Editors, 1989, Plenum Publishers, p. 369.

34. Ohmart, C. P., *Forest Ecol. Management*, 1991, **39**, 35.

35. Nicholsorians, C., *J. Cem. Ecol.*, 1991, **17**, 1177.

36. Raubenheimer, D., *Ecology*, 1992, **73**, 1012.

37. Dhir, K. K., Raul, L., Shing, K. J. and Chark, K. S., *Biologia Plantarum*, 1992, **34**, 409.

38. Gonzalezcoleoma, A., C.S., W. and Rundel, P. W., *J. Biosci. (Zeitschrift Fur Naturforschung)*, 1993, **48**, 722.

39. Micheli, F., 1993, **171**, 165.

40. Mule, S., *Biochem. Systematics Ecol.*, 1993, **21**, 833.

41. Butler, L. G., in *Chemistry and significance of Condensed Tannins*, R. W. Hemingway and J. J. Karchesy, Editors, 1989, Plenum Publishers, p. 391.

42. Reed, J. D., *J. Animal Sci.*, 1995, **73**, 1516.

43. Dietz, B. A., Hagerman, A. E. and Barrett, G. W., *J. Mammalogy*, 1994, **75**, 880.

44. Beart, J. E., Lilley, T. H. and Haslam, E., *Phytochemistry*, 1985, **24**, 33.

45. Harborne, J. B., *Introduction to Ecological Biochemistry*. 1982, London, Academic Press.

46. Bate-Smith, E. C., *Phytochemistry*, 1973, **12**, 907.

47. Purushotham, H., Koshy, A., Sundar Rao, V. S., Latha, P., Gurumoorthy, M. M., Ananthanarayanan, S., Haridoss, V., Venkataboopathy, K., Sundaram, R., Lajapathy, C., Rao, P. G., Malikarjunan, M. M. and Raghavan, K. V., *J. Soc. Leather Tech. Chem.*, 1994, **78**, 178.

48. Steiner, P. R., in *Chemistry and significance of Condensed Tannins*, R. W. Hemingway and J. J. Karchesy, Editors, 1989, Plenum Publishers: p. 517.

49. Pizzi, A., Rossouw, D. duT., Knuffel, W. E. and Singmin, M., *Holzforsch. und Holzverwer*, 1980, **32**, 140.

50. Yamaguchi, H., Higuchi, M. and Sakata, I., *J. Appl. Pol. Sci.*, 1992, **45**, 1455.

51. Pizzi, A., Vunleyser, E. P., Valenzuela, J. and Clark, J. G., *Holzforschung*, 1993, **47**, 168.

52. Pizzi, A. and Stephanou, A., *J. Appl. Pol. Sci.*, 1994, **51**, 2109.

53. Fuwape, J. A., *Bioresource Technology*, 1994, **48**, 83.

54. Kehr, E., Riehl, G., Hoherichter, E., Roffael, E. and Dix, B., *Holz Als Roh-und Werkstoff.*, 1994, **52**, 253.

55. Pizzi, A., Valenzuela, J. and Westermeyer, C., *Holz Als Roh-und Werkstoff*, 1994, **52**, 311.

56. Zhua, L., Cau, B., Wang, F. and Yazaki, Y., *Holz Als Roh-und Werkstoff*, 1995, **53**, 117.

57. Calve, L., Mwalungu, G. C. J., Mwingira, B. A., Riedl, B. and Shields, J. A., *Holzforschung*, 1995, **49**, 259.

58. Laks, P. E., in *Chemistry and significance of Condensed Tannins*, R. W. Hemingway and J. J. Karchesy, Editors, 1989, Plenum Publishers: p. 503.

59. Kakiuchi, N., Hattori, M., Nishizawa, M., Yanagishi, T., Okuda, T. and Namba, T., *Chem. Pharm. Bull.*, 1986, **34**, 720.

60. Ooshima, T., Minami, T., Aonu, W., Tamora, Y. and Hamada, S., *Caries Research*, 1994, **28**, 146.

61. Castonguay, A., Boukharta, M. and Jalbert, G., *ACS Symp. Series*, 1994, **546**, 294.

62. Martz, W., *Toxicon*, 1992, **30**, 1131.

63. Haslam, E., Lilley, T. H., Warminski, E., Liao, H., Cai, Y., Martin, R., Gaffney, H., Goulding, P. N. and Genevieve, L., *ACS Symp. Series*, 1992, **509**, 8.

64. Bate-Smith, E. C., *Food*, 1954, **23**, 124.

65. Bate-Smith, E. C., *Adv. Food Res.*, 1954, **5**, 262.

66. Goldstein, J. L. and Swain, T., *Phytochemistry*, 1965, **4**, 185.

67. Oh, H. I., Hoff, J. E., Armstrong, G. A. and Haff, L. A., *J. Agric. Food Chem.*, 1980, **28**, 394.

68. Hagerman, A. E. and Butler, L. G., *J. Biol. Chem.*, 1981, **256**, 4494.

69. Goldstein, J. L. and Swain, T., *Phytochemistry*, 1963, **2**, 371.

70. Haslam, E., *Biochem. J.*, 1974, **139**, 285.

71. Loomis, W. D. and Battaile, J., *Phytochemistry*, 1966, **5**, 423.

72. Ellis, S. C. and Pankhurst, K. G. A., *Discuss. Faraday Soc.*, 1954, **16**, 170.

73. Gustavson, K. H., *J. Pol. Sci.*, 1954, **12**, 317.

74. Russel, A. E., Shutleworth, S. G. and Williams-Wynn, D. A., *J. Soc. Leather Trade Chemists*, 1968, **52**, 459.

75. Gutsche, C. D., *Calixarenes*. RSC Monographs in Supramolecular Chemistry, 1989, Canbridge.

76. Gutsche, C., Iqbal, M. and Stewart, J., *J. Org. Chem.*, 1986, **51**, 742.

77. Aoyama, Y., Tanaka, Y., Toi, H. and Ogoshi, H., *J. Am. Chem. Soc.*, 1988, **110**, 634.

78. Adams, H., Davis, F. and Stirling, C. J. M., *J. Chem. Soc. Chem. Commun.*, 1994, **21**, 2527.

79. Trigg, W. and Haslam, E., 1994, Unpublished observations, University of Sheffield.

CHAPTER TWO

EXPERIMENTAL PROCEDURE

2.1 Materials

All the proteins, peptides and synthetic macromolecules were obtained from Sigma Chemical Company Ltd. Caffeine and methyl gallate were purchased from Fisons and Aldrich Chemical Co. Ltd, respectively. The above compounds were used as received from the suppliers without further purification. The deuteriated solvents dimethylsulfoxide $((CD_3)_2SO)$ and chloroform $(CDCl_3)$ were obtained from Aldrich Chemical Co. Ltd. and deuterium oxide (D_2O), acetone $((CD_3)_2CO)$, methanol (CD_3OD) were supplied by Fluorochem Ltd. For the synthesis of calix[4]resorcinarene and calix[4]pyrogallolarene resorcinol and pyrogallol were purchased from BDH Ltd. and heptanal was obtained from Aldrich Chemical Co. Ltd.

The natural polyphenols: (-)epicatechin, procyanidin B-2, procyanidin B-3, procyanidin B-4, (-)epigallocatechin-3-O-gallate, β-1,2,3,4,6-penta-O-galloyl-D-glucopyranose (PGG), β-1,2,3,6-tetra-O-galloyl-D-glucopyranose (TeGG), β-1,3,6-tri-O-galloyl-D-glucopyranose (TGG) and 2,6-di-O-galloyl-D-glucopyranose (DGG) were prepared using a standard technique (section 2.2). Other natural polyphenols procyanidin A-2 and 2,6-di-O-galloyl-1,5-anhydro-D-glucitol were kindly donated by Prof. E Haslam.

In the precipitation experiments, all aqueous solutions were made using deionised (mixed resin) water which was then distilled.

2.2 Preparation of plant polyphenols

Polyphenols were isolated using the technique described in reference [1].

34

General Standard Procedure:

Between 1-2 Kg of plant materials (freshly picked leaves or fruits) were crushed in a high speed blender with 1-2 litres of cold methanol. Plant debris was removed and the methanolic extract was concentrated to a small volume using a rotary evaporator under reduced pressure at 30°C. The residual aqueous-methanolic solution of plant polyphenols was then filtered to remove unwanted materials such as chlorophyll, fats and waxes, etc. The crude phenolic extract was obtained by extracting the aqueous solution (250 ml) with ethyl acetate (6-8 times, 500 ml) and subsequently evaporating the combined ethyl acetate extract. Polyphenols were then separated on a Sephadex LH-20 chromatographic column using ethanol as eluting solvent. Two-dimensional paper chromatography was used to monitor the separation process. Chromatograms were prepared using (a) 6% aqueous acetic acid(v/v) in the first dimension and and (b) butan-2-ol-acetic acid-water (14:1:5, v/v) in the second dimension and were developed using ferric chloride-potassium ferricyanide spray. Appropriate fractions were combined and evaporated to dryness. Repurification was performed where necessary.

(-)Epicatechin:

This compound was separated from the extract of Hawthorn berries (*Crataegus monogyna*) using the standard procedure and the pure compound was obtained by crystallisation from water. Physical data: m.p. 218°C (decomp.), R_f(a) 0.37 and R_f(b) 0.51.

(-)Epigallocatechin-3-O-gallate:

This compound was prepared from green tea (*Camellia sinensis*) following the standard procedure. The compound was repurified using a Sephadex

35

LH-20 column eluting with chloroform-ethanol mixture (5:1, v/v). Physical data: R_f (a) 0.36 and R_f (b) 0.60.

Procyanidin B-2 (Epicatechin-(4β-8)-epicatechin):

This compound was separated from the extract of Hawthorn berries (*Crataegus monogyna*) using the standard procedure. Physical data: R_f(a) 0.58 and R_f(b) 0.42.

Procyanidin B-3 (Catechin-(4α-8)-catechin):

This was isolated from the extract of Sallow Willow catkins (*Salix caprea*) using the standard procedure. The compound was repurified on Sephadex LH-20 eluting with chloroform-ethanol mixture (4:1, v/v). Physical data: R_f(a) 0.43 and R_f(b) 0.34.

Procyanidin B-4 (Catechin-(4α-8)-epicatechin):

This compound was obtained from phenolic extracts of Raspberry leaf (*Rubus idaeaus*) following the standard procedure and repurified with chloroform-ethanol mixture (4:1, v/v). Physical data: R_f(a) 0.50 and R_f(b) 0.40.

2,6-Di-O-galloyl-D-glucopyranose:

This compound was prepared from Turkish galls (*Quercus infectoria*) along with β-1,2,3,6-tetra-O-galloyl-D-glucopyranose using the standard procedure described for the preparation of TeGG. Physical data: R_f(a) 0.43 and R_f(b) 0.43.

β-1,3,6-Tri-O-galloyl-D-glucopyranose:

This compound was prepared [2] from myrabolans (*Terminalia chebula*). Chebulinic acid was prepared by extracting crushed myrabolans powder in

acetone and by subsequent crystallisation from water. Chebulinic acid (12.5 g) was dissolved in a mixture of acetone-water (400 ml, 1:3, v/v). The solution was refluxed at 60°C under a nitrogen atmosphere for 7-8 days. Hydrolysis was monitored by 2D paper chromatography. When a substantial amount of chebulinic acid was converted to β-1,3,6-tri-O-galloyl-D-glucopyranose, the acetone was evaporated at 30°C. β-1,3,6-Tri-O-galloyl-D-glucopyranose and other compounds were extracted with ethyl acetate and dried to give a powder. β-1,3,6-Tri-O-galloyl-D-glucopyranose was separated using a Sephadex LH-20 column eluting with ethanol and further purified by crystallisation from water. Physical data: R_f(a) 0.12, and R_f(b) 0.44.

β-1,2,3,6-Tetra-O-galloyl-D-glucopyranose:

β-1,2,3,6-Tetra-O-galloyl-D-glucopyranose was prepared from the phenolic extracts of Turkish galls (*Quercus infectoria*) [3, 4]. Turkish galls (250 g), crushed into a fine powder, were extracted with methanol (2 x 1000ml). The solvent was then removed by evaporation at 30°C under reduced pressure to give the crude extract (~150 g). The crude gallotannin extract (6 g) was dissolved in an acetate buffer (60 ml) (prepared from acetic acid and sodium acetate) and refluxed for 24 hours and maintained at 37°C for 7 days under a nitrogen atmosphere. The hydrolysis reaction was monitored by 2D paper chromatography each day. When a substantial amount of gallotannin was converted to the product, the solution was reduced to a small volume and extracted with ethyl acetate (5 x 300 ml). The ethyl acetate extract was evaporated to dryness (gum). β-1,2,3,6-Tetra-O-galloyl-D-glucopyranose was purified using Sephadex LH-20 column eluting with ethanol. Physical data: R_f(a) 0.09, and R_f(b) 0.48.

β-1,2,3,4,6-Penta-O-galloyl-D-glucopyranose:

β-1,2,3,4,6-Penta-O-galloyl-D-glucopyranose was prepared from tannic acid [3]. The methanolysis reaction and purification of β-1,2,3,4,6-penta-O-galloyl-D-glucopyranose are similar to the preparation of β-1,2,3,6-tetra-O-galloyl-D-glucopyranose. Physical data: R_f(a) 0.08 and R_f(b) 0.51.

2.3 NMR studdies of procyanidin B-2

2.3.1 Preparation of the acetate derivative of procyanidin B-2

Procyanidin B-2 decaacetate was prepared [5] using the following method. 100 mg of procyanidin B-2 (crude) was dissolved in a mixture of 1 ml absolute pyridine and 1 ml distilled acetic anhydride. The solution was maintained for 24 hours at room temperature with constant stirring. Small pieces (5-6, ~ 2 cm³ in size) of ice were added to the solution which was then left for few hours at 4°C (melting ice), during which time the procyanidin B-2 decaacetate was precipitated. The solid was dissolved in a solvent mixture of chloroform-ethyl acetate (6:4, v/v) and applied to a silica gel column and eluted with the same solvent mixture. Chromatography was repeated three times to give the pure procyanidin B-2 deca-acetate (85 mg). Physical data: m.p. 141.1°C.

2.3.2 NMR experimentation

One- and two-dimensional NMR experiments were acquired using Bruker AM250, Bruker AMX400 and Bruker AMX500 spectrometers, the specific use of each machine depended upon the experimental requirements and availability. Specifications for the spectrometers are given in Table 2.1. All two-dimensional spectra acquired with AMX500 were processed, viewed and analysed using FELIX (Biosym Technologies Inc.) operating on a Silicon Graphics workstation. Other two-dimensional spectra were

38

processed within Bruker Win-NMR (1D and 2D) software installed on IBM Windows PC workstation. Hard copy plots of spectra were printed using a laser printer fitted with a postscript cartridge. All NMR studies were carried out on samples 0.6 ml in volume prepared in 5 mm standard NMR tubes.

Table 2.1 Specifications of NMR Spectrometers

Spectrometer	Facilities	Operating Frequency
Bruker AM250	Equipped with Aspect 3000 computer and variable temperature probe	250 MHz for ^{1}H and 62.5 MHz for ^{13}C
Bruker AMX400	Equipped with Aspect X32 computer and variable temperature probe	400 MHz for ^{1}H and 100 MHz for ^{13}C
Bruker AMX500	Equipped with Aspect X32 computer, inverse proton probe and variable temperature probe	500 MHz for ^{1}H and 125 MHz for ^{13}C

2.3.2.1 One-dimensional experiments

^{13}C variable temperature experiments for procyanidin B-2 were conducted with the Bruker AMX500 spectrometer and acquired into 16 K data points. ^{1}H variable temperature experiments for procyanidin B-2 were recorded with the Bruker AM250 spectrometer. The data were zero-filled to 64 K data points in all cases. Window functions such as exponential multiplication using a line broading (LB) of 2 Hz for ^{13}C data and Lorentz-Gauss enhancement or Lorentz-Gauss convert functions were employed with appropriate line broadening (LB = -1 or -2 Hz and GB = 0.2-0.3) before Fourier transformation.

2.3.2.2 Two-dimensional experiments

Proton detected inverse one-bond (HSQC, Heteronuclear Single Quantum Coherence) as well as long-range (HMBC, Heteronuclear Multiple Bond Correlation) ^{1}H-^{13}C correlation experiments for procyanidin B-2 were acquired using a Bruker AMX500 spectrometer. Similar experiments for decaacetate derivative of procyanidin B-2 were recorded on a Bruker AMX400 spectrometer. All experiments were recorded in phase-sensitive mode with TPPI (time-proportional phase increamentation) into 1000, 8 K complex files over a spectral width of 12.5 kHz in F_2 and 17.5 kHz in F_1. Before Fourier transformation, Lorentz-Gaussian window functions and sine-bell window functions shifted by 90° were employed in t_2 and t_1, respectively. ROESY (rotating-frame nuclear Overhauser effect spectroscopy) and COSY (correlation spectroscopy) experiments were acquired using a Bruker AMX400 spectrometer and were processed employing appropriate parameters.

2.4 Tannin-protein precipitation experiments

The experimental methodology and analytical techniques used in the precipitation experiments are essentially the same as those described in reference [6].

2.4.1 Equipment used

All operations , including centrifugation and the acquisition of UV spectra were carried out in the temperature range 293-295 K. Hand-held pipettes (Finnpipette) for 0.2-1.0 ml and a macropipette (BCL 3000) for 2.0-10.0 ml were used to achieve pipetting. All volumetric flasks were calibrated prior to use. A MSE Superspeed 65 machine was used to centrifuge samples at 30 000 rpm using 10 ml capacity polycarbonate tubes. UV spectra were recorded using a Phillips PU8700 UV/visible spectrophotometer.

Volumetric flasks were washed by soaking in aqua regia (a mixture of concentrated nitric acid, concentrated hydrochloric acid and water, 1:3:1, v/v for one hour, followed by extensive rinsing with distilled water. The wet glassware was allowed to drain and then dried in an oven at 45°C overnight.

A Janway 3030 pH meter coupled to a compatible glass electrode was used to measure pH and the system was calibrated using solutions of pH 3 and pH 4 (± 0.1 pH unit) made from buffer tablets supplied by the manufacturer.

2.4.2 Experimental methods

Tannin-protein precipitation was monitored as a function of protein concentration i.e., a series of tannin-protein solutions were prepared with a progressive increment of protein concentration keeping the tannin concentration constant. The following methodology was adopted: 1 ml of tannin 'stock' solution was added to a number of 10 ml volumetric flasks. Such an amount of solvent (buffer, salt solution or water) was added so that subsequent addition of protein solution gave the approximate desired experimental concentration thereby requiring only a minimal volume of solvent (1-4 drops) to make up the final volume. An example of the aliquot volumes of protein and tannin and experimental mole ratio values are shown in Table 2.2. Protein solution was added to each flask in turn in progressively increasing volume aliquots. Even mixing was ensured by rapid inversion of the flask. About 22 hours was allowed for the precipitation reaction. Then the samples were centrifuged and the supernatant were analysed by UV/visible spectrophotometry at ambient temperature (293-295 K).

41

Table 2.2 An example of tannin-protein mixing protocol.

Formal volume of tannin stock solution (102 μM) used ml	Formal volume of protein stock solution (2.4 μM) added ml	Final volume after adding required solvent ml	Concentration of Protein μM	Mole ratio (tannin/ protein)
1	0.0	10	0.000	-
1	0.2	10	0.048	212.5
1	0.4	10	0.096	106.3
1	0.6	10	0.144	070.8
1	0.8	10	0.192	053.1
1	1.0	10	0.240	042.5
1	1.2	10	0.288	035.4
1	1.4	10	0.336	030.4
1	1.6	10	0.384	026.6
1	1.8	10	0.432	023.6
1	2.0	10	0.480	021.3
1	3.0	10	0.720	014.2
1	3.4	10	0.816	012.5
1	3.8	10	0.912	011.2
1	4.2	10	1.008	010.1
0	10.0	10	2.400	-

2.4.3 Analysis of precipitation experiments

According to Beer-Lambert law:

$$A_i^{\lambda_x} = \varepsilon_i^{\lambda_x} . [C] . L \tag{2.1}$$

where $A_i^{\lambda_x}$ is the measured absorbance of a solute i, at concentration [C] (M) taken at wavelength λ_x (nm), L (cm) is the path length (the length of the absorbing medium) and $\varepsilon_i^{\lambda_x}$ (mol^{-1} cm^2) is the molar extinction coefficient which depends on the absorbing species and the wavelength of measurement. The Beer-Lambert law was found to be valid for all compounds used in the concentration ranges employed in this study.

2.4.4 Stoichiometric calculations of tannin/protein complexes in precipitates

The following equations [6] were used to calculate residual concentration of tannins and proteins:

$$[T]^{res} = \frac{\left[A^{\lambda_2}_{Total} \cdot \varepsilon^{\lambda_1}_P - A^{\lambda_1}_{Total} \cdot \varepsilon^{\lambda_2}_P \right]}{\left[\varepsilon^{\lambda_2}_T \cdot \varepsilon^{\lambda_1}_P - \varepsilon^{\lambda_1}_T \cdot \varepsilon^{\lambda_2}_P \right]} \cdot \frac{1}{L} \tag{2.2}$$

$$[P]^{res} = \frac{\left[A^{\lambda_2}_{Total} \cdot \varepsilon^{\lambda_1}_T - A^{\lambda_1}_{Total} \cdot \varepsilon^{\lambda_2}_T \right]}{\left[\varepsilon^{\lambda_1}_T \cdot \varepsilon^{\lambda_2}_P - \varepsilon^{\lambda_2}_T \cdot \varepsilon^{\lambda_1}_P \right]} \cdot \frac{1}{L} \tag{2.3}$$

where,

$[T]^{res}$ and $[P]^{res}$ = residual concentration of tannin and protein respectively (i.e., that remaining in the supernatant following the removal of the precipitate by centrifugation)

$A^{\lambda_1}_{Total}$ and $A^{\lambda_2}_{Total}$ = total observed absorbance at chosen wavelengths λ_1 and λ_2 of characteristic absorption maxima exhibited by tannins

$\varepsilon^{\lambda_1}_T$ and $\varepsilon^{\lambda_2}_T$ = molar extinction coefficient of tannins at λ_1 and λ_2

$\varepsilon^{\lambda_1}_P$ and $\varepsilon^{\lambda_2}_P$ = molar extinction coefficient of proteins at λ_1 and λ_2

Thus the measurement of: (a) the absorbance of the mixture at wavelengths corresponding to the absorption maxima in the spectrum of the pure tannin, (b) the molar extinction coefficient of the tannin alone at its absorption maxima and (c) the molar extinction coefficient of the protein alone at wavelengths corresponding to the maxima in the tannin absorption spectrum facilitates the calculation of residual concentration of both tannin and protein.

Precipitation indices can be calculated from the following equations:

$$RA = \left(\frac{A_0^{\lambda_2} - A_{Total}^{\lambda_2}}{A_0^{\lambda_2}} \right).100\% \tag{2.4}$$

$$M_T^{ppt} = \left([T]^{init} - [T]^{res} \right).\left(\frac{RMM_T}{1000} \right).v \tag{2.5}$$

$$M_P^{ppt} = \left[[P]^{init} - [P]^{res} \right].\left(\frac{RMM_P}{1000} \right).v \tag{2.6}$$

$$\%[T]^{ppt} = 100.\frac{[T]^{init} - [T]^{res}}{[T]^{init}} \tag{2.7}$$

and

$$MR = \frac{M_T^{ppt}}{M_P^{ppt}}.\left(\frac{RMM_P}{RMM_T} \right) = \frac{[T]^{init} - [T]^{res}}{[P]^{init} - [P]^{res}} \tag{2.8}$$

where

RA $\qquad$ = relative absorbance

$A_0^{\lambda_2}$ $\qquad$ = absorbance of tannin alone (i.e., in the absence of protein or other reagent

$[T]^{init}$ and $[P]^{init}$ $\qquad$ = initial concentration of tannin and orotein species, respectively

M_T^{ppt} and M_P^{ppt} $\qquad$ = mass of tannin and protein in the precipitate

MR $\qquad$ = mole ratio of the precipitates

RMM_T and RMM_P =relative molar mass of tannin and protein

v $\qquad$ = volume of the reaction flask.

2.5 Caffeine-tannin binding studies by NMR spectroscopy

2.5.1 Caffeine-tannin titration experiments

The caffeine-tannin titration experiments were carried out in the solvent system D_2O/CD_3OD (1:1, v/v). Solutions of each polyphenol (60 mM) were prepared. Solution of the tannins was accomplished by using a sonic bath and short heating. Solutions of polyphenols were titrated into a solution of caffeine of concentration 2 mM, prepared in the same solvent.

A Bruker WH400 (equipped with Aspect 2000 computer and operating at 400 MHz for ^1H) spectrometer was used to follow the titration experiments. Changes in proton chemical shift of caffeine (chemical shift data for caffeine is presented in Table 2.3) were measured from one-dimensional experiments. Deuterated methanol present in the solvent system was used both as an internal reference and for the deuterium lock. The sodium salt of 3-trimethylsilyl (2,2,3,3-D_4 propionate (TSP) (**1**) dissolved in the same solvent, sealed in a glass capillary tube and inserted in the NMR tube, served as the secondary reference. All the titration experiments were performed in the temperature range 293-295 K.

Table 2.3 ^1H Chemical shifts (400 MHz) for caffeine at 2 mM concentration in D_2O/CD_3OD (1:1, v/v) at 295 K, and are given relative to external TSP 0.000 ± 0.005 ppm.

Proton	δ (ppm)	Multiplicity	Coupling constant (Hz)
methyl 1	3.355	singlet	-
methyl 3	3.538	singlet	-
methyl 7	3.968	doublet	$^4J_{H8,Me7} = 0.68$
H8	7.916	doublet	$^4J_{H8,Me7} = 0.68$

45

$$\text{Me} - \underset{\underset{\text{Me}}{|}}{\overset{\overset{\text{Me}}{|}}{\text{Si}}} \diagdown\diagup \text{COO}^- \text{Na}^+$$
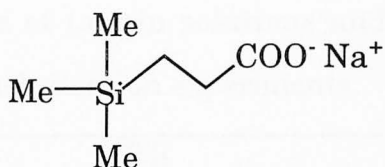
(1) (sodium) 3-trimethylsilyl (2,2,3,3-D$_4$) propionate

NMR data were processed and analysed using Bruker Win-NMR software installed on a Windows PC workstation. A high digital resolution was achieved by recording NMR data into 32 K data points, using a shorter spectral window (2968 Hz). The data were zero-filled to 64 K data points to give a final resolution of 0.1 Hz/point. A Lorentz-Gauss window function was employed prior to Fourier transformation. A built-in curve-fitting program within Win-NMR was used to measure the chemical shifts with an approximate accuracy of ± 0.0003 ppm.

Table 2.4 shows the aliquot volumes (µl) and the resulting caffeine:tannin mole ratio values produced by the titration of the tannin solution into 600 µl, 2 mM solutions of caffeine.

2.5.2 Analysis of caffeine-tannin titration data

The binding constants (K_a) for the heterotactic association of caffeine and tannins were calculated using the proton chemical shift data measured during the titration experiments. The values of K_a and maximum chemical shift change ($\Delta\delta_{max}$) were determined from non-linear least-square fitting of the equations presented in section 2.8. The equations were expressed as formulae in spreadsheets within the program EXCEL (Microsoft Corporation). The procedure adopted to calculate K_a and $\Delta\delta_{max}$ was as follows: Estimated values for K_a and $\Delta\delta_{max}$ were initially entered resulting in calculated chemical shift values (δ_{calc}) at each of the observed chemical shift (δ_{obs}) vs [solute] data points. The difference between the δ_{obs} and δ_{calc}

Table 2.4 Aliquot volumes of tannin solutions and resulting mole ratio values of caffeine-polyphenol titration experiments.

V_i µl added to 600µl of 2mM solution of caffeine	$[T]_i$ mM	Mole ratio (caffeine:tannin)
0	0.00	1:0.0
10	0.98	1:0.5
20	1.94	1:1.0
30	2.86	1:1.5
40	3.75	1:2.0
50	4.62	1:2.5
60	5.46	1:3.0
70	6.27	1:3.5
80	7.06	1:4.0
90	7.83	1:4.5
100	8.57	1:5.0
120	10.00	1:6.0
140	11.35	1:7.0
160	12.63	1:8.0

where V_i = total volume of polyphenol added
          $[T]_i$ = total concentration of polyphenols added.

at each data point was calculated and the resulting value was squared. The calculation of the squared differences and a minimisation of the sum of the squares produces the best-fit curve and the best-fit values of K_a and $\Delta\delta_{max}$. To fit equations to the experimental data, a standard non-linear least-square curve-fitting routine was followed and the quality of fit was judged by the residual sum of least-squares ($\Sigma_{squares}$). The success of the curve-fitting procedure relied on the curvature of (δ_{obs}) vs [solute] plots. An example of the ilustration of curve-fitting is presented in Fig. 2.1.

The results obtained following the above procedure were cross checked by performing additional curve-fitting using the program Host-Guest-NMR written in PASCAL by Dr C. A. Hunter of the Department of Chemistry, University of Sheffield.

47
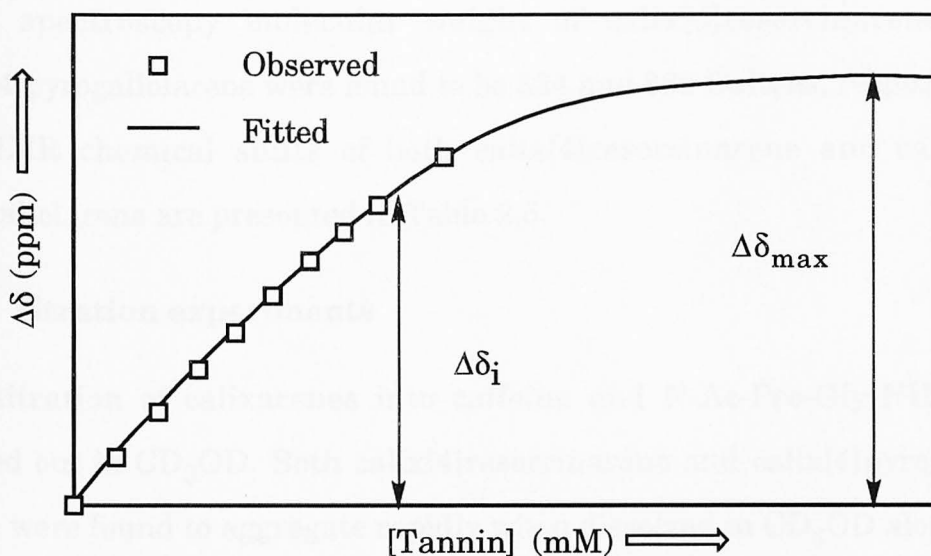
Fig. 2.1 Graphical display of the curve fitting of substrate-tannin titration data.

2.6 Binding studies of calixarenes with caffeine and proline containing peptide

The binding of caffeine and a small peptide (N-acetyl-Pro-Gly-NH$_2$) with two different calixarenes, calix[4]resorcinarene and calix[4]pyrogallol-arene, were studied.

2.6.1 Synthesis of calixarenes

The calixarenes were synthesised using the following method. A solution of resorcinol or pyrogallol (0.15 moles) was prepared in distilled ethanol (60 ml) and concentrated hydrochloric acid (12 N, 20 ml) was added and the solution cooled to 5°C. Heptanal (0.15 moles, 17.13 g) was added dropwise over an hour. A precipitate formed which dissolved on heating. The mixture was then refluxed for 16 hours at 65-70°C. The precipitate became

crystals. Physical data: m.p. of calix[4]resorcinarene and calix[4]pyrogallol-arene were determined to be 375°C and 339°C, respectively. Calix[4]-pyrogallolarene was found to decompose at between 300°C to 339°C. From mass spectroscopy molecular weight of calix[4]resorcinarene and calix[4]pyrogallolarene were found to be 824 and 889 Daltons, respectively. ^{1}H NMR chemical shifts of both calix[4]resorcinarene and calix[4]-pyrogallolarene are presented in Table 2.5.

2.6.2 Titration experiments

The titration of calixarenes into caffeine and N-Ac-Pro-Gly-NH$_2$ was carried out in CD$_3$OD. Both calix[4]resorcinarene and calix[4]pyrogallol-arene were found to aggregate rapidly when dissolved in CD$_3$OD alone but interestingly, the mixtures of caffeine or N-Ac-Pro-Gly-NH$_2$ and calix[4]arenes were highly soluble at the concentration range required for this study. On the basis of this observation a different strategy was adopted. A 2 mM solution (excess) of caffeine or peptide was prepared and the calix[4]arenes were dissolved in the required volume of caffeine or peptide solution to give a concentration of 30 mM. The caffeine or peptide solutions were used as a solvent the calix[4]arenes. Solutions of the calix[4]arenes were titrated into the caffeine or the peptide solutions (600 μl, 2 mM). The concentration of caffeine or N-Ac-Pro-Gly-NH$_2$ thus remained absolutely constant throughout the titration. Titrations were performed in the respective temperature range 293-295 K.

Table 2.5 ^{1}H Chemical shifts (400 MHz) for calix[4]resorcinarene and calix[4]pyrogallolarene at 2 mM concentration in CD_3OD at 295 K, and are given relative to internal methanol (3.300 ppm) ± 0.005 ppm.
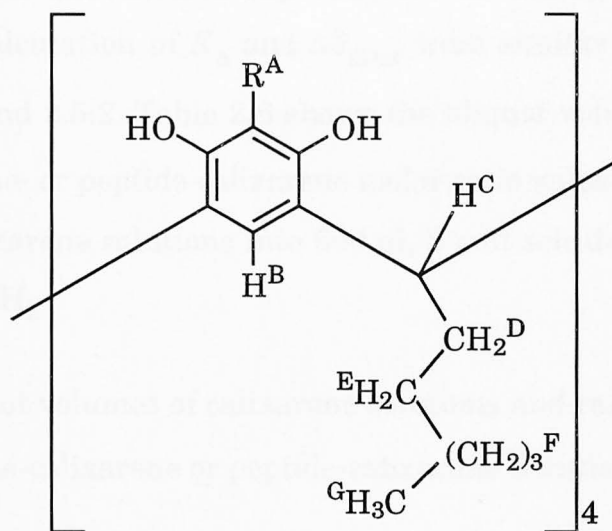
Calix[4]resorcinarene, R = H
Calix[4]pyrogallolarene, R = OH

Proton	Calix[4]resorcinarene			Calix[4]pyrogallolarene		
	δ (ppm)	Multiplicity	Coupling Constant (Hz)	δ (ppm)	Multiplicity	Coupling Constant (Hz)
A	7.178	s	-	-	-	-
B	6.197	s	-	6.747	s	-
C	4.258	t	7.8, 7.8	4.296	t	7.9, 7.9
D	2.160	qua	7.8, 7.5	2.137	qua	7.9, 7.8
E	≈1.398	qui	-	≈1.391	qui	-
F	≈1.308	m	-	≈1.304	m	-
G	0.911	t	6.7, 7.0	0.908	t	6.8, 6.9

s = singlet, d = doublet, t = triplet, qua = quartet, qui = quintet and m = multiplet.

2.6.3 Analysis of chemical shift data

Changes in proton chemical shift of caffeine and N-Ac-Pro-Gly-NH$_2$ were monitored by one-dimensional experiments. Recording of spectra, their analysis and calculation of K_a and $\Delta\delta_{max}$ were similar to as detailed in sections 2.5.1 and 2.5.2. Table 2.6 shows the aliquot volumes (μl) and the resulting caffeine- or peptide-calixarene molar ratio values produced by the titration of calixarene solutions into 600 μl, 2 mM solution of caffeine and N-Ac-Pro-Gly-NH$_2$.

Table 2.6: Aliquot volumes of calixarene solutions and resulting mole ratio values of caffeine-calixarene or peptide-calixarene titration experiments.

V_i μl added to 600 μl of 2 mM solution of caffeine or peptide	$[T]_i$ mM	Mole ratio (caffeine : calixarenes) (peptide : calixarenes)
0	0.00	1:0.0
10	0.49	1:0.3
20	0.97	1:0.5
30	1.43	1:0.7
40	1.88	1:0.9
50	2.31	1:1.2
60	2.73	1:1.4
70	3.13	1:1.6
80	3.53	1:1.8
100	4.29	1:2.1
120	5.00	1:2.5
140	5.68	1:2.8
160	6.32	1:3.2
180	6.92	1:3.5
200	7.50	1:3.8
220	8.05	1:4.0
240	8.57	1:4.3
260	9.07	1:4.5
300	10.00	1:5.0

where V_i = total volume of calixarene added

$[T]_i$= total concentration of calixarene added.

2.7 Binding investigation of bradykinin and its analogues with tannins

2.7.1 Chemical shift assignment of bradykinin

One-dimensional ^{1}H variable temperature experiments and homonuclear two-dimensional experiments TOCSY (total correlation spectroscopy) and ROESY were carried out on a Bruker AMX500 spectrometer. Two-dimensional experiments were recorded with water presaturation in phase-sensitive mode using time-proportional phase increamentation (TPPI). The spectra were acquired into 512, 8 K complex files over a spectral width of 12.5 kHz in F_2 and 4.17 kHz in F_1. A Lorentz-Gauss or sine-squared bell window function shifted by 90° was applied in t_2 and sine-squared bell window shifted by 90° was applied in t_1 prior to Fourier transformation. All experiments were performed in solution mixture $D_2O/(CD_3)_2SO$ (4:1, v/v).

2.7.2 Titration of peptides with tannins

All experiments were performed in solution mixture $D_2O/(CD_3)_2SO$ (4:1, v/v). Solutions of tannins (60 mM) were titrated into a solution of peptide (2 mM). The titration was monitored by one-dimensional ^{1}H NMR spectroscopy. All room-temperature (293-295 K) experiments were recorded with a Bruker WH400 spectrometer. Bradykinin-tannin titration experiments were repeated at 278 K and were recorded with a Bruker AMX500 spectrometer. Deuterated DMSO was used for the deuterium lock and also served as an internal reference. Spectra were referenced downfield from external TSP as detailed in section 2.5.1.

A similar procedure was employed to record and analyse spectra and to calculate K_a and $\Delta\delta_{max}$ values as detailed in section 2.5.1 The aliquot volumes (μl) and resulting peptide:polyphenol molar ratio values produced

52

by the titration of polyphenol solution into 600 µl, 2 mM solution of peptide are detailed in Table 2.7.

Table 2.7 Aliquot volumes of polyphenol solutions and resulting mole ratio values of peptide-polyphenol titration experiments.

V_i µl added to 600 µl of 2 mM solution of peptide	$[T]_i$ mM	Mole ratio (peptide:tannin)
0	0.00	1:0.0
10	0.98	1:0.5
20	1.94	1:1.0
30	2.86	1:1.5
40	3.75	1:2.0
50	4.62	1:2.5
60	5.46	1:3.0
70	6.27	1:3.5
80	7.06	1:4.0
90	7.83	1:4.5
100	8.57	1:5.0
120	10.00	1:6.0

where V_i = total volume of polyphenol added
            $[T]_i$= total concentration of polyphenols added.

2.7.3 Self-association studies of tannins

Self-association experiments were performed in $D_2O/(CD_3)_2SO$ (4:1, v/v) at 293-295 K and were recorded with a Bruker AM250 spectrometer. External TSP was used to reference the spectra. Polyphenol solutions (60mM) were prepared. Volume aliquots of polyphenol solutions were added to 600 µl solvent to give increasing concentrations of polyphenols from 0 mM to 15 mM.

Changes in the proton chemical shift of polyphenols during titrations were used to determine the homotactic association constant K_a and $\Delta\delta_{max}$ using the equations presented in section 2.8.2 and procedures detailed in section 2.5.1.

2.8 Determination of association constant K_a

This section presents heterotactic and homotactic binding equations which enable the equilibrium constants for substrate-tannin interactions and tannin self-association to be determined. All the equations presented below were expressed as formulae in the software program EXCEL (Microsoft Corporation). The association constant K_a and maximum chemical shift change $\Delta\delta_{max}$ were determined from NMR chemical shift data using a least-square fitting routine.

2.8.1 Heterotactic binding interaction

The following equation was employed to determine the heterotactic association constant K_a for 1:1 binding interaction of independent species and maximum change in chemical shift $\Delta\delta_{max}$ using the chemical shift data for protons of caffeine or peptides obtained from the titration of the polyphenols into caffeine or peptides. The equation was taken and adapted from reference [7].

$$\Delta\delta_i = \frac{\Delta\delta_{max}}{2}\left[\left(1+\frac{1}{K_a[P]_i}+\frac{[T]_i}{[P]_i}\right)-\left\{\left(1+\frac{1}{K_a[P]_i}+\frac{[T]_i}{[P]_i}\right)^2-4\frac{[T]_i}{[P]_i}\right\}^{\frac{1}{2}}\right] \qquad (2.9)$$

where

$\Delta\delta_i$ = observed change in chemical shift (ppm)

$\Delta\delta_{max}$ = maximum change in chemical shift (ppm

K_a = association constant (M^{-1})

$[P]_i$ = total concentration of caffeine or peptide (M)

$[T]_i$ = total concentration of polyphenol (M)

54

and

$$[P]_i = \frac{[P]_0 . V_0}{V_0 + V_i}$$

$$[T]_i = \frac{[T]_a . V_i}{V_0 + V_i}$$

where,

$[P]_0$ = initial concentration of peptide or caffeine solution (M)

$[T]_0$ = concentration of added polyphenol solution (M)

V_i = volume of polyphenol solution added (µl)

V_0 = initial volume of peptide or caffeine solution (µl)

2.8.2 Self-association

2.8.2.1 Dimerisation model

The following equation was used to determine the dimerisation constant of tannin molecules from NMR chemical shift data. The equation was taken from reference [8]. This model assumes that the molecules of tannin T (momomers) self-associate to form dimers.

$$\delta - \delta_T = (\delta_{max} - \delta_T)\frac{(1 + 8K_a[T]_0)^{1/2} - 1}{(1 + 8K_a[T]_0)^{1/2} + 1} \qquad (2.10)$$

where

δ = observed chemical shift

δ_T = chemical shift of T as monomer

δ_{max} = maximum chemical shift of T (dimer) ($\delta_{max} - \delta_T = \Delta\delta_{max}$)

55

K_a = dimerisation constant

$[T]_0$ = total concentration of tannin

2.8.2.2 Isodesmic or self-association model

The equation for the isodesmic model was taken and corrected from reference [9] and was used to obtain self-association constants from NMR chemical shift data. This model assumes that tannin molecules associate to form stacks of tannin molecules (dimers, trimers, etc.) where the equilibrium constant for each step is the same.

$$\delta - \delta_T = (\delta_{max} - \delta_T) K_a [T]_o \left\{ \frac{2}{1 + (4K_a[T]_o + 1)^{1/2}} \right\}^2$$
$$\times \left[2 - K_a[T]_o \left\{ \frac{2}{1 + (4K_a[T]_o + 1)^{1/2}} \right\}^2 \right] \tag{2.11}$$

where,

δ = observed chemical shift

δ_T = chemical shift of T as monomer

δ_{max} = the chemical shift of T present in a tannin stack

K_a = self-association constant constant

$[T]_0$ = total concentration of tannin

Equations (2.10) and (2.11) give δ as a function of δ_T (known), $\Delta\delta_{max}$ (unknown), $[T]_0$ (known) and K_a (unknown). Using the chemical shift values measured for proton resonances at concentrations of tannin, values of K_a and $\Delta\delta_{max}$ for the dimerisation and stacking of tannin association can be obtained from least-square fitting routine.

References

1. Jacques, D. and Haslam, E., *J. Chem. Soc. Perkin Trans. 1*, 1974, 2663.

2. Schmidt, O. T. and Demmler, K., *Liebigs Ann. Chem.*, 1957, **609**, 192.

3. Armitage, R., Bayliss, G. S., Gramshaw, J. W., Haslam, E., Hawarth, R. D., Jones, K., Rogers, H. J. and Searle, T., *J. Chem. Soc.*, 1961, 1842.

4. Thompson, R. R., Jacques, D. J., Haslam, E. and Tanner, R. J. N., *J. Chem. Soc. Perkin Trans. 1*, 1972, 1387.

5. Weinges, K., Kaltenhauser, W., Marx, H., Nader, E., Nader, F., Perner, J. and Seiler, D., *Liebigs Ann. Chem.*, 1968, **711**, 184.

6. Warminski, E. E., Ph. D. Thesis, 1992, University of Sheffield, U. K.

7. Fairbrother, W. J., D. Phil. Thesis, 1989, University of Oxford, U. K.

8. Murray, N. J., Ph. D. Thesis, 1994, University of Sheffield, U. K.

9. Lilley, T. H., Linsdell, H. and Maestre, A., *J. Chem. Soc. Faraday Trans.*, 1992, **88**, 2865.

CHAPTER THREE

NMR STUDIES OF PROCYANIDIN B-2

3.1 Introduction

B-type [1] proanthocyanidins are widely distributed in nature. Extracts of hawthorn and meadowsweet are rich in B-type procyanidins along with other compounds that typically form the basis for many herbal medicines [2], which are still widely used. Interestingly, plants produce polyphenols selectively, that is to say, certain types of plants biosynthesise mainly certain types of products. As for example, in Hawthorn plants (-)epicatechin and its higher oligomers are found to be predominantly synthesised. Similarly, willowcatkins produces (+)catechin and its oligomers. Procyanidin B-2 (**1a**) is a dimer of (-)epicatechin. This compound along with other B-type procyanidins has been extensively studied at Sheffield [3-5] and elsewhere [1, 6-9] by using conventional techniques as well as spectroscopic and molecular mechanics calculations.
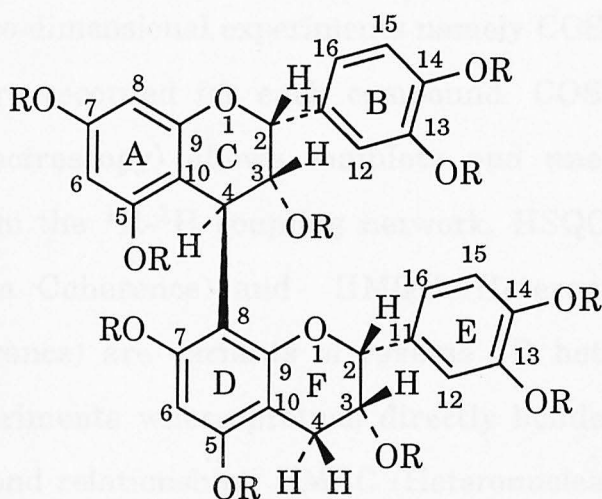
Procyanidin B-2

(**1a**, R = H)
(**1b**, R = Ac)

58

The monomeric unit (-)epicatechin of procyanidin B-2 has absolute stereochemistry of 2R and 3R. The absolute stereochemistry at C4 was established as 4R by the Sheffield group [4, 5] by extensive use of ^{13}C NMR and C.D. spectroscopy. From earlier times it has been speculated [1, 4, 5] that the compound which is called procyanidin B-2 is a dimer of (-)epicatechin linked through C4 of the top unit and C8 of the bottom unit on the basis that the C8 carbon is more nucleophilic and less sterically hindered than C6. There has been, however, no direct proof so far for this C4C → C8D linkage (the second uppercase letters in the atom expression indicate the rings that the atoms belong to).

The aim of the present study is to provide spectroscopic proof for the interflavan linkage, whether it is C4C→C8D or C4C→C6D. The overall conformation of the molecule will be interpreted from the Molecular Mechanics calculations combined with NMR data. Details of the preparation of procyanidin B-2 from Hawthorn fruits and its acytylation have been presented in Chapter 2.

3.2 Methods of ^{1}H and ^{13}C resonance assignments

A set of three two-dimensional experiments namely COSY, HSQC/HMQC and HMBC were recorded for each compound. COSY (homonuclear Correlation Spectroscopy) allows complete and unequivocal proton assignments from the ^{1}H-^{1}H coupling network. HSQC (Heteronuclear Single Quantum Coherence) and HMQC (Heteronuclear Multiple Quantum Coherence) are variants of reverse 2D heteronuclear shift correlation experiments where protons directly bonded to carbon are observed (one bond relationship). HMBC (Heteronuclear Multiple Bond Correlation) is the long-range variant of the HSQC or HMQC, i.e., in this experiment protons bonded to carbons separated by normally 2 and 3

bonds are observed. In extremely favourable situations, however, correlations of up to 4 bonds may be observed.

For this study, the reverse ^{1}H-^{13}C correlation experiments HSQC and its long-range variant HMBC were recorded for procyanidin B-2 (natural, **1a**). On the other hand, HMQC and its long-range variant were recorded for the decaacetate derivative (**1b**). There is essentially no difference between HSQC and HMQC experiments, as far as the appearance and analysis of the spectra are concerned, except in the pulse sequence. There is a little difference in the appearance of two variants of HMBC spectra. The HSQC derived HMBC spectra provides an additional one-bond correlation as carbon satellites (separated by H-C coupling constants) along with 2 and 3 bond correlations. This additional one-bond relationship can be advantageously exploited. There was, however, no specific reason for choosing different versions of the same kind of experiments, but for the convenience and availability of the machines and associated pulse programmes.

The ^{1}H and ^{13}C frequency for the experiments recorded for natural procyanidin B-2 were 500 and 125 MHz, respectively. The same for the decaacetate derivative were 400 and 100 MHz, respectively. Recording and processing of NMR data are detailed in Chapter 2.

3.3 Chemical shift results and discussion

3.3.1 ^{1}H and ^{13}C shift assignments

Natural procyanidin B-2 was a troublesome compound with respect to ^{1}H NMR spectroscopy. The ^{1}H spectrum at ambient temperature (ca. 295K, Fig. 3.1) was not resolved, rather almost all the signals were broad and ^{1}H-^{1}H coupling information was absent, except for a few signals appearing at high field. Aromatic proton chemical shifts were found to move with

60

temperature and at ambient temperature few proton signals, particularly protons attached to the B and E rings, were degenerate. COSY experiment allowed unequivocal assignments for protons attached to pyran rings only. For ^{1}H assignments a convenient starting point was two double doublets appearing at 2.91 and 2.74 ppm, respectively, separated from each other by 16.7 Hz, (typical geminal coupling constant) which were assigned to H4Cβ and H4Cα, respectively. H4Cβ and H4Cα were identified from their cis and trans coupling with H3C proton, such as 4.7 Hz and 3.8Hz, respectively. Assignments of other pyran protons were straightforward. H6A and H8A were identified from their metacoupling relationship. Considerable ambiguity remained for protons attached to the B and E rings.

At 268K the aromatic proton signals were found to be suitably dispersed and COSY experiments allowed assignments for them. Their assignments remained to be verified by other means. At this stage it was not possible to comment with certainty which proton groups belonged to rings B and E. This ambiguity, however, was removed by subsequent examination of the HMBC spectra combined with HSQC spectra.

^{13}C chemical shifts were assigned by the combined analysis of HSQC and HMBC spectra. Key starting points were C4C and C4F carbons that occurred at distinct chemical shifts at 36.5 ppm (295 K) or 35.4 ppm (268 K) (typical of doubly benzylic carbon) and 28.6 ppm (295 K) or 27.6 ppm (268K), respectively. The rest of the shift assignments were made by systematic use of the long-range ^{1}H-^{13}C correlation map. C9A, C10A, C9D and C10D (unprotonated carbons) assignments were verified from correlation with at least two protons.

A similar approach was adopted to assign ^{1}H and ^{13}C chemical shifts for the decaacetate of procyanidin B-2. Here assignments were less

complicated compared to the native compound because almost all the ^{1}H-^{1}H coupling information was available in the one-dimensional ^{1}H spectrum. Two sets of assignments for both ^{1}H and ^{13}C were obtained for major and minor conformers without much difficulty. ^{1}H and ^{13}C chemical shift assignments are presented in Tables 3.1 and 3.2.
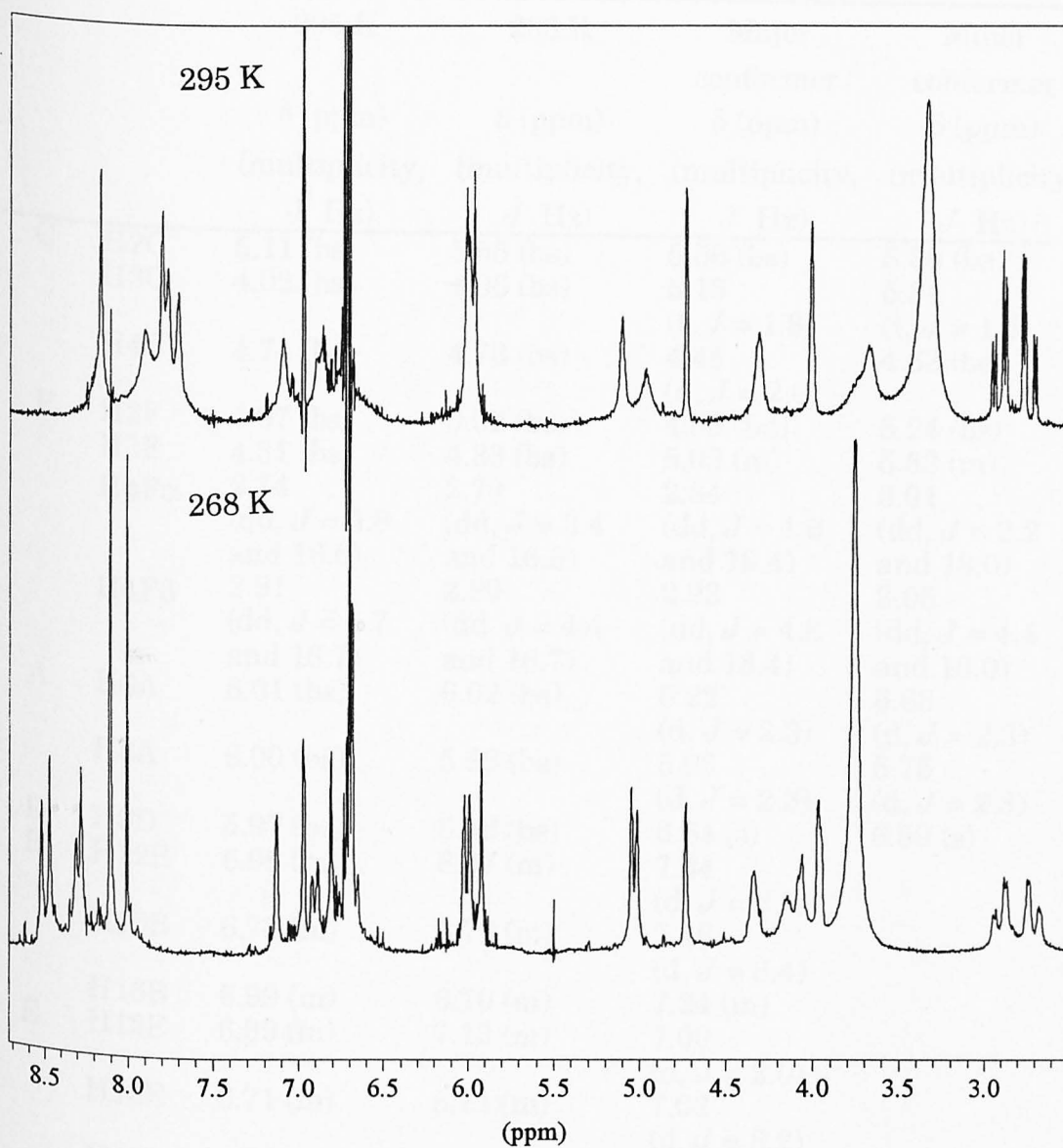
Fig. 3.1 ^{1}H NMR spectra of natural procyanidin B-2 recorded in $(CD_3)_2CO$ at 250 MHz.

Table 3.1 ^{1}H chemical shifts for procyanidin B-2. Shifts are given relative to the internal $(CD_3)_2CO$ residual proton signal at 2.04 ppm or $CDCl_3$ residual proton signal at 7.25 ppm.

Ring	Proton	Natural compound (**1a**) (500 MHz, $(CD_3)_2CO$)		Decaacetate derivative (**1b**) (400 MHz, $CDCl_3$) 295 K	
		295 K	268 K	Major conformer	Minor conformer
		δ (ppm) (multiplicity, J Hz)	δ (ppm) (multiplicity, J Hz)	δ (ppm) (multiplicity, J Hz)	δ (ppm) (multiplicity, J Hz)
C	H2C	5.11 (bs)	5.05 (bs)	5.56 (bs)	5.39 (bs)
	H3C	4.02 (bs)	4.06 (bs)	5.15 (t, J = 1.8)	5.31 (t, J = 1.5)
	H4C	4.74 (bs)	4.73 (bs)	4.45 (d, J = 2.0)	4.63 (bs)
F	H2F	4.97 (bs)	5.02 (bs)	4.53 (bd)	5.24 (bs)
	H3F	4.31 (bs)	4.33 (bs)	5.09 (m)	5.53 (m)
	H4Fα	2.74 (dd, J = 3.8 and 16.6)	2.70 (dd, J = 3.4 and 16.9)	2.84 (dd, J = 1.6 and 18.4)	3.01 (dd, J = 2.2 and 18.0)
	H4Fβ	2.91 (dd, J = 4.7 and 16.7)	2.90 (dd, J = 4.4 and 16.7)	2.92 (dd, J = 4.8 and 18.4)	3.05 (dd, J = 4.4 and 18.0)
A	H6A	6.01 (bs)	6.02 (bs)	6.22 (d, J = 2.3)	6.63 (d, J = 2.3)
	H8A	6.00 (bs)	5.99 (bs)	5.95 (d, J = 2.3)	6.75 (d, J = 2.3)
D	H6D	5.97 (bs)	5.92 (bs)	6.64 (s)	6.59 (s)
B	H12B	6.99 (m)	6.97 (m)	7.34 (d, J = 2.0)	
	H15B	6.73 (m)	6.72 (m)	7.16 (d, J = 8.4)	
	H16B	6.99 (m)	6.70 (m)	7.24 (m)	
E	H12E	6.99 (m)	7.13 (m)	7.00 (d, J = 2.0)	
	H15E	6.71 (m)	6.71 (m)	7.02 (d, J = 8.2)	
	H16E	6.99 (m)	6.91 (m)	6.87 (dd, J = 8.3 and 2.0)	
	CH_3CO			1.86 - 2.35	1.54 - 2.35

bs = broad singlet, bd = broad doublet, d = doublet, t = triplet and m = multiplet.

63

Table 3.1 ^{13}C chemical shifts for procyanidin B-2. Shifts are given relative to the internal $(CD_3)_2CO$ carbon signal at 29.8 ppm or the $CDCl_3$ carbon signal at 77.0 ppm.

Ring	Carbon	Natural compound (125 MHz, $(CD_3)_2CO$)		Decaacetate derivative (100 MHz, $CDCl_3$) 295 K	
		295 K	268 K	Major conformer	Minor conformer
		δ (ppm)	δ (ppm)	δ (ppm)	δ (ppm)
C	C2C	76.6	75.5	73.5	74.3
	C3C	72.6	71.6	71.0	70.5
	C4C	36.5	35.4	34.0	34.1
F	C2F	79.0	77.6	77.2	76.6
	C3F	66.1	65.0	66.9	66.3
	C4F	28.6	27.6	26.7	26.5
A	C5A	158.0	156.7	147.2	149.1
	C6A	96.3	95.0	108.6	108.9
	C7A	157.2	154.6	148.6	149.1
	C8A	95.9	94.4	107.2	108.1
	C9A	155.6	157.6	154.8	154.4
	C10A	100.3	99.5	111.0	111.2
D	C5D	155.5	154.9	147.2	146.7
	C6D	96.5	95.6	110.2	110.8
	C7D	157.4	154.9	148.6	146.7
	C8D	106.7	106.1	116.2	117.2
	C9D	153.8	153.1	153.9	151.3
	C10D	100.3	99.2	111.3	109.3
B	C11B	132.0	131.2	136.1	
	C12B	115.1	114.1	122.1	
	C13B	145.1	144.4	140.9	
	C14B	145.1	144.1	141.4	
	C15B	115.3	114.4	123.0	
	H16B	119.0	118.0	124.4	
E	C11E	130.4	130.9	133.9	
	C12E	115.8	112.9	122.4	
	C13E	145.1	144.4	141.1	
	C14E	145.1	144.1	141.1	
	C15E	115.1	114.4	122.7	
	H16E	120.3	117.7	125.0	
	CH$_3$ of the acetates			19.8 - 21.2	
	Carbonyls of CH$_3$CO			167.9 - 170.4	

3.3.2 Location of the interflavan linkage

One of the important goals for this study was to locate the interflavan linkage, whether it is C4→C8 or C4→C6. A similar strategy as described in reference [10] was adopted to confirm the location.

Depending on the type of linkage, the H4C proton should show long-range correlations as displayed in Table 3.3 (and see Scheme 3.1). The only difference would be the correlation with the C9D in C4→C8 dimer compared with C5D in the C4→C6 dimer. Thus it was necessary to discriminate those two carbon resonances.

Table 3.3 Comparison of the expected long-range correlations for H4C proton in (-)epicatechin dimer in a HMBC experiment.

Nature of the correlation	C4→C8 dimer		C4→C8 dimer	
	^2J	^3J	^2J	^3J
Upper flavan unit	C3C, C10A	C2C, C9A, C5A	C3C, C10A	C2C, C9A, C5A
Lower flavan unit	C8D	C7D, C9D	C6D	C5D, C7D

As expected, the H4C proton showed correlations with all possible eight carbons in the HMBC experiment recorded for native procyanidin B-2. ^{13}C resonances showing correlation to H4C were 72.6, 76.5, 99.5, 106.7, 153.8, 155.6, 157.4 and 158.0 ppm, respectively. But this was not sufficient to discriminate C5D (155.5 ppm, identified from correlation with H4F protons) and C9D (153.8 ppm, identified from correlation with H2F) carbon resonances, because they were too close, and could easily be interchanged.

C4-C8 linkage

(**1a**, R = H)
(**1b**, R = Ac)

C4-C6 linkage

(**2a**, R = H)
(**2b**, R = Ac)
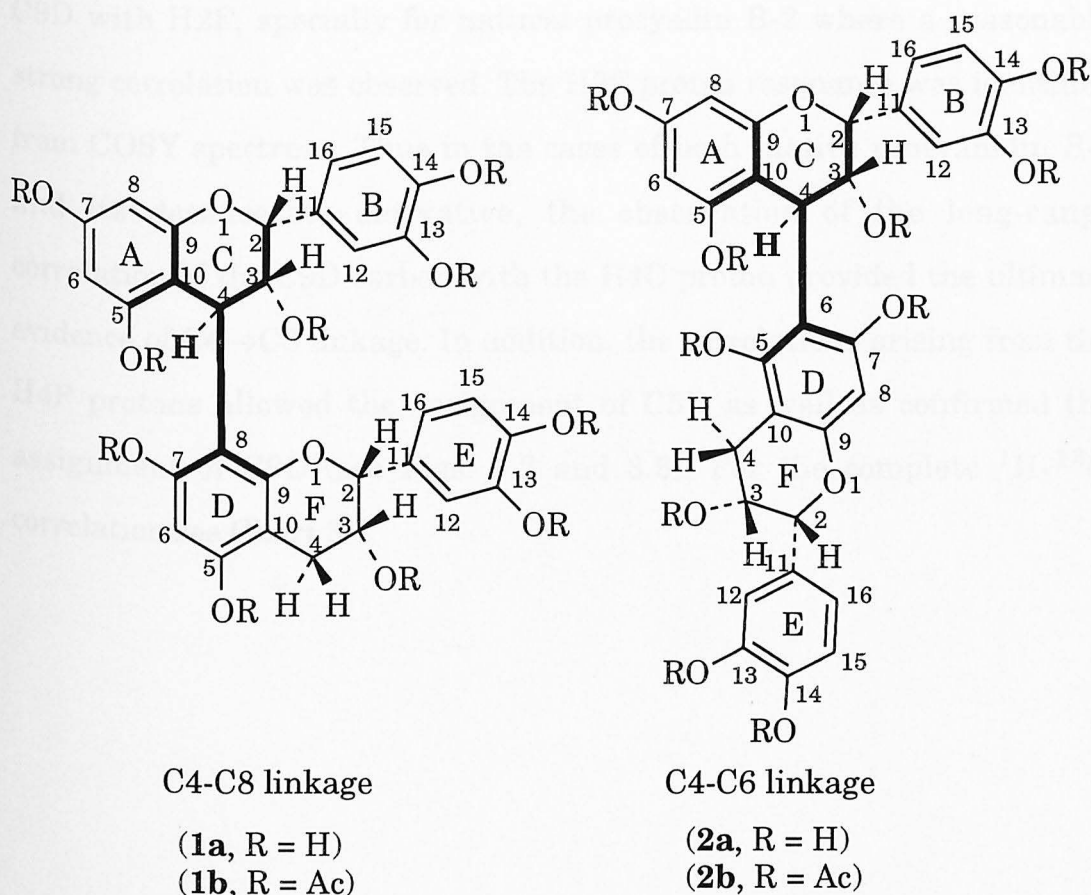
Scheme 3.1 Expected long-range correlations arising from H4C proton in (-)epicatechin dimers.

Acetylation of the natural procyanidin B-2 provided aid to resolve the problem in a way that on acetylation an upfield shift ($\approx$ 8 ppm) of all the aromatic carbon atoms bearing a hydroxyl group was observed, whereas C9A and C9D carbon resonances remained almost unaffected. After acetylation H4C proton showed correlation with the following carbon resonances- 71.0, 73.5, 111.0, 116.2, 147.2, 148.6, 153.9 and 154.8 ppm, respectively. H4C proton would show correlation with at least three carbon resonances in the range of 147 - 148 ppm if the compound was C4→C6 connected, because 3 hydroxylated aromatic carbons then would become available for correlation (see Scheme 3.1). Clearly, that was not the case. This partially helped to discriminate C9D from C5D. Finally, the discrimination of C9D from C5D was confirmed from the correlation of

66

C9D with H2F, specially for natural procyadin B-2 where a reasonably strong correlation was observed. The H2F proton resonance was identified from COSY spectrum. Thus in the cases of both native procyanidin B-2 and its decaacetate derivative, the observation of the long-range correlation of the C9D carbon with the H4C proton provided the ultimate evidence of C4→C8 linkage. In addition, the correlations arising from the H4F protons allowed the assignment of C5D as well as confirmed the assignment of C9D (see Figs. 3.2 and 3.3). For the complete ^{1}H-^{13}C correlation see Chart 3.1.

(a)
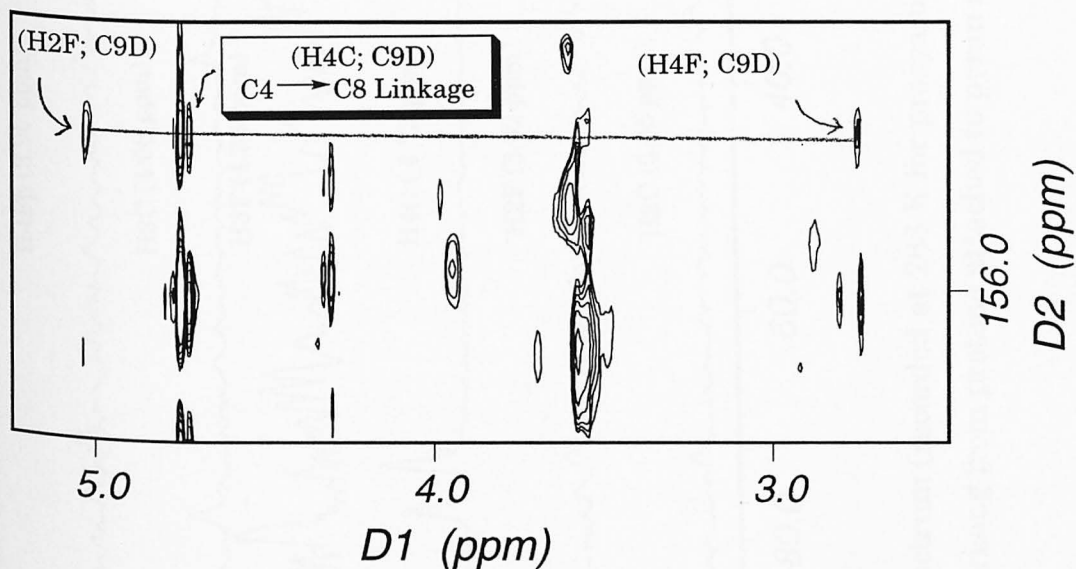
(b)
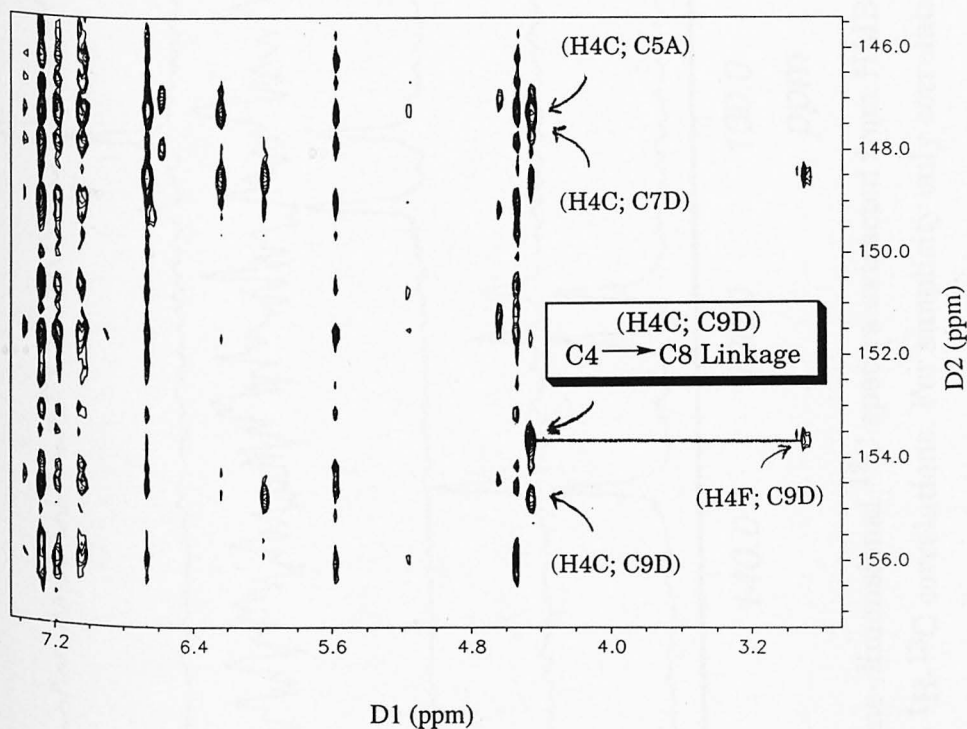
Fig. 3.2 Expansion of the proton-detected long-range heteronuclear chemical shift correlation (HMBC) of procyanidin B-2. (a) For natural procyanidin B-2, recorded at [1]H 500 and [13]C 125 MHz (268 K) and (b) for decaacetate derivative, recorded at [1]H 400 and [13]C 100 MHz (295 K).
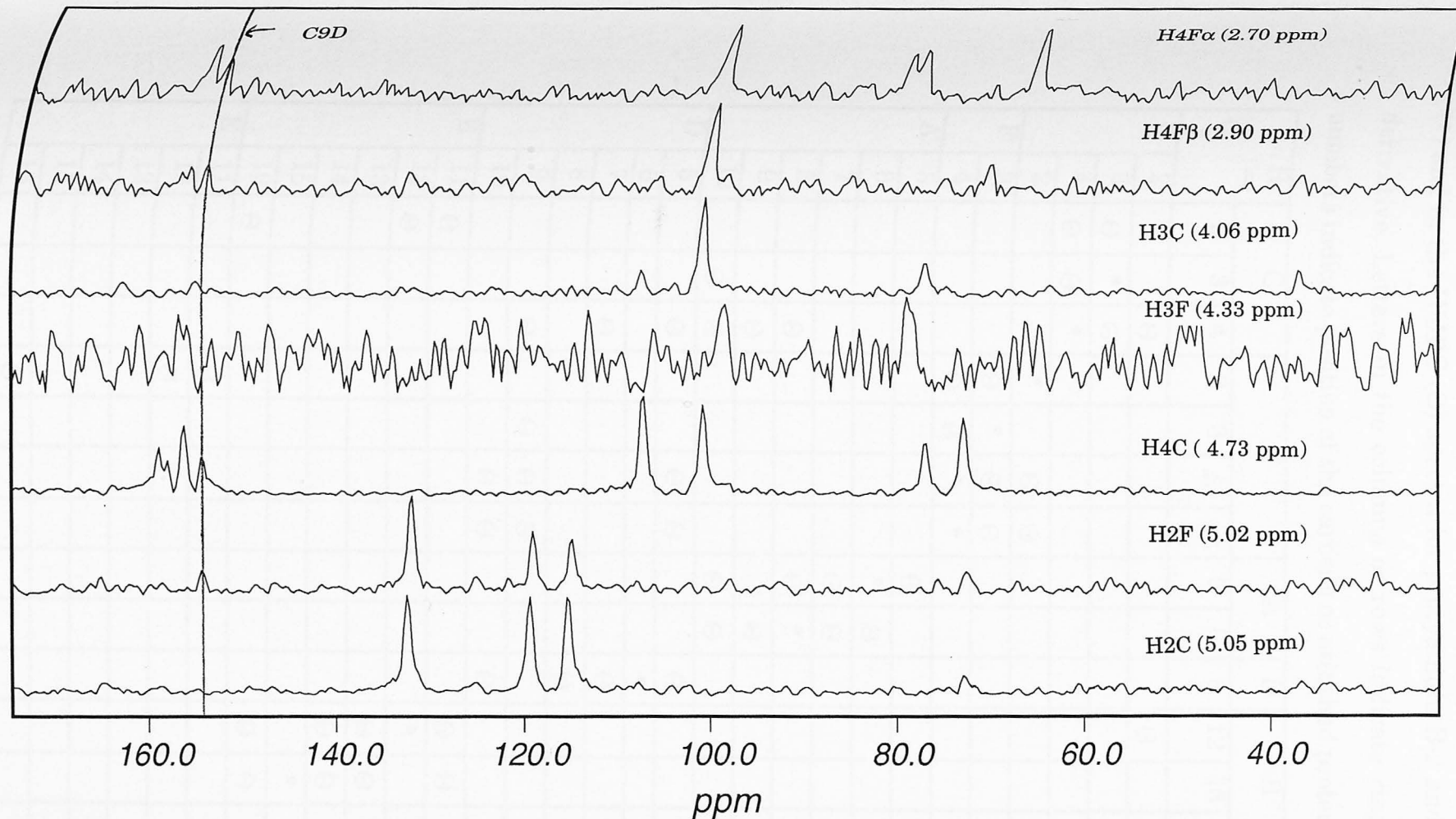
Fig. 3.3 Stack plot of one-dimensional ^{13}C spectra extracted from HMBC spectrum (recorded at 268 K for procyanidin B-2 in $(CD_3)_2CO$ showing the ^1H-^{13}C correlations. For simplicity only correlations arising from protons attached to pyran rings were plotted.

Chart 3.1 Documentation of the ^{1}H-^{13}C cross peaks in the HSQC/HMQC (•) and in the HMBC (Θ) spectra for procyanidin B-2 and its decaacetate derivative. Letters in the columns or rows indicate ring types and the numbers indicate position of the carbons or attached protons.

	H⇒	C			F				A		D	B			E		
C⇓		2	3	4	2	3	4α	4β	6	8	6	12	15	16	12	15	16
C	2	•		Θ								Θ					
	3	Θ	•	Θ													
	4	Θ	Θ	•													
F	2				•		Θ	Θ									
	3				Θ	•	Θ	Θ									
	4				Θ	Θ	•	•									
A	5								Θ								
	6								•	Θ							
	7								Θ	Θ							
	8			Θ					Θ	•							
	9			Θ						Θ							
	10		Θ	Θ					Θ	Θ							
D	5			Θ			Θ	Θ			Θ						
	6										•						
	7			Θ							Θ						
	8										Θ						
	9			Θ		Θ	Θ	Θ									
	10						Θ	Θ			Θ						
B	11	Θ										Θ	Θ	Θ			
	12	Θ										•		Θ			
	13											Θ	Θ				
	14											Θ	Θ	Θ			
	15												•	Θ			
	16	Θ										Θ	Θ	•			
E	11				Θ										Θ	Θ	Θ
	12				Θ										•		Θ
	13														Θ	Θ	
	14														Θ	Θ	Θ
	15															•	Θ
	16				Θ										Θ	Θ	•

3.4 Conformational analysis

The absolute stereochemistry at C2, C3 and C4 for procyanidin B-2 have been established as 2R, 3R and 4R, respectively by various spectroscopic as well as conventional means [1, 4, 5]. As said before, the ^{1}H NMR spectrum of procyanidin B-2 at ambient temperature produces broad signals. The reason for this behavior has been speculated [4, 11-13] to be that the compound exhibits atropisomerism and this phenomenon has been attributed to the restricted rotation about the C4 to C8 interflavan bond. Indeed, a ^{1}H NMR (250 MHz) spectrum recorded at 226 K showed duplication of signals, particularly visible were the signals for the sharp aromatic signals, with a population ratio of roughly 15:1. ^{1}H NMR (400 MHz) of the decaacetate derivative of the same compound clearly produced two sets of signals with a population ratio of 3:1, providing further evidence to the rotational hindrance phenomenon. Obviously, incorporation of the acetate groups to the molecule would increase the existing restricted rotation. Molecular mechanics calculations [8, 9] of the structure (**1a**) gave two preferred local energy minima around the interflavan torsion angle ± 90° that too supports the phenomenon of hindered rotation.

3.5 Molecular modelling

3.5.1 Method of structure optimization

To supplement the NMR results simple molecular mechanics calculations were performed for structures of natural procyanidin B-2 and its decaacetate derivative. Molecules were built starting from the templates implemented in the software programme MacroModel (Version 4.5) installed within a Silicon Graphics local networked work station. The force field chosen was the modified MM2 (1987 parameters) [14, 15]. The structures were rapidly preminimized using PRCG (Polak-Ribiere Conjugate Gradient) [16] method with 100-iterations cycle. Before starting final optimization, these structures were submitted to find a profile of local minima. A standard dihedral driver was employed to examine the minima by varying dihedral angle about the interflavan bond with a step size of 10°. The same was repeated manually to verify the profile. The minima found were very close to $\pm 90^\circ$ (see Table 3.4). A similar observation was reported before [8, 9].

Now the structures were minimized starting from an interflavan dihedral angle at around $\pm 90^\circ$ using the TNCG (Truncated Newton Conjugate Gradient) [17] method. Finally, structures obtained from the TNCG method were reminimized using the FMNR (Full Matrix Newton Raphson) [18] method. Final structures are presented in Fig. 3.4.

$^3J_{HH}$ values were calculated from the optimized structures by way of the Altona formulation [19] of the Karplus equation [20] incorporated into the MacroModel programme. Calculated and observed coupling constants are compared in Table 3.5.

(a)
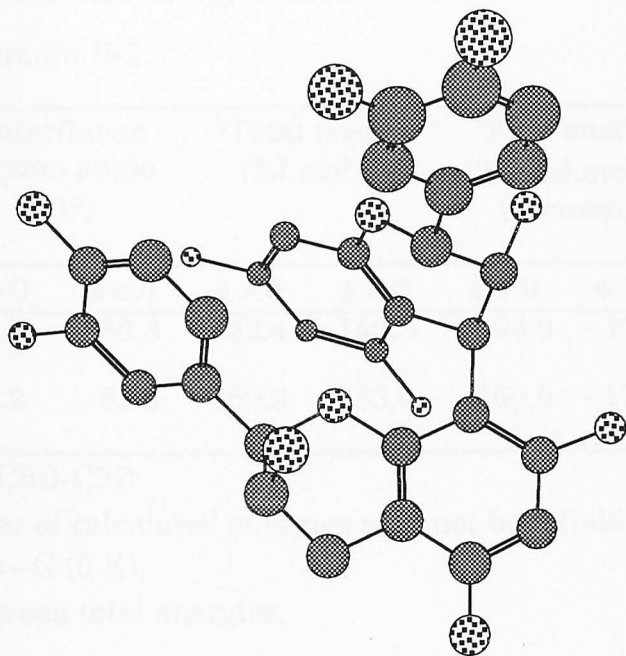
(b)
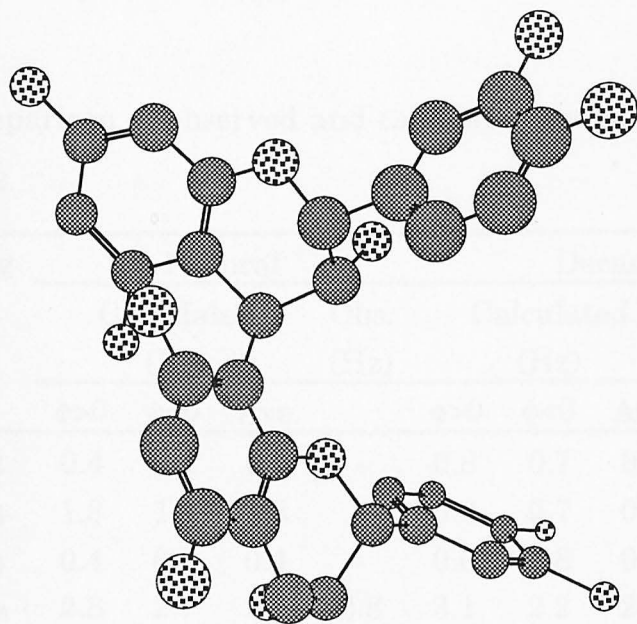
Fig 3.4 Procyanidin B-2. Interflavan dihedral angles (ϕ) (a) 98.2° and (b) – 80.8°. Protons and lone pairs were removed for clarity. Shaded and dotted balls refer to carbon and oxygen atoms, respectively. Relative sizes of the balls indicate distance from the viewer: bigger means closer and smaller means further.

Table 3.4 Location and energy differences between local minima for the molecule procyanidin B-2.

Molecules	[a]Interflavan torsion angle ϕ, (°)		[b]Total energy (kJ.mol^{-1})		[c]Free energy (ΔG, kJ.mol^{-1}) (vacuum)		[d]Energy difference (kJ.mol^{-1})
	$\phi > 0$	$\phi < 0$	$\phi > 0$	$\phi < 0$	$\phi > 0$	$\phi < 0$	
Natural compound	98.2	- 80.8	142.4	140.8	- 106.0	- 108.9	1.6
Acetate derivative	95.2	- 83.8	559.9	583.0	- 160.5	- 173.7	23.1

[a] ϕ = C3C-C4C-C8D-C9D
[b] Absolute values of calculated energies may not be reliable.
[c] ΔG = G(295 K) - G (0 K).
[d] difference between total energies.

Table 3.5 Comparison of observed and calculated coupling constants for procyanidin B-2.

Ring	Coupling	Natural				Decaacetate				
		Calculated (Hz)			Obs. (Hz)	Calculated (Hz)			Obs. (Hz)	
		$\phi>0$	$\phi<0$	Ave.		$\phi>0$	$\phi<0$	Ave.	Maj.	Min.
C	$^3J_{H2\text{-}H3}$	0.4	0.4	0.4	-	0.6	0.7	0.7	-	-
	$^3J_{H3\text{-}H4}$	1.3	1.1	1.2	-	0.9	0.7	0.8	1.8	1.5
F	$^3J_{H2\text{-}H3}$	0.4	0.4	0.4	-	0.6	0.8	0.7	-	-
	$^3J_{H3\text{-}H4a}$	2.8	2.7	2.8	3.8	3.1	2.2	2.7	1.6	2.2
	$^3J_{H3\text{-}H4b}$	3.2	3.3	3.3	4.7	2.9	4.1	3.5	4.8	4.4

3.5.2 Analysis of molecular modelling results

There was a twofold rotation about the interflavan bond C4-C8 for both natural procyanidin B-2 and its decaacetate derivative (Table 3.5) which is in line with previous calculations [8, 9]. The difference in the energy at the

minima for the native compound is sufficiently small (1.6 kJ.mol^{-1}) so that both minima can be populated to a significant extent. This is consistant with the observed ^{1}H NMR behaviour of the compound at ambient temperature where broad ^{1}H signals are normally observed. Broad signals can be interpreted in terms of the dynamics of two conformers with a small energy barrier, i.e. the exchange between the two conformers is too fast for NMR time limit to be recognised as a separate entity and hence an average of the signals from different rotational conformers are observed. However, at very low temperature (ca. 226 K, in acetone) two different conformers apparently appear in the ^{1}H NMR spectrum with a population ratio of 15:1.

When acetates were incorporated into the natural procyanidin B-2 molecule, the energy difference between the minima became large compared to that of the native compound (ca. 23 kJ.mol^{-1}). The presence of two separate conformers was predicted. Again the calculated results were supported by the ^{1}H NMR behaviour of the derivative at ambient temperature where clearly two sets of signals were observed with a population ratio of 3:1.

Comparisons of the calculated and observed coupling constants are reasonably close if the effect of solvent is taken into account. So the conformational data for pyran rings extracted from molecular modelling calculations may be taken as fair estimates of the real conformations (Table 3.6). Both the pyran rings C and F obtained half-chair or sofa (2) conformations placing C2 above and C3 below the plane of the benzopyran fused ring systems. Catechol rings B and E were placed at quasi-equatorial positions. (Fig. 3.5).
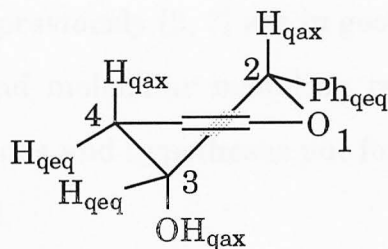
Fig 3.5 Conformation of the pyran rings.

Table 3.6 Conformation of pyran rings of procyanidin B-2.

ϕ = C3C-C4C-C8C-C9D (interflavan torsion angle).

Torsion angle	Natural compound (°)				Decaacetate derivative (°)			
	Ring C		Ring F		Ring C		Ring F	
	$\phi>0$	$\phi<0$	$\phi>0$	$\phi<0$	$\phi>0$	$\phi<0$	$\phi>0$	$\phi<0$
C10-C9-O1-C2	-15.7	-16.0	-13.8	-14.7	-18.2	-17.1	-11.0	-19.6
C9-O1-C2-C3	45.2	45.9	44.9	46.5	48.1	47.4	42.9	49.7
O1-C2-C3-C4	-61.6	-60.3	-61.1	-62.1	-61.1	-61.3	-61.9	-60.4
C2-C3-C4-C10	47.0	43.6	47.6	46.3	44.1	44.5	50.2	42.0
C3-C4-C10-C9	-17.9	-14.8	-19.2	-16.8	-14.8	-15.0	-21.1	-14.5
C4-C10-C9-O1	1.2	-0.2	0.4	0.6	0.4	-0.2	0.3	1.1
H2-C2-C3-H3	-66.0	-66.0	-66.0	-66.3	-63.8	-64.3	-63.7	-61.2
H3-C3-C4-H4	-77.1	-80.1			-82.4	82.2		
H3-C3-C4-H4$_\alpha$			-68.0	-69.0			67.4	68.9
H3-C3-C4-H4$_\beta$			49.6	48.9			50.2	43.7

3.6 Conclusion

The combined and systematic use of two-dimensional homo- and heteronuclear shift correlation spectroscopy allowed complete ^{1}H and ^{13}C assignments of the natural procyanidin B-2 and its decaacetate derivative. From the HMBC spectra the interflavan connectivity has been unequivocally established as C4→C8, for the first time.

Spectral data reported previously [3, 7] are in good agreement with the ^{1}H and ^{13}C NMR data and molecular modeling results presented in this study. So, the speculations and hypotheses put forward by earlier workers [4, 11-13] are confirmed.

References

1. Weinges, K., Kaltenhauser, W., Marx, H. -D., Nader, D., Nader, F. Perner, J. and Seiler, D., *Liebigs Ann. Chem.*, 1968, **711**, 184.

2. Haslam, E., *Plant Polyphenols - Vegetable Tannins Revisited.* 1989, Cambridge, Cambridge University Press.

3. Thompson, R. S., Jacques, D., Haslam, E. and Tanner, R. J. N., *J. Chem. Soc. Perkin Trans. 1*, 1972, 1387.

4. Fletcher, A. C., Porter, L. J., Haslam, E. and Gupta, R. K., *J. Chem. Soc. Perkin Trans. 1*, 1977, 1628.

5. Haslam, E. *Phytochemistry*, 1977, **16**, 1625.

6. Weinges, K., Goritz, K. and Nader, F., *Liebigs Ann. Chem.*, 1968, **715**, 164.

7. Porter, L. J., Newman, R. H., Foo, L. Y. and Wong, H., *J. Chem. Soc. Perkin Trans. 1*, 1982, 1217.

8. Viswanadhan, V. N. and Mattice, W. L., *J. Comp. Chem.*, 1986, **7**, 711.

9. Viswanadhan, V. N. and Mattice, W. L., *J. Chem. Soc. Perkin Trans. 2*, 1987, 739.

10. Balas, L. and Vercauteren, J., *Mag. Res. Chem.*, 1994, **32**, 386.

11. Weinges, K., Marx, H. D. and Goritz, K., *Chem. Ber.*, 1970, **103**, 2336.

12. Jurd, L. and Lundin, R., *Tetrahedron*, 1968, **24**, 2653.

13. du Preez, I. C., Rowan, A. C., Roux, D. G. and Feeny, J., *J. Chem. Soc. Chem. Commun.*, 1971, 315.

14. Allinger, N. L., *J. Am. Chem. Soc.*, 1977, **99**, 8127.

15. Mohamadi, F., Richards, N. G. J., Guida, W. C., Liskamp, R., Lipton, M., Caufield, C., Chang, G., Hendrickson, T. and Still, W. C., *J. Comp. Chem.*, 1990, **11**, 440.

16. Polak, E. and Ribiere, G., *Rev. Fr. Inf. Rech. Oper.*, 1969, **16**, 35.

17. Ponder, J. W. and Richards, F. M., *J. Comp. Chem.*, 1989, **8**, 1016.

18. Burkert, U. and Allinger, N. L., *Molecular Mechanics.* 1982, Washington D.C., American Chemical Society, pp. 67-72.

19. Haasnoot, C. A. G., de Leeuw, F. A. A. M. and Altona, C., *Tetrahedron*, 1980, **36**, 2783.

20. Karplus, M., *J. Chem. Phys.*, 1959, **30**, 11.

CHAPTER FOUR

TANNIN-PROTEIN PRECIPITATION

4.1 Introduction

Tannins are a major constituent of some plants and are characterized by their distinctive ability to associate with various biomolecules, such as proteins, alkaloids and carbohydrates, as discussed previously. One of the oldest examples of tannin-protein association is the making of leather – treating animal hide proteins with the tannin rich infusions of plant materials. The astringent taste of foods and beverages is believed to be due to the binding and precipitation of proteins and polysaccharides present in the oral cavity by tannins.

4.2 A brief review of the tannin-protein complexation

Tannin-protein complexation is either reversible or irreversible. The complexation process [1] is influenced by (a) characteristics of the proteins such as size, amino acid composition, pI, and extent of post translational modification; (b) characteristics of the tannin such as size, structure, heterogeneity of the preparation; and (c) conditions of the reaction such as pH, temperature, solvent composition, time.

One of the earliest historical uses of tannin-protein complexation is leather making. Earlier investigations of tannin-protein interactions were hampered by the nonavailability of pure tannins and proteins of known structure. Emergence of newer and sophisticated methods of purification and spectroscopic methods of analysis has greatly improved techniques to

examine this problem and firm information on the nature of tannin-protein complexation at the molecular level is now available.

4.2.1 Nature of tannin-protein complexation: reversibility

It is believed that tannin-protein complexes are generally formed by a combination of hydrophobic effects and hydrogen bonds. Hydrogen bonds (Fig. 4.1) are preferentially established between the carbonyl oxygen of the peptide bond and the phenolic hydroxyl groups, with the peptide oxygen acting as acceptor. Hydrophobic interactions between nonpolar domains of proteins and nonpolar regions of tannin molecules bring the protein and tannin molecules in close proximity to facilitate hydrogen bonding, particularly at acidic pH [2]. Polydentate tannins bind at more than one point of the protein surface through different phenolic groups [3]. Low protein concentration favours the formation of less hydrophilic monolayers (Fig. 4.2a) and high protein concentration creates a relatively hydrophobic surface and cross-linking of different protein molecules (Fig. 4.2b); in both cases this may be followed by precipitation, which is pH dependent. The optimum pH of precipitation is usually around the isoelectric point of the protein [4, 5]. The reversibility of the tannin-protein complex formation is supported by observations of dissociation by acetone [6], caffeine [7, 8], detergents [9], urea [10], PVP [11], etc.

Fig. 4.1

(a)

low protein
concentration

(b)

high protein
concentration
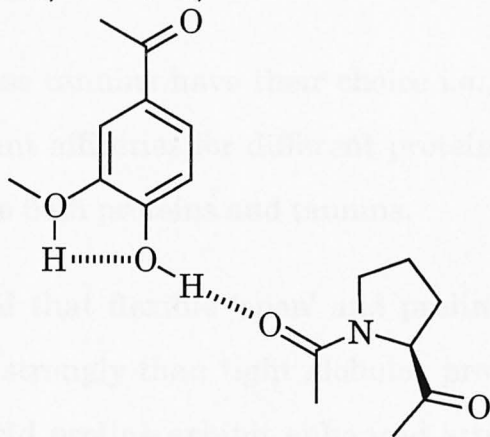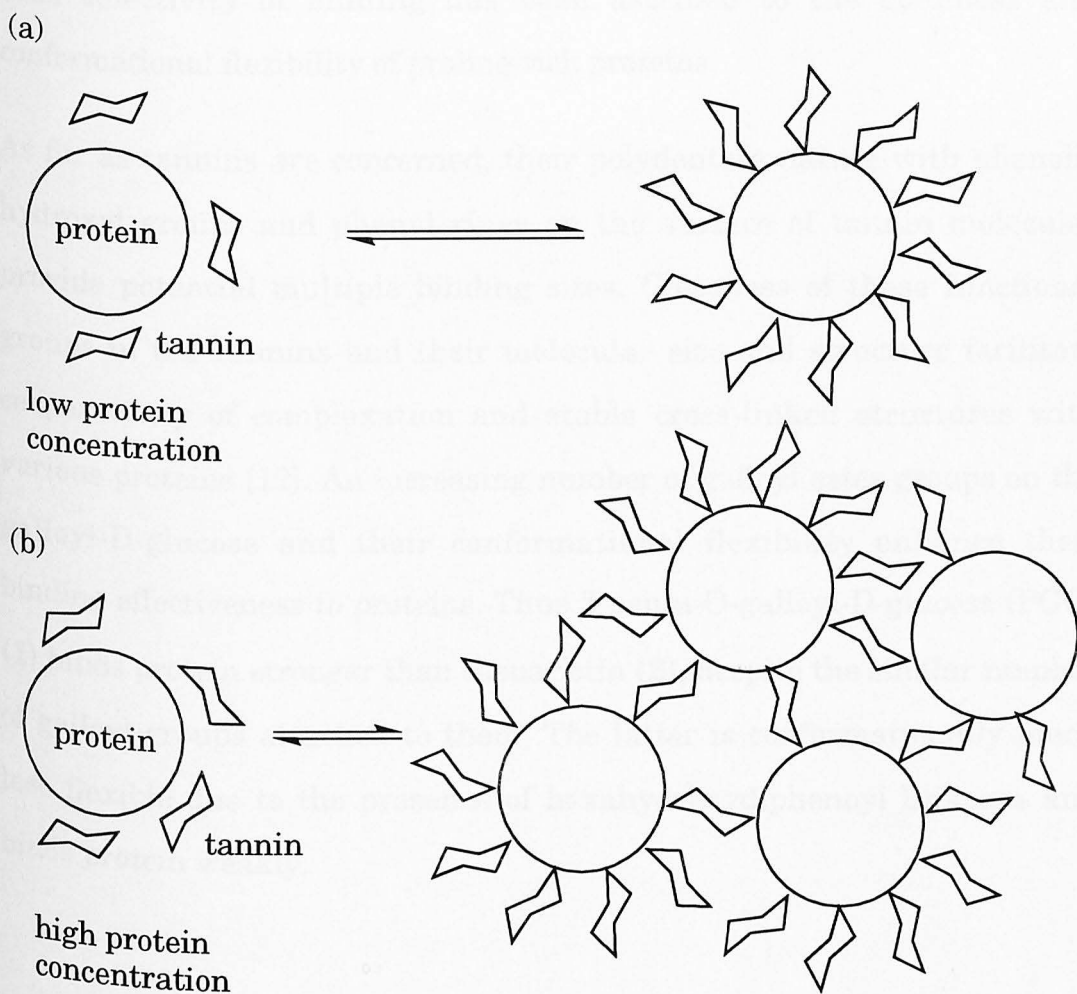
Fig. 4.2 Possible modes of tannin-protein precipitation. (Figures taken and adapted from reference [12]).

4.2.2 Structure-activity relationship (or specificity) of tannin-protein complexation

In the binding process tannins have their choice i.e., a particular type of tannin shows different affinities for different proteins. Structure-activity relationships apply to both proteins and tannins.

It has been observed that flexible 'open' and proline rich proteins bind tannins much more strongly than tight globular proteins. Thus proteins rich in the amino acid proline exhibit enhanced attractions for tannins.

This selectivity of binding has been ascribed to the openness and conformational flexibility of proline-rich proteins.

As far as tannins are concerned, their polydentate nature with phenolic hydroxyl groups and phenyl rings on the surface of tannin molecules provide potential multiple binding sites. Closeness of these functional groups in the tannins and their molecular size and structure facilitate cooperativity of complexation and stable cross-linked structures with various proteins [12]. An increasing number of galloyl ester groups on the galloyl-D-glucose and their conformational flexibility enhance their binding effectiveness to proteins. Thus β-penta-O-galloyl-D-glucose (PGG) (1) binds protein stronger than casuarictin (2), despite the similar number of galloyl groups attached to them. The latter is conformationally much less flexible due to the presence of hexahydroxydiphenoyl linkages and binds protein weakly.

(1) PGG

(2) Casuarictin
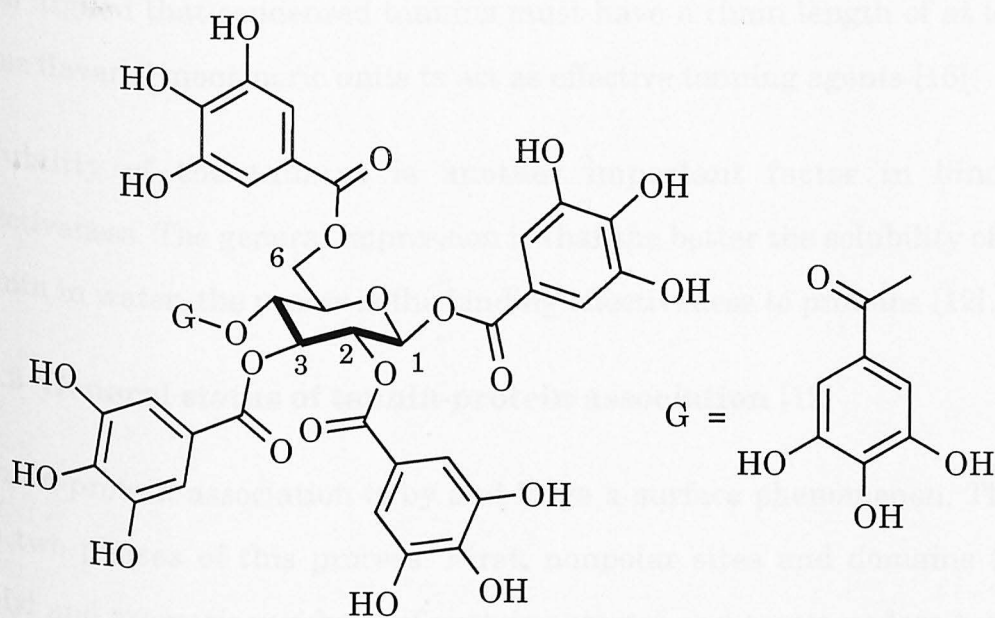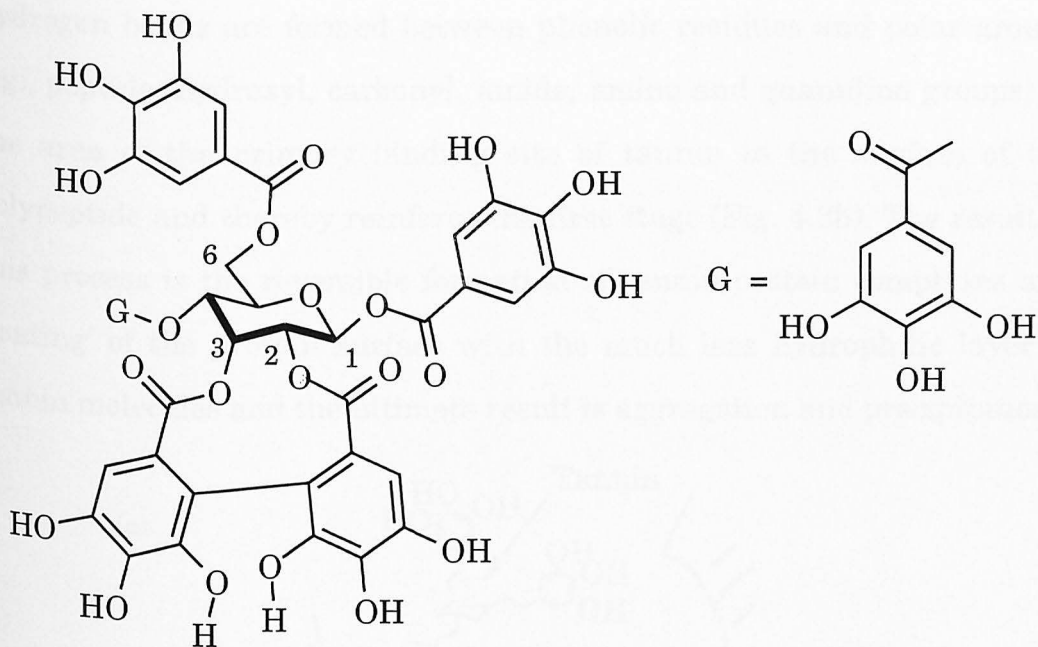
The relative ranking of hydrolysable and condensed tannins in terms of their binding to proteins is not very clear although some investigators have found that hydrolysable and condensed tannins precipitate proteins (hemoglobin or BSA) with similar effectiveness [13, 14]. However it has been argued that condensed tannins must have a chain length of at least three flavanol monomeric units to act as effective tanning agents [15].

Solubility of the tannins is another important factor in binding effectiveness. The general impression is that the better the solubility of the tannin in water, the poorer is the binding effectiveness to proteins [12].

4.2.2 General status of tannin-protein association [12]

Tannin-protein association is by and large a surface phenomenon. There are two phases of this process. First, nonpolar sites and domains (eg., prolyl and aromatic residues) of proteins attract and accommodate tannin molecules via hydrophobic interaction. Facilitated by conformational flexibility of the protein polypeptide chains, several apolar side chains come into close contact to form a 'hydrophobic pocket' (Fig. 4.3a). Second,

83

hydrogen bonds are formed between phenolic residues and polar groups (eg., peptide, hydroxyl, carbonyl, amide, amino and guanidino groups) in the area of the primary binding site of tannin to the surface of the polypeptide and thereby reinforce the first stage (Fig. 4.3b). The result of this process is the reversible formation of tannin-protein complexes and 'coating' of the protein surface with the much less hydrophilic layer of tannin molecules and the ultimate result is aggregation and precipitation.
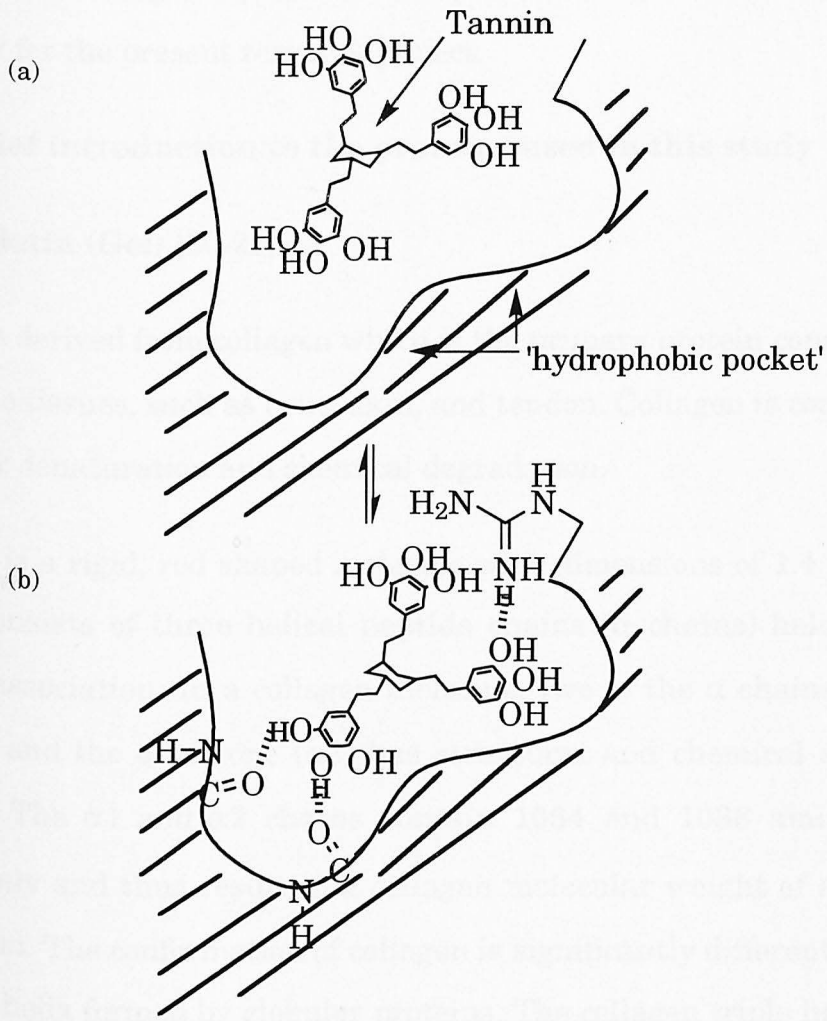
Fig. 4.3 Tannin-protein complexation. (a) Docking to the hydrophobic cavity; (b) Hydrogen bonding to the surface of the protein. Figure taken and adapted from reference [12].

4.3 Aim of the present study

Tannin-protein precipitation has already been explored [16] in some detail. The present attempts should be viewed as demonstrations and extensions of the previous work [16-19] at Sheffield. Important and relevant comments in this chapter were mainly extracted from reference [16]. The aim was to have an overview of tannin-protein precipitation (and complexation) using the present attempts as examples. This was judged necessary for the present research project.

4.4 A brief introduction to the proteins used in this study

4.4.1 Gelatin (Gel) [20-22]

Gelatin is derived from collagen which is the primary protein component of connective tissues, such as bone, skin, and tendon. Collagen is converted to gelatin by denaturation and chemical degradation.

Collagen is a rigid, rod shaped molecule with dimensions of 1.4 nm x 300 nm. It consists of three helical peptide chains (α chains) held in close parallel association. In a collagen molecule, two of the α chains ($\alpha 1$) are identical and the other one ($\alpha 2$) has structural and chemical similarity with $\alpha 1$. The $\alpha 1$ and $\alpha 2$ chains contain 1054 and 1038 amino acids, respectively and thus result in a collagen molecular weight of about 290 kilo Dalton. The conformation of collagen is significantly different from the typical α helix formed by globular proteins. The collagen triple helix is left handed and needs a special amino acid sequence. Except at each end of the collagen molecule a sequence of triplets, $-(-\text{glycine-X-Y-})_n-$ is found to repeat unfailingly, where X and Y are frequently proline and hydroxyproline, respectively. The occurrence of the glycine-I-I sequence is about four times less common than glycine-I-Z and glycine-Z-I sequences, where Z may be any amino acid and I is either proline or hydroxyproline.

Thus a significant proportion of prolyl residues are separated from one another.

When a collagen molecule is converted to gelatin, three different gelatin species can be formed, such as monomer, dimer and trimer, respectively, of either $\alpha 1$ or $\alpha 2$ chains or a mixure of the two. During the thermal denaturation of collagen, only noncovalent bonds such as coulombic, hydrogen bonds and van der Waals forces are ruptured.

Commercial gelatin molecules are heterogeneous with respect to amino acid composition, except for glycine. Invariably, gelatin has a glycine content of 33 mol %. The major amino acid composition of typical gelatin and collagen is presented in Table 4.1.

4.4.2 Bovine Serum Albumin (BSA) [23-25]

BSA is a high molecular weight globular protein that occurs in blood plasma at a concentration of 30-40 g/litre. It also occurs in milk but only at levels of 0.1-0.4 g/litre. BSA is a principal factor contributing to the osmotic pressure and plasma volume of blood. It is also regarded as a transport or temporary storage protein. It has up to six distinct binding regions and can bind various molecules. BSA binds and transports long chain fatty acids and bilirubin, resulting in larger water solubility and decreased toxicity of these compounds, respectively.

Detailed 3D structural features of BSA are not known due to an inability to crystallise it. However, it contains about 582 amino acid residues (including 17 disulphide bonds) resulting in a relative molecular mass of approximately 65 kilo Dalton. It is thought to have an overall ellipsoidal shape composed of three domains. The domain feature of the BSA structure, each being composed of two large and one small double loop,

Table 4.1 Amino acid composition of gelatin and collagen, Residues per 1000 Residues (Reference [21]).

Name	Three letter code	Lime-pretreated gelatin	Collagen
alanine	Ala	117	119
arginine	Arg	48	51
aspartic acid	Asp	46	29
glutamic acid	Glu	72	48
glycine	Gly	335	332
hydroxyproline		93	104
phenylalanine	Phe	14	13
proline	Pro	124	115

provides a degree of flexibility to the molecule. This flexibility plays an important role when it binds to substrates.

4.4.3 Polyvinylpyrrolidone (PVP) [26]

PVP consists of vinylpyrrolidone (3) units that have a structural similarity with the amino acid proline. PVP of varying molecular weights are commercially available. For this study a PVP of molecular weight 10 kilo Dalton was chosen.

(3)
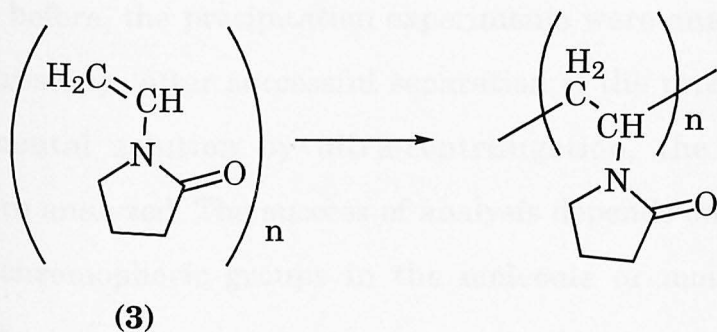
The individual unit in the PVP chain, consisting of the polar imide group, four nonpolar methylene groups, and a methine group, is expected to be amphiphilic in character. As a consequence of the hydrophobic-hydrophilic balance, the polymer is soluble in a variety of solvents including water. Water molecules are attached to the polymer due to hydrogen-bonded hydration on the amide group and hydrophobic hydration around the methylene groups.

PVP forms a variety of compounds as a consequence of its unique structure, the exposed cyclic imido group and the balance of hydrophobic-hydrophilic segments. The hydrophobic character is attributed to the methylene groups in the ring and the linear aliphatic backbone, whereas the polar lactam moiety of the pyrrolidone ring provides the hydrophilicity. The pyrrolidone structure is highly susceptible to hydrogen bonding and easily forms insoluble complexes with phenolic substances in aqueous solution.

4.5 Background of the analytical technique

β-1,2,3,4,6-Penta-O-galloyl-D-glucopyranose (PGG) (1) was chosen as a model tannin for the tannin-protein precipitation experiments. Throughout this chapter it will be referred to as PGG. The experimental protocol, techniques to analyze precipitation experiments and subsequent treatment of experimental data are detailed in section 2.4.

As was said before, the precipitation experiments were analyzed by UV-visible spectroscopy. After successful separation of the precipitates from the experimental solution by ultra-centrifugation, the supernatant solutions were analyzed. The success of analysis depends on the presence of suitable chromophoric groups in the molecule or molecules under investigation.

PGG is a polyfunctional tannin molecule that has five identical functional groups, i.e. the galloyl functions. These galloyl ester groups are the principal UV absorbants. In water PGG was found to absorb characteristically at wavelengths around 215 nm (λ_1) and 280 nm (λ_2). The *fundamental* chromophore benzene absorbs at the primary band $\approx$ 200 nm and at the secondary band $\approx$ 260 nm. The absorption at the primary band is more intense ($\varepsilon_{max}^{\lambda_{200}} \approx 7.0$ µmol^{-1}.cm^2) than that at the secondary band ($\varepsilon_{max}^{\lambda_{260}} \approx 0.2$ µmol^{-1}.cm^2). The presence of the 'perturbing' carbonyl ester and auxochromic OH groups exert bathochromic effects on the fundamental chromophore and shifts the absorption bands towards 215 nm and 280 nm (red shift). The galloyl ester chromophoric unit, together with its relevant features is presented in Fig. 4.4.
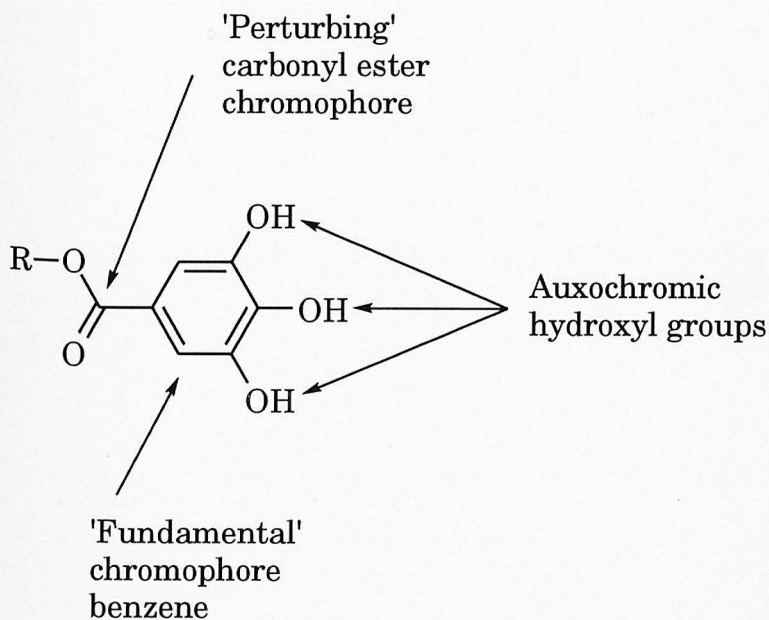
Fig. 4.4 Elements of galloyl ester chromophore.

4.6 Precipitation of PGG with gelatin, BSA and PVP

Gelatin and BSA were chosen as representative proteins of fibrous and globular types, respectively. PVP can model gelatin or other unstructured fibrous proteins. Precipitation experiments of PGG-Gel, PGG-BSA, PGG-PVP and TGG-Gel were performed in distilled water at a temperature range 293-295 K. A standard precipitation technique was followed in each case, as detailed in Section 2.4. pH 5.4 was maintained for PGG-Gel, PGG-BSA and TGG-Gel systems using 10 mM acetate buffer. PGG-BSA experiments were repeated at pH 4.0. PGG-PVP experiments were conducted in 50mM NaCl (aq) solution.

After centrifugation, the supernatant solutions were analyzed by using a UV-vis spectrophotometer. Fig 4.5 exemplifies the UV-vis spectra of supernatant solutions.

Fig. 4.5 UV absorption spectra of the supernatants from PGG-PVP : 50mM NaCl(aq) system; (a) the precipitation region, numbered spectra (1-5) correspond to spectra of the supernatants resulting from the addition of 0.0, 0.3, 0.7, 1.0 and 1.3 µM of PVP, respectively to about 10 µM of PGG. and (b) the resolubilization region, numbered spectra (6-10) correspond to spectra of the supernatants resulting from the addition of 1.7, 2.3, 3.3, 4.2 and 5.0 µM of PVP, respectively to about 10 µM of PGG.

4.7 Results

4.7.1 Calculation of precipitation indices

Several parameters such as % relative absorbance, concentration of tannin or protein in the precipitate, mass of tannin or protein in the precipitate, total mass of protein of the precipitate or % mass of tannin in the precipitate can be used to characterize precipitation experiments. These may be generally termed precipitation indices.

Two different methods were employed to calculate precipitation indices. The first was 'standard n measurements for n variables' using the equations laid out in section 2.4.4. This method was based on absorbance maxima at selected wavelengths (such as 215 nm and 280 nm). The second method involved a matrix inversion operation carried out by computer (the programme was written by S. Young [27] and supplied by Professor Cappas of South Alabama University). This latter method uses the entire UV spectrum rather than chosen absorption maxima to calculate the concentration of the components in the supernatants and can cope with extremely overlapping spectra.

Of the precipitation indices mentioned above, relative absorbance was found to show exceptionally good correlation to the mass or concentration of tannin in the precipitate (see Fig. 4.6). Examination of Fig. 4.6 shows that the % relative absorbance is almost directly proportional to the mass of tannin in the precipitate. Fig. 4.7 compares the % relative absorbance as a function of initial concentration of proteins for PGG-Gel and PGG BSA systems, and Fig. 4.8 shows the same for the PGG-PVP system.
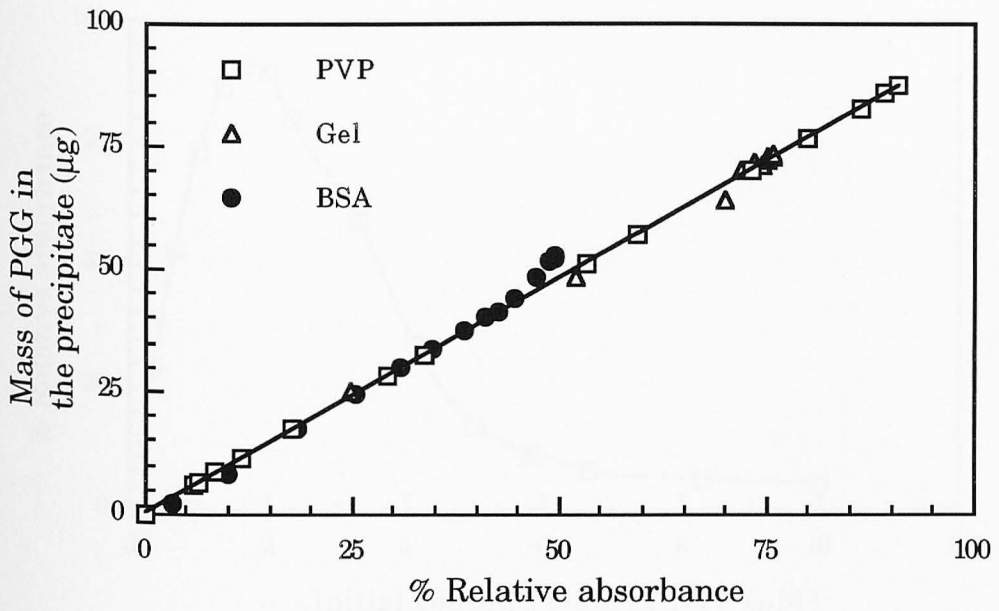
Fig. 4.6 The correlation of % relative absorbance with the mass of tannin in the precipitate.
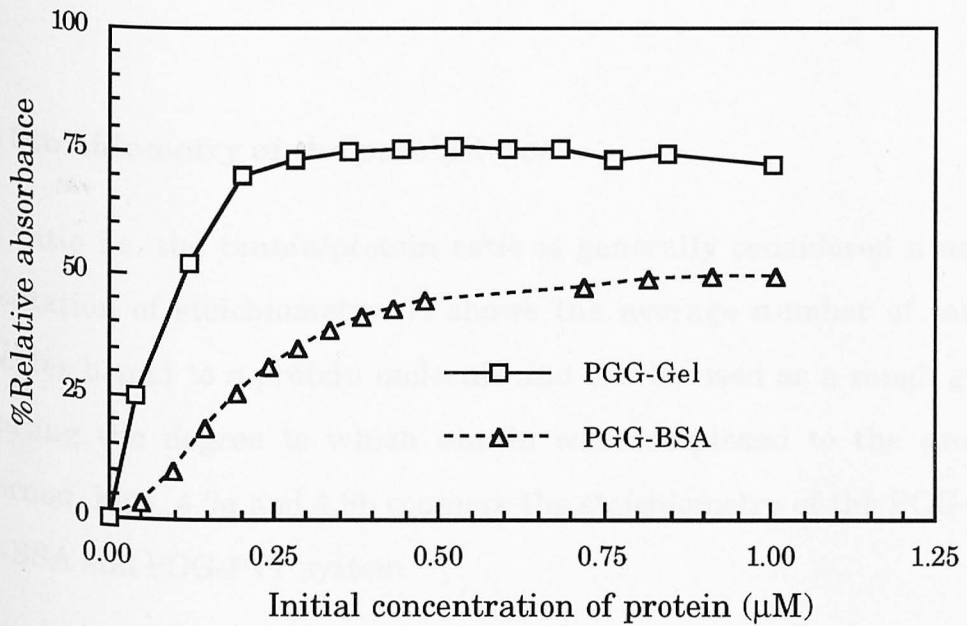
Fig. 4.7 A comparison of the precipitation of two PGG-protein systems; pH 5.4; temperature 293-295 K. Plot of % relative absorbance as a function of initial concentration of proteins.
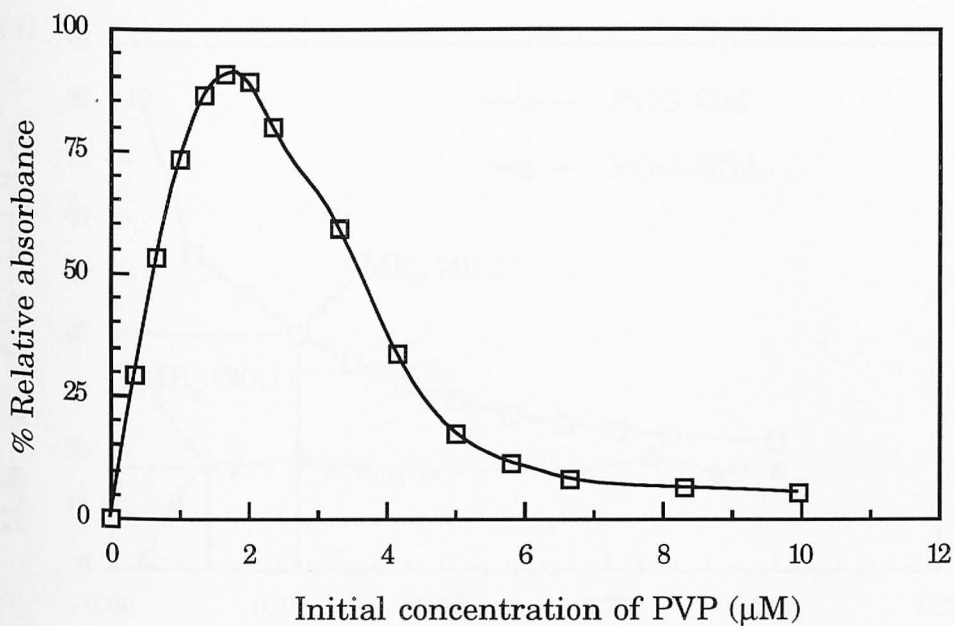
Fig. 4.8 Plot of % relative absorbance as a function of initial concentration of PVP in 10 mM NaCl(aq), 293-295 K.

4.7.2 Stoichiometry of the precipitates

Mole ratio i.e. the tannin/protein ratio is generally considered a useful presentation of stoichiometry. It shows the average number of tannin molecules bound to a protein molecule and can be used as a rough guide indicating the degree to which tannin was complexed to the protein concerned. Figs. 4.9a and 4.9b compare the stoichiometry of the PGG-Gel, PGG-BSA and PGG-PVP system.
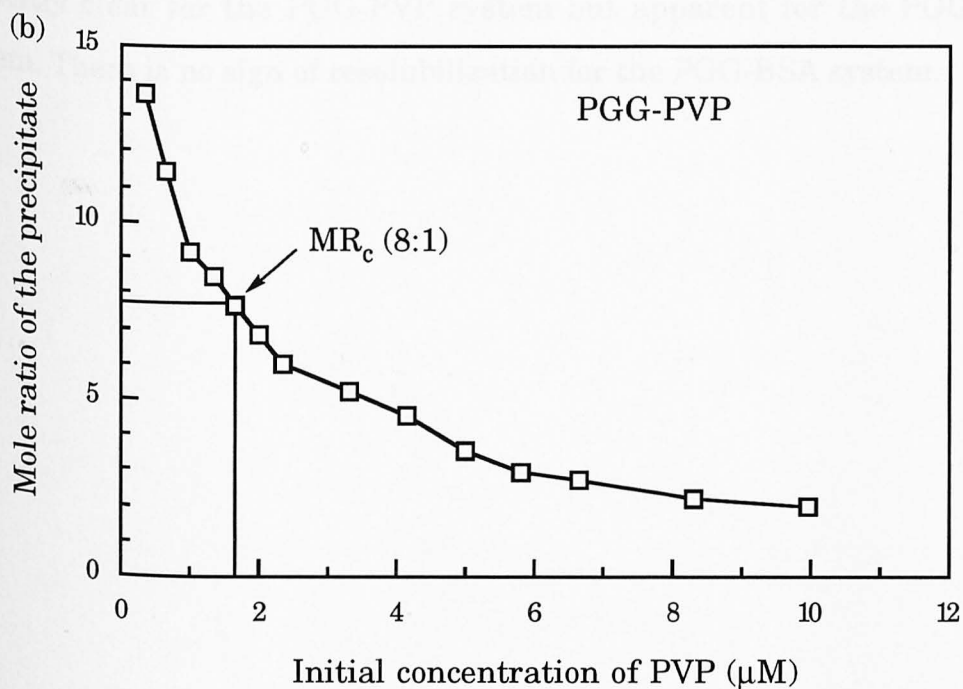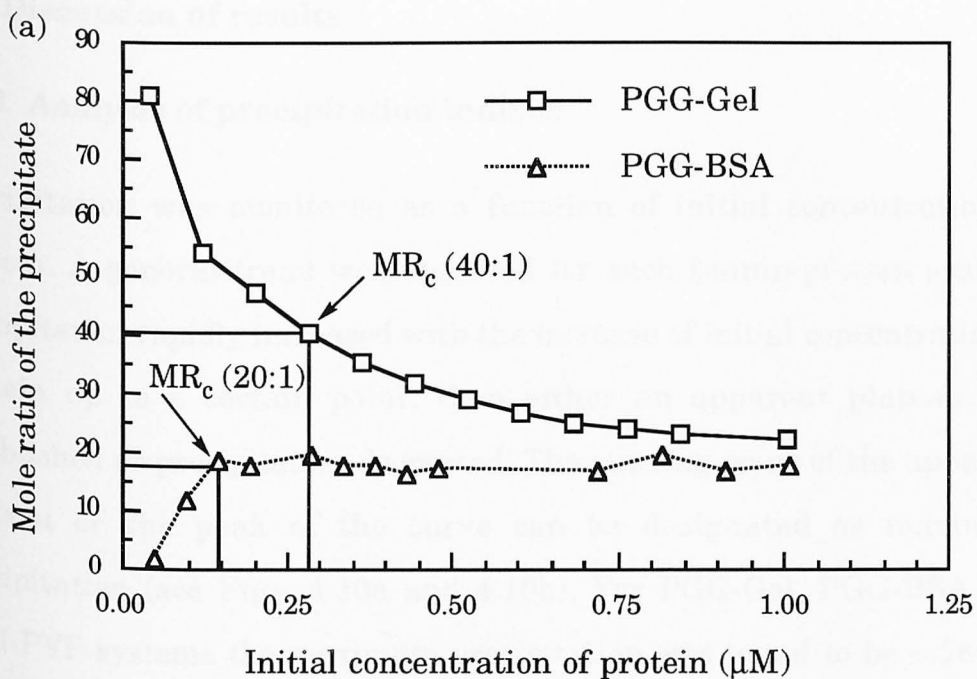
Fig. 4.9 Comparison of the mole ratio (MR, PGG/protein) in precipitate as a function of initial concentration of protein. (a) PGG-Gel and PGG-BSA systems ; pH 5.4; 293-295 K. (b) PGG-PVP system; 50 mM NaCl(aq); 293-295 K. MR_c is the critical mole ratio (see section 4.8.2).

4.8 Discussion of results

4.8.1 Analysis of precipitation indices

Precipitation was monitored as a function of initial concentration of protein. A general trend was observed for each tannin-protein system. Precipitation rapidly increased with the increase of initial concentration of protein up to a certain point, then either an apparent plateau was established or precipitation decreased. The starting point of the apparent plateau or the peak of the curve can be designated as maximum precipitation (see Figs. 4.10a and 4.10b). For PGG-Gel, PGG-BSA and PGG-PVP systems the maximum precipitation was found to be $\approx$ 76%, $\approx$ 55% and $\approx$ 91%, respectively. The decrease in precipitation with increase of protein concentration may be termed as 'resolubilization'. This trend is explicitly clear for the PGG-PVP system but apparent for the PGG-Gel system. There is no sign of resolubilization for the PGG-BSA system.
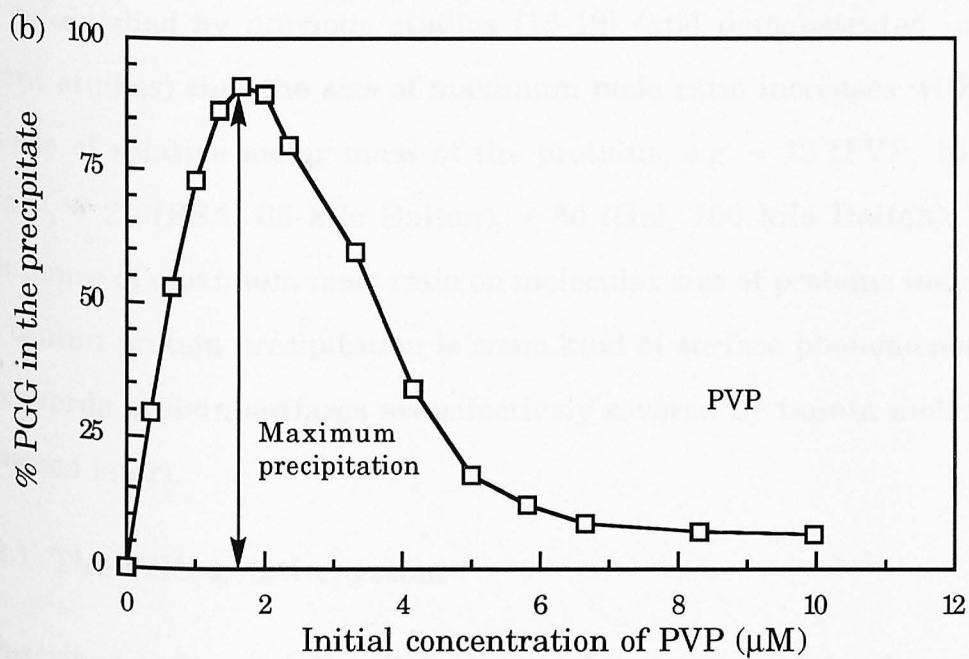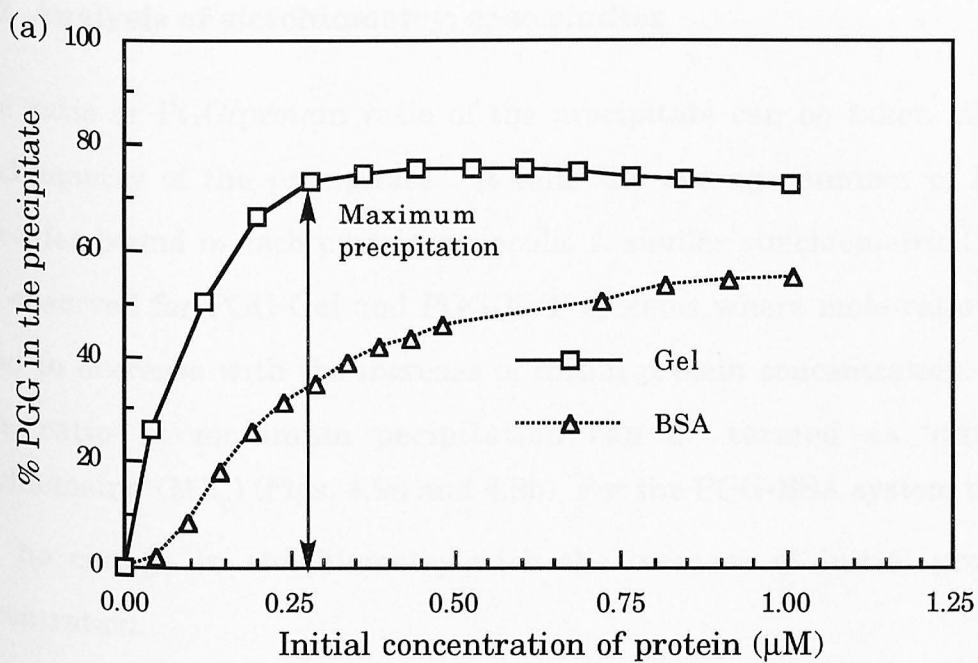
Fig. 4.10 Plot of % PGG in the precipitate as a function of initial protein concentration; (a) PGG-Gel and PGG-BSA systems ; pH 5.4; 293-295 K. (b) PGG-PVP system; 50 mM NaCl(aq); 293-295 K.

4.8.2 Analysis of stoichiometry: case studies

Mole ratio or PGG/protein ratio of the precipitate can be taken as the stoichiometry of the precipitate. It tells the average number of PGG molecules bound to each protein molecule. A similar stoichiometric trend was observed for PGG-Gel and PGG-PVP systems where mole ratio was found to decrease with the increase of initial protein concentration. The mole ratio at maximum pecipitation can be termed as 'critical stoichiometry' (MR$_c$) (Figs. 4.9a and 4.9b). For the PGG-BSA system there was no change in stoichiometry with the increase of initial protein concentration.

In general at lower protein concentrations, the stoichiometry of the precipitates shows a remarkable difference. A broad correlation, however, was established by previous studies [16-19] (and demonstrated in the present studies) that the size of maximum mole ratio increases with the increase of relative molar mass of the proteins, e.g. $\approx$ 13 (PVP, 10 kilo Dalton), $\approx$ 20 (BSA, 65 kilo Dalton), $\approx$ 80 (Gel, 100 kilo Dalton). This dependence of maximum mole ratio on molecular size of proteins indicates that tannin-protein precipitation is some kind of surface phenomenon. In other words protein surfaces are effectively covered by tannin molecules (discussed later).

4.8.2.1 The PGG-gelatin system

As described before, gelatin (Gel) is a soluble protein obtained from the hydrolysis or thermal degradation of the insoluble fibrous protein collagen. Its chemical nature is expected to be heterogeneous in both amino acid sequence, relative molar mass and possible higher levels of protein structure (parent collagen).

The sample used in this study was assumed to be α chains present as single strands with an average relative molar mass of 100 kilo Dalton. Gelatin consists of 124 (≈ 120) proline, 93 (≈90) hydroxyproline and 335 glycine residues (see Table 4.1) and each proline residue is preceded by a glycine residue. There are at least two amino acids between each proline residue.

Gelatin is a soluble protein derived from hydrolysis of the insoluble fibrous protein collagen. Being a degradation product, its chemical nature is heterogeneous in both relative molar mass and possible higher levels of protein structure surviving the hydrolytic process. This soluble form of collagen has a relative molar mass of 300 kiloDaltons and exists in solution as rod-like particles about 280 nm in length and 1.5 nm in diameter. When denatured, these particles are made up of three polypeptide (α) chains. One of these (α2) has a slightly different primary amino acid sequence from the other two (α1) chains but this difference is comparatively small. The amino acid composition of tropocollagen is unusual, in that it contains a very high proportion of glycine, proline, hydroxyproline and alanine (about 33, 12, 9 and 11 residues per 100 residues, respectively).

The lack of uniformity in the gelatin amino acid sequence makes the estimation of the degree of secondary structure (if any) in the α chain single strand difficult. Assuming that a random coil is not present and the conformation adopted by the single stand is a mixture of the polyglycine II and the polyproline II helical forms (both of which have 3 residues per turn and a translation along the helix axis of about 0.3 nm per residue), the overall length of the strand is roughly 300 nm. On the other hand PGG may be deemed as a disc-like molecule and using standard covalent radii, bond angles and basic trigonometric rules, the maximum end to end

distance of the molecule can be estimated to be about 2 nm. This can be taken as the approximate diameter of the PGG molecule. Thus, theoretically, an extended gelatin molecule can accommodate ≈ 150 (300/2) PGG molecules. Examination of Fig. 4.9a reveals that roughly a maximum of 90 PGG molecules (estimated by extrapolation of the curve to infinitely dilute initial protein concentration) can complex with a single gelatin molecule. This figure falls to 40 at maximum precipitation.

The maximum stoichiometry experimentally observed in the precipitates (≈90) is roughly the same as the theoretical maximum limit of ≈150, and this suggests that binding to gelatin is simply determined by the surface area accessible to PGG molecules. The theoretical maximum stoichiometry is probably not observed because of regions of incompatibility along the polypeptide chain and possibly by partial protein envelopment of bound PGG molecules. It is possible that the correspondence of the observed stoichiometry with the number of proline residues is merely coincidental.

4.8.2.2 The PGG-PVP system

The sample of PVP used in this study had a relative molar mass of 10 kilo Dalton. Considering the mass of each vinylpyrolidone unit as 111 Dalton, the number of such units per molecule can be estimated to be 90. Each repeat unit has an approximate length of 0.25 nm which leads to a total length of 22.5 nm for the PVP molecule. So the expected theoretical stoichiometry is ≈ 11 PGG molecules per PVP molecule if the PGG molecules are laid side by side. The experimental maximum stoichiometry was found to be ≈ 13 (Fig. 4.9b) which is roughly similar to the theoretical value. At maximum precipitation, the stoichiometry falls to ≈ 8 indicating that a PGG molecule is shared by at least 11 pyrolidone units.

4.8.2.3 The PGG-BSA system

A marked difference in the stoichiometry of the PGG-BSA system was observed compared to that of the PGG-Gel and PGG-PVP systems. The PGG-BSA system exhibited a virtually constant or single stoichiometry throughout the range of intial protein concentration (Fig. 4.9a).

As described before, BSA is thought to have an ellipsoidal shape with three domains containing one small and two large double loops. These features of BSA provide a degree of flexibility to the molecule and determine its ability to bind tannins. The total surface area of BSA can be estimated roughly as 920 nm^2 using the formula [28]

$$surface\ area = 5.56\ M^{2/3}$$

where M is the relative molar mass of BSA. The surface area of PGG can be estimated as 31 nm^2 using the formula

$$surface\ area = 4\pi r^2$$

from its diameter (2r) of 2 nm. The above estimated quantities lead to a theoretical stoichiometry of 29:1, which is roughly the same as the single stoichiometry experimentally observed in the precipitate ($\approx$20:1).

4.8.3 Resolubilization of precipitates

The PGG-PVP system showed complete resolubilization (Fig. 4.10b) with increased initial concentration of PVP. Resolubilization was virtually absent in the PGG-BSA system (Fig. 4.10a). The PGG-Gel system also shows [16-19] complete resolubilization with excess gelatin. The demonstrative experiments performed for this study did not show complete resolubilization. This apparently anomalous behaviour of gelatin may be due to (a) a difference in sample homogeneity, i.e. a significant proportion

of the gelatin sample may have retained helical conformation (survived entity of collagen degradation) which may encapsulate PGG molecules and thus provide some degree of irreversibility; (b) a difference in applied g-force in the separation of precipitates (a higher rpm value (30,000) was employed compared to that (20,000) of previous works which may have caused [16] this apparent plateau in the curve; and (c) change in the characteristics of PGG chromophore (e.g. the value of the molar absorption coefficient, ε) which may have caused error in the estimation of the concentration of PGG in the precipitate after the maximum precipitation.

Certain interesting points can be noted from the analysis of the resolubilization region of PGG-protein precipitation experiments. These are:

(i) A critical mole ratio (MR_c) of precipitates exists before which precipitation increases sharply and after which resolubilization begins. After MR_c the PGG-protein complex starts to become more and more protein rich. (MR_c for PGG-Gel and PGG-PVP are 40:1 and 8:1, respectively).

(ii) During resolubilization the absorption maxima of the PGG chromophore suffer a red shift (shifts toward longer wavelength). The change is remarkable for PGG-PVP system ($\approx$ 7 nm) (see Fig. 4.11) but is less significant for the PGG-Gel system ($\approx$ 2 nm).

(iii) The absorption of PGG becomes slightly broader at the resolubilization region.
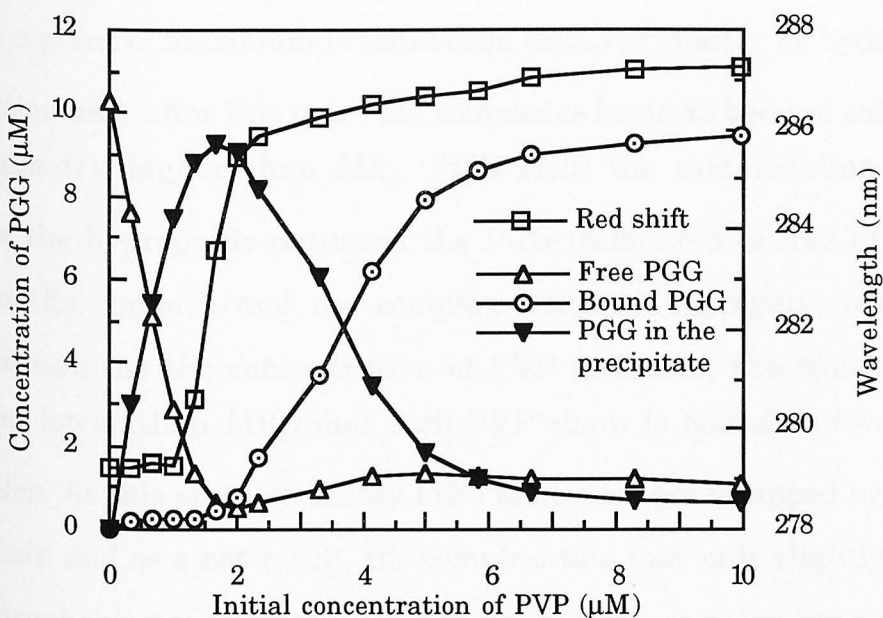
Fig. 4.11 Correlation of bound PGG and red shift for PGG-PVP system (supernatants).

The evidence that the PGG absorption maximum suffers a red shift and slightly broadens during resolubilization indicates that PGG molecules in the supernatant solution do not necessarily exist in a free state, rather they probably exist as both 'free' and 'bound' forms. Relying on the above hypothesis of 'free' and 'bound' PGG, UV spectra of PGG-PVP supernatant solutions were analysed using computerized methods (Deconvolution) to quantify free and bound PGG in the supernatant solution and the results obtained are displayed in Fig. 4.11. The curves for 'free' and 'bound' PGG cross each other just at the point of maximum precipitation and then precipitaion falls symmetrically with the rise of bound PGG but 'free' PGG remains almost unchanged.

PVP in salt (NaCl aq) solution adopts essentially an extended random coil conformation [29]. PVP is an amphiphilic compound which in its extended

form may easily attract many PGG molecules that are also amphiphilic in nature but hydrophobicity is dominant. Thus the PGG-PVP system quickly attains a point of maximum precipitation (MR_c) primarily by hydrophobic interaction and after this point the complexes begin to become soluble. At stoichiometry higher than MR_c (PGG rich) the complexation largely reduces the hydrophilic nature of the PGG (compared to free PGG) and PVP in the complex and the complex tends to aggregate, leading to precipitation. As the concentration of PVP increases, the stoichiometry becomes lower than MR_c, and each PVP chain is bound to fewer PGG molecules. At this stage, probably PGG molecules are wrapped around by PVP chain and as a net result, the complexation may only slightly change the hydrophobic nature of the PVP chain, and the complex can remain in solution. It is also likely that due to the presence of fewer PGG molecules and their entrapment by the PVP chain, a smaller number of PGG molecules is available to cross-link PVP chains, which reduces the possibility of aggregation. A similar explanation for the resolubilization of the PGG-Gel system should also hold.

BSA (a globular protein) did not show any similar resolubilization trend. Once maximum precipitation was reached, some kind of irreversibility in the complexation process was established. A constant mole ratio arises because it is only when this stoichiometry is reached that insolubility ensues. More protein rich complexes are simply too soluble to enter into the aggregation process. It has been speculated [16] that no polyphenolic cross-linking between BSA molecules is necessary for the aggregation, rather the stoichiometry may be a result of the interplay between the complexation and the aggregation equilibrium constants.

It has been seen that the interaction of PGG with PVP perturbs the chromophore of the PGG to an extent which depends on the nature and

strength of the interaction (a parallel increment of bound PGG with the red shift, Fig. 4.11). As suspected before all PGG-PVP complexes do not necessarily precipitate. Before maximum precipitation occurs, an increasing amount of PGG is precipitated by PVP, and the remaining PGG molecules exist in the solution in a free state and in a varying form of soluble complexes (bound PGG). The concentration of bound PGG may be very low at this stage compared to free PGG. As a result, the absorption maximum at λ_2 ($\approx$ 280 nm) remains unchanged. When resolubilization takes place, bound PGG becomes predominant and consequently the red shift continues to increase until full resolubilization of PGG has occurred (Fig. 4.11).

Hydrogen bonding has been proposed [16] between PGG and PVP involving the phenol groups of PGG and the amide groups of PVP. It is possible that the soluble PGG-PVP and PGG-gelatin complexes demonstrate different spectroscopic effects because of the different interplay of the hydrophobic effect and hydrogen bonding to the total binding strength between PGG and the macromolecules. For the PGG-PVP system, predominance of the bathochromic shift may be explained by complexation being dominated by hydrogen bonding involving the phenol groups of PGG and the amide groups of polyvinylpyrrolidone (Fig. 4.12). In partially donating its hydrogen atom, the phenol group takes on partial phenoxide ion character and therefore is more able, through the resonance effect, to interact with the π molecular orbitals of the benzene ring. The result of this would be a bathochromic shift in the PGG spectrum, which is observed experimentally. A hypsochromic shift would be expected for the n $\rightarrow \pi^*$ transition of the carbonyl chromophore of polyvinylpyrrolidone if it was involved in binding.

A very crude approximation of the overall strength of such a binding process may be gained from the difference in energy between the two peak maxima (*i.e.* 'free' PGG and 'bound' PGG). The bands at 280 nm and 287 nm when converted to wavenumbers and then through to the usual units of energy correspond to about 428.6 and 418.1 $kJ.mol^{-1}$, respectively. The difference in energy and a measure of strength of binding between PGG and polyvinylpyrrolidone is therefore, about 10 $kJ.mol^{-1}$, a fairly reasonable estimate of the strength of a hydrogen bond.

It is suggested that the hypochromic effect produced by gelatin comes about through the restriction of the vibrations necessary to 'avoid' the prohibitive symmetry selection rules. This may be caused by the encapsulation of PGG. In other words, PGG is enclosed within the flexible gelatin molecule such that there is a restriction in the vibrational modes it can adopt. Consequently there is a reduction in intensity of the λ_2 electronic absorption band. Corroboration of this suggestion may be inferred from the observation that neither type of effect was seen in the systems involving the use of globular proteins.

The absence of significant bathochromic shift in the PGG-Gel system thus may have been due to counteracting of the bathochromic shift by a hypsochromic shift involving the carbonyl chromophore ($n \rightarrow \pi^*$). So a similar hydrogen bond can be expected involving the phenol groups of PGG and the carbonyl oxygen of peptide as said before (Fig. 4.1, section 4.2.1).
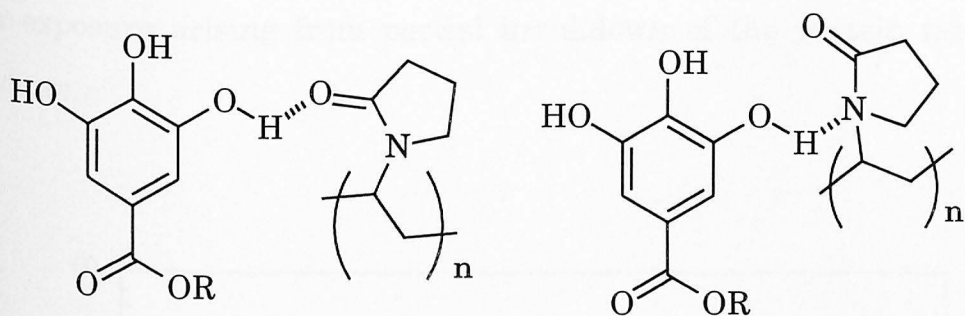
Fig 4.12 Possible hydrogen bonding in tannin-PVP complexation.

4.8.4 Effect of pH on tannin-protein precipitation

The change of pH of a protein directly or indirectly affects its conformation or ligand binding ability. It has been seen [4, 5, 30, 31] that maximum tannin-protein precipitation is obtained at a pH close to the isoelectric point (pI) of the protein involved. At its pI a protein has a minimum net electric charge and hence there is little coulombic repulsion that minimizes the obstacle to aggregation and precipitation.

In the present study, precipitation experiments were conducted at pH 5.4 which was just above or close to the pI of the proteins involved (BSA, pI = 4.8, pI of gelatin depends on sample). Precipitation of PGG-BSA was repeated at pH 4.0 and almost no precipitation was observed compared to that at pH 5.4 (Fig. 4.13). The effect of pH change on PGG-protein precipitation was studied in detail by Warminski [16]. It has been commented that pH changes seem to modify precipitation primarily through alteration of the solubility of polyphenol-protein complexes from an increase in the net charge of the protein component. Proteins having smaller increased charge *density* are not so markedly affected. It seems that pH does not alter the PGG-protein complexation equilibrium constant to any significant extent but its effect is mainly exercised on the aggregatory equilibrium processes. However, the stoichiometry of complexes formed was found to increase because of greater protein surface

area exposure arising from partial breakdown of the protein tertiary structure.
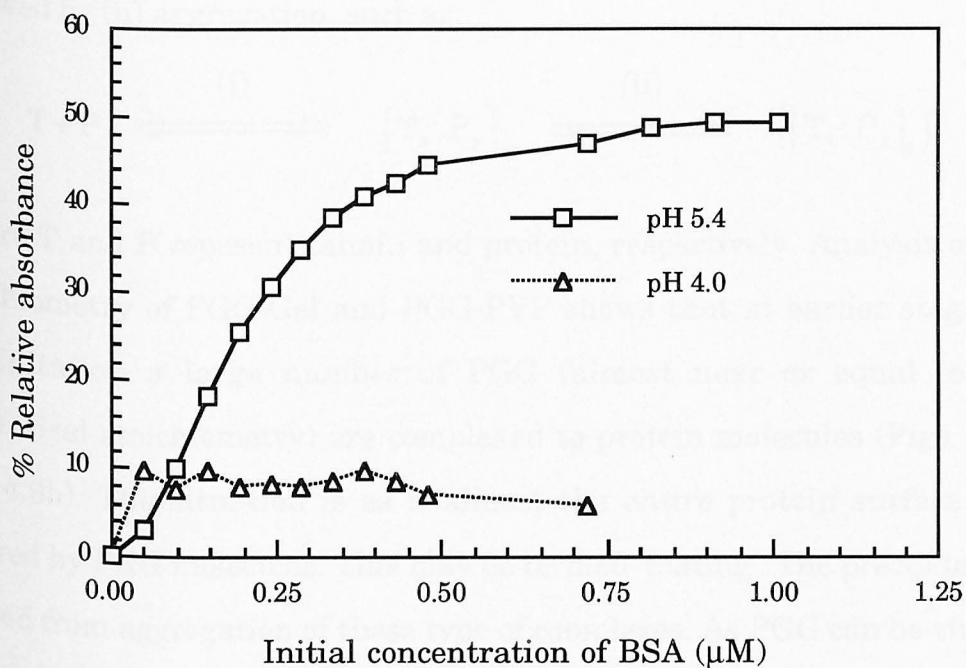
Fig. 4.13 Effect of pH on PGG-BSA precipitation.

At first glance, the increase in stoichiometry seems inconsistent with the concomitant decrease in precipitation. This apparent paradox is quite simply resolved because the increased charge held by the protein increases the critical stoichiometry (*i.e.* that needed to allow aggregation) to a level that can not be readily compensated from the increase in PGG complexation brought about by the increased surface area produced by partial denaturation.

To conclude, the solubility of polyphenol-protein complexes, which can have a huge bearing upon the systems' propensity to demonstrate precipitation, is mainly determined by the protein component. Therefore pH is a vital parameter to control when attempting to compare polyphenol-protein precipitation.

4.9 General discussion and mechanism of tannin-protein precipitation

Precipitation may be crudely viewed as (i) complexation which is then followed by (ii) aggregation, such as:

$$
T + P \xrightleftharpoons{\text{(i)}} \left[T_x \cdot P_y\right]_{aq} \xrightleftharpoons{\text{(ii)}} \left(\left[T_x \cdot P_y\right]_z\right)_s
$$
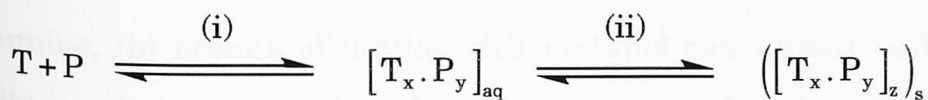
Where T and P repesent tannin and protein, respectively. Analysis of the stoichiometry of PGG-Gel and PGG-PVP shows that at earlier stages of precipitation a large number of PGG (almost near or equal to the theoretical stoichiometry) are complexed to protein molecules (Figs. 4.9a and 4.9b). The situation is as if almost the entire protein surface was covered by PGG molecules. This may be termed 'coating'. The precipitate is formed from aggregation of these type of complexes. As PGG can be viewed as multidentate, so it can act as an anchor between protein molecules. This situation can be described as 'crosslinking'.

The two binding modes 'coating' and 'crosslinking' have been proposed in reference [16]. These binding modes are consistent with the variable stoichiometry observed for various PGG-protein systems. They also justify general trends in precipitation, i.e. a rise to a maximum followed by resolubilization as the initial protein concentration is increased. It is thought that at initial stages of precipitation there are excess PGG over protein (coated). When this excess decreases further, crosslinking probably becomes predominant, thus precipitation reaches its most efficient state. Once the point of maximum crosslinkage of protein by PGG is reached any further addition of protein can reverse the crosslinkage because protein molecules at this stage compete with one another for the available PGG and hence resolubilization ensues.

The tannin-protein precipitation has been proposed to be a general, nonspecific, surface phenomenon from the experimental facts that proteins with large surface area bind more PGG and also large proteins reach maximum precipitation point at very low initial protein concentration. It has been concluded that (a) proline does not act as a specific binding site for tannins, (b) proline of proline rich proteins can impart sufficient flexibility so that it encapsulates bound tannin molecules, thus maximises binding strength to occur, (c) encapsulation may provide a degree of 'irreversibility' to complex thereby making resolubilization more difficult. It has been suggested that tannin-protein interaction arises primarily from the hydrophobic effect but this effect may be supplemented by a complementary network of hydrogen bonding and the overall balance probably depends on the nature of the participating components, particularly flexibility of the protein. The modes of tannin-protein precipitation are summarised in Fig. 4.14.
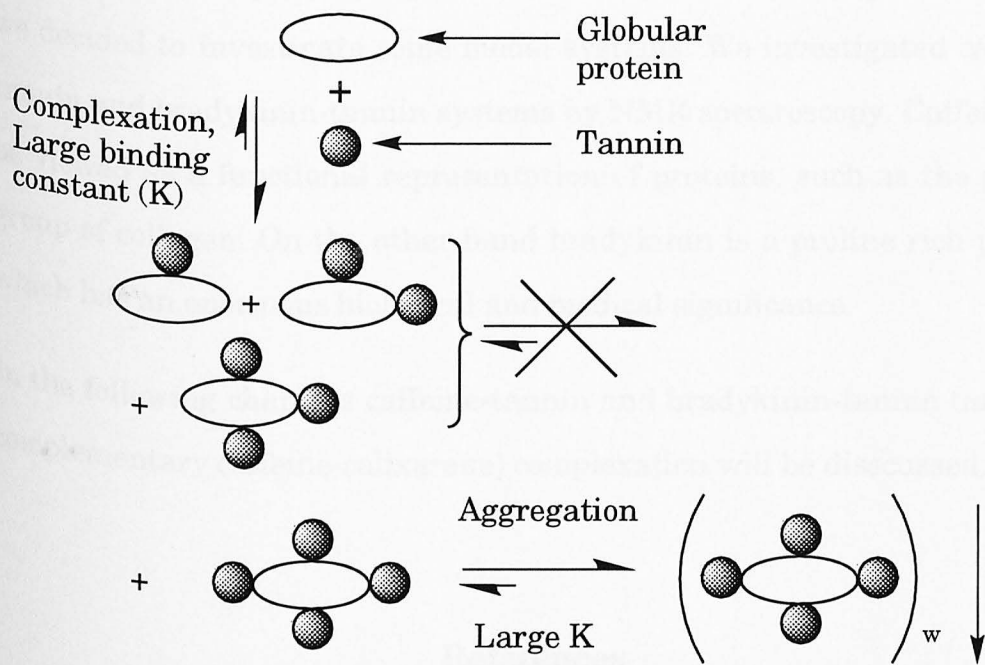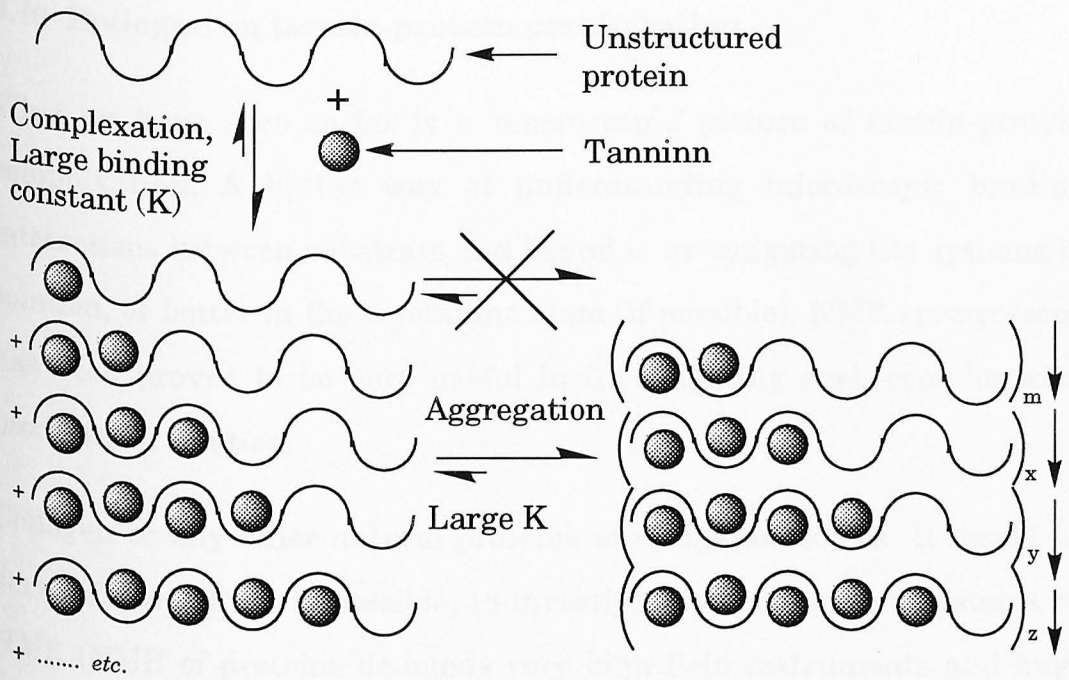
Fig. 4.14 Schematic illustration of the general mechanism of tannin-protein precipitation. Figure adapted from reference [16].

4.10 Epilogue on tannin-protein precipitation

What we have seen so far is a 'macroscopic' picture of tannin-protein complexation. A better way of understanding microscopic binding interactions between substrate and ligand is investigating the systems in solution, or better in the crystalline state (if possible). NMR spectroscopy has been proved to be very useful in investigating such complexation processes in solution.

Collagen or any other natural proteins are huge molecules. It would be very difficult, if not impossible, to investigate tannin-protein systems by NMR (NMR of proteins demands very high field instruments and huge instrument time, particularly to run multi-dimensional experiments). So we decided to investigate some model systems. We investigated caffeine-tannin and bradykinin-tannin systems by NMR spectroscopy. Caffeine can be viewed as a functional representation of proteins, such as the proline group of collagen. On the other hand bradykinin is a proline rich peptide which has an enormous biological and medical significance.

In the following chapters caffeine-tannin and bradykinin-tannin (and also complementary caffeine-calixarene) complexation will be disscussed.

References

1. Hagerman, A. E., in *Significance of Condensed Tannins,* R. W. Hemingway and J. J. Karchesy, Editors, 1989, Plenum Publishers, p. 323.

2. McManus, J. P., Davis, K. G., Beart, J. E., Gaffney, S. H., Lilley, T. H. and Haslam, E., *J. Chem. Soc. Perkin Trans. 2,* 1985, 1429.

3. McManus, J. P., Davis, K., Haslam, E. and Lilley, T. H., *J. Chem. Soc. Chem. Comm.*, 1981, 309.

4. Hagerman, A. E. and Butler, L. G., *J. Agric. Food Chem.*, 1978, **26**, 809.

5. Hagerman, A. E. and Butler, L. G., *J. Biol. Chem.*, 1981, **256**, 4494.

6. Hestrin, S., Feingold, D. S. and Schramm, M., *Methods in Enzymol.*, 1955, **1**, 236.

7. Mejbaum-Katzenellenbogan, W., Dobryszchka, W. M., Jawarska, K. and Morawaiecka, B., *Nature*, 1959, **184**, 1799.

8. Mejbaum-Katzenellenbogan, W. and Dobryszchka, W. M., *Nature*, 1962, **193**, 1288.

9. Goldstein, J. L. and Swain, T., *Phytochemistry*, 1965, **4**, 185.

10. Gustavson, K. H., *The Chemistry of Tanning Processes*. 1956, New York, Academic Press.

11. Hulme, A. C. and Jones, J. D., in *Enzyme Chemistry of Phenolic Compounds*, J.B. Pridham, Editor, 1963, Pergamon Press, Oxford, p. 97.

12. Haslam, E., *Plant Polyphenols - Vegetable Tannins Revisited*. 1989, Cambridge, Cambridge University Press.

13. Porter, L. J. and Woodroffe, J., *Phytochemistry*, 1984, **23**, 1255.

14. Hagerman, A. E. and Klucher, K. M., in *Plant Flavonoids in Biology and Medicine: Biochemical, Pharmacological and Structure Activity Relationships*, V. Cody, E. Middleton, and J. Harborne, Editors, 1986, p. 67.

15. Roux, D. G., *Phytochemistry*, 1972, **11**, 1219.

16. Warminski, E. E., Ph. D. Thesis, 1992, University of Sheffield, U. K.

17. Liao, H., Ph. D. Thesis, 1993, University of Sheffield, U. K.

18. Haslam, E., Lilley, T. H., Warminski, E., Liao, H., Cai, Y., Martin, R., Gaffney, S. H., Goulding, P. N. and Luck, G., *ACS Symposium Series*, 1992, 506.

19. Luck, G., Liao, H., Murray, N. J., Grimmer, H. R., Warminski, E. E., Williamson, M. P., Lilley, T. H. and Haslam, E., *Phytochemistry*, 1994, **37**, 357.

20. Stryer, L., *Biochemistry*. 1995, New York, W. H. Freeman and Company.

21. Rose, P. I., *Gelatin,* in *Encyclopedia of Polymer Science and Engineering,* H. F. Mark, N. M. Bikales, C. G. Oberberger and G. Manges, Editors, 1989, p. 488.

22. Piez, K. A., *Collagen,* in *Encyclopedia of Polymer Science and Engineering,* H. F. Mark, N. M. Bikales, C. G. Oberberger and G. Manges, Editors, 1989, p. 699.

23. Swaisgood, H. E., *Chemistry of Milk proteins,* in *Development in Dairy Chemistry-1 (Proteins),* P. F. Fox, Editor, 1982, Applied Science Publications, London.

24. Whitney, R. M., *Proteins of Milk,* in *Fundamentals of Dairy Chemistry,* N. P. Wong, R. Jennes, M. Keeney and E. H. Marth, Editors, 1988, New York.

25. Kragh-Hansen, U., *Pharm. Rev.*, 1981, **33**, 17.

26. Barabas, E. S., *N-Vinyl Amide Polymer,* in *Encyclopedia of Polymer Science and Engineering,* H. F. Mark, N. M. Bikales, C. G. Oberberger and G. Manges, Editors, 1987, p. 198.

27. Cappas, C., Hoffman, N., Jones, J. and Young, S., *J. Chem. Educ.,* 1991, **68**, 300.

28. Creighton, T. E., *Proteins: Structure and Molecular Properties.* 1984, W.H. Freeman and Company, p. 241.

29. Bergman, W. R. and Mattice, W. L., *ACS Symposium Series*, 1987, **358**, 162.

30. Asquith, T. H. and Butler, L. G., *Phytochemistry*, 1986, **25**, 1591.

31. Oh, H.-I. and Hoff, J. E., *J. Food Sci.*, 1987, **52**, 1267.

CHAPTER FIVE

A STUDY OF THE INTERACTION OF CAFFEINE WITH TANNINS

5.1 Introduction

Caffeine (1) is usually described as an alkaloid but it also resembles a peptide to some extent in its structural features, in that it has two -CO-N(Me)- tertiary amide functional groups in its six-membered ring. These functional groups have similarities to those in the imino acid proline which occurs in proteins. Caffeine has attracted the attention of food chemists and others because of its presence in tea and coffee and its association with the physiological effects of these beverages.
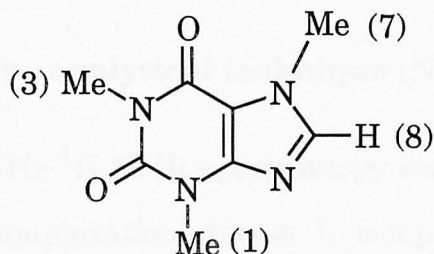
(1) Caffeine

Caffeine binds strongly and ultimately precipitates tannins from aqueous media; the precipitates have a variable stoichiometry. Earlier studies [1, 2] involving tanning showed that caffeine competes effectively with protein for tannins and that protein may be regenerated protein from tannin-protein precipitates. The caffeine-tannin complexation process is reversible and in many ways mimics protein-tannin complexation which thus provides a reasonable model system for the examination of the general mechanism of protein-tannin complexation [3]. However, there are

limitations to this model. Caffeine is small in size and has a rigid structure compared to peptides which display conformational flexibility. Any inference taken from the caffeine-tannin system may not be a true reflection of the real picture of protein-tannin systems.

A great deal of information is already available for caffeine-tannin systems in aqueous media. Because of the poor solubility of tannins in water, most of the data available for caffeine-tannin complexation are at temperatures higher than ambient (~ 318-333 K). For the present study a solvent mixture of D_2O/CD_3OD (1:1, v/v) was chosen in which both solutes and their complexes were sufficiently soluble for high resolution NMR experiments at ambient temperature (293-295 K). The objective was to re-examine the existing information available for caffeine-tannin systems and also to determine how the solvent composition affects the caffeine-tannin binding process.

5.2 Background of the analytical technique (NMR spectroscopy)

High resolution 400 MHz ^{1}H NMR spectroscopy was employed to monitor the substrate-tannin complexation process. In complex formation, an NMR observable nucleus (say, ^{1}H) can 'partition' between two magnetically nonequivalent sites (pure compound and complex, respectively). The nucleus is said to undergo *chemical exchange* between these sites. The exchange process determines the nature of the observable signal. In the fast exchange limit, an NMR signal is an average of the two sites and is a sharp line (or lines for a multiplet), whereas in the intermediate exchange limit the line is broadened and in the slow exchange limit separate lines are observed which correspond to the free and complexed forms. It has been pointed out [4] that the intermediate or slow exchange may indicate very tightly bound complexes whereas fast exchange usually applies to loosely bound complexes.

117

In this study, the proton NMR signals of caffeine were recorded and the relative changes in chemical shifts measured during the titration with tannins were used to assess quantitatively the binding of caffeine to tannin. The change in chemical shift is defined in this work as the difference between the chemical shift of free proton resonance of caffeine or peptide and that of the same proton resonance bound to tannin. This change in chemical shift for any caffeine or peptide proton is believed to be caused largely by the induction of aromatic ring currents provided by the aromatic rings. An aromatic ring can be envisaged as a current loop where the π-electrons are free to move on a circle formed by the σ framework. When these compounds are influenced by an external magnetic field B (Fig. 5.1a), a diamagnetic ring current is induced.

The secondary field resulting from this current affects the protons in its vicinity. Thus protons in the molecular plane and outside the ring are deshielded (downfield shift) and protons in the region above or below the plane of the ring are shielded (upfield shift) (Fig. 5.1b). A quantitative assessment of these chemical shifts effects ($\Delta\delta$) can be made by using the following equation:

$$\Delta\delta = \mu(1 - 3\cos^2\theta) / r^3$$

where μ is the equivalent dipole; r is the distance of the proton from the benzene ring and θ is as shown in Fig. 5.1 [5]. Thus, for a proton above the ring plane, $\theta = 0°$ and $\Delta\delta$ is negative (upfield shift) and vice-versa for a proton in the ring plane.

(a)

Applied magnetic field →

B

θ   r

Ring current   Benzene ring

(b)

Shielded protons (upfield shift)

Me

O

N — Me

H

N

N

N

O

Me Me

O

O

N

H

N

N — Me

N

O

Me

Deshielded Proton (downfield shift)
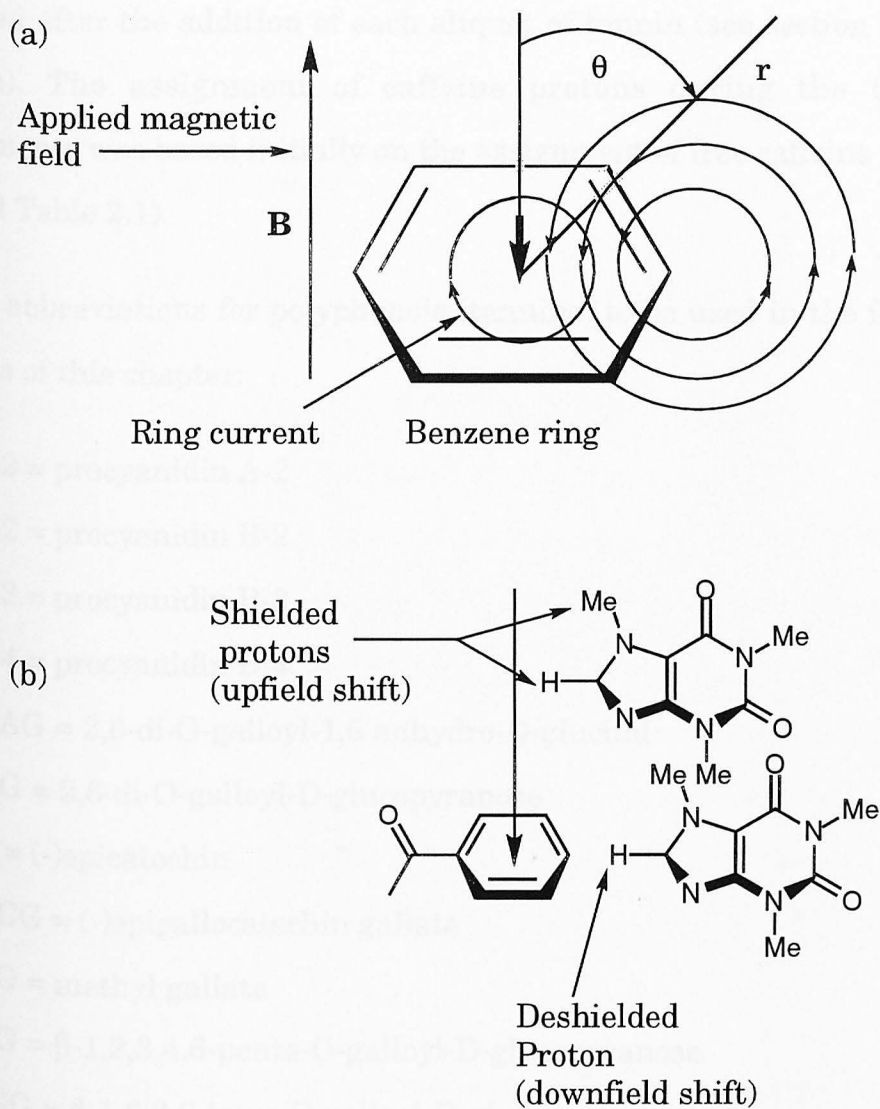
Fig 5.1 The aromatic ring current of benzene. Figure (a) taken and adapted from reference [5]

5.3 Titration of tannins into caffeine

The titration of the phenolic substances methyl gallate (**7**), 2,6-di-O-galloyl-D-glucopyranose (**5**), 2,6-di-galloyl-1,5-anhydro-D-glucitol (**6**), β-1,3,6-tri-O-galloyl-D-glucopyranose (**4**), β-1,2,3,6-tetra-O-galloyl-D-glucopyranose (**3**), β-1,2,3,4,6-penta-O-galloyl-D-glucopyranose (**2**), (-)epicatechin (**8**), (-)epi-gallocatechin-gallate (**9**), proanthocyanidin A-2 (**10**), procyanidin B-2 (**11**), procyanidin B-3 (**12**), and procyanidin B-4 (**13**), was followed by one dimensional ^{1}H NMR experiments which were

recorded after the addition of each aliquot of tannin (see section 2.5.1 for details). The assignment of caffeine protons during the titration experiments was based initially on the assignment of free caffeine (see Fig. 5.7 and Table 2.1).

Key to abbreviations for polyphenols (tannins) to be used in the following sections of this chapter:

(10) A-2 = procyanidin A-2

(11) B-2 = procyanidin B-2

(12) B-3 = procyanidin B-3

(13) B-4 = procyanidin B-4

(6) DGAG = 2,6-di-O-galloyl-1,5 anhydro-D-glucitol

(5) DGG = 2,6-di-O-galloyl-D-glucopyranose

(8) EC = (-)epicatechin

(9) EGCG = (-)epigallocatechin gallate

(7) MeG = methyl gallate

(2) PGG = β-1,2,3,4,6-penta-O-galloyl-D-glucopyranose

(3) TeGG = β-1,2,3,6-tetra-O-galloyl-D-glucopyranose

(4) TGG = β-1,3,6-tri-O-galloyl-D-glucopyranose

Caffeine assignments for the following titrations: caffeine-PGG (Appendix A.2.1), caffeine-TeGG (Appendix A.2.2), caffeine-TGG (Appendix A.2.3), caffeine-DGG (Appendix A.2.4), caffeine-DGAG (Appendix A.2.5), caffeine-MeG (Appendix A.2.6), caffeine-EC (Appendix A.2.7), caffeine-EGCG (Appendix A.2.8), caffeine-A-2 (Appendix A.2.9), caffeine-B-2 (Appendix A.2.10), caffeine-B-3 (Appendix A.2.11), caffeine-B-4 (Appendix A.2.12), are presented in appendices A.2.1- A.2.12.

5.4 Results

5.4.1 Observed chemical shift effects during the titration of caffeine with tannins

For the protons H8 and Me7 weak doublets (long range coupling between H8 and Me7 protons) were observed which became broad singlets with the progressive addition of tannins. The Me1 and Me3 signals, however, remained sharp singlets. The order of the magnitude of the observed chemical shift changes ($\delta_{free}-\delta_{caffeine}$: tannin mole ratio values) was invariably found to be: H8> Me7> Me3> Me1 (Fig. 5.2) for all tannin studied. The change in chemical shift ($\delta_{free}-\delta_{caffeine}$: tannin mole ratio, 1:8) for proton H8 of caffeine after addition of the final aliquot of tannin during titration is presented in Fig. 5.3. Similarly Fig. 5.4 displays the average change in chemical shift ($\delta_{free}-\delta_{caffeine}$: tannin molar ratio, 1:8) after addition of the final aliquot of tannin for protons H8, Me7, Me3 and Me1 of caffeine during each titration.
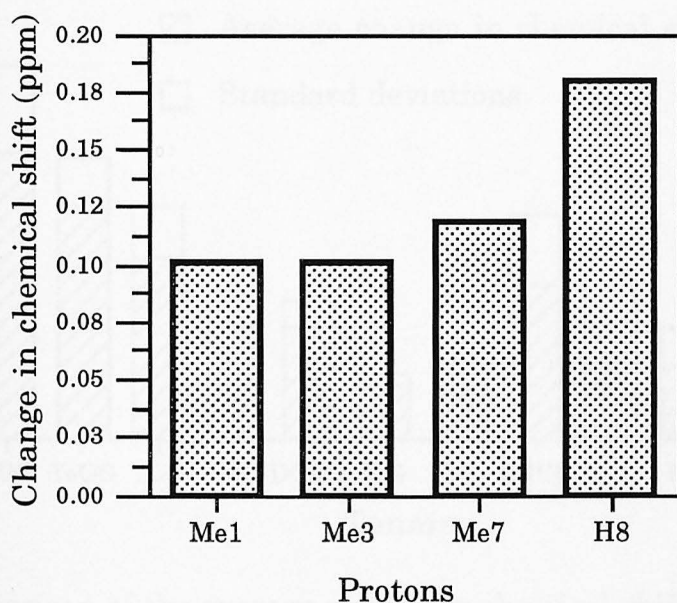
Fig. 5.2 Comparison of the change in chemical shift (ppm) ($\delta_{free}-\delta_{caffeine}$: PGG molar ratio, 1:8) for the protons of caffeine during caffeine-PGG titration in D_2O/CD_3OD (1:1, v/v) at 295 K.
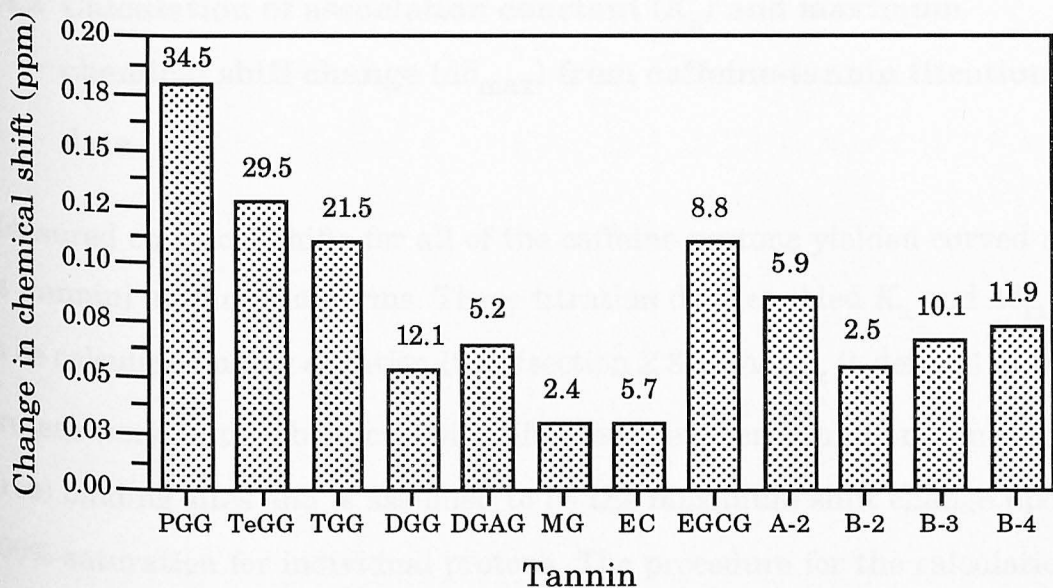
Fig. 5.3 Comparison of the change in chemical shift (ppm) ($\delta_{\text{free}} - \delta_{\text{caffeine}}$: tannin molar ratio, 1:8) of caffeine H8 resonance observed on titration with tannins in D_2O/CD_3OD (1:1, v/v) at 295 K. Numbers printed on top of each bar indicate the association constants (M^{-1}) determined using the chemical shift changes observed for H8 of caffeine for individual tannins.
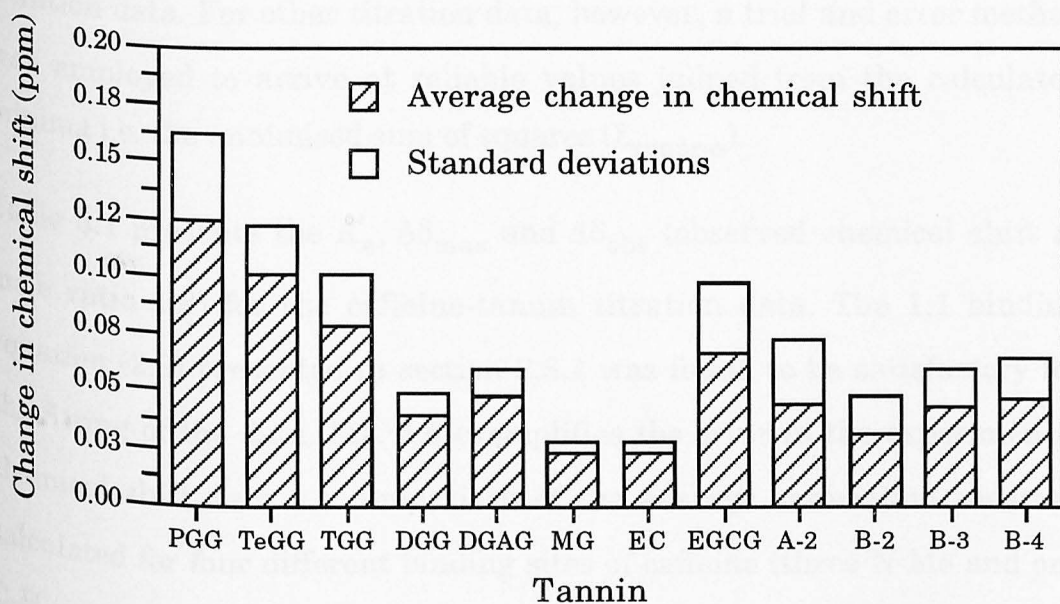
Fig. 5.4 Comparison of the average change in chemical shift (ppm) ($\delta_{\text{free}} - \delta_{\text{caffeine}}$: tannin molar ratio, 1:8) of caffeine proton resonances observed on titration with tannins in D_2O/CD_3OD (1:1, v/v) at 295 K.

5.4.2 Calculation of association constant (K_a) and maximum chemical shift change ($\Delta\delta_{max}$) from caffeine-tannin titration data

Measured chemical shifts for all of the caffeine protons yielded curved $\Delta\delta$ vs [tannin] binding isotherms. These titration data enabled K_a and $\Delta\delta_{max}$ to be calculated using equation (2.9) (section 2.8.1). $\Delta\delta_{max}$ is defined in the present work as the chemical shift difference between bound and unbound (free) binding sites and is assumed to be the maximum shift change upon 100% saturation for individual protons. The procedure for the calculation of K_a and $\Delta\delta_{max}$ is detailed in section 2.5.1.

The calculation of K_a and $\Delta\delta_{max}$ for curved $\Delta\delta$ vs [tannin] isotherms was straightforward and the calculation outputs were almost independent of the initial estimates entered for the calculation. This was found to be so for caffeine-PGG, caffeine-TeGG, caffeine-TGG, caffeine-B-3 and caffeine-B-4 titration data. For other titration data, however, a trial and error method was employed to arrive at reliable values judged from the calculated minima i.e. the minimised sum of squares ($\Sigma_{squares}$).

Table 5.1 presents the K_a, $\Delta\delta_{max}$ and $\Delta\delta_{obs}$ (observed chemical shift at mole ratio 1:8) for the caffeine-tannin titration data. The 1:1 binding equation (2.9) presented in section 2.8.1 was found to be satisfactory for the fitting of the data. Fig. 5.5 exemplifies the error in the experimental chemical shift data. A comparison of the average association constant calculated for four different binding sites of caffeine (three N-Me and one C-H protons) during titrations with various tannins is displayed in Fig. 5.6.

Table 5.1 The association constant, K_a, for caffeine-tannin complexation, maximum chemical shift change upon 100% saturation, $\Delta\delta_{max}$, calculated by curve fitting the caffeine-tannin chemical shift data for protons of caffeine (using equation (2.9)); solvent = D_2O/CD_3OD, (1:1 v/v); temperature 295 K. $\Delta\delta_{obs}$ values are the observed chemical shift change at caffeine to tannin molar ratio 1:8 ($\Delta\delta_{obs}$ values at 1:8 mole ratio for caffeine-TeGG, caffeine-DGAG systems were extrapolated from a best-fit polynomial equation).

Caffeine-PGG Average K_a = 32.2 ($\pm$ 1.6) M^{-1}.

Proton	K_a (M^{-1})	$\Delta\delta_{max}$(ppm)	$\Delta\delta_{obs}$(ppm)	Σsquares
methyl 1	31.9	0.358	0.100	9.45×10^{-7}
methyl 3	31.0	0.369	0.101	8.13×10^{-7}
methyl 7	31.5	0.429	0.118	1.35×10^{-7}
H8	34.5	0.609	0.179	2.22×10^{-6}

Caffeine-TeGG Average K_a = 30.3 ($\pm$ 0.9)M^{-1}.

Proton	K_a (M^{-1})	$\Delta\delta_{max}$(ppm)	$\Delta\delta_{obs}$(ppm)	Σsquares
methyl 1	31.4	0.312	0.080	3.45×10^{-6}
methyl 3	30.54	0.337	0.088	2.30×10^{-6}
methyl 7	29.74	0.389	0.108	2.79×10^{-6}
H8	29.52	0.600	0.128	2.81×10^{-6}

Caffeine-TGG Average K_a = 18.7 ($\pm$ 2.0) M^{-1}.

Proton	K_a (M^{-1})	$\Delta\delta_{max}$(ppm)	$\Delta\delta_{obs}$(ppm)	Σsquares
methyl 1	18.2	0.345	0.061	1.09×10^{-6}
methyl 3	16.6	0.434	0.071	1.26×10^{-6}
methyl 7	18.7	0.415	0.074	1.55×10^{-6}
H8	21.45	0.549	0.110	1.63×10^{-6}

Table 5.1 (contd.)

Caffeine-DGG Average K_a = 11.8 (± 0.9) M^{-1}.

Proton	K_a (M^{-1})	$\Delta\delta_{max}$(ppm)	$\Delta\delta_{obs}$(ppm)	Σsquares
methyl 1	12.9	0.234	0.032	2.41×10^{-7}
methyl 3	11.3	0.320	0.040	6.28×10^{-7}
methyl 7	10.8	0.286	0.034	2.51×10^{-7}
H8	12.1	0.404	0.053	3.80×10^{-7}

Caffeine-DGAG Average K_a = 4.4 (± .6) M^{-1}.

Proton	K_a (M^{-1})	$\Delta\delta_{max}$(ppm)	$\Delta\delta_{obs}$(ppm)	Σsquares
methyl 1	4.1	0.678	0.040	1.05×10^{-6}
methyl 3	4.0	0.809	0.048	2.25×10^{-6}
methyl 7	4.1	0.679	0.040	1.28×10^{-6}
H8	5.2	0.861	0.064	2.73×10^{-6}

Caffeine-methyl gallate Average K_a = 1.9 (± 0.5) M^{-1}.

Proton	K_a (M^{-1})	$\Delta\delta_{max}$(ppm)	$\Delta\delta_{obs}$(ppm)	Σsquares
methyl 1	1.3	1.242	0.020	7.13×10^{-8}
methyl 3	1.9	0.977	0.023	9.64×10^{-8}
methyl 7	2.0	0.813	0.020	4.61×10^{-8}
H8	2.4	1.038	0.030	4.83×10^{-7}

Caffeine-(-)epicatechin Average K_a = 4.7 (± 1.0) M^{-1}.

Proton	K_a (M^{-1})	$\Delta\delta_{max}$(ppm)	$\Delta\delta_{obs}$(ppm)	Σsquares
methyl 1	4.1	0.397	0.020	2.47×10^{-7}
methyl 3	3.6	0.471	0.020	2.53×10^{-7}
methyl 7	5.4	0.352	0.022	8.86×10^{-7}
H8	5.7	0.442	0.029	1.55×10^{-7}

Table 5.1 (contd.)

Caffeine-(-)epigallocatechingallate Average K_a = 7.8 (± 0.7) M^{-1}.

Proton	K_a (M^{-1})	$\Delta\delta_{max}$(ppm)	$\Delta\delta_{obs}$(ppm)	Σsquares
methyl 1	7.2	0.540	0.045	2.62×10^{-7}
methyl 3	7.5	0.564	0.048	3.23×10^{-7}
methyl 7	7.5	0.773	0.066	4.17×10^{-7}
H8	8.8	1.101	0.109	2.15×10^{-6}

Caffeine-A-2 Average K_a = 5.3 (± 0.5) M^{-1}.

Proton	K_a (M^{-1})	$\Delta\delta_{max}$(ppm)	$\Delta\delta_{obs}$(ppm)	Σsquares
methyl 1	5.5	0.386	0.025	1.60×10^{-7}
methyl 3	4.6	0.462	0.025	2.31×10^{-7}
methyl 7	5.3	0.709	0.044	6.68×10^{-7}
H8	5.9	1.248	0.085	4.85×10^{-7}

Caffeine-B-2 Average K_a = 2.0 (± 0.5) M^{-1}.

Proton	K_a (M^{-1})	$\Delta\delta_{max}$(ppm)	$\Delta\delta_{obs}$(ppm)	Σsquares
methyl 1	2.2	0.748	0.020	2.32×10^{-7}
methyl 3	1.4	1.429	0.025	2.97×10^{-7}
methyl 7	2.0	1.185	0.030	2.15×10^{-7}
H8	2.5	1.734	0.054	1.65×10^{-6}

Caffeine-B-3) Average K_a = 8.2 (± 1.5) M^{-1}.

Proton	K_a (M^{-1})	$\Delta\delta_{max}$(ppm)	$\Delta\delta_{obs}$(ppm)	Σsquares
methyl 1	8.8	0.299	0.030	1.52×10^{-7}
methyl 3	6.8	0.445	0.035	3.77×10^{-7}
methyl 7	7.1	0.515	0.042	3.00×10^{-7}
H8	10.1	0.592	0.066	5.29×10^{-7}

Table 5.1 (contd.)

Caffeine-B-4 Average K_a = 9.7 ($\pm$ 1.8) M^{-1}.

Proton	K_a (M^{-1})	$\Delta\delta_{max}$(ppm)	$\Delta\delta_{obs}$(ppm)	Σsquares
methyl 1	9.8	0.295	0.032	2.15×10^{-7}
methyl 3	7.6	0.432	0.037	5.11×10^{-7}
methyl 7	9.4	0.447	0.047	9.74×10^{-7}
H8	11.9	0.556	0.072	1.43×10^{-6}
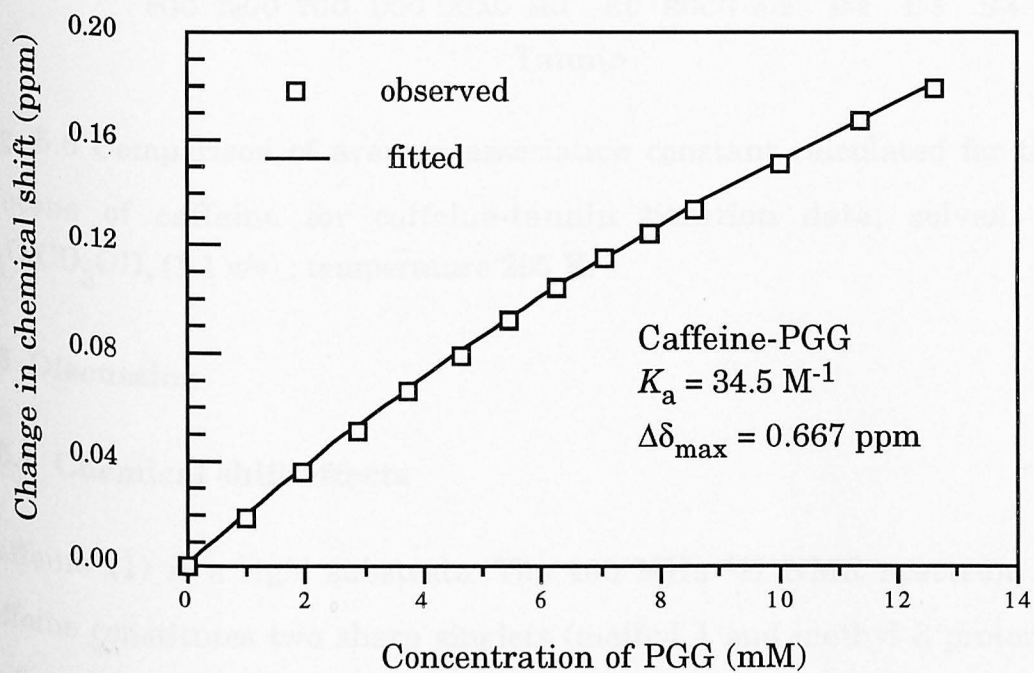
Fig. 5.5 Comparison of observed and fitted chemical shift differences for the H8 resonance of caffeine as a function of PGG concentration.

127
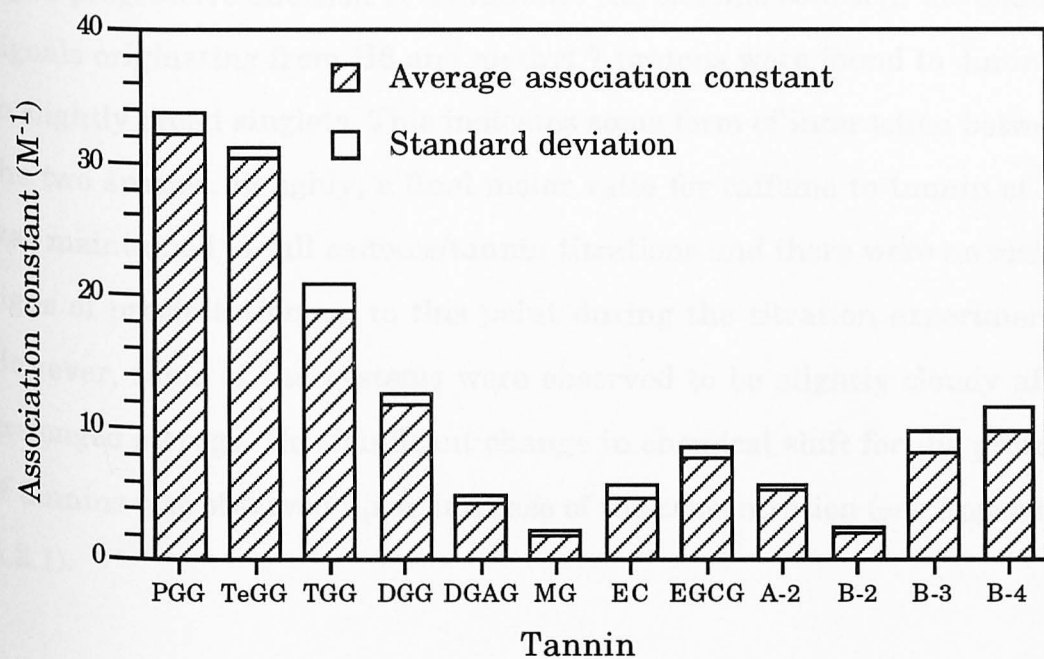
Fig. 5.6 Comparison of average association constant calculated for the protons of caffeine for caffeine-tannin titration data; solvent = D_2O/CD_3OD, (1:1 v/v) ; temperature 295 K.

5.5 Discussion

5.5.1 Chemical shift effects

Caffeine (1) is a rigid substrate. The 400 MHz ^{1}H NMR spectrum of caffeine constitutes two sharp singlets (methyl 1 and methyl 3 protons) and two narrow doublet signals (arising from weak long range coupling between methyl 7 and H8 protons, $^4J_{H8,Me7}$ = 0.68 Hz) (see Fig. 5.7). On addition of tannins to caffeine, all the caffeine protons were found to shift upfield. The magnitude of the chemical shift displacement, however, was not equal for all the four spin systems. The general order of the magnitude of change in chemical shift was found to be: H8 > methyl 7 > methyl 3 > methyl 1 with an exception for the caffeine-DGG and caffeine-MG systems where the order found was H8 > methyl 3 > methyl 7 > methyl 1.

Upon progressive addition of tannin into the caffeine solution, the doublet signals originating from H8 and methyl 7 protons were found to diminish to slightly broad singlets. This indicates some form of interaction between the two species. Roughly, a final molar ratio for caffeine to tannin of 1:8 was maintained for all caffeine/tannin titrations and there were no visible signs of precipitation up to this point during the titration experiments. However, some of the systems were observed to be slightly cloudy after prolonged storage. No significant change in chemical shift for the protons of tannins was observed upon increase of the concentration (see Appendix-A.2.1).
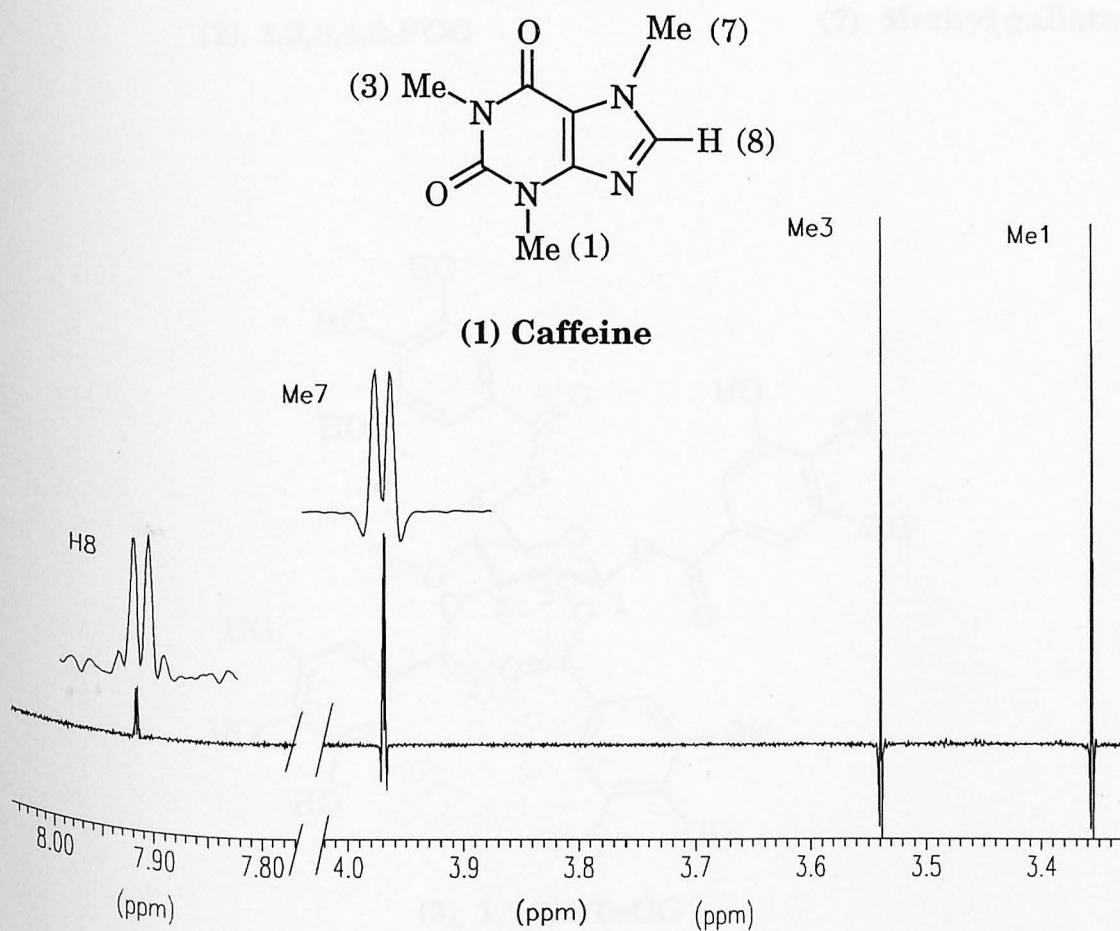
Fig 5.7 Molecular structure and ^{1}H chemical shift assignment (400 MHz) for caffeine (2 mM) in D_2O/CD_3OD (1:1, v/v) at 295 K.
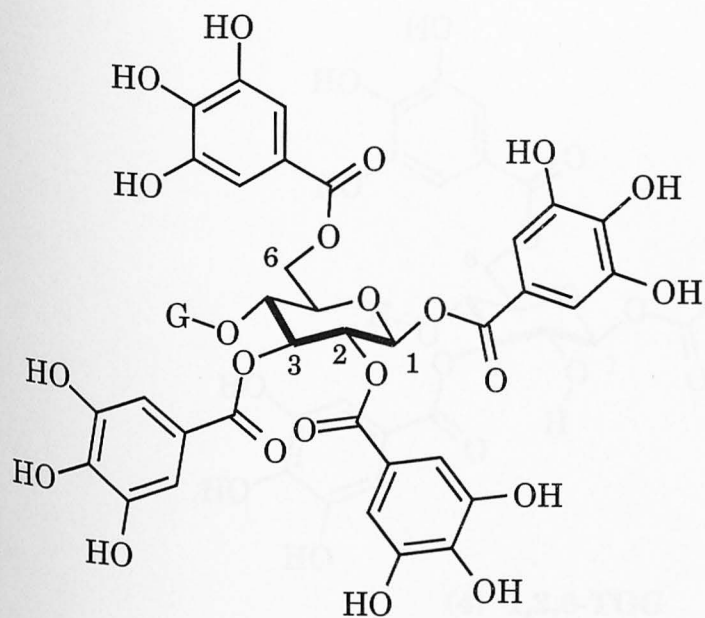
(2) 1,2,3,4,6-PGG

$G =$
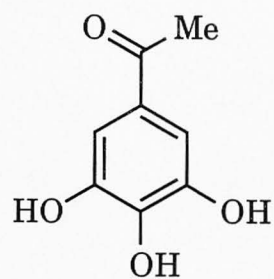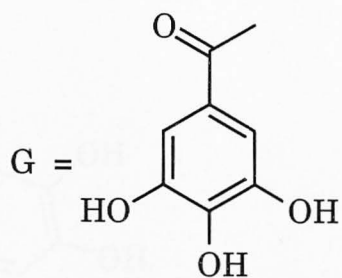
(7) Methyl gallate
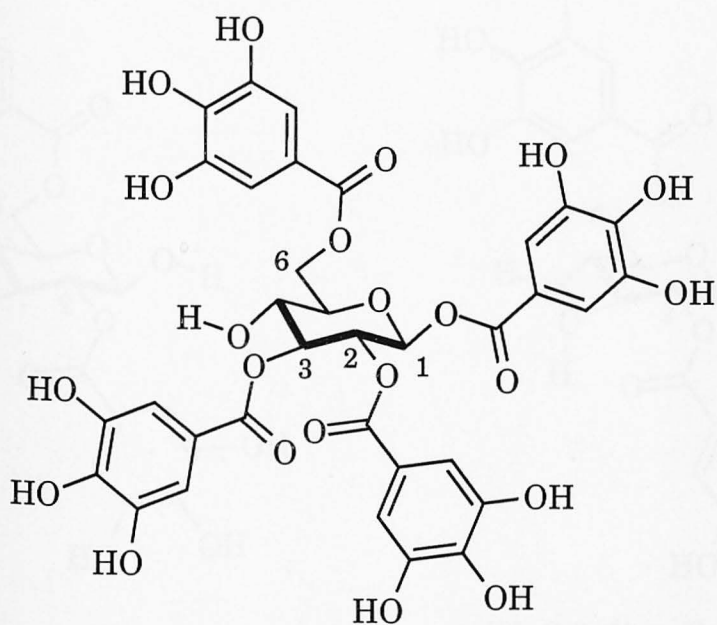
(3) 1,2,3,6-TeGG
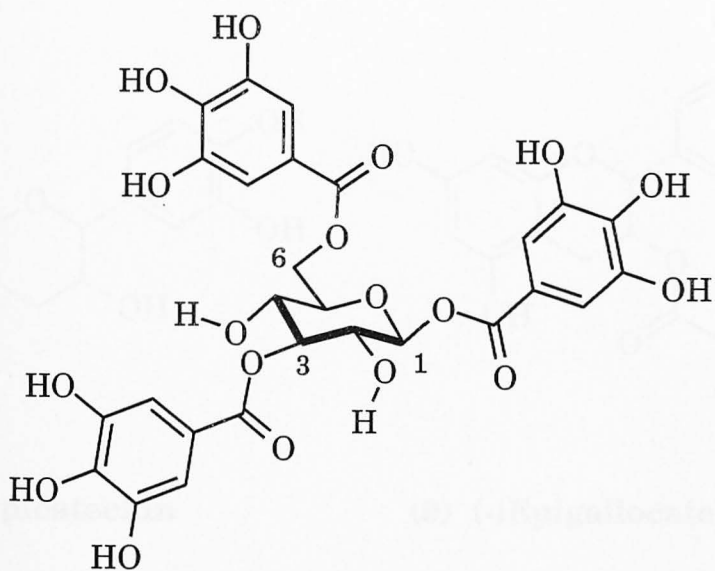
(4) 1,3,6-TGG
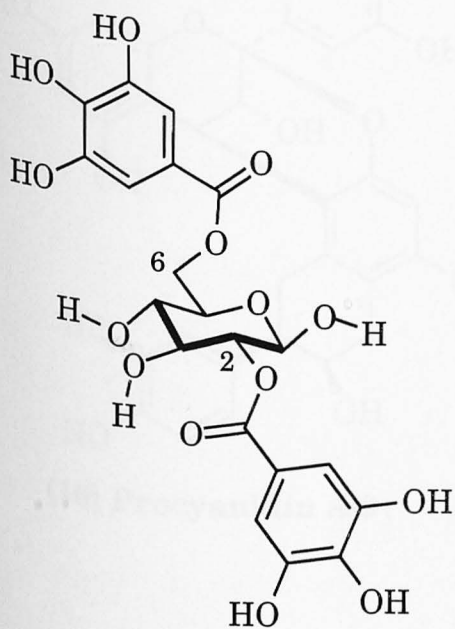
(5) 2,6-DGG
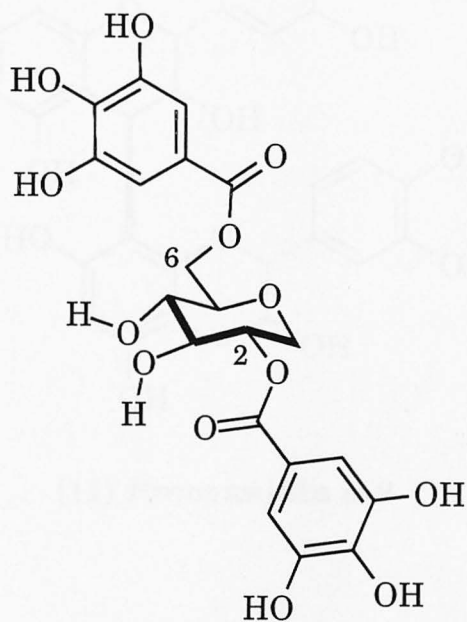
(6) 2,6-di-galloyl -1,5-anhydro-glucitol

131
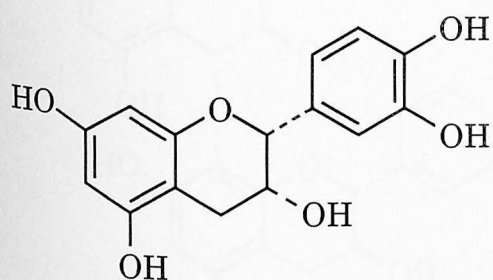
(8) (-)Epicatechin
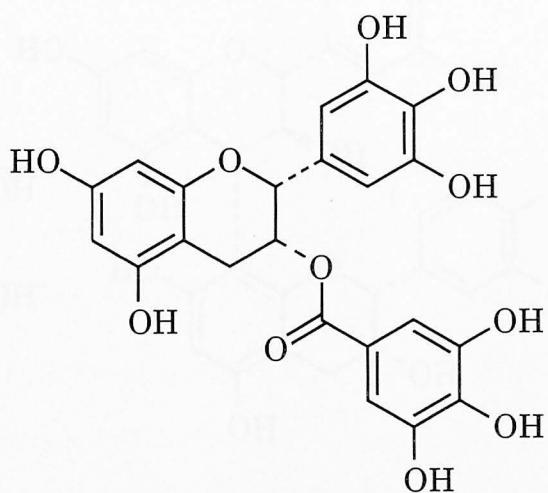
(9) (-)Epigallocatechingallate
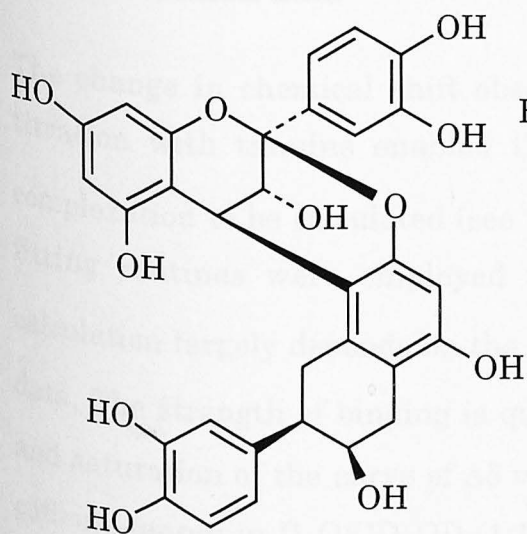
(10) Procyanidin A-2

(11) Procyanidin B-2

OH

HO O OH

OH

OH

HO O OH

OH

OH

HO O OH

OH

OH

OH

HO O OH

OH

OH
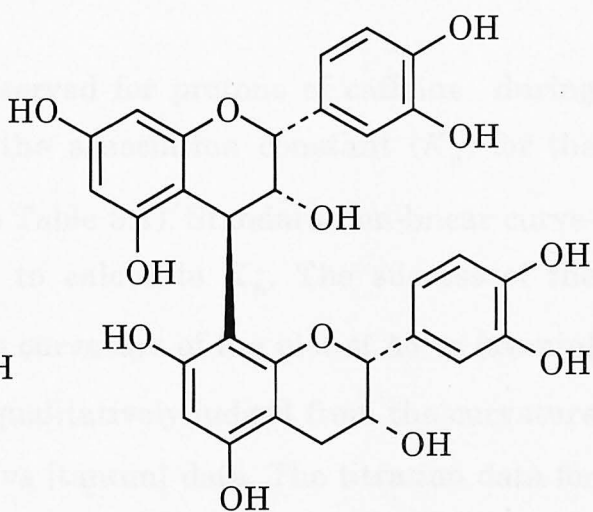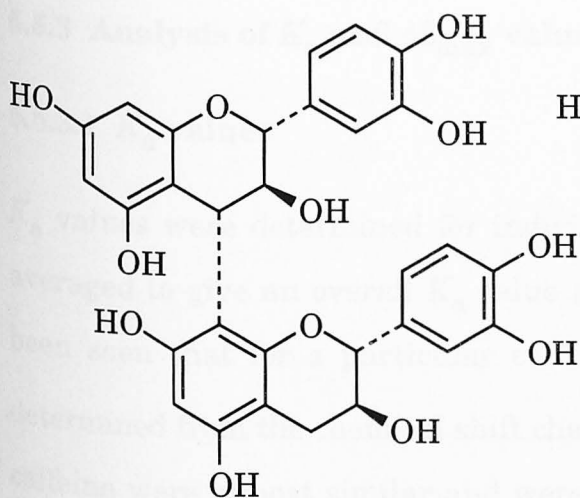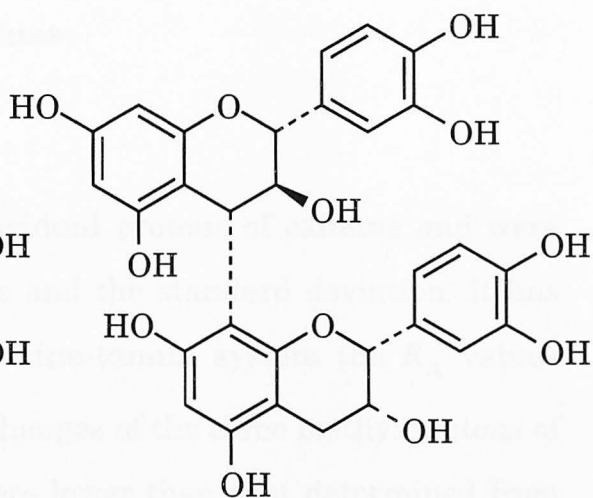
(12) Procyanidin B-3   **(13) Procyanidin B-4**

5.5.2 Calculation of K_a and $\Delta\delta_{max}$ from the caffeine-tannin titration data

The change in chemical shift observed for protons of caffeine during titration with tannins enabled the association constant (K_a) for the complexation to be calculated (see Table 5.1). Standard non-linear curve-fitting routines were employed to calculate K_a. The success of the calculation largely depends on the curvature of the plot of $\Delta\delta$ vs [tannin] data. The strength of binding is qualitatively judged from the curvature and saturation of the curve of $\Delta\delta$ vs [tannin] data. The titration data for caffeine-tannin in D_2O/CD_3OD (1:1, v/v) do not indicate strong binding (< 35 M^{-1}) and as a result the saturation point for the caffeine-tannin binding isotherms was not possible to attain. So the $\Delta\delta$ vs [tannin] binding curve should be considered truncated and this factor could limit the success and reliability of the calculation of K_a and $\Delta\delta_{max}$, especially where $\Delta\delta$ vs [tannin] is not substantially curved (very weak binding). In spite of the above limitations, K_a and $\Delta\delta_{max}$ values were successfully calculated in each case for all the protons of caffeine.

5.5.3 Analysis of K_a and $\Delta\delta_{max}$ values

5.5.3.1 K_a values

K_a values were determined for individual protons of caffeine and were averaged to give an overall K_a value and the standard deviation. It has been seen that for a particular caffeine-tannin system the K_a values determined from the chemical shift changes of the three methyl protons of caffeine were almost similar and were lower than that determined from the chemical shift changes of the H8 proton. Invariably, K_a value determined from the H8 shift changes was the largest for any caffeine-tannin system. The experimental data probably indicate that the rate of exchange between H8 binding site and any potential binding site of tannin is slower compared to the methyl groups of caffeine. This is reflected in the calculated K_a values. This greater accessibility of H8 proton for tannins and the fact that caffeine proton resonances are shifted upfield induced by aromatic rings of tannins probably indicate the specific and preferred mode of the flexible stacking of aromatic rings on caffeine in solution.

K_a data, either determined for H8 proton or an average value of K_a value determined for all the four proton groups of caffeine, can be used to rank the tannins in order of their binding effectiveness to caffeine; hydrolysable tannins: PGG > TeGG > TGG > DGG > DGAG > MG, and condensed tannins: B-4 $\approx$ B-3 > EGCG > A-2 > EC > B-2. Previous studies [6, 7] of caffeine-tannin complexation in water indicated the similar ranking order for hydrolysable tannins but the same is not true for condensed tannins (see Table 5.4). The experimental results indicate that the nature of the solvent has a greater and non-linear influence on the binding of caffeine/condensed tannins systems than that of caffeine-hydrolysable tannin systems. The differential binding affinities of DGG and DGAG for

134

caffeine indicates that the presence of hydroxyl group in C-1 position of glucopyranose has a great influence on the complexation process (DGG binds 3 times stronger than DGAG).

The galloyl groups in hydrolysable tannins are considered to be the principal binding functions of tannin for any substrate. This is supported by the experimental data that caffeine proton resonances were observed to move upfield and this upfield movement is believed to be induced by the aromatic ring current of the aromatic groups of tannins. Although with the increasing number of galloyl groups, the K_a values were found to increase steadily but not as a multiple of the galloyl function (see Fig 5.8 and Table 5.2). This implies that the galloyl function alone is not responsible for the total effectiveness of association, but that the tannin molecule as a whole accords the binding properties of caffeine.
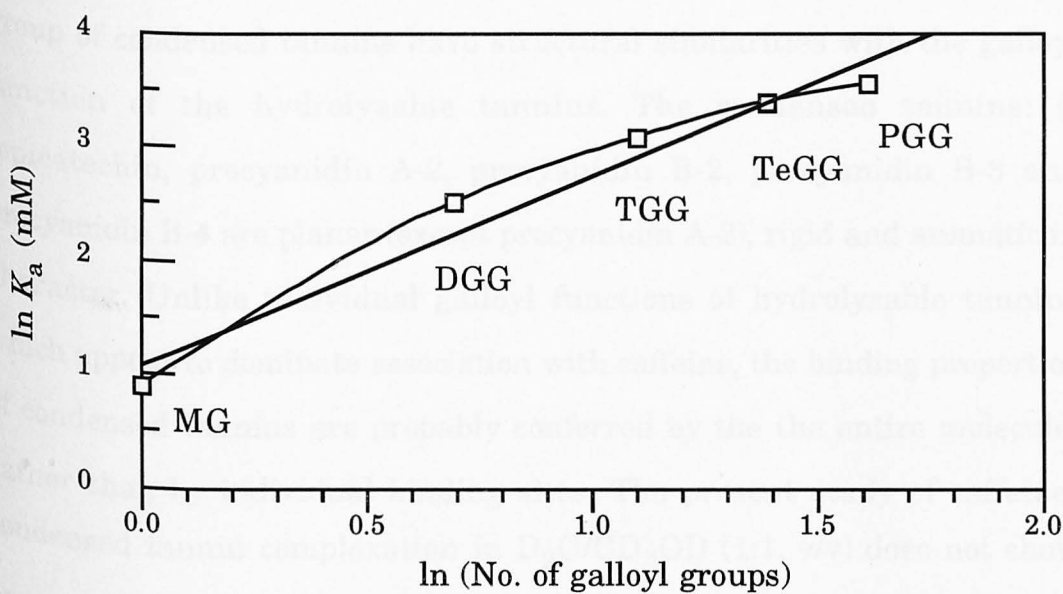
Fig. 5.8 Correlation between association constant (K_a) and no. of gallyol groups per molecule of galloyl esters. The K_a values calculated for H8 of caffeine are plotted.

135

Table 5.2 Comparison of the K_a values for caffeine/tannin complexation in D_2O/CD_3OD (1:1, v/v) with the 'ideal' association constant K_i determined for H8 proton of caffeine.

Tannin	K_a (M^{-1})	K_i (M^{-1})	Deviation (M^{-1})
MG	2.4	2.4x1	00.0
DGAG	5.2	2.4x2	00.4
DGG	12.1	2.4x3	07.3
TGG	21.5	2.4x3	14.3
TeGG	29.5	2.4x4	19.3
PGG	34.5	2.4x5	22.5

The upfield chemical shift change of caffeine protons on titration with condensed tannins indicates that the aromatic rings of the condensed tannins playing the principal role in binding. The 3,4-dihydroxyphenyl group of condensed tannins have structural similarities with the galloyl function of the hydrolysable tannins. The condensed tannins: (-)epicatechin, procyanidin A-2, procyanidin B-2, procyanidin B-3 and procyanidin B-4 are planar (except procyanidin A-2), rigid and aromatic in character. Unlike individual galloyl functions of hydrolysable tannins which appear to dominate association with caffeine, the binding properties of condensed tannins are probably conferred by the the entire molecule, rather than by individual binding sites. The present study of caffeine-condensed tannin complexation in D_2O/CD_3OD (1:1, v/v) does not show any specific binding pattern compared to previous similar types of studies in D_2O (see Table 5.4). It is a general experience that the solubility of condensed tannins (and also hydrolysable tannins) increases when switched from water to methanol or acetone. Thus improved tannin-solvent interactions may have caused this apparent anomaly.

5.5.3.2 $\Delta\delta_{obs}$ and $\Delta\delta_{max}$ values

It is a general belief that the larger the magnitude of the change in chemical shift, the tighter is the binding i.e. larger K_a values. This was found broadly true for the caffeine-hydrolysable tannin systems and apparently true for the caffeine-condensed tannin systems. The experimental data indicate that with the increase in the number of galloyl groups in the hydrolysable tannin molecules, a sharp increase in the magnitude of $\Delta\delta_{obs}$ value is observed (Fig. 5.3). A linear relationship between K_a and $\Delta\delta_{obs}$ values is apparently established by the experimental data for the caffeine-hydrolysable tannin systems.

Deviation of the observed $\Delta\delta_{obs}$ values for hydrolysable tannins (Table 5.3) from ideality probably indicates the effect of the geometry of the tannin molecules as a whole and the cooperativity between binding sites. No straight forward trend was observed for caffeine-condensed tannin titration data.

Table 5.3 Deviation of the $\Delta\delta_{obs}$ values at molar ratio 1:8 for caffeine-tannin complexation in D_2O/CD_3OD (1:1, v/v) from the 'ideal' $\Delta\delta_{obs}$ values observed for H8 proton of caffeine.

Tannin	$\Delta\delta_{obs}$ (ppm)	$\Delta\delta_{obs}$ (ideal) (ppm)	Deviation (ppm)
MG	0.030	0.030x1	0.000
DGG	0.053	0.030x2	0.007
TGG	0.110	0.030x3	0.020
TeGG	[a]0.128	0.030x4	0.008
PGG	0.179	0.030x5	0.029

[a] value was extrapolated from best-fit polynomial curve-fitting of experimental caffeine-TeGG chemical shift data.

As far as $\Delta\delta_{max}$ values are concerned, there is no straight forward relationship between $\Delta\delta_{max}$ and K_a values, but the apparent trend is that

the magnitude of $\Delta\delta_{max}$ values decreases with a decrease in K_a values upto a certain limit (Fig. 5.9). Again this broadly applies to caffeine-hydrolysable tannin systems. It has been noticed that loosely bound caffeine-tannin systems, i.e. smaller K_a values predicted very high magnitude of $\Delta\delta_{max}$ values. A point should be remembered here that the caffeine-tannin isotherms ($\Delta\delta_{max}$ vs [tannin]) were truncated due to the fact that the saturation point were not possible to attain. So the higher magnitude of $\Delta\delta_{max}$ values for smaller K_a values (i.e. poorly curved isotherms) could be simply due to the calculational uncertainty and may not be very reliable.
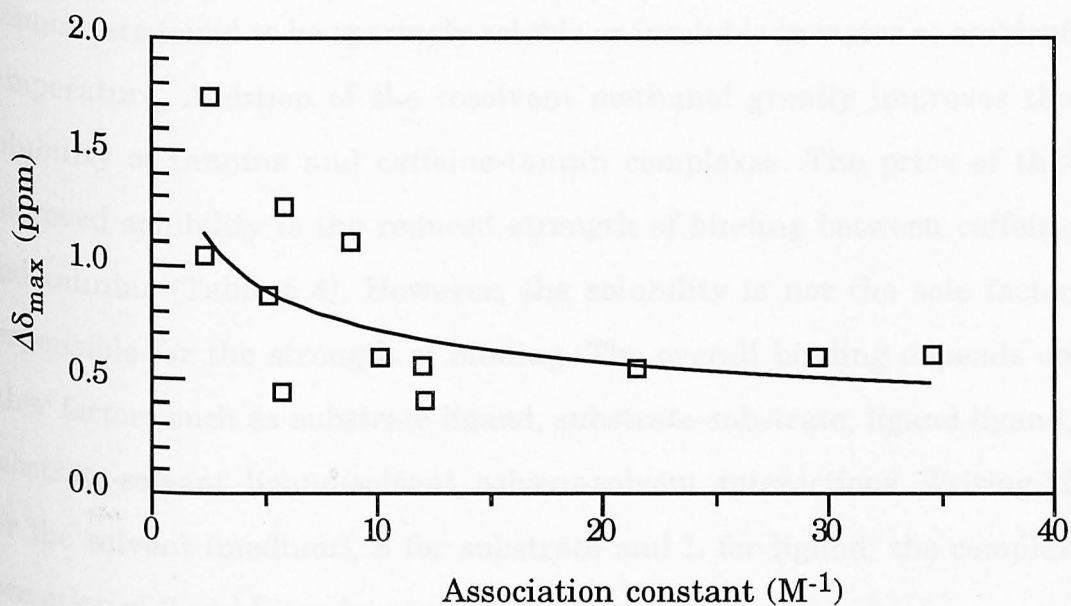
Fig. 5.9 Correlation between calculated association constant (K_a) and maximum change in chemical shift ($\Delta\delta_{max}$). For convenience, values calculated for H8 of caffeine are plotted.

5.5.4 The effect of solvent on caffeine-tannin association

The strength of association and hence the value of the association constant (K_a) of complexes depend on the solvent used [8]. The formation of complexes (homotactic or heterotactic) is greatly influenced by the

solubility of the solutes (including the complexes) in the solvent. A mixed solvent can improve the solubility of given solutes. The solubility of a given solute in a given solvent (say, water) is closely related to the tendency of the solute(s) to engage in molecular interaction with an added cosolvent (say, methanol). When the solute-solute interaction is stronger than solute-solvent interaction, a poor solubility results. However, the apparent solubility of solutes may be increased when a cosolvent is added because of the additional solute-cosolvent interaction.

The present study of caffeine-tannin complexation was conducted in a mixture of D_2O/CD_3OD (1:1, v/v) at ambient temperature (295 K). Tannins are found to be sparingly soluble or insoluble in water at ambient temperature. Addition of the cosolvent methanol greatly improves the solubility of tannins and caffeine-tannin complexes. The price of this improved solubility is the reduced strength of binding between caffeine and tannins (Table 5.4). However, the solubility is not the sole factor responsible for the strength of binding. The overall binding depends on other factors such as substrate-ligand, substrate-substrate, ligand-ligand, substrate-solvent, ligand-solvent, solvent-solvent, interactions. Writing M for the solvent (medium), S for substrate and L for ligand, the complex formation of S and L can be approximately represented as

$$SM + LM \rightleftharpoons SL + MM$$
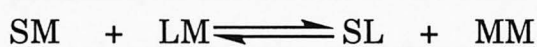
where SM and LM represent solvated species and MM indicates solvent-solvent interaction. When the system molecular properties do not experience strong solute-solvent or solvent-solvent interaction, then the complex formation is predominantly governed by the substrate-ligand (SL) interactions. The following equation represents the profile of the overall free energy change (ΔG) for this process.

$$\Delta G = \Delta G_{MM} + \Delta G_{MS} + \Delta G_{SL}$$

where,

ΔG_{MM} = contribution from solvent-solvent interaction;

ΔG_{MS} = contribution from all solvent-solute interactions, i.e.

solvation parameters; and

ΔG_{SL} = contribution from all substrate-ligand interactions.

These three energy terms: ΔG_{MM}, ΔG_{MS} and ΔG_{SS} are thought to be the 'driving force' for the complex formation. The ΔG_{SS} term makes a stabilizing contribution to ΔG at equilibrium. The substrate-medium, ligand-medium and complex-medium interactions are included in the ΔG_{MS} term and play an important role in stabilizing or destabilizing the system because the SM and LM interactions compete with SL interaction. The ΔG_{MM} term is the most important one for the present study. In aqueous solvents the MM interactions are very strong and dominate the system. ΔG_{MM} constitutes the hydrophobic effect.

When predominantly hydrophobic or nonpolar solutes are dissolved in water, the strong intermolecular hydrogen bonding characteristic of water must be modified, so that a new network of water-water hydrogen bonds may develop in the proximity of the solute. If two such dissolved molecules are brought into mutual contact, the structured solvent shells which originally accompany each of them are found to reorganize; some of the formerly structured solvent may be released to the bulk water. This contributes a positive or favourable entropy contribution (ΔS) to the energy of association. This is the 'classical' picture of molecular aggregation or association through hydrophobic effects, a process driven by favourable entropy changes.

Both caffeine and tannins are predominantly hydrophobic in nature. The hydrophobicity in tannins is manifested by the presence of aromatic groups in the molecules. When these compounds are dissolved in water, they are virtually 'squeezed out' from water due to very strong water-water (MM) interactions and hydrophobic character of the tannins. This leads to self-association (or aggregation) and complexation. Which process ultimately dominates (self-association or complexation) depends on the capability of the mutual recogniton between substrate and ligand.

When a cosolvent methanol is added to the system, MS interactions are reorganized (improved solvation) and overall MM interactions become weaker and are no longer dominant. As a result the strength of binding between caffeine and tannin becomes substantially weaker. Indeed, manyfold lowering ($\approx$ 8 times for caffeine-PGG) of binding constants for caffeine-tannin association was observed when switched from water to the water-methanol solvent (Table 5.4). This type of behaviour of tannins in 'better' solvents is supported by thermodynamic studies [9, 10]. The hydrophobic methyl group of methanol provides improved solvation for both caffeine and tannin and thus the ΔG_{SS} term does not contribute significantly, i.e. the self-assocation is not significant. This is evidenced by the fact that no significant change in the chemical shift of tannin protons was observed with the increasing concentration of tannins; either tannins alone or during titration into caffeine. The experimental results thus suggest that the overall process is dominated by the attraction between caffeine and tannins.

From a comparision of the association results determined for the caffeine-tannin titrations in D_2O/CD_3OD(1:1, v/v) and D_2O [6, 7] respectively, the effect of solvent on the molecular association can be established. The

results indicate that the primary mode of complexation is hydrophobic association.

Table 5.4 Comparision of association constants for caffeine-tannin titration data in D_2O/CD_3OD (1:1, v/v) and D_2O [6, 7] , determined for H8 proton of caffeine. Data recorded at 300K for galloyl esters were taken from reference [6] and corrected from molality to molarity scale.

Tannin	K_a (M^{-1}) in D_2O/CD_3OD (1:1, v/v)	K_a (M^{-1}) in D_2O	
	295 K	298 K	318 K
EC (8)	5.7		34.5
EGCG (9)	8.8		52.8
A-2 (10)	5.9		
B-2 (11)	2.5		26.2
B-3 (12)	10.1		22.4
B-4 (13)	11.9		22.4
MG(7)	2.4	33.8	
DGAG (6)	5.2	-	
DGG (5)	12.1	-	
TGG (4)	21.5	88.9	
TeGG (3)	29.5	153.8	
PGG (2)	34.5	302.2	

5.5.5 Modes of caffeine-tannin complexation

Caffeine (1) strongly binds tannin [3]. It is a bicyclic molecule having proline like features within the structure (the two -CO-N(Me)- groups). It has four tertiary N centres which are believed to be relatively poorly solvated by water [11, 12]. Thus, when caffeine interacts with hydrogen bonding compounds in aqueous media, a smaller number of solvating hydrogen bonds need to be broken and hence the process may be energetically favourable. The tertiary amide carbonyl (-CO(NMe)-) groups of caffeine are good proton acceptors. This is supported by the evidence

142

that the carbonyl function in tertiary amides is a much more effective hydrogen bond acceptor than that in primary and secondary amides [11-15].

Earlier studies [6, 7] established that galloyl groups attached to tannins are mainly responsible for caffeine-tannin complexation (and also protein-tannin complexation). The galloyl functions at position 1 and 6 in the glucose core of hydrolysable tannins are the preferred binding sites for caffeine complexation. In another study the galloyl groups have been shown to be good donors but poor acceptors for hydrogen-bonding [13].

X-ray crystallographic studies [6, 16] of caffeine-methyl gallate complexes have revealed that a layer-lattice structure exists in which the caffeine and the methyl gallate are stacked in an alternating layers, approximately 3.3-3.4 Å apart (Fig. 5.10a). It is believed that for methyl gallate this stacking structure is stabilized by an extensive in-plane system of hydrogen-bonding between the three hydroxy groups (donors) and the two keto amide groups and the basic N-9 of caffeine (Fig. 5.10b). This stacking structure of caffeine-methyl gallate complex is supported by recent NMR studies in solution [17]. There is, however, a marked contrast between the structure of caffeine-methyl gallate in solid state and in solution. X-ray studies [6, 16] of the solid caffeine-methyl gallate complex suggest that the phenolic groups and the associated aromatic nuclei are generally stacked above the 6-membered ring of caffeine. From ^{1}H NMR solution studies of caffeine-methyl gallate (present work and work described in reference [17]) it has been seen that H8 proton (of the five membered ring) was generally perturbed the most (the order of chemical shift change was found to be H8 > Me3 > Me7 ≈ Me1). The reason for this differential behaviour of caffeine in solid state and in solution is not clear. Greater mobility of the methyl gallate in a caffeine-methyl gallate stack in solution compared to that in

(a)

(b)
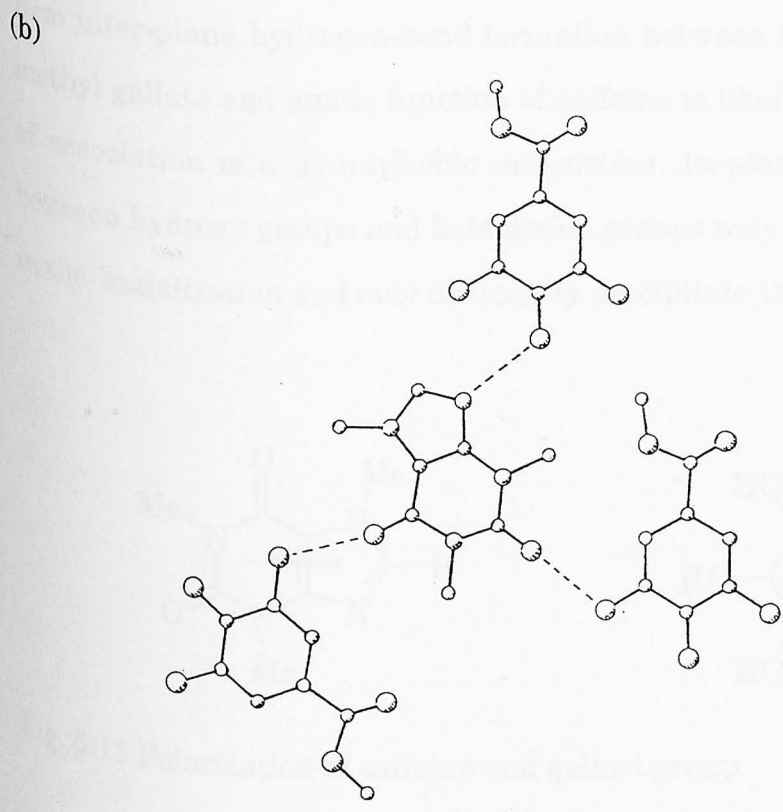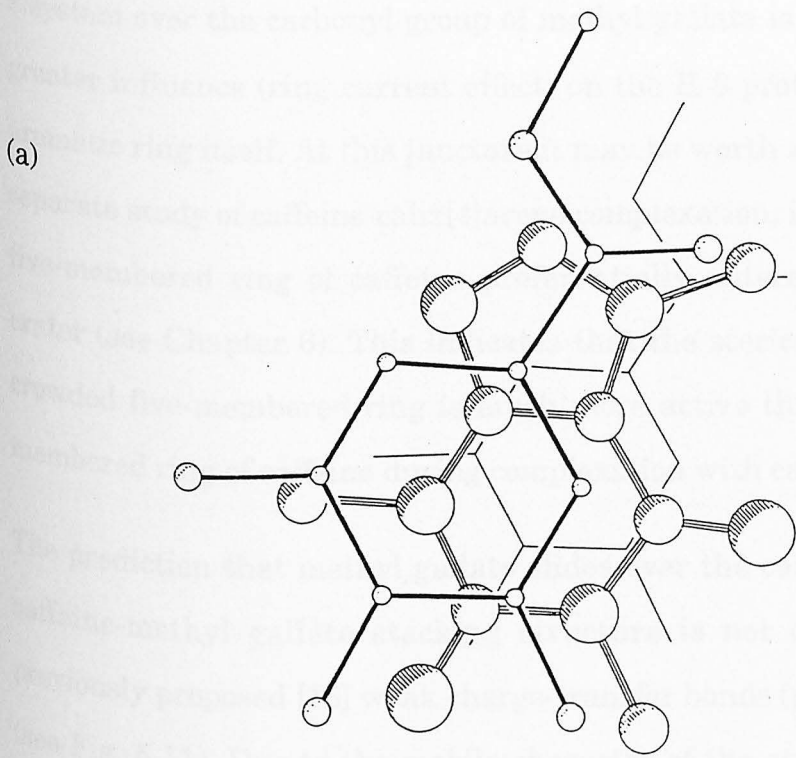
Fig. 5.10 Caffeine-methyl gallate complex: (a) layer-lattice structure and (b) in-plane hydrogen bonding. Figures taken from reference [3].

solid state may have caused this. Another reason may be that the extended π system over the carbonyl group of methyl gallate is probably imparting greater influence (ring current effect) on the H-8 proton compared to the aromatic ring itself. At this juncture it may be worth mentioning that in a separate study of caffeine-calix[4]arene complexation, it was found that the five-membered ring of caffeine preferentially entered the calix[4]arene crater (see Chapter 6). This indicates that the sterically simple and less crowded five-membered ring is much more active than the crowded six-membered ring of caffeine during complexation with calixarene.

The prediction that methyl gallate slides over the caffeine surface in the caffeine-methyl gallate stacking structure is not consistent with the previously proposed [16] weak charge-transfer bonds (polarization binding) (see Fig. 5.11). Due to the mobile character of the stacking structure, no firm inter-plane hydrogen-bond formation between hydroxyl functions of methyl gallate and amide function of caffeine is likely. The principal force of association is a hydrophobic interaction. In-plane hydrogen bonding between hydroxy groups and keto amide groups may play a secondary role in the stabilization and may ultimately precipitate the complex.
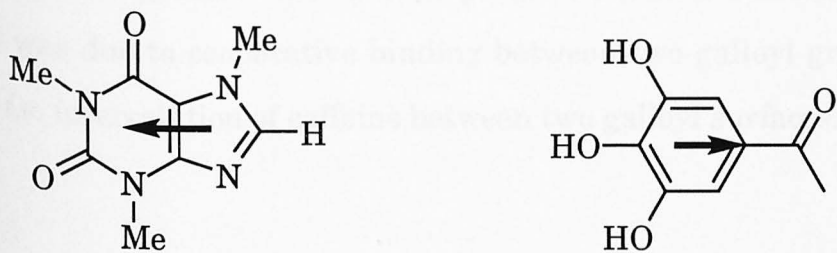
Fig. 5.11 Polarization of caffeine and galloyl group.

The stacking structure of the caffeine-galloyl function is further constrained when methyl gallate is replaced by a larger tannin molecule with more than one galloyl function. The order of chemical shift changes (H8 > Me7 > Me3 > Me1, Fig. 5.2) again suggests that the five-membered ring is the most perturbed region of the caffeine substrate. The H8 proton receives the largest exposure to the aromatic galloyl functions. Similar behaviour was observed in all other recent NMR studies of caffeine-tannin complexation processes [7, 17].

An explanation for this behaviour could be that caffeine is intercalated between two galloyl functions (for example, connected to position 1 and 3 of glucose) in a fashion that one galloyl function stacks above the six-membered ring of caffeine and the other one stacks above the five-membered ring of caffeine but on the opposite face (see Fig. 5.12). The interplanar distance of galloyl/six-membered ring may be higher than that of galloyl/five-membered ring. This explanation is consistent with the chemical shift data that shift change for Me1 and Me3 are almost equal and much lower than those of Me7 and H8. This is also consistent with the earlier explanation [3, 6, 7] of the deviation from linearity in the caffeine-tannin binding strength when an increasing number of galloyl functions are added to the glucose. It has been predicted that the deviation from linearity was due to cooperative binding between two galloyl groups and caffeine, i.e. intercalation of caffeine between two galloyl surfaces.
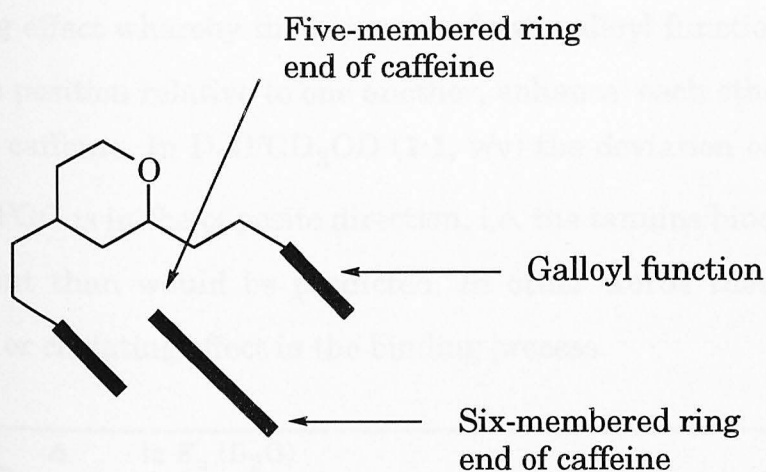
Fig 5.12 Caffeine-tannin association. Figure taken and adapted from reference [3].

The nature of the solvent has an enormous effect on the complexation of caffeine and tannin. For caffeine-PGG complexation, an eight times decrease in the strength of binding was obtained on switching from D_2O (302.2 M^{-1}) to D_2O/CD_3OD(1:1, v/v) (34.5 M^{-1}). No significant change in chemical shift for any protons of tannins was observed during titration of caffeine with tannin with increasing concentration of tannin in D_2O/CD_3OD (1:1, v/v). This implies that tannins do not self-associate in D_2O/CD_3OD (1:1, v/v). No precipitation of caffeine-tannin complexes was observed even at higher molar ratios (>1:8). On the other hand there is evidence that tannins (especially hydrolysable tannins) strongly self-associate in D_2O [6, 7].

It has been seen that with the increase of galloyl functions within the tannin molecule, the strength of binding between caffeine and tannin does not increase linearly, but rather deviates from the statistical line. The deviation is much pronounced for PGG and TeGG (Fig. 5.13). In D_2O the deviation of the binding of TeGG and PGG for caffeine shows that the tannins bind caffeine to a much greater extent than would be predicted. This greater binding was predicted [3, 6] to be a co-operative binding effect

or chelating effect whereby the presence of two galloyl functions oriented in a certain position relative to one another, enhance each other's binding affinity for caffeine. In D_2O/CD_3OD (1:1, v/v) the deviation of binding of TeGG and PGG is in the opposite direction, i.e. the tannins bind caffeine to a less extent than would be predicted. In other words there is no co-operativity or chelating effect in the binding process.
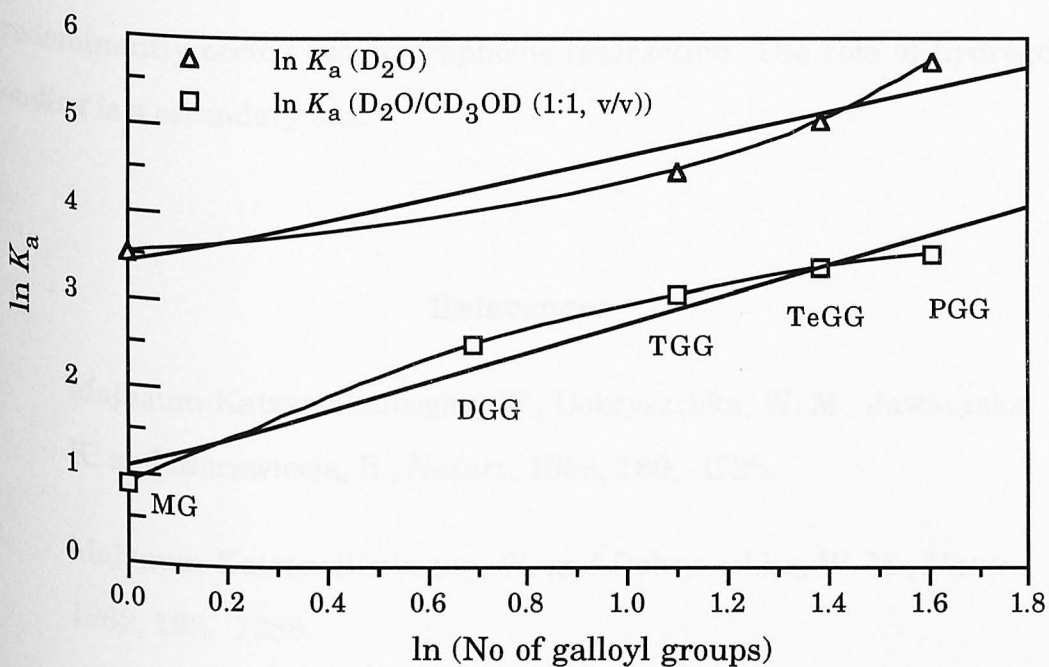
Fig. 5.13 Illustration of the effect of the nature of solvent on the caffeine-tannin complexation process.

The evidence presented above establishes the profound effect on the relative contribution of the types of interactions responsible for caffeine-tannin complexation. Methanol is a amphipathic molecule containing a weakly hydrophilic OH group and hydrophobic methyl group. The solvation of the hydrophobic molecules by methanol would decrease the hydrophobic effect thereby leading to weaker molecular association. In D_2O , the hydrophobic interaction between caffeine and tannin molecules is more effective than in D_2O/CD_3OD (1:1, v/v). In D_2O/CD_3OD(1:1, v/v), the hydrophobic tannin molecules and hydrophobic groups of caffeine are

148

primarily solvated by methanol that provides apoorer tannin-caffeine hydrophobic interaction.

The upfield chemical shift changes for the protons of caffeine during the caffeine-tannin titration and the overall weakening of the binding association between caffeine and tannin by the presence of the hydrophobic solvent methanol reinforces the view that caffeine-tannin association predominantly occurs *via* hydrophobic interaction. The role of hydrogen bonding is a secondary one.

References

1. Majbaum-Katzenellenbogan, W., Dobryszchka, W. M., Jawaorska, K. and Morawiecja, B., *Nature*, 1959, **180**, 1799.

2. Majbaum-Katzenellenbogan, W. and Dobryszchka, W. M., *Nature*, 1962, **193**, 1288.

3. Cai, Y., Gaffney, S. H., Lilley, T. H., Magnolato, D., Martin, R., Spencer, C. M. and Haslam, E., *J. Chem. Soc. PerkinTrans. 2*, 1990, 2197.

4. Feeney, J., Batchelor, J. G., Albrand, J. P. and Roberts, G. C. K., *J. Magn. Reson.*, 1979, **33**, 519.

5. Abraham, R. J., Fisher, J. and Loftus, P., *Introduction to NMR Spectroscopy*. 1988 (1991), John Wiley & Sons Ltd.

6. Martin, R., 1988, Ph. D. Thesis, University of Sheffield, U. K.

7. Cai, Y., 1989, Ph. D. Thesis, University of Sheffield, U. K.

8. Grant, D. J. W. and Highuchi, T., *Solubility Behavior of Organic Chemistry,* in *Techniques of Chemistry*, 1990, Wiley Interscience Publication Ltd.

9. Lilley, T. H., *Pure & Appl. Chem.*, 1993, **65**, 2551.

10. Lilley, T. H., *Pure & Appl. Chem.*, 1994, **66**, 429.

11. Fernandez, J. and Lilley, T. H., *J. Chem. Soc. Faraday Trans.*, 1992, **88**, 2503.

12. Wolfenden, R., *Science*, 1983, **222**, 1087.

13. Abraham, M. H., Druce, P. P., Prior, D. V., Barratt, D. G., Morris, J. J. and Taylor, P. J., *J. Chem. Soc. Perkin Trans. 2*, 1989, 1355.

14. Taft, R., Gurke, D., Joris, L., Schleyr, P. von R. and Rakshys, J. W., *J. Am. Chem. Soc.*, 1969, **91**, 4801.

15. Cheek, P. J. and Lilley, T. H., *J. Chem. Soc. Faraday Trans. 1*, 1988, **84**, 1927.

16. Martin, R., Lilley, T. H., Bailey, N. A., Falshaw, C. P., Haslam, E., Magnolato, D. and Begley, M. J., *J. Chem. Soc. Chem. Commun.*, 1986, 105.

17. Murray, N. J., 1994, Ph. D. Thesis, University of Sheffield, U. K.

CHAPTER SIX

A STUDY OF THE MOLECULAR RECOGNITION OF CAFFEINE AND A PROLINE-PEPTIDE BY CALIXARENES

6.1 Introduction

Calixarenes have been found to bind effectively to various molecular species including metal cations, organic anions and neutral organic molecules [1]. They have become a popular tool in the synthesis or purification of many compounds. They are generally called synthetic 'hosts'. The success in their use as 'hosts' lies in their unique bowl shape, easy synthesis and functionalization.

Calixarenes or their modified versions bind smaller molecules selectively. This selectivity is conferred by multiple hydrogen bonding involving adjacent hydroxy groups of the macrocycle which stabilises the resulting complex [2]. Suitably modified calixarenes can replace many bioactive natural hosts such as enzymes or antibodies and perform their physiological functions. Molecular recognition is the secret of this process. Molecular recognition can be defined as a process where the host molecules recognise the electronic and geometric shape of the guest molecule so well that only a particular guest molecule is able to bind to it. This selective binding triggers the biological function. Molecular recognition processes have some common features. They are (i) complementarity - size, shape (van der Waals surface) and electrostatics; (ii) preorganisation - both free and bound host should have the same conformation; and (iii) competition with the solvent (desolvation).

The present work was intended to provide a better understanding of the tannin-protein interaction. Caffeine was taken as a functional model of proline-rich proteins to supplement the knowledge of tannin-protein interaction at the molecular level. Caffeine (1) has certain structural features which resemble proline groups of peptides, such as it has two -CO-N(Me)- tertiary amide functional groups in its six-membered ring. On the other hand calixarenes (resorcin or pyrogallol based) have a similarity with tannins. Thus they have strongly hydrophobic domains (aromatic rings and alkyl side-chains) in their structures and they also possess a strong hydrophilic character by virtue of the hydroxy groups on the aromatic rings. Due to their unique natural arrangement of OH groups, calixarenes may show good selectivity towards caffeine and prolyl peptide (2). The present investigation was aimed at the understanding of the molecular recognition of caffeine and proline group by calixarenes and at the same time to throw some light on the similarity (or dissimilarity) of caffeine with proline functions of proteins.

Two calixarenes - calix[4]resorcinarene (3) and calix[4]pyrogallolarene (4) were synthesised by acid catalysed condensation of heptanal and appropriate phenols (resorcin and pyrogallol, respectively) (see section 2.6 for the details of synthesis). There are no reports so far on the binding of caffeine with calix[4]arenes. However, it has been reported [2] that calix[4]resorcinarene binds polyvinylpyrrolidone (5) that has a functional similarity with proline-rich proteins.

(1)   (2)
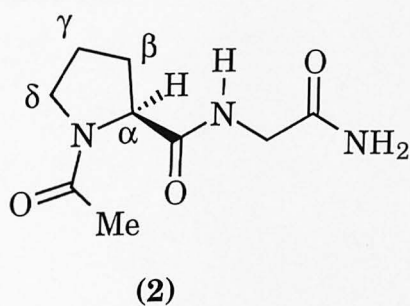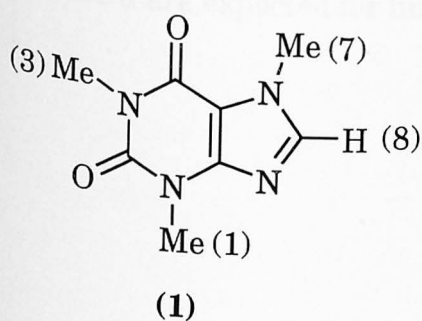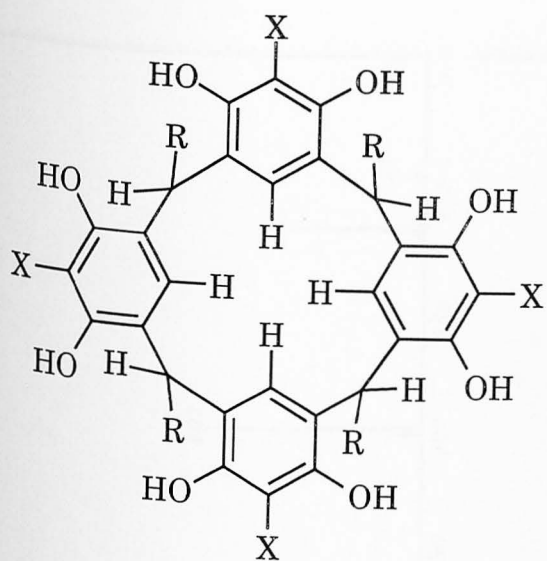
(3); R = (CH₃)₅CH₃; X = H
(4); R = (CH₃)₅CH₃; X = OH
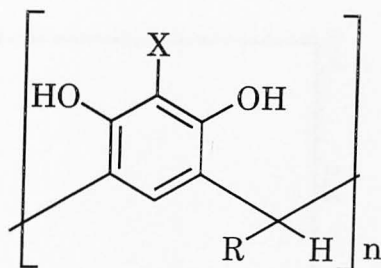
(6) X = H or OH
     R = -C₆H₁₃
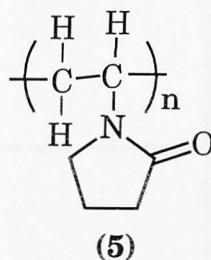
(5)

6.2 Structures of calix[4]resorcinarene and calix[4]pyrogallol-arene

After synthesis and separation, the calixarenes were characterised by the application of high resolution mass and ^{1}H NMR spectroscopy. From the analysis of mass spectra (see Fig 6.1) the molecular weights for the resorcinol and pyrogallol based compounds were determined to be 824.52 and 888.50 Daltons, respectively. These molecular weights confirmed that the compounds were tetramers (6). The simplicity of the ^{1}H NMR spectra (one and two singlet signals for 4 or 8 aromatic protons of resorcin and pyrogallol based compounds, respectively) (see Fig. 6.2) proved that the compounds were essentially cyclotetramers. Complex one-dimensional ^{1}H NMR spectra are expected for linear tetramers (6).

153
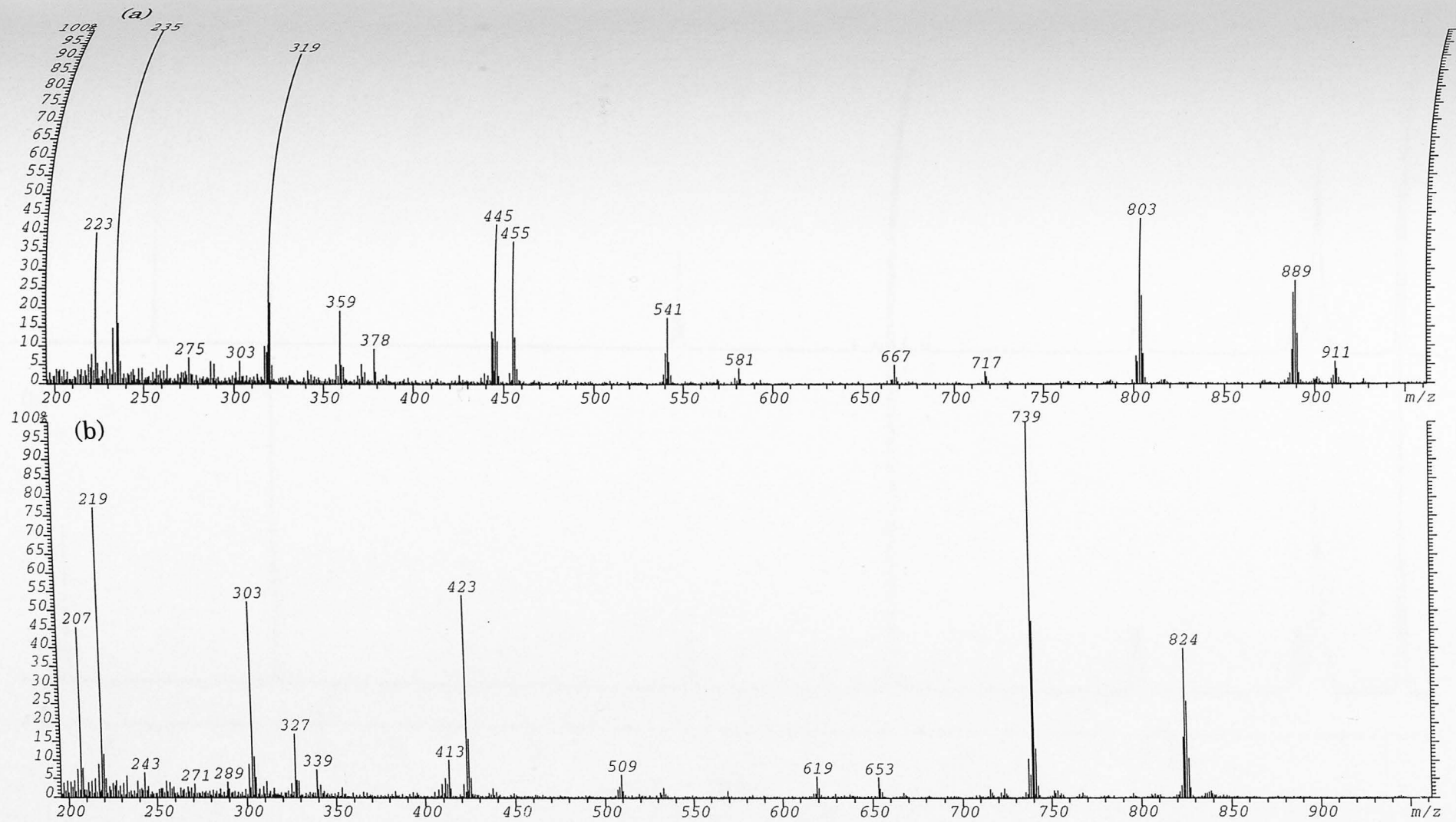
Fig. 6.1 Mass spectra of calix[4]arenes. (a) Pyrogallol and (b) resorcin derived.
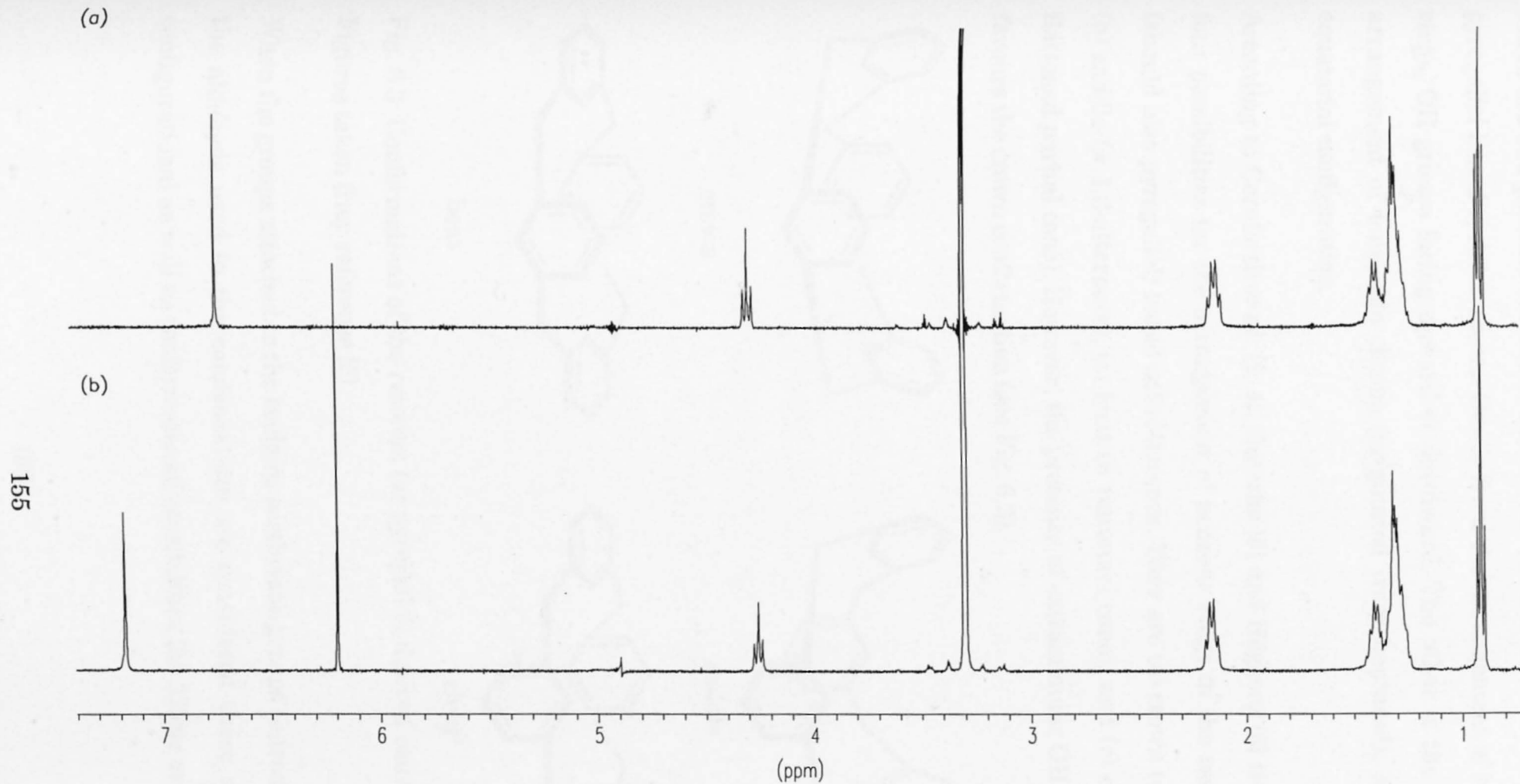
Fig. 6.2 ^1H NMR spectra of calix[4]arenes recorded in CD_3OD, 400 MHz at 295K. (a) Pyrogallol and (b) resorcin derived.

There are two possible sources of diasterioisomerism in the resorcinol or pyrogallol based cyclotetramers. One is from the arrangement of benzene rings, OH groups facing upward or downward. The other is the spatial arrangement of long side chains (originated from heptanal); axial or equatorial configuration.

According to Cornforth et al. [3, 4], Gutsche [5] and Högberg [6] there are four possibilities for the arrangement of benzene rings in the resorcinol (should also pyrogallol) based calix[4]arenes. They are (a) crown (= cone), (b) saddle (= 1,3-alternate), (c) boat (= flattened cone), and (c) chair (= flattened partial cone). However, the presence of extraannular OH groups favours the crown conformation (see Fig. 6.3).

crown   saddle

boat   chair
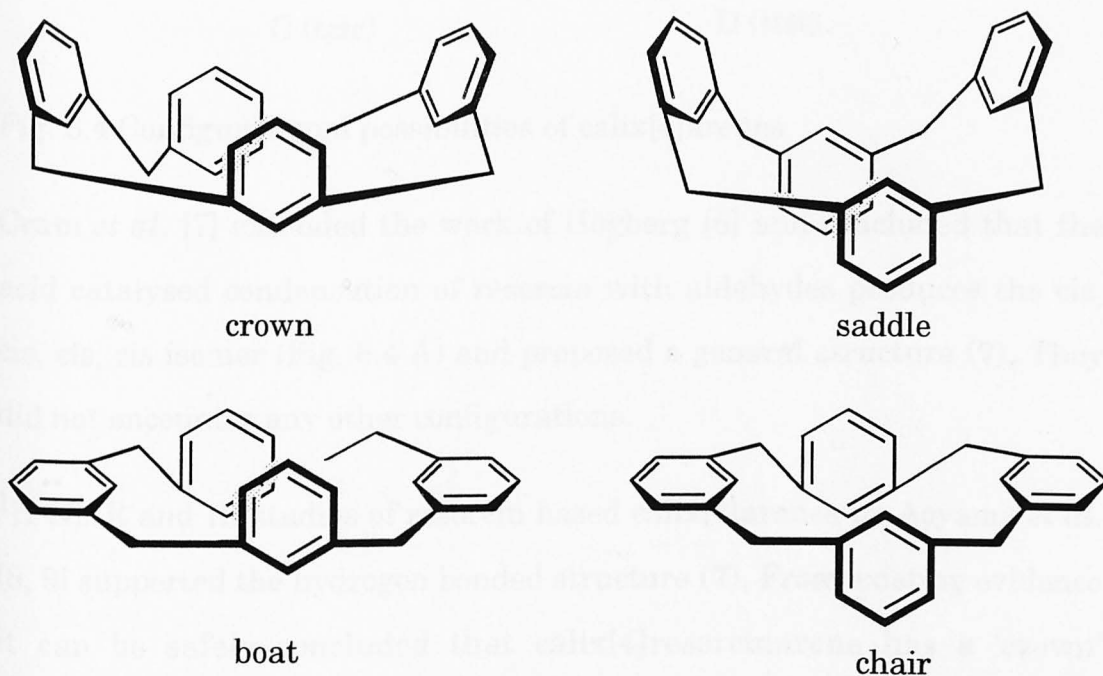
Fig. 6.3 Conformations of the resorcin (or pyrogallol) derived calixarenes. Figures taken from reference [5]

When the groups attached to the bridging methylene groups (introduced by the aldehyde used in the condensation) are considered there are four configurational as well as conformational possibilities [5]. These are A (cis,

cis, cis, cis), B (trans, cis, cis,trans), C (trans, cis, trans, cis) and D (trans, trans, trans trans) (see Fig 6.4).
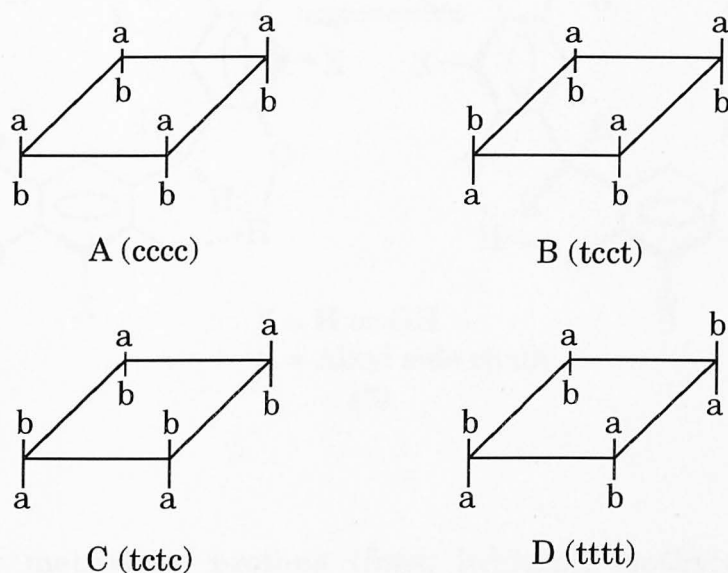
Fig. 6.4 Configurational possibilities of calix[4]arenes

Cram *et al.* [7] extended the work of Högberg [6] and concluded that the acid catalysed condensation of resorcin with aldehydes produces the cis, cis, cis, cis isomer (Fig. 6.4 A) and proposed a general structure (7). They did not encounter any other configurations.

^{1}H NMR and IR studies of resorcin based calix[4]arenes by Aoyama *et al.* [8, 9] supported the hydrogen bonded structure (7). From existing evidence it can be safely concluded that calix[4]resorcinarene has a 'crown' conformation. There is little comparable evidence from the study of calix[4]-pyrogallolarene (4) that it is assumed to possess the same general features as (3). The nature of the ^{1}H NMR spectra of calix[4]resorcinarene and calix[4]pyrogallolarene in CD_3OD recorded for the present study were found to be almost similar. Calix[4]resorcinarene has two different sets of aromatic protons, four from upper rim and four from the lower rim and a

X = H or OH
R = Alkyl side chain
(7)
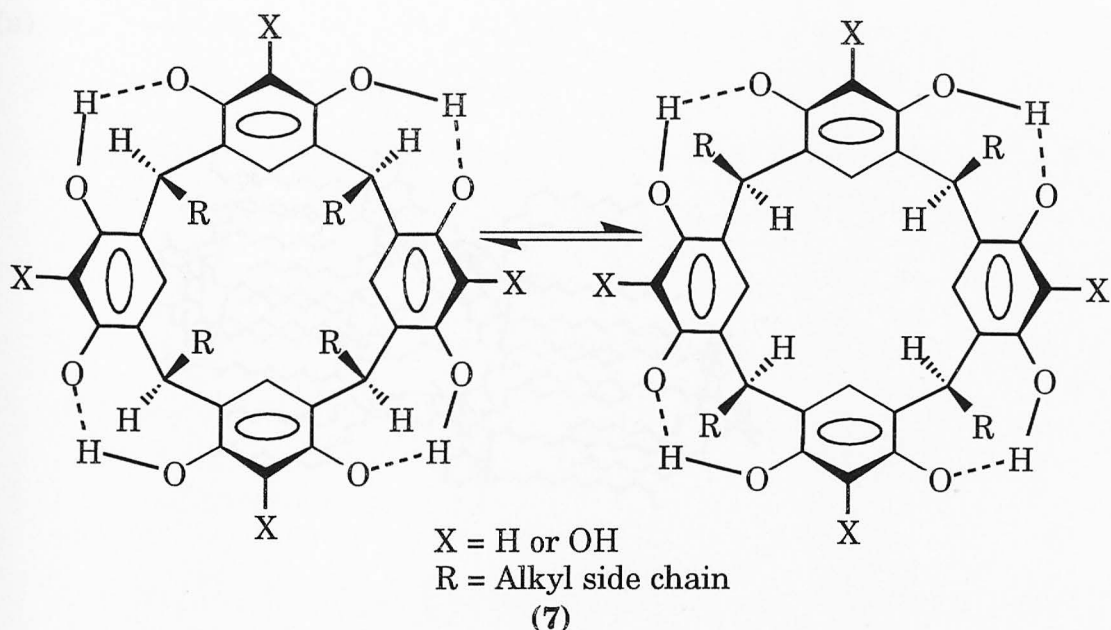
set of four methylene protons (from bridging methylene groups). Strikingly, two singlet signals for those of aromatic protons and one triplet for methylene protons were observed which implies that there are two equivalent sets of aromatic protons and one equivalent set of methylene protons (see Fig. 6.2). A similar situation was encountered for calix[4]pyrogallolarene where a singlet for aromatic and a triplet for methylene protons were observed (Fig. 6.2). These ^{1}H NMR data imply that both alkyl side chains and aromatic rings are symmetrically arranged and the two compounds have a similar structure. Asymmetry in the arrangement of the benzene rings and/or alkyl side chains would have produced more than one set of signals for the aromatic as well as the methylene protons.

In recent X-ray crystallographic studies [9a, 9b], aromatic rings in both calix[4]resorcinarene and calix[4]pyrogallolarene have been found to be arranged in an all-cis structure which confirms the structures (7) suggested by NMR [8] (see Fig. 6.5). The hydroxy groups are juxtaposed, indicating hydrogen bonding around the ring system.

(a)
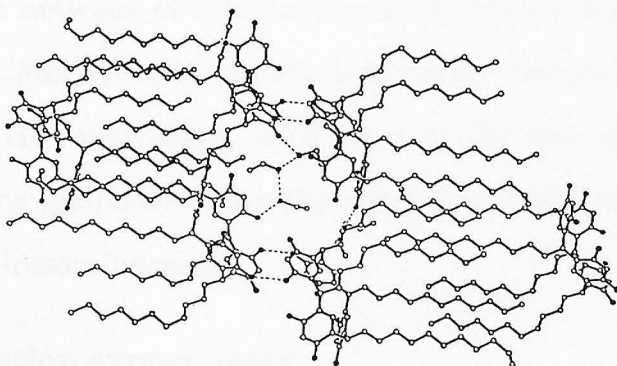
(b)
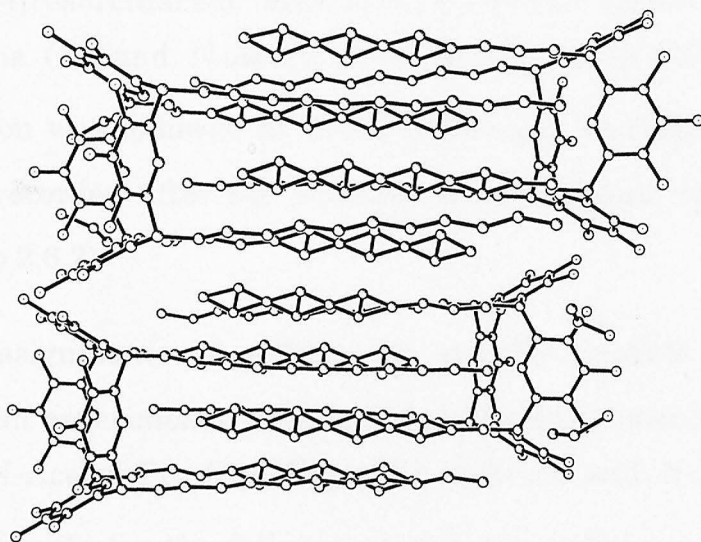
Fig. 6.5 X-ray structures of (a) calix[4]resorcinarene and (b) calix[4]pyrogallol-arene. Figures (a) and (b) are taken from references [9a] and [9b], respectively.

Calix[4]resorcin-arene packs in a bowl-to-bowl fashion and alkyl side chains interdigitate with those of the adjacent calix[4]resorcinarene. An extensive network of intermolecular hydrogen bonding between adjacent bowls of Calix[4]-resorcinarene is probably responsible for this type of close packing. However, there is no evidence for bowl-to-bowl close packing in calix-[4]pyrogallolarene but the alkyl side chains interdigitate similarly as in calix[4]resorcinarene.

6.3 Titration experiments

High resolution 400 MHz ^{1}H NMR spectroscopy was employed to monitor the substrate-calix[4]arene complexation processes. The analytical technique adopted was similar to that employed for caffeine-tannin binding studies and is detailed section 5.2.

Calix[4]resorcinarene and calix[4]pyrogallolarene were titrated into caffeine (1) and N-Acetyl-Pro-Gly-NH$_2$ (2) in CD$_3$OD at 295 K. The titration was followed by one-dimensional ^{1}H NMR experiments which were recorded after the addition of each aliquot of calix[4]arenes (see section 2.6.2).

The assignments of caffeine (1) and the peptide protons during the titration experiments were based on the assignment of free caffeine and free N-Acetyl-Pro-Gly-NH$_2$. The caffeine and N-Acetyl-Pro-Gly-NH$_2$ assignments for the following titrations: caffeine-calix[4]resorcinarene, caffeine-calix[4]pyrogallolarene, N-Acetyl-Pro-Gly-NH$_2$-calix[4]resorcin-arene, and N-Acetyl-Pro-Gly-NH$_2$-calix[4]pyrogallolarene are presented in appendices A.3.1-A.3.4, respectively.

6.4 Results

6.4.1 Observations

Both calix[4]resorcenarene and calix[4]pyrogallolarene easily aggregate or crystallise in CD_3OD at ambient temperature when they are pure. Calix[4]pyrogallolarene was found to be more soluble compared to calix[4]resorcinarene. Both compounds readily dissolved in a 2 mM solution of caffeine or N-Acetyl-Pro-Gly-NH_2. The bowl-to-bowl packing is probably disturbed by caffeine or N-Acetyl-Pro-Gly-NH_2, and they become soluble.

For caffeine-calix[4]arene systems only the H8 and Me7 proton resonances of caffeine were found to move upfield during the titration, whereas Me3 and Me1 protons remained unaffected (see Fig. 6.6). Similarly, for N-Acetyl-Pro-Gly-NH_2-calix[4]arene systems only the proline ring protons moved upfield whereas the glycine protons remained unaffected (see Fig 6.7).
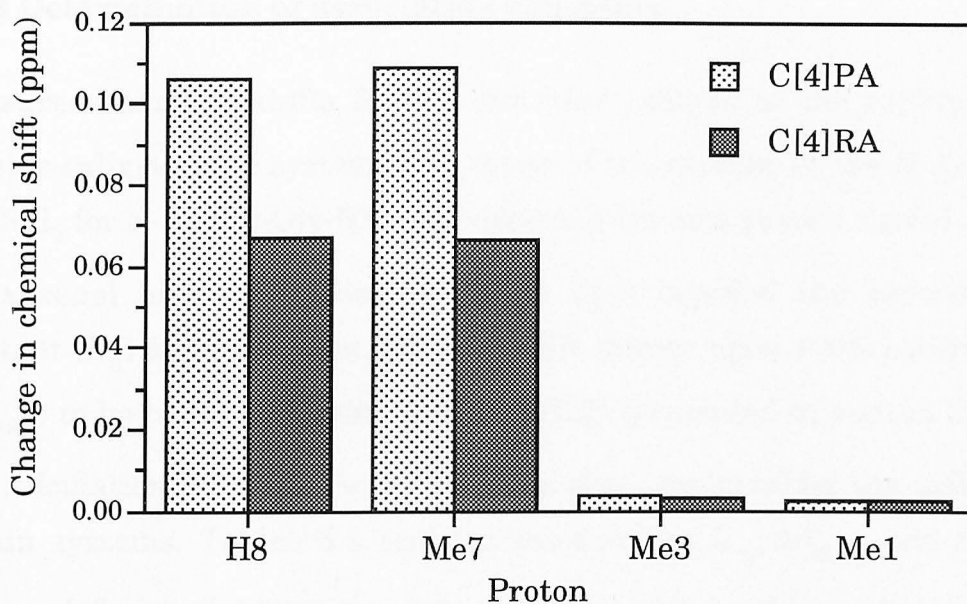
Fig. 6.6 The comparison of the change in chemical shift (ppm) ($\delta_{free}-\delta_{caffeine\ :\ calixarene\ mole\ ratio,\ 1:5}$) of caffeine (3) proton resonances observed on titration with calix[4]pyrogallolarene (C[4]PA) and calix[4]resorcin-arene (C[4]RA) in CD_3OD at 295K.
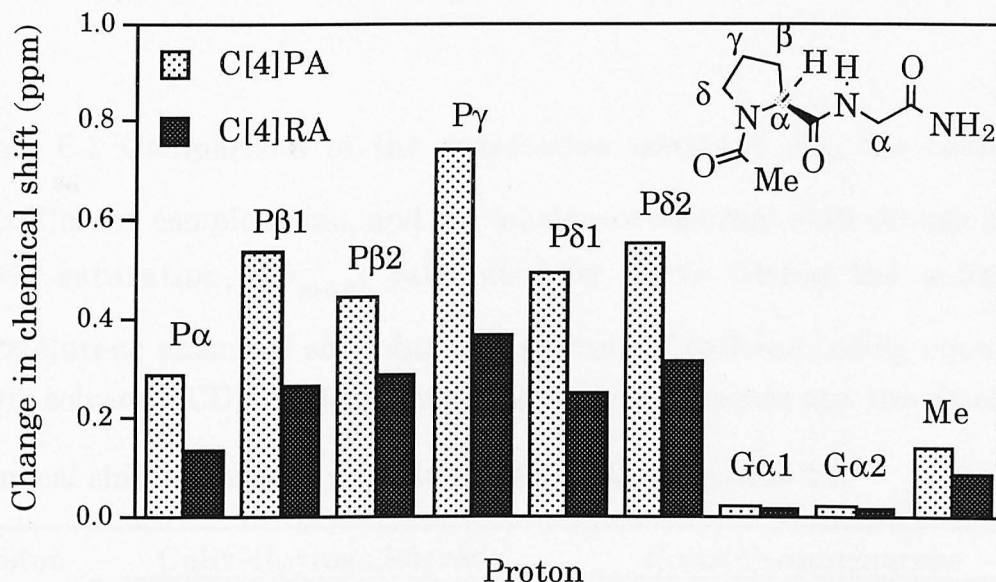
Fig. 6.7 The comparison of the change in chemical shift (ppm) ($\delta_{free}-\delta_{peptide\ :\ calixarene\ mole\ ratio,\ 1:5}$) of N-Ac-Pro-Gly-$NH_2$ (2) proton resonances observed on titration with calix[4]pyrogallolarene (C[4]PA) and calix[4]resorcinarene (C[4]RA) in CD_3OD at 295K. Key to abbreviations: P = prolin residue, G = glycine residue and Me = methyl group.

162

6.4.2 Determination of association constants

Measured chemical shifts for H8 and Me7 protons of the caffeine for caffeine-calix[4]arene systems and many of the protons of the N-Ac-Pro-Gly-NH$_2$ for N-Ac-Pro-Gly-NH$_2$-calix[4]arene systems yielded curved $\Delta\delta$ vs [calixarene] binding isotherms. These data enabled the association constant (K_a) and maximum chemical shift change upon 100% saturation ($\Delta\delta_{max}$) to be calculated using equation (2.9) (presented in section 2.8.1). The calculation procedure was similar to that employed for the caffeine-tannin systems. Tables 6.1 and 6.2 present the K_a, $\Delta\delta_{max}$ and $\Delta\delta_{obs}$ (observed chemical shift change at mole ratio 1:5) for caffeine-calix[4]arene and N-Ac-Pro-Gly-NH$_2$-calix[4]arene titration data, respectively. The 1:1 binding equation was found satisfactory for the fitting of the data. Fig. 6.8 exemplifies the error in the experimental data.

Table 6.1 Comparison of the association constant, K_a, for caffeine-calix[4]arene complexation, and the maximum chemical shift change upon 100% saturation, $\Delta\delta_{max}$, calculated by curve fitting the caffeine-calix[4]arene chemical shift data for protons of caffeine (using equation (2.9)); solvent = CD$_3$OD; temperature 295 K. $\Delta\delta_{obs}$ values are the observed chemical shift changes at peptide to calixarene mole ratio 1:5.

Proton	Calix[4]pyrogallolarene			Calix[4]resorcinarene		
	K_a (M^{-1})	$\Delta\delta_{max}$ (ppm)	$\Delta\delta_{obs}$ (ppm) (mole ratio 1:5)	K_a (M^{-1})	$\Delta\delta_{max}$ (ppm)	$\Delta\delta_{obs}$ (ppm) (mole ratio 1:5)
H8	8.9	1.798	0.145	5.5	1.905	0.067
Me7	16.0	1.093	0.147	4.9	2.074	0.066

163

Table 6.2 Comparison of the association constant, K_a, for N-Ac-Pro-Gly-NH$_2$-calix[4]arene complexation, and the maximum chemical shift change upon 100% saturation, $\Delta\delta_{max}$, calculated by curve fitting the N-Ac-Pro-Gly-NH$_2$-calix[4]arene chemical shift data for protons of N-Ac-Pro-Gly-NH$_2$ (using equation (2.9)); solvent = CD$_3$OD; temperature 295 K. $\Delta\delta_{obs}$ values are the observed chemical shift change at peptide to calixarene mole ratio 1:5.

Proton	Calix[4]pyrogallolarene			Calix[4]resorcinarene		
	K_a (M^{-1})	$\Delta\delta_{max}$ (ppm)	$\Delta\delta_{obs}$ (ppm)	K_a (M^{-1})	$\Delta\delta_{max}$ (ppm)	$\Delta\delta_{obs}$ (ppm)
Pα	47.4	0.923	0.285	10.0	1.350	0.135
Pγ	36.1	2.923	0.744	-	-	-
Pδ1	48.7	1.559	0.491	11.3	2.654	0.246
Gα1	51.2	0.062	0.020	6.4	0.241	0.016
Me	43.1	0.482	0.140	13.2	0.669	0.085

Average K_a for C[4]PA = 45.4 ± 6.0 M^{-1}

Average K_a for C[4]RA = 10.2 ± 2.9 M^{-1}
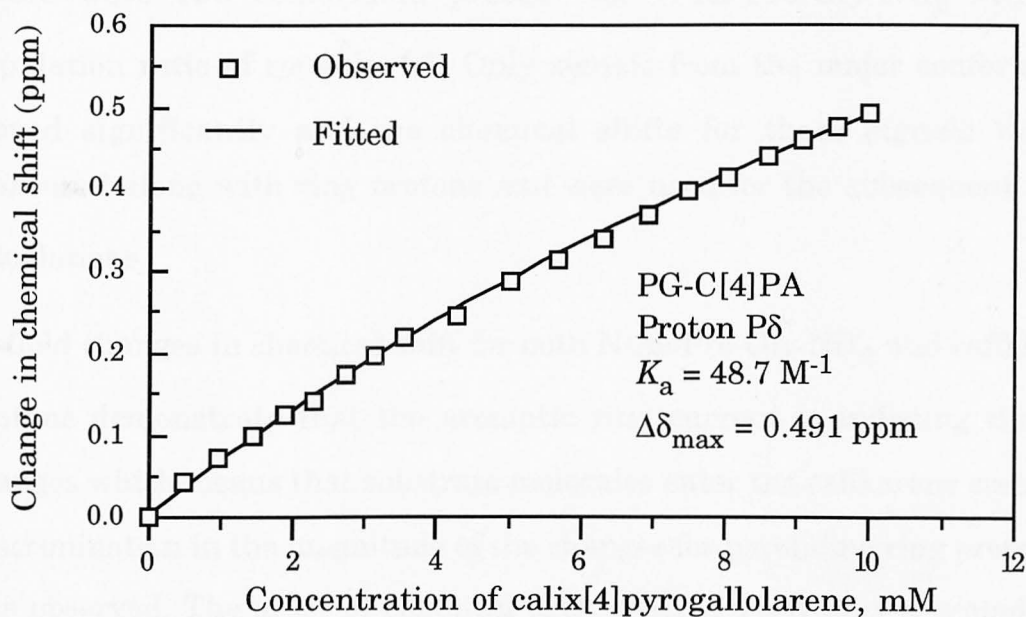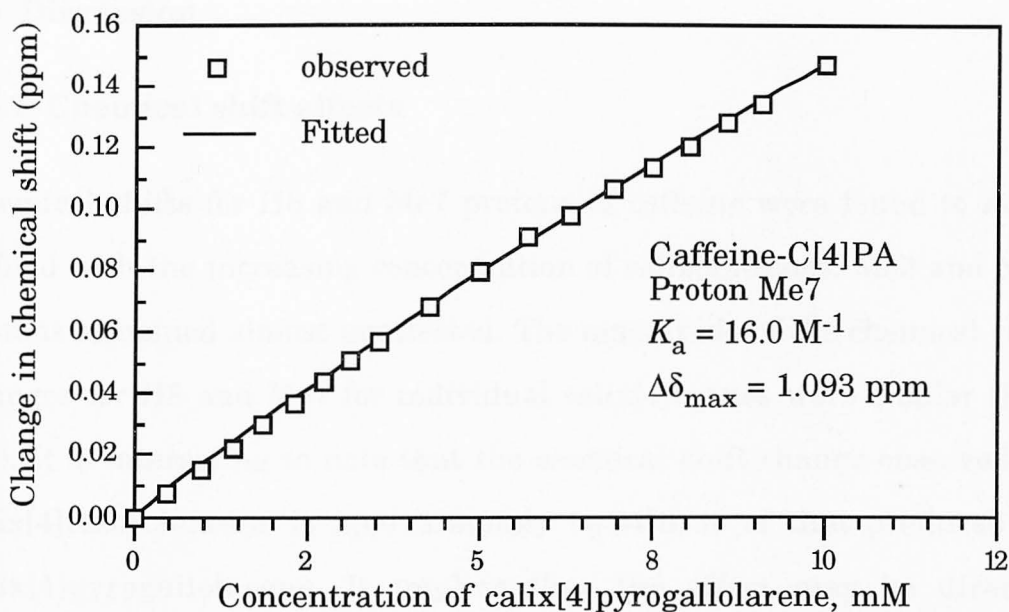
Fig. 6.8 Comparison of observed and fitted chemical shift differences for the proton resonances of substrates as a function of concentration of calixarene. Key to abbreviations: C[4]PA = calix[4]pyrogallolarene, PG = N-Ac-Pro-Gly-NH$_2$, Pδ = proton attached to δ carbon of proline residue.

165

6.5 Discussion

6.5.1 Chemical shift effects

Chemical shifts for H8 and Me7 protons of caffeine were found to move upfield with the increasing concentration of calix[4]arenes. Me3 and Me1 protons remained almost unaffected. The magnitude of the chemical shift changes for H8 and Me7 for individual calix[4]arenes were similar (Fig. 6.6). It is interesting to note that the chemical shift change observed by calix[4]resorcinarene is approximately two-thirds of that produced by calix[4]pyrogallolarene. It implies that the effect may be directly proportional to the number of OH groups attached to the aromatic rings.

Roughly a similar situation was encountered for the N-Ac-Pro-Gly-NH$_2$-calix[4]arene systems. Proline ring protons were largely affected (Fig. 6.7). There were two conformers present for N-Ac-Pro-Gly-NH$_2$ with a population ratio of roughly 4:1. Only signals from the major conformer moved significantly and the chemical shifts for these signals were measured along with ring protons and were used for the subsequent K_a calculations.

Upfield changes in chemical shift for both N-Ac-Pro-Gly-NH$_2$ and caffeine protons demonstrate that the aromatic ring current is inducing these changes which means that substrate molecules enter the calixarene crater. Discrimination in the magnitude of the changes for pyrolidine ring protons was observed. The order of chemical shift change: $\gamma > \beta \approx \delta > \alpha$ probably indicates the preferred orientation of the ring inside the calix[4]arene crater (see Fig. 6.9).

166

6.5.2 Analysis of K_a values

K_a values were obtained for individual protons of N-Ac-Pro-Gly-NH$_2$ that yielded curved isotherms and were averaged to give an overall K_a value and standard deviation.

The strength of binding was found roughly to depend on the number of OH groups in the calix[4]arene molecule. The binding strength of the N-Ac-Pro-Gly-NH$_2$-calix[4]resorcinarene complex was roughly two-thirds of that of the N-Ac-Pro-Gly-NH$_2$-calix[4]pyrogallolarene complex. This implies that additional OH group is an important factor in the binding process.

Only H8 and Me7 protons of caffeine were found to give rise to $\Delta\delta$ vs [calixarene] binding isotherms. Differential K_a values were obtained for H8 and Me7 protons for caffeine-calix[4]pyrogallolarene system. The reason for this is not known. However, the caffeine-calix[4]resorcinarene system gave similar K_a values for H8 and Me7 protons.

Calix[4]pyrogallolarene binds both caffeine and N-Ac-Pro-Gly-NH$_2$ more strongly, roughly three times, compared to calix[4]resorcinarene (see Tables 6.1 and 6.2).

6.5.3 Binding of caffeine and N-Ac-Pro-Gly-NH$_2$ to calix[4]arene

Caffeine and N-Ac-Pro-Gly-NH$_2$ have several common features such as (a) a strong hydrophobic ring face, (b) tertiary amine groups and (c) a carbonyl oxygen linked to a tertiary nitrogen function. Carbonyl groups attached to tertiary amides are good proton acceptors [10-14].

The equivalency of the benzene rings and four methylene moieties in the ^{1}H NMR spectra implies that both calix[4]resorcinarene and calix[4]pyrogallolarene have a symmetrical macrocyclic skeleton. The OH

groups situated on the upper rim of the calix crater are internally hydrogen bonded [8]. Both calix[4]resorcinarene and calix[4]pyrogallol-arene have two important features:

(a) they have two (resorcin based) or three (pyrogallol based) hydrogen bonded OH groups as the unit-binding sites for guest substrates containing hydrogen bonding accepting groups, and

(b) the availability of multiple independent hydrophobic surfaces which are separated by m-phenylene bridges.

Examination of the chemical shift data implies that the five-membered ring part of caffeine enters into the calix[4]arene crater. This is evident from the perturbations of equal magnitude for the H8 and Me7 protons whereas the Me3 and Me1 protons remained unaffected. Probable reasons for this selective association could be that the five-membered ring is more hydrophobic and smaller in size than the six-memberd ring. Close inspection of molecular models of caffeine and calix[4]arenes indicates that the orientation of caffeine inside the crater facilitates multiple hydrogen bonding via tertiary amide (position 9) and carbonyl oxygen attached to tertiary N (position 4) with the opposite facing aromatic OH groups (see Fig. 6.10).

The pyrollidine ring of N-Ac-Pro-Gly-NH$_2$ enters the calixarene crater. This is consistent with the chemical shift data in which the proline ring protons were perturbed and glycine protons remained unaffected. The methyl proton signal moved upfield significantly. This implies that the dominant rotational isomer of N-Ac-Pro-Gly-NH$_2$ is one in which the methyl group lies on the side of proline (Fig. 6.11).
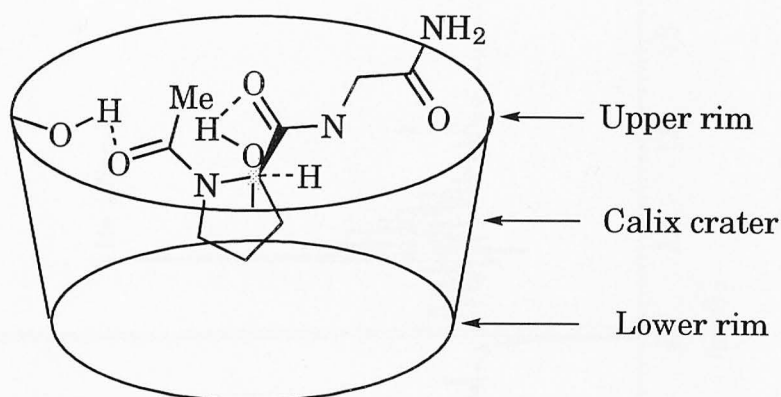
Fig. 6.9 Mode of N-Ac-Pro-Gly-NH$_2$-calix[4]arene binding.
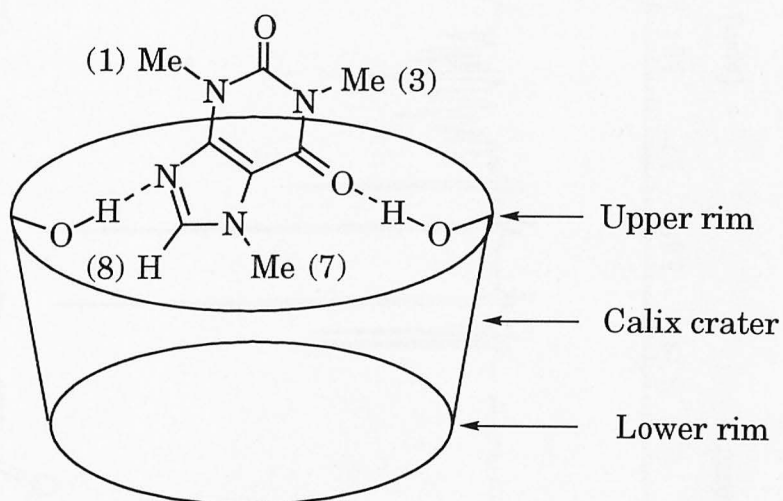
Fig. 6.10 Mode of caffeine-calix[4]arene binding.
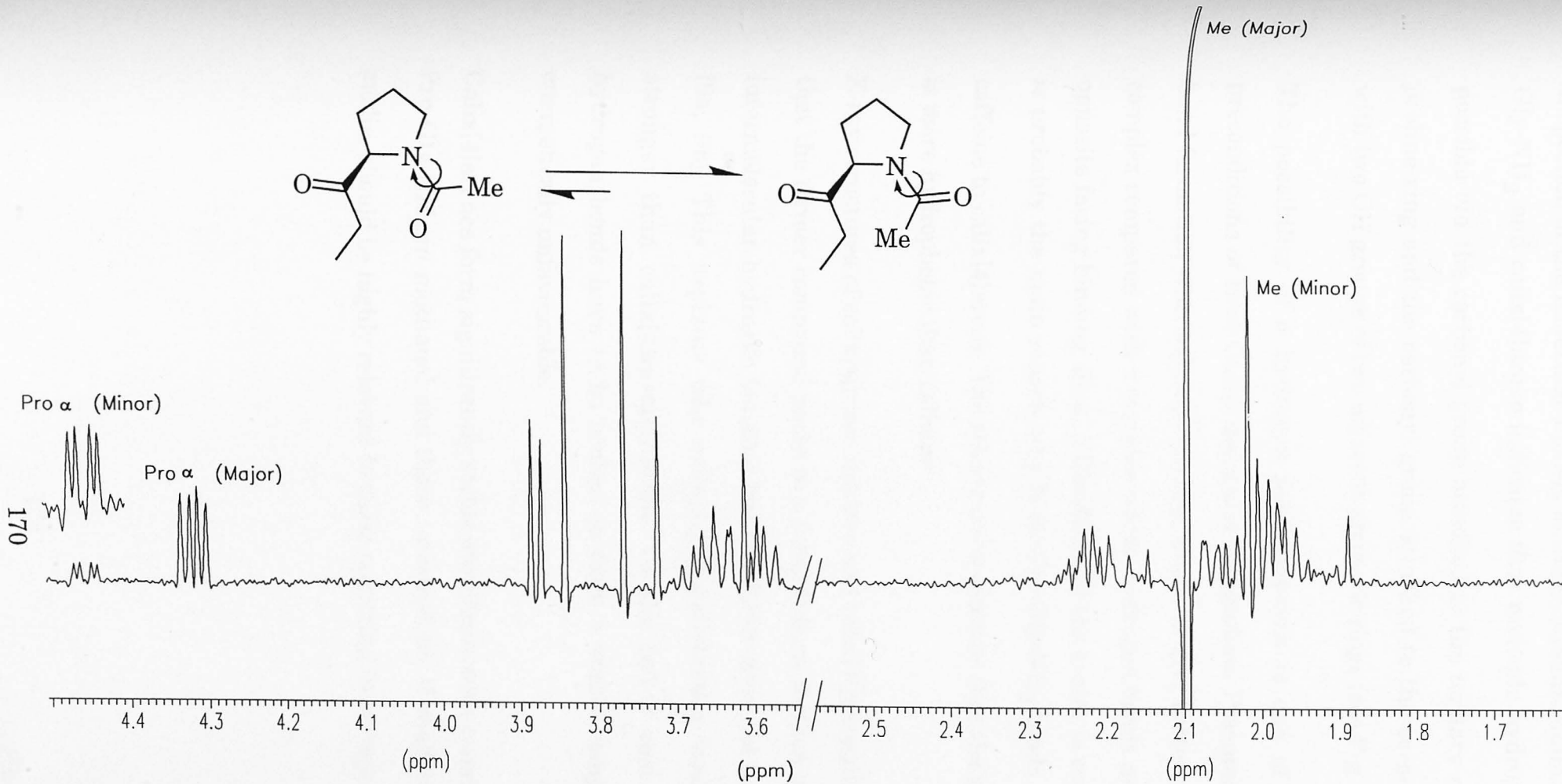
Fig. 6.11 Molecular formula and ^{1}H NMR spectrum of N-Ac-Pro-Gly-NH$_2$ recorded in CD$_3$OD, 400 MHz at 295K, showing major and minor rotamers.

Inspection of the molecular models of the dominant rotamer of N-Ac-Pro-Gly-NH$_2$ and calix[4]arene indicates that multiple hydrogen bonding is possible *via* the carbonyl group attached to the tertiary nitrogen of the proline ring and the carbonyl group attached to the secondary nitrogen with two OH groups of two adjacent aromatic rings (see Fig. 6.9).

The possibility of a hydrogen bond network is one of the essential preconditions of Host-Guest molecular recognition. Presumably, hydrogen bond formation with adjacent binding sites will give better stability to the complex compared with a complex where hydrogen bonds are formed with opposite facing binding sites, if flexibility of the crater is considered. This is probably the main reason why N-Ac-Pro-Gly-NH$_2$ binds stronger than caffeine to calix[4]arene. The other reason could be that the pyrolidine ring is more hydrophobic than caffeine.

X-ray structures of calix[4]resorcinarene and calix[4]pyrogallolarene reveal that the former compound packs in a bowl-to-bowl fashion with extensive intermolecular hydrogen bonding but the latter does not pack so tightly [9a, 9b]. This explains why calix[4]pyrogallolarene binds substrates stronger than calix[4]resorcinarene. In the latter case many more hydrogen bonds have to be broken to form a stable complex which is energetically unfavourable.

Calix[4]arenes form significantly stable complexes with caffeine and N-Ac-Pro-Gly-NH$_2$ in methanol and these interactions, if realised in aqueous media, should be highly relevant to those occurring in biological systems.

References

1. Linnane, P. and Shinai, S., *Chemistry & Industry*, 1994, 811.

2. Kurihara, K., Ohto, K., Tanaka, Y., Aoyama, Y. and Kunitake, T., *J. Am.Chem. Soc.*, 1994, **113**, 444.

3. Cornforth, J. W., Hart, P. D., Nicholls, G. A., Rees, R. J. W. and Stock, J. A., *Br. J. Pharmacol.*, 1955, **10**, 73.

4. Cornforth, J. W., Morgan, E. D., Potts, K. T. and Rees, R. J. W., *Tetrahedron*, 1973, **29**, 1659.

5. Gutsche, C. D., *Calixarenes*. Monographs in Supramolecular Chemistry, J. F. Stoddart, Editor, 1989, Cambridge, The Royal Society of Chemistry,

6. Hogberg, A. G. S., *J. Am. Chem. Soc.*, 1980, **102**, 6046.

7. Cram, D. J. and Cram, J. M., *Container Molecules and their Guests*. Monographs in supramolecular Chemistry, J. F. Stoddart, Editor, 1994, Cambridge, The Royal Society of Chemistry.

8. Aoyama, Y., Tanaka, Y. and Suguhara, S., *J. Am. Chem. Soc.*, 1989, **111**, 5397.

9a. Adams, H., Davies, F. and Stirling, C. J. M., *J. Chem. Soc.. Chem. Commun.*, 1994, 2527.

9b Davis, F., Unpublished observations, University of Sheffield, 1995.

10. Fernandez, J. and Lilley, T. H., *J. Chem. Soc. Faraday Trans.*, 1992, **88**, 2503.

11. Wolfenden, R., *Science*, 1983, **222**, 1087.

12. Abraham, M. H., Druce, P. P., Prior, D. V., Barratt, D. G., Morris, J. J. and Taylor, P. J., *J. Chem. Soc. Perkin Trans. 2*, 1989, 1355.

13. Taft, R., Gurke, D., Joris, L., Schleyr, P. v. R. and Rakshys, J. W., *J. Am. Chem. Soc.*, 1969, **91**, 4801.

14. Cheek, P. J. and Lilley, T. H., *J. Chem. Soc. Faraday Trans. 1*, 1988, **84**, 1927.

CHAPTER SEVEN

AN INVESTIGATION INTO THE BINDING OF BRADYKININ AND ITS ANALOGUES WITH TANNINS

7.1 Introduction

Bradykinin is a proline-rich hormone peptide with the amino acid sequence Arg^1-Pro^2-Pro^3-Gly^4-Phe^5-Ser^6-Pro^7-Phe^8-Arg^9. It is released by the activation of its precursor plasma kallikren-kinin (K-K) cascade [1] by certain snake venoms or enzymes with trypsin-like activity and is directly or indirectly involved in a wide variety of physiological processes. Known physiological functions of bradykinin include: stimulation of smooth muscle inhibition of neurotransmission in the spinal cord, strong vasodilation, the release of catecholamines in the adrenal medulla, increased capillary permeation induction of acute arterial hypotension, leucocyte migration and accumulation and initiation of pain and hyperanalgesia, lowering of systemic blood pressure. There is evidence [2] that bradykinin causes inflammatory response, asthma, sepsis, and symptoms related with rhinoviral infection. Bradykinin may also mediate functional vasodilation to acute inflammation in the human body.

Many peptide derived bradykinin antagonists are known but their clinical use is limited due to their poor oral absorption and the short duration of their effects. Efforts have been made to develop bradykinin antagonists from plant sources and known plant derived antagonists [3] include many flavonoids and terpenes although there is no report to date of any plant polyphenols with definite bradykinin antagonistic activity. This study is

intended to give some understanding of the interaction of tannins with bradykinin.
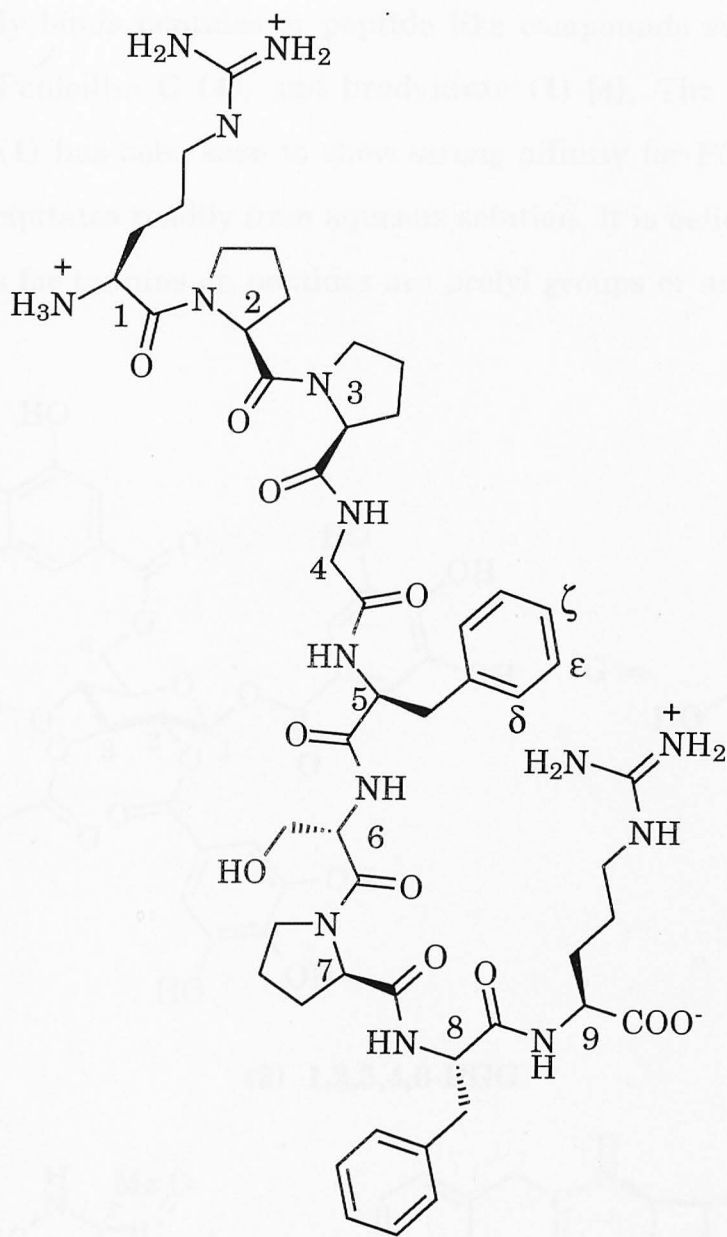
(1) **Bradykinin**

7.2 Current knowledge of tannin-peptide complexation

Generally tannins do not bind effectively to simple peptides but there is evidence that simple peptides, containing one or more prolyl and/or

175

phenylalanyl residues within their molecular structures, have affinity for tannins, and especially for β-penta-O-galloyl-D-glucopyranose (PGG) (2). PGG strongly binds peptides or peptide like compounds such as prolyl amide (3), Penicillin G (4), and bradykinin (1) [4]. The oligopeptide bradykinin (1) has been seen to show strong affinity for PGG (2) and a complex precipitates readily from aqueous solution. It is believed that the binding sites for tannins on peptides are prolyl groups or aromatic rings [5].
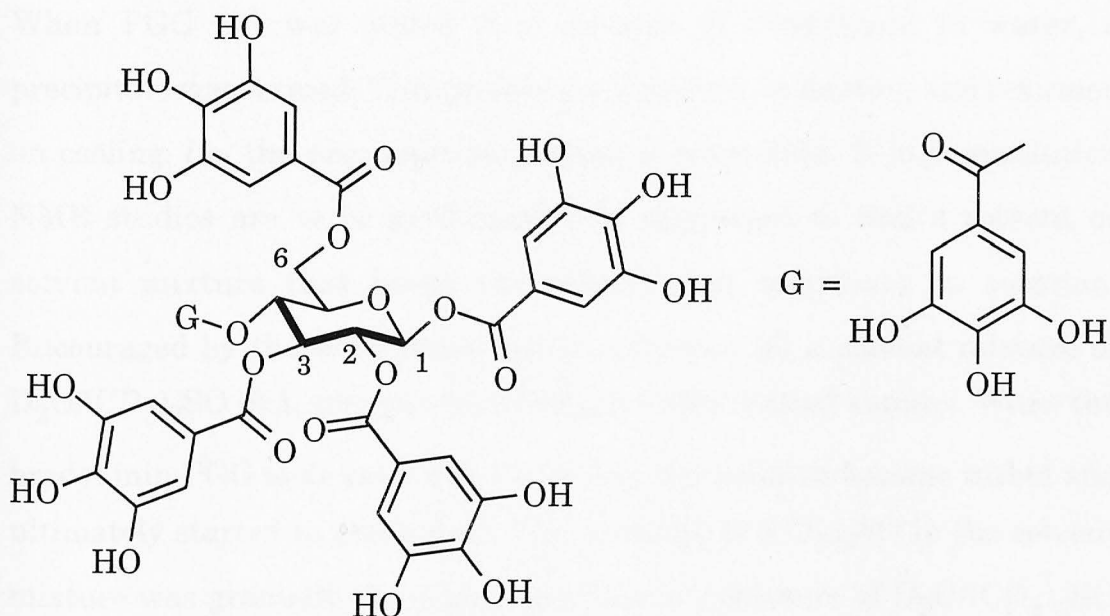
(2) 1,2,3,4,6-PGG
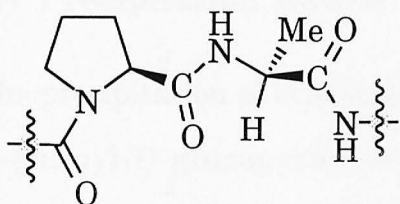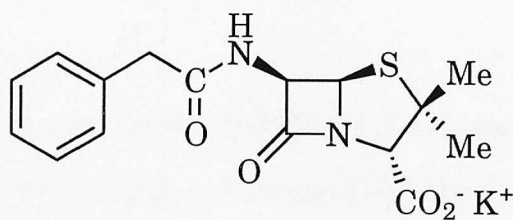
(3)   (4)

Recent NMR studies at Sheffield [6-8] of medium order proline-rich peptides (19 and 22 residues in length) and tannin systems have revealed a great deal of information on tannin-peptide complexation processes. It

176

has been suggested that the main interactions which promote complexation are (a) hydrophobic association between the galloyl rings of tannin and the pyrolidine ring face containing the C_α proton; and (b) hydrogen bonding. The precipitation of peptides with higher concentration of tannins is believed to be caused by a kinetic competition between aggregation and dissociation of the complex.

7.3 Initial studies: addition of PGG to bradykinin

When PGG (2) was added to a solution of bradykinin in water, a precipitate was formed. This precipitate dissolved on heating and reformed on cooling, *i.e.* the precipitation process is reversible. If high resolution NMR studies are to be performed it is important to find a solvent or solvent mixture that keeps the solutes and complexes in solution. Encouraged by the work described in reference [6] a solvent mixture of $D_2O/(CD_3)_2SO$ (9:1, v/v) was tried but gave only limited success. When the bradykinin-PGG mole ratio was 1:2 or less, the solution became turbid and ultimately started to precipitate. The quantity of $(CD_3)_2SO$ in the solvent mixture was gradually increased and finally a mixture of $D_2O/(CD_3)_2SO$ (4:1, v/v) was found satisfactory for NMR studies.

7.4 Precipitation studies

The precipitation of bradykinin (BK) (1) with the tannins β-1,2,3,4,6-penta-O-galloyl-D-glucopyranose (PGG) (2), β-1,2,3,6-tetra-O-galloyl-D-glucopyranose (TeGG) (5), β-1,3,6-tri-O-galloyl-D-glucopyranose (TGG) (6) and procyanidin B-2 (7) was conducted in H_2O at 295K. Aliquots of a 15 mM solution of individual tannins were added (5, 10, 15 µl aliquots) to 300 µl of a 2.0 mM solution of bradykinin. Similarly, precipitation experiments of the bradykinin analogues bradykinin (1-5) (BK(1-5)) (Arg[1]-Pro[2]-Pro[3]-Gly[4]-Phe[5]), desArg[9]-bradykinin (desArg[9]-BK) (Arg[1]-Pro[2]-Pro[3]-Gly[4]-Phe[5]-

Ser[6]-Pro[7]-Phe[8]), and desArg[1]-bradykinin (desArg[1]-BK) (Pro[2]-Pro[3]-Gly[4]-Phe[5]-Ser[6]-Pro[7]-Phe[8]-Arg[9]) with PGG (2) were conducted. The stoichiometry of solutions (threshold) required for precipitation are shown in Table 7.1.

Table 7.1 Precipitation threshold in H_2O at 295 K for the complexation of bradykinin and its analogues with tannins.

System	Onset of precipitation in H_2O (Peptide : tannin)	Comments
BK-B-2	[a]1: 4.00	Redissolved on heating
BK-TGG	1: 0.35	,,
BK-TeGG	1: 0.25	,,
BK-PGG	1: 0.10	,,
BK(15)-PGG	≈1: 0.10	,,
desArg[9]-BK-PGG	≈1: 0.10	,,
desArg[1]-BK-PGG	≈1: 0.10	,,

[a] Value may not be very accurate, colour of procyanidin B-2 prevented accurate assessment.
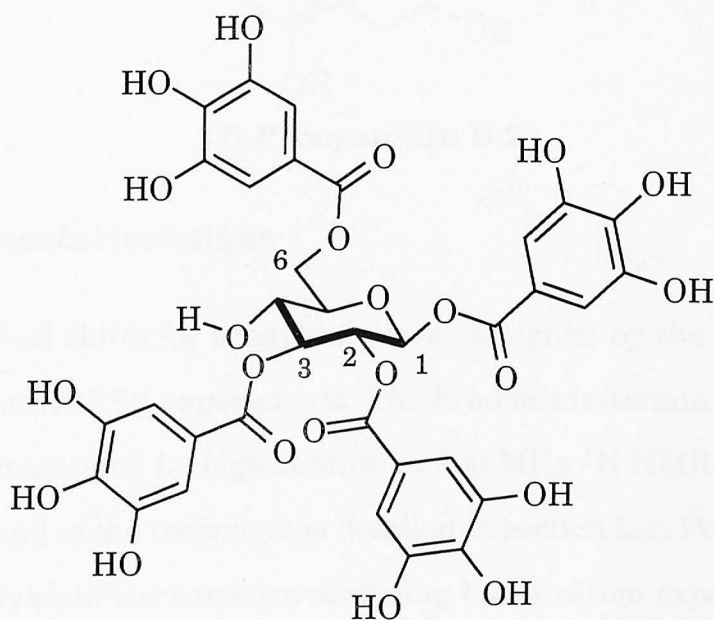
(5) 1,2,3,6-TeGG
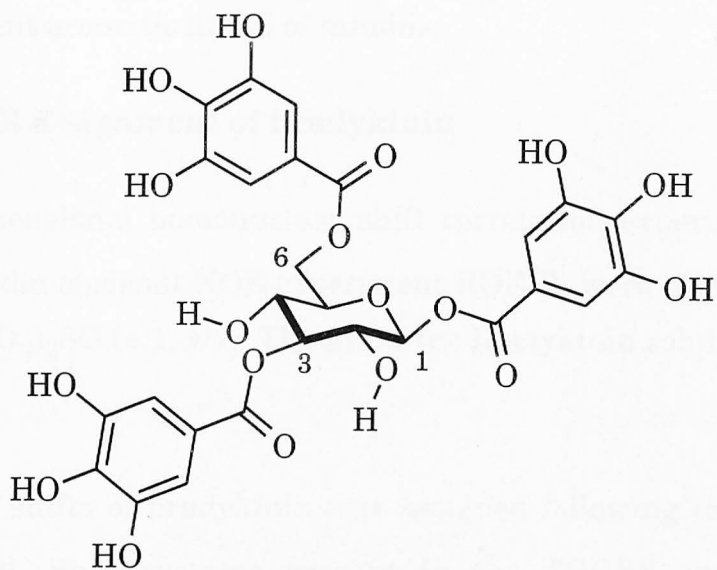
(6) 1,3,6-TGG
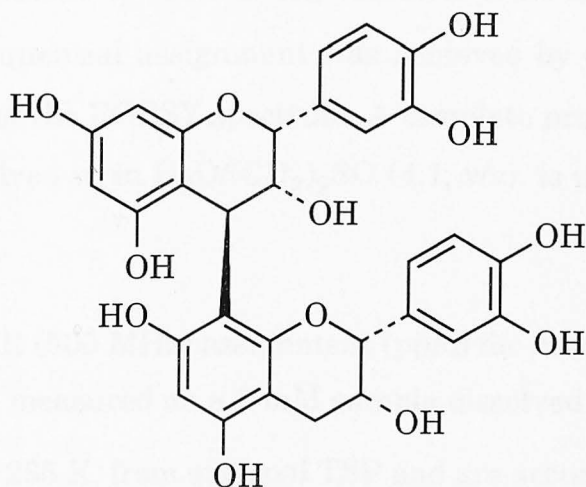
(7) Procyanidin B-2

7.5 Experimental technique

Proton chemical shifts for bradykinin were assigned by the combined use of TOCSY and ROESY experiments. The bradykinin-tannin complexation process was monitored by high resolution 400 MHz ^{1}H NMR spectroscopy. The background of the technique is detailed in section 5.2. Proton chemical shifts of bradykinin were measured during the titration experiments. The change in chemical shifts of bradykinin protons upon addition of tannins is

179

believed to be primarily due to the aromatic ring current effect induced by the constituent aromatic nuclei of tannins.

7.6. ^{1}H NMR assignment of bradykinin

The two-dimensional homonuclear shift correlation experiment TOCSY and the two-dimensional NOE experiment ROESY were performed at 295 K in $H_2O/(CD_3)_2SO$ (4:1, v/v). The pH of the bradykinin solution measured was 5.9.

^{1}H chemical shifts of bradykinin was assigned following the strategy of Wüthrich [9]. Spin systems present in the TOCSY spectrum were identified by reference to random-coil chemical shift tables published in reference [9]. Sequential assignment was achieved by comparison of the NH-CαH region of the ROESY spectrum. A complete proton assignment of bradykinin dissolved in in $H_2O/(CD_3)_2SO$ (4:1, v/v). is presented in Table 7.2.

Table 7.2 ^{1}H NMR (500 MHz) assignment (ppm) for bradykinin. Chemical shift values were measured on a 2 mM sample dissolved in $H_2O/(CD_3)_2SO$ (4:1, v/v), pH 5.9, 295 K, from external TSP and are accurate to ± 0.01 ppm.

Residue	NαH	CαH	CβH	CβH	CγH	CγH	CδH	CδH	NεH
Arg[1]	-	4.31	1.87	1.69	1.69	-	3.11	-	-
Pro[2]	-	4.78	2.42	1.91	2.01	-	3.74	3.48	-
Pro[3]	-	4.42	2.28	1.90	2.05	1.82	3.82	3.68	-
Gly[4]	8.40	3.92, 3.85	-	-	-	-	-	-	-
Phe[5]	8.08	4.58	3.04	3.04	-	-	-	-	-
Ser[6]	8.20	4.68	3.74	3.74	-	-	-	-	-
Pro[7]	-	4.32	1.65	2.14	1.87	-	3.59	-	-
Phe[8]	8.00	4.62	3.22	2.91	-	-	-	-	-
Arg[9]	7.69	4.13	1.82	1.69	1.55	-	3.16	-	7.27

7.7 Titration of tannins into bradykinin and its analogues

The titration of the tannins PGG (2), TeGG (5), TGG (6), and procyanidin B-2 (7), with bradykinin was conducted in $D_2O/(CD_3)_2SO$ (4:1, v/v) at 295K. The pH of the bradykinin solution was measured as 5.9.

One-dimensional ^1H NMR spectra were recorded after addition of each aliquot of tannins (detailed in section 2.7). The free bradykinin proton resonances were assigned by 2D NMR spectra (see section 7.6) and the relative assignments of bradykinin proton resonances during titration were based on these free bradykinin assignments.

The three bradykinin analogues bradykinin (1-5), desArg9-bradykinin and desArg1-bradykinin were chosen for further study. and PGG was titrated into these solutions and the experiments were similarly monitored by ^1H NMR spectroscopy as described above. The proton resonances of the uncomplexed bradykinin analogues were assigned by comparison with the appropriate random coil proton assignments of amino acid residues [9] Experiments were recorded in similar conditions to those described for bradykinin-tannin systems. Chemical shift data showing the assignments of bradykinin and its analogues for the following titrations: bradykinin-PGG, bradykinin-TeGG, bradykinin-TGG, bradykinin-B-2, bradykinin (1-5)-PGG, desArg^9-bradykinin-PGG and desArg^1-bradykinin-PGG, respectively, are presented in Appendices A.4.1-A.4.7.

7.8 Results:

7.8.1 Observed changes in chemical shifts and intermolecular ROE

When tannins were added to solutions of bradykinin, many of the proton resonances of bradykinin were observed to shift upfield and a few were found to move downfield. The largest change in chemical shift was

observed for the N-terminal proline residue (Pro^2) and the two phenylalanyl residues. For the Pro^2 residue, all Cα, Cβ and Cγ proton resonances moved upfield to almost the same extent. Compared to the changes in the chemical shifts for the aromatic protons of phenylalanyl residues, the changes for the nonaromatic (Cα and Cβ) protons of the same residues were not significant. In general Cα protons of all residues (except Pro^2) moved insignificantly compared to Cβ and Cγ protons. The analogues of bradykinin, desArg^9-bradykinin and desArg^1-bradykinin, showed similar behaviour. The residues Pro^2 of bradykinin and Pro^3 of of desArg^1-bradykinin behaved similarly when tannins were added. For bradykinin-PGG and bradykinin-TeGG systems, the Arg$^9\alpha$ protons were found to move downfield, whereas the corresponding protons moved upfield for bradykinin-TGG and bradykinin-B-2 systems. Figs. 7.1-7.7 compare the observed changes in chemical shifts, δ_{free}-δ_{final} peptide-tannin mole ratio, for the Cα, Cβ and aromatic protons of peptides for the following titrations: bradykinin-PGG, bradykinin-TeGG, bradykinin-TGG, bradykinin-B-2, bradykinin (1-5)-PGG, desArg^9-bradykinin-PGG and desArg^1-bradykinin-PGG, respectively.

Interestingly, for the system bradykinin (1-5)-PGG, proton resonances of Arg^1 and Pro^2 residues started to become broad when PGG was added and the signals at the final molar ratio (1:6) were extremely broad (see Fig. 7.8). Consequently the measurements of the chemical shifts for those particular protons were less accurate.

Two ROESY experiments were conducted at 500 MHz for bradykinin alone and bradykinin-PGG at a 1:1 mole ratio, using similar conditions to those used in the titration studies. No intermolecular ROEs were observed.

(a)

(b)
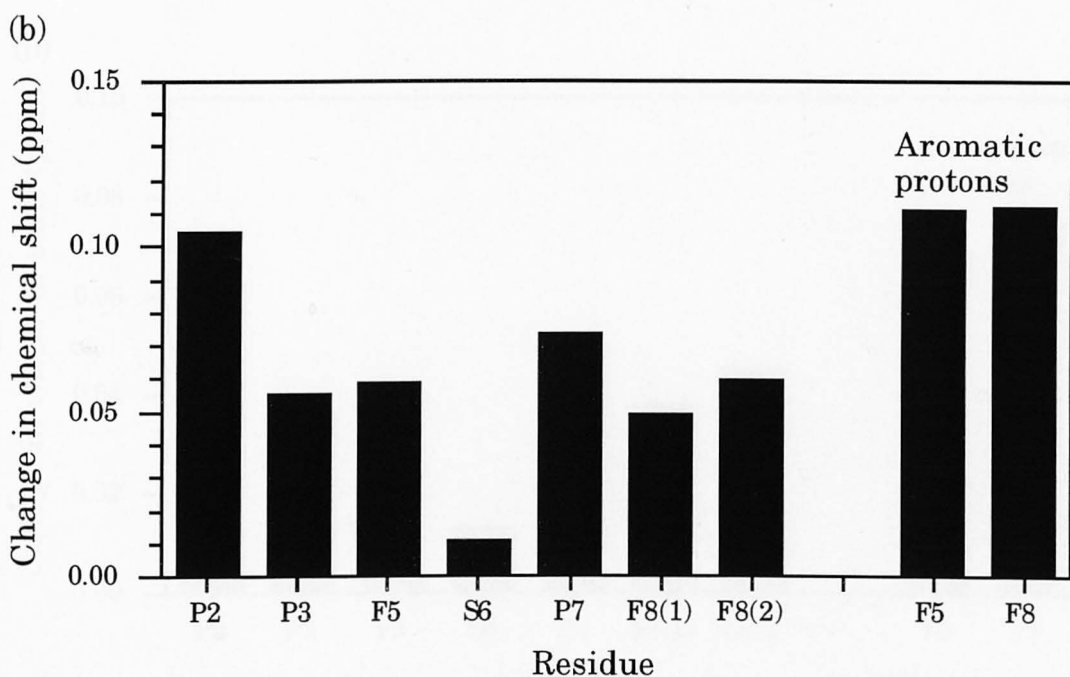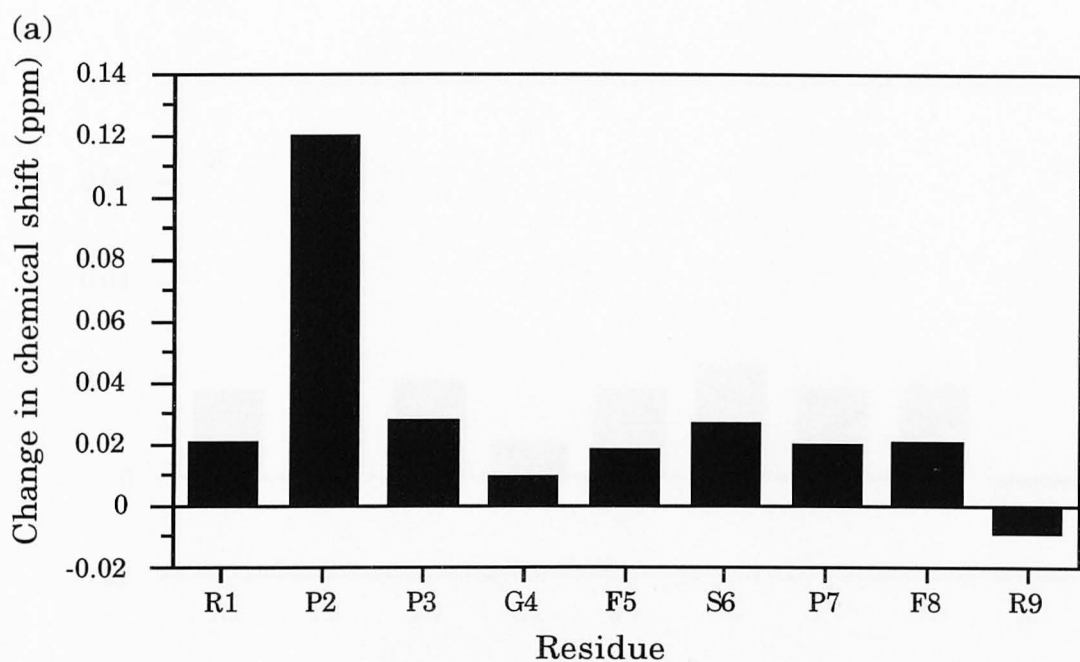
Fig. 7.1 Comparison of the observed change in chemical shift for bradykinin protons during the titration with PGG in $D_2O/(CD_3)_2SO$ (4:1, v/v) at 295 K, pH 5.9. (a) α protons and (b) β and aromatic (averaged) protons. The chemical shift change for the P2α proton was taken from similar titration experiments recorded at 278 K and corrected to 295 K because the signal for this proton was overlapped by the residual HDO protons and measurement was not possible.

Fig. 7.2 Comparison of the observed change in chemical shift for bradykinin protons during the titration with TeGG in $D_2O/(CD_3)_2SO$ (4:1, v/v) at 295 K, pH 5.9. (a) α protons and (b) β and aromatic (averaged) protons. The chemical shift change for the $P2\alpha$ proton was taken from similar titration experiments recorded at 278 K and corrected to 295 K because the signal for this proton was overlapped by the residual HDO protons and measurement was not possible.
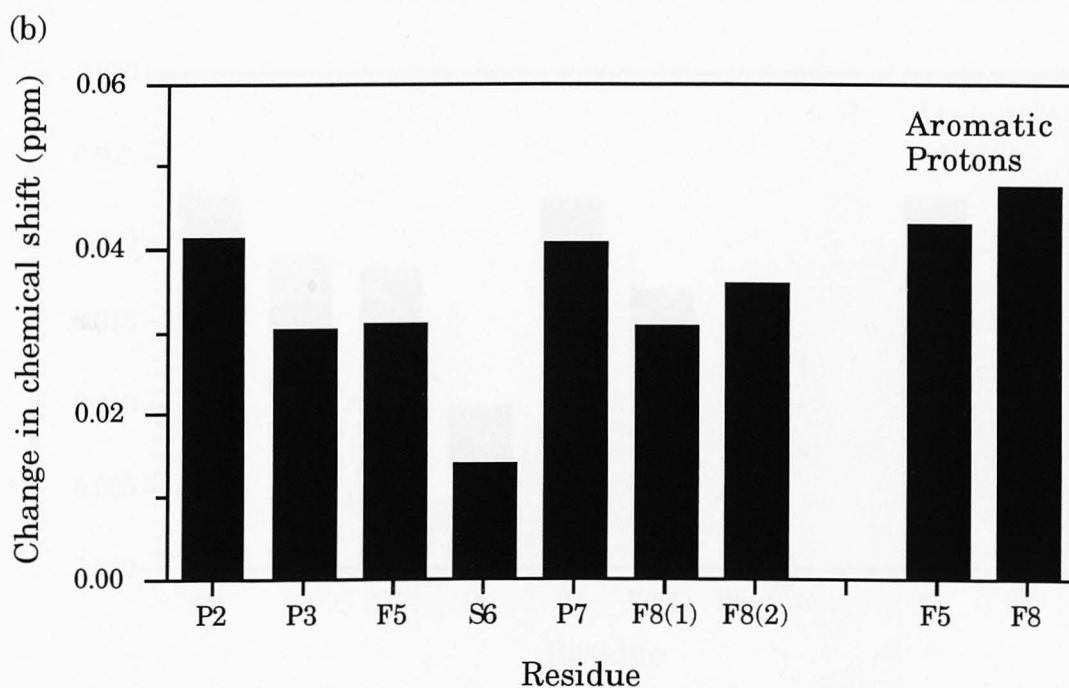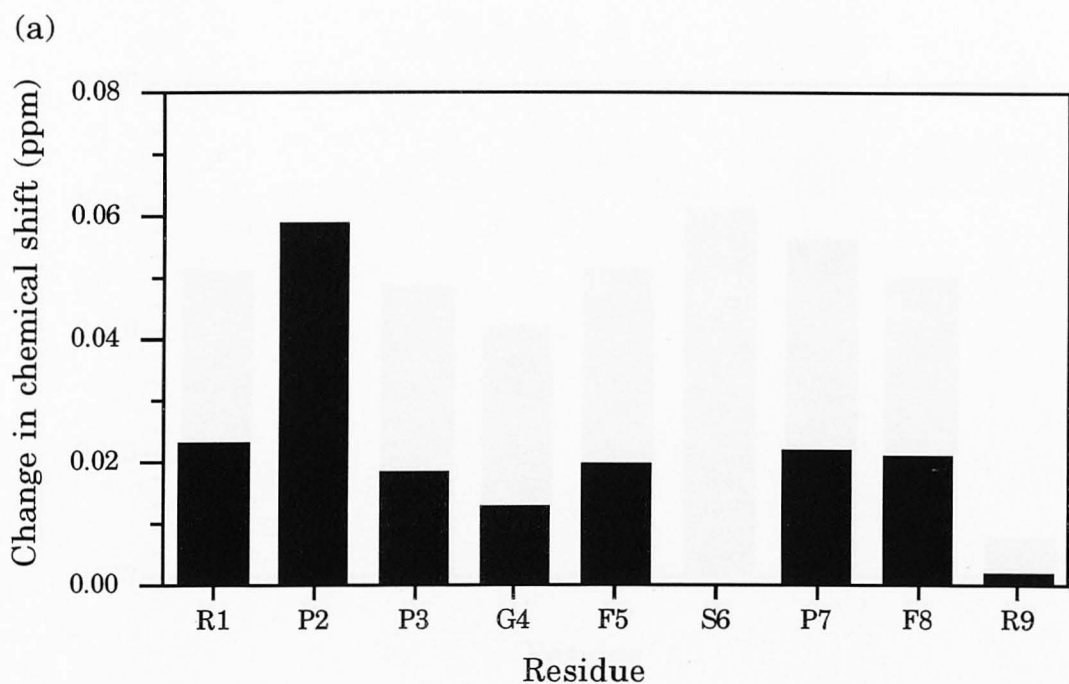
Fig. 7.3 Comparison of the observed change in chemical shift for bradykinin protons during the titration with TGG in $D_2O/(CD_3)_2SO$ (4:1, v/v) at 295 K, pH 5.9. (a) α protons (S6α proton was overlapped by tannin protons) and (b) β and aromatic (averaged) protons. The chemical shift change for the P2α proton was taken from similar titration experiments recorded at 278 K and corrected to 295 K because the signal for this proton was overlapped by the residual HDO protons and measurement was not possible.
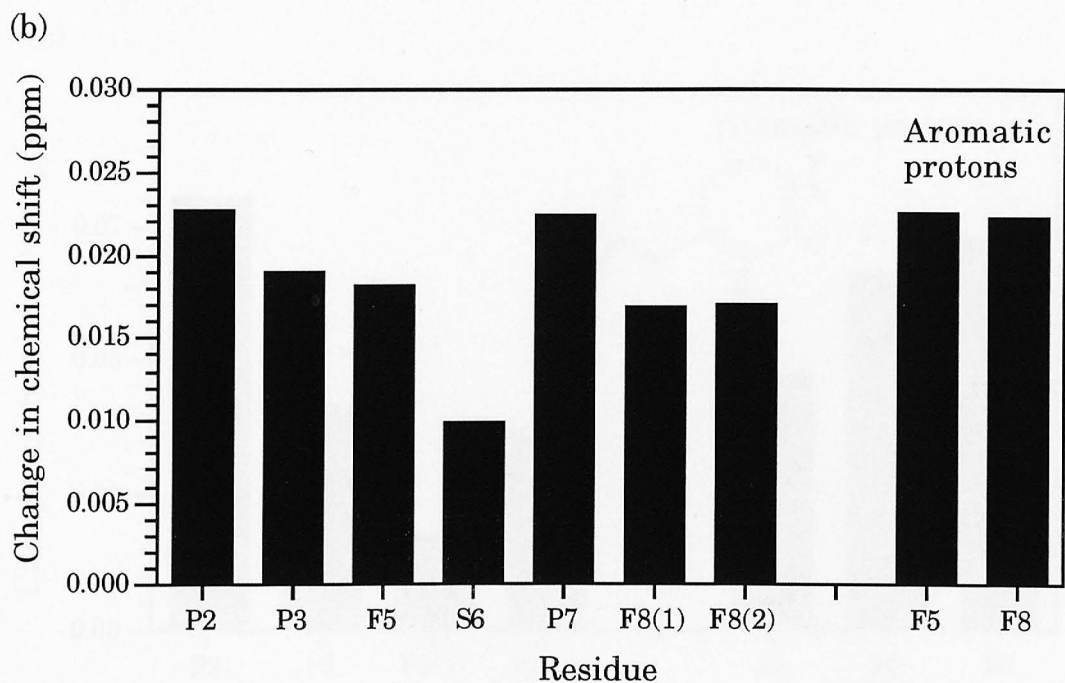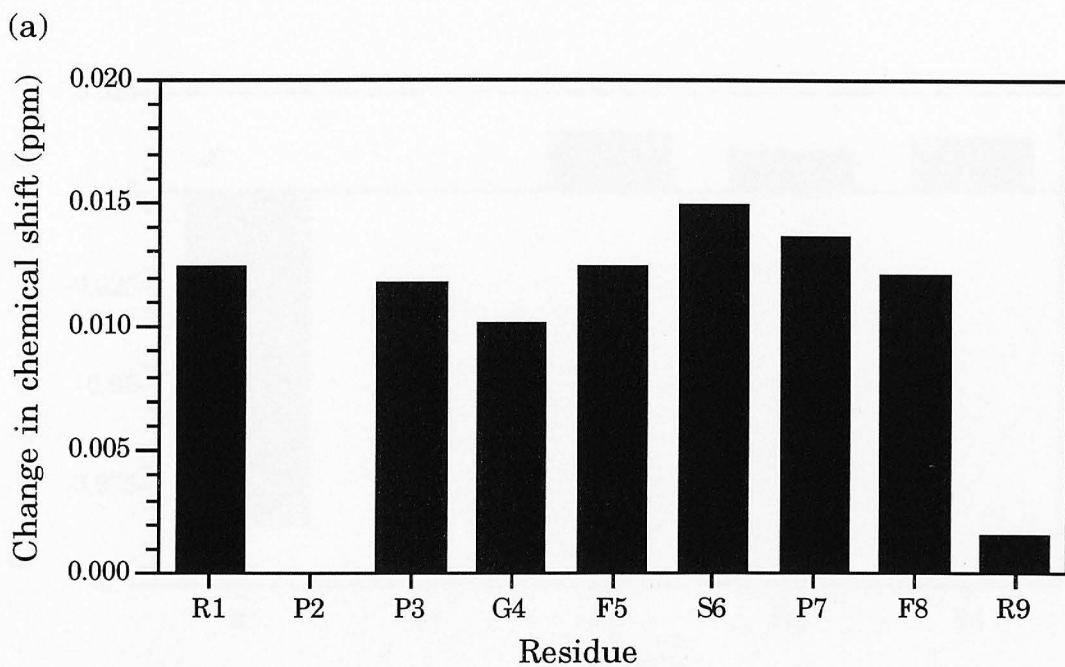
Fig. 7.4 Comparison of the observed change in chemical shift for bradykinin protons during the titration with procyanidin B-2 in $D_2O/(CD_3)_2SO$ (4:1, v/v) at 295 K, pH 5.9. (a) α protons and (b) β and aromatic (averaged) protons. The chemical shift change for the P2α proton was overlapped by the residual HDO signal.

(a)

(b)

Fig. 7.5 Comparison of the observed change in chemical shift for bradykinin (1-5) protons during the titration with PGG in $D_2O/(CD_3)_2SO$ (4:1, v/v) at 295 K. (a) α protons and (b) β and aromatic (averaged) protons. The P2α proton was overlapped by the residual HDO signals.
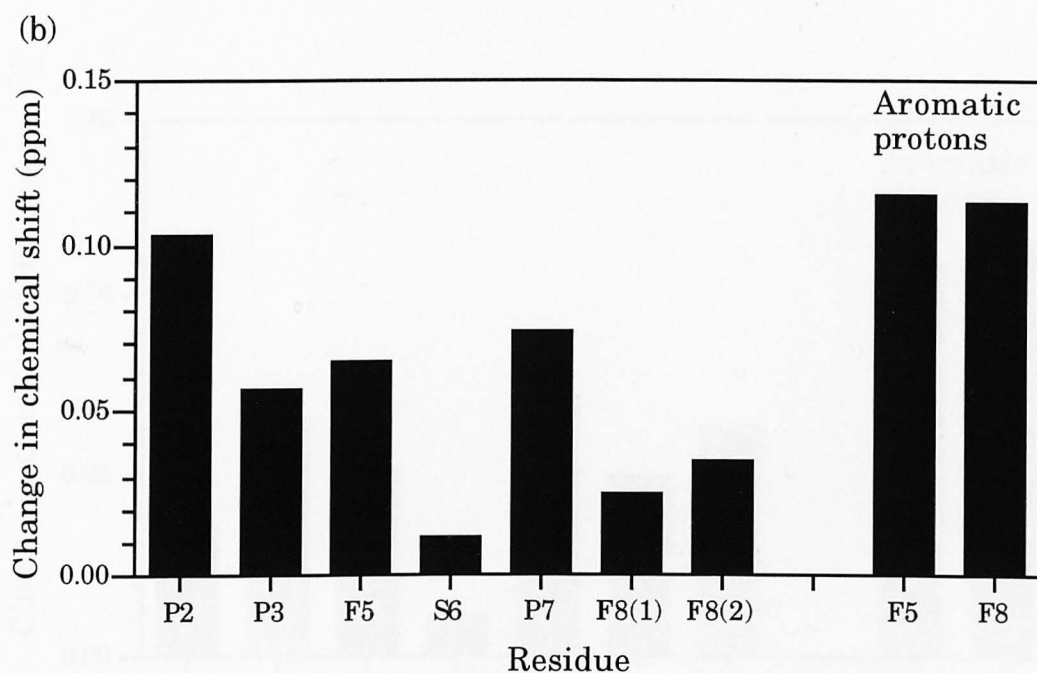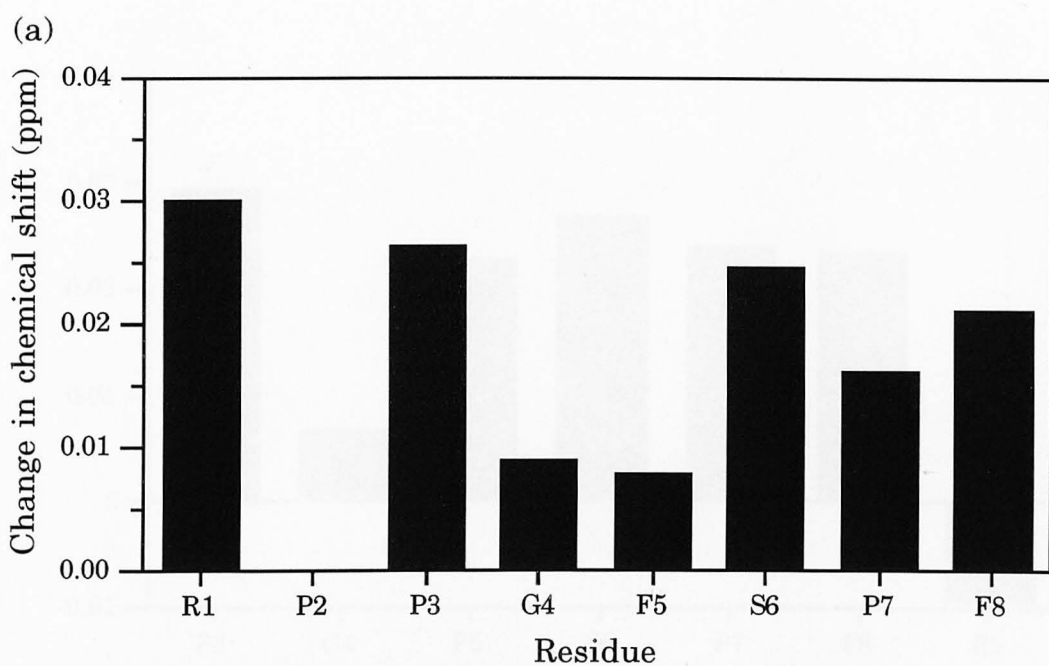
Fig. 7.6 Comparison of the observed change in chemical shift for desArg^{9}bradykinin protons during the titration with PGG in D$_2$O/(CD$_3$)$_2$SO (4:1, v/v) at 295 K. (a) α protons and (b) β and aromatic (averaged) protons. the P2α proton was was overlapped by the residual HDO signal.
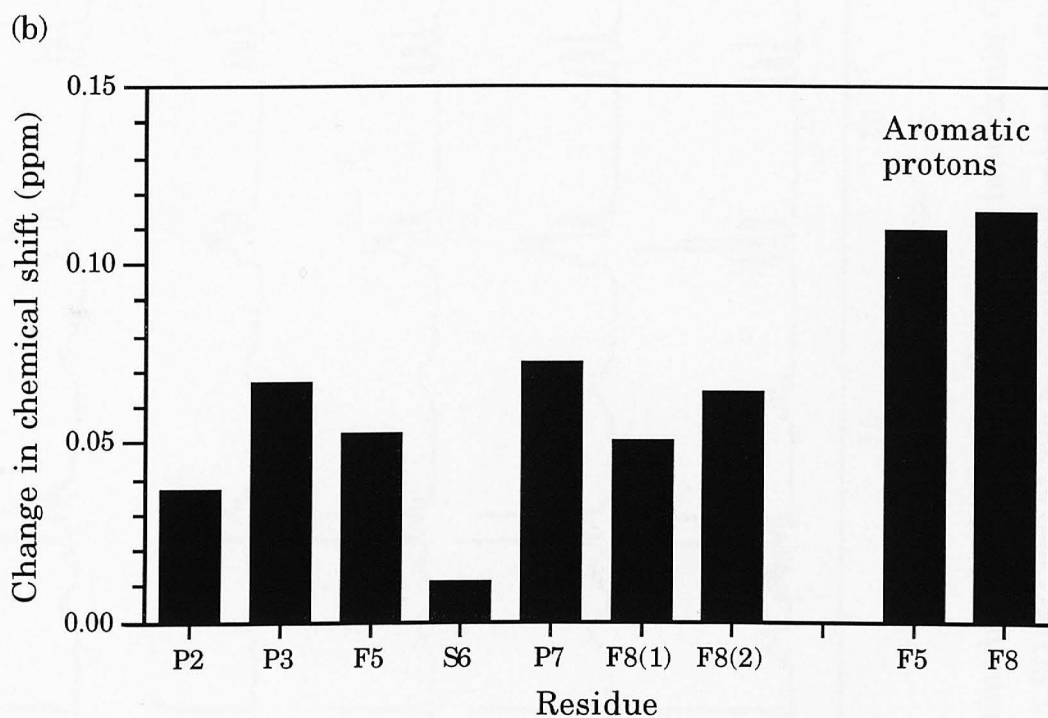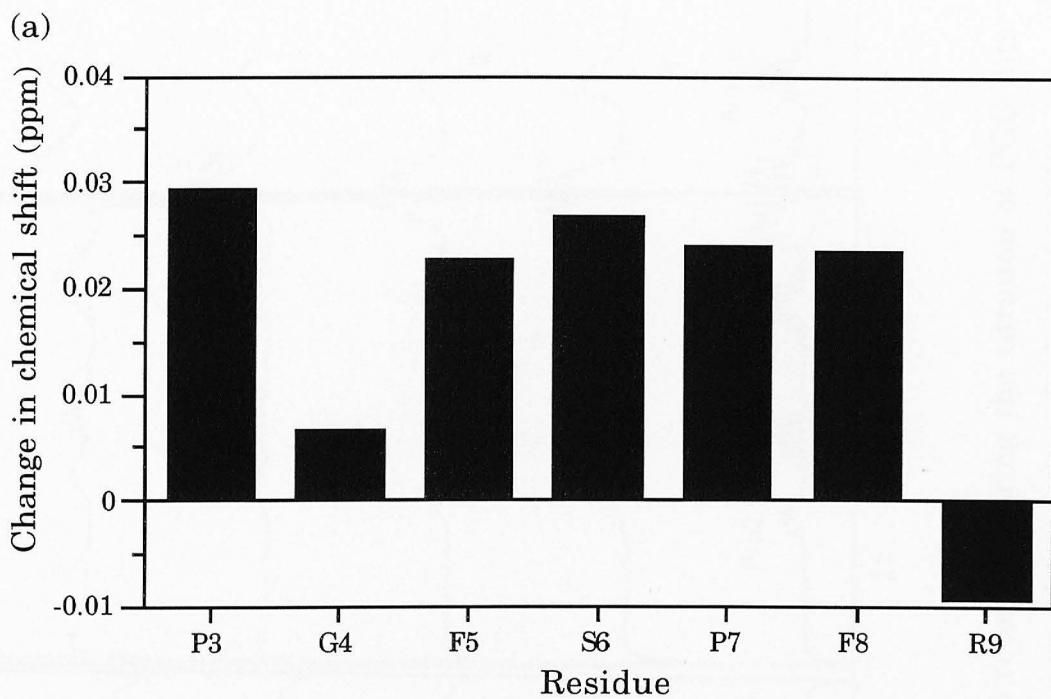
Fig. 7.7 Comparison of the observed change in chemical shift for desArg[1]bradykinin protons during the titration with PGG in $D_2O/(CD_3)_2SO$ (4:1, v/v) at 295 K. (a) α protons and (b) β and aromatic (averaged) protons. The P2α proton was was overlapped by the residual HDO signal.
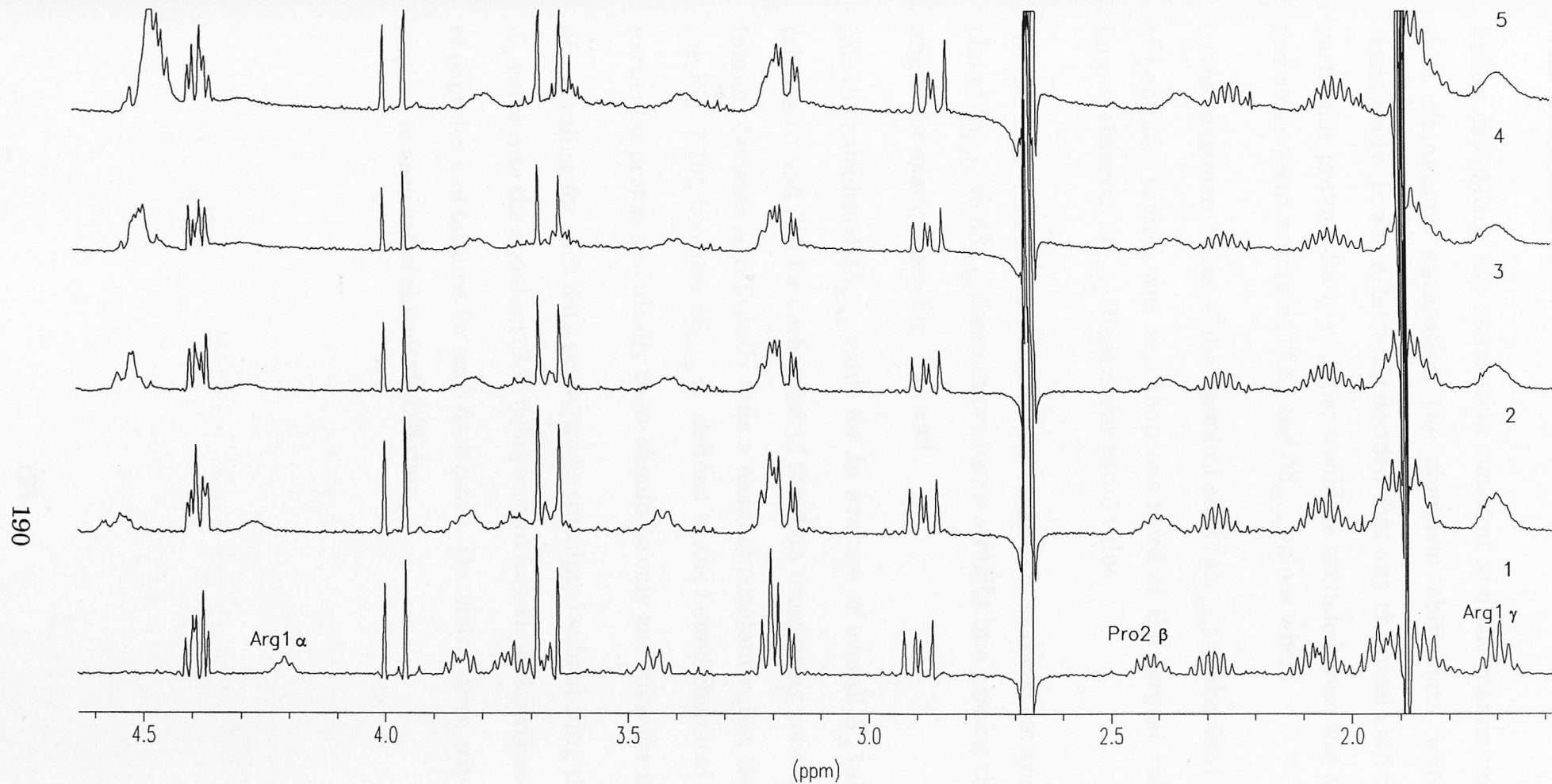
Fig. 7.8 Stack plot of one-dimensional ^{1}H NMR spectra for bradykinin (1-5) recorded during the titration of PGG into bradykinin (1-5) in $D_2O/(CD_3)_2SO$ (4:1 v/v) at 295 K. Numbered spectra (1-5) correspond to spectra of solutions resulting from the addition of 0, 20, 40, 60, and 100 µl of 60 mM PGG to 600 µl, 2 mM solution of bradykinin (1-5).

7.8.2 Treatment of data

Before calculating the association constant and the maximum chemical shift change on saturation the chemical shift data were treated statistically. It was arbitrarily decided that any chemical shift data (for a particular proton of any residue) would be excluded from the calculation and subsequent averaging of K_a and $\Delta\delta_{max}$ values when:

(i) the maximum value of the chemical shift ($\Delta\delta_{i,obs}$) at the final mole ratio of peptide : tannin was less than one-third of the largest value of the largest observed $\Delta\delta_{i,obs}$ (final molar ratio) value;

(ii) the data were not consistent with other data of the same system, i.e. a plot of $\Delta\delta_{i,obs}$ vs $\Delta\delta_{i,obs}$ does not produce a straight line passing through the origin (for example see Fig. 7.9); and

(iii) the calculated $\Delta\delta_{max}$ value for an average or overall K_a value (using criteria (i) and (ii)) for each point of the data (increasing concentration of tannin) deviates significantly from a mean or constant value, (for example see Fig. 7.10), because $\Delta\delta_{max}$ is defined as the bound chemical shift for a particular proton and ideally there should be only one value for it.

$\Delta\delta_{max}$ values for each data point can be calculated substituting the average K_a value into the equation (2.9) using known experimental concentrations of peptides and tannins for each data point. The above three criteria were applied to each set of chemical shift data.
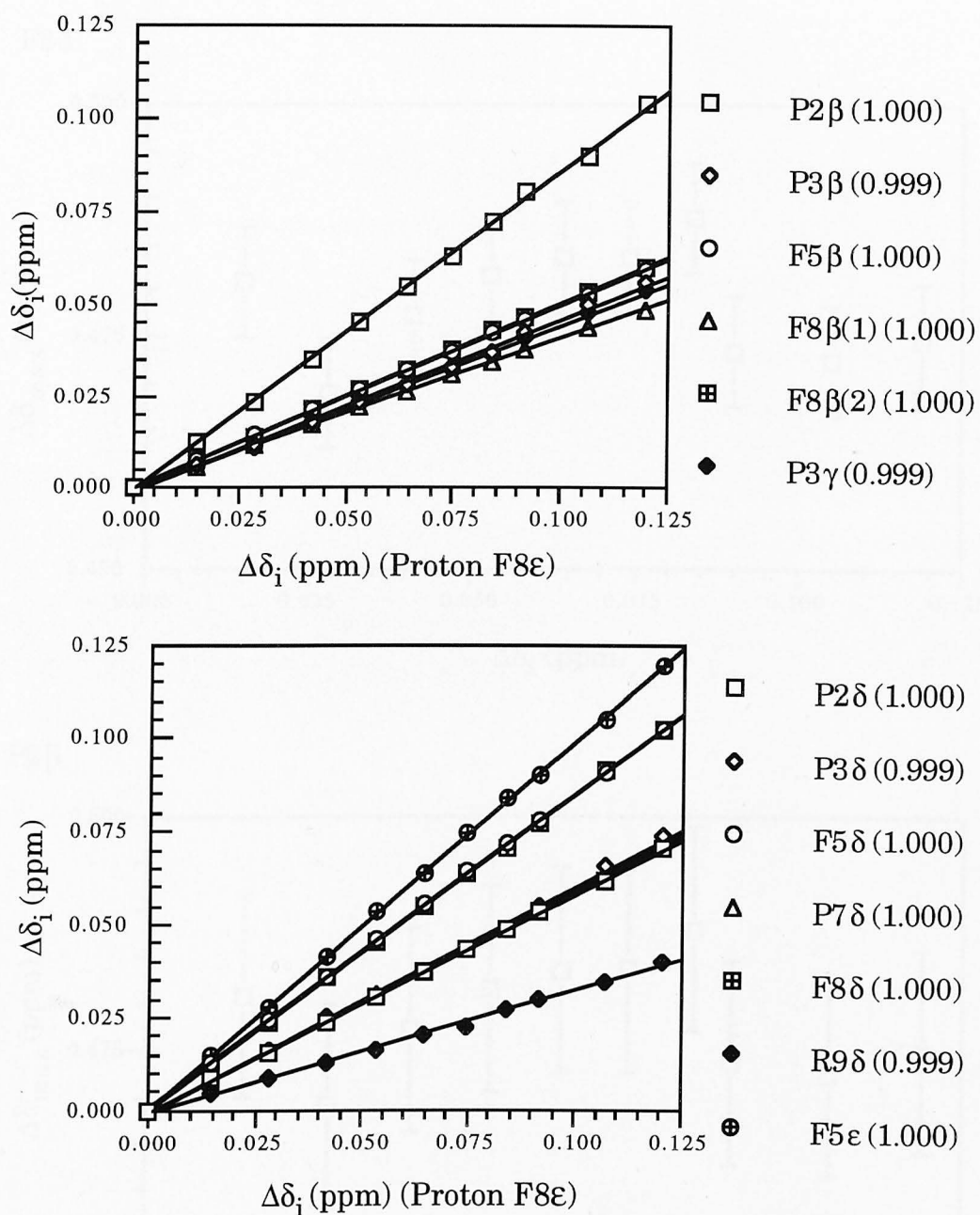
Fig. 7.9 The test of self-consistency of chemical shift data ($\Delta\delta_i = \delta_{free} - \delta_{peptide/tannin}$) for bradykinin-PGG titration in $D_2O/(CD_3)_2SO$ (4:1, v/v) at 295 K, final molar ratio = 1:6. The values given in parentheses indicate the correlation coefficient between respective data sets, such as F8ε v P2δ. (R = Arg, P = Pro and F = Phe).

F8δ

P2β
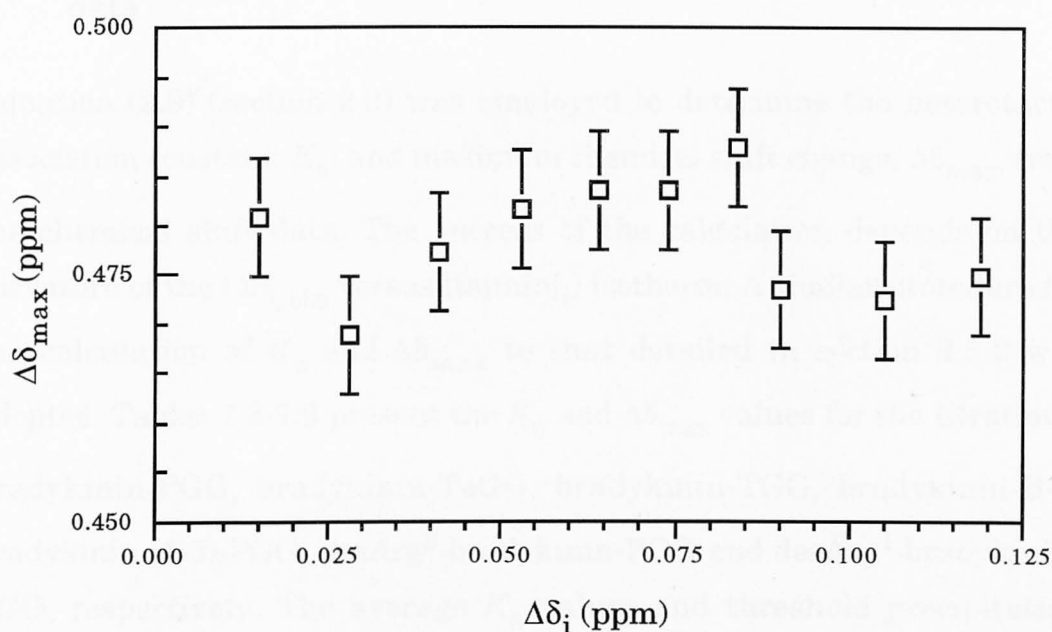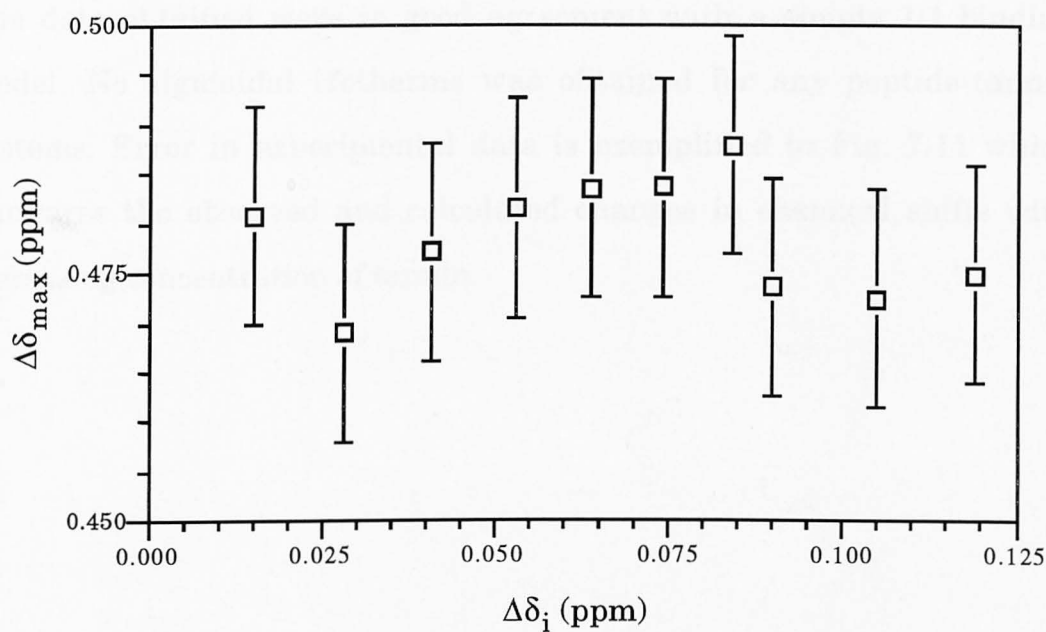
Fig. 7.10 The test of self-consistency of calculated association constants (K_a) determined using the chemical shift data ($\Delta\delta_i = \delta_{free} - \delta_{peptide/tannin}$) vs [tannin]$_i$ for bradykinin-PGG titration in $D_2O/(CD_3)_2SO$ (4:1, v/v). For an ideal system there should be only one $\Delta\delta_{max}$ value, i.e. the plot $\Delta\delta_i$ v $\Delta\delta_{max}$ should give a straight line with a slope of zero.

7.8.3 Calculation of K_a and $\Delta\delta_{max}$ from peptide-tannin titration data

Equation (2.9) (section 2.8) was employed to determine the heterotactic association constant, K_a, and maximum chemical shift change, $\Delta\delta_{max}$, from the chemical shift data. The success of the calculation depends on the curvature of the ($\Delta\delta_{i,\,obs}$ versus [tannin]$_i$) isotherm. A similar procedure for the calculation of K_a and $\Delta\delta_{max}$ to that detailed in section 2.5.2 was adopted. Tables 7.3-7.9 present the K_a and $\Delta\delta_{max}$ values for the titrations: bradykinin-PGG, bradykinin-TeGG, bradykinin-TGG, bradykinin-B-2, bradykinin (1-5)-PGG, desArg^9-bradykinin-PGG and desArg^1-bradykinin-PGG, respectively. The average K_a values and threshold precipitation point are summarized in Table 7.10.

The data obtained were in good agreement with a simple 1:1 binding model. No sigmoidal isotherms was obtained for any peptide-tannin systems. Error in experimental data is exemplified in Fig. 7.11 which compares the observed and calculated changes in chemical shifts with increasing concentration of tannin.

Table 7.3 The association constant, K_a, for bradykinin-PGG complexation and the chemical shift change on complexation, $\Delta\delta_{max}$, calculated using equation (2.9). $\Delta\delta_{obs}$ values are the observed chemical shift change at peptide to tannin molar ratio 1:6; solvent = $D_2O/(CD_3)_2SO$ (4:1, v/v); temperature 295 K; approximate pH 5.9 ± 0.3.

Proton	K_a (M^{-1})	$\Delta\delta_{max}$ (ppm)	$\Delta\delta_{obs}$ (ppm)
P2β	29.2	0.479	0.104
P3β	28.4	0.256	0.056
F5β	45.0	0.197	0.059
F8β(1)	41.2	0.174	0.049
F8β(2)	42.3	0.209	0.060
P3γ	26.1	0.267	0.054
P2δ	32.2	0.298	0.070
P3δ	28.4	0.341	0.074
F5δ	41.5	0.361	0.102
P7δ	32.6	0.298	0.071
F8δ	37.1	0.390	0.102
R9δ	27.7	0.185	0.040
F5ϵ	38.8	0.441	0.120
F8ϵ	38.2	0.451	0.120

Average K_a=34.9 ($\pm$ 6.4) M^{-1}

Table 7.4 The association constant, K_a, for bradykinin-TeGG complexation and the chemical shift change on complexation, $\Delta\delta_{max}$, calculated using equation (2.9). $\Delta\delta_{obs}$ values are the observed chemical shift change at peptide to tannin molar ratio 1:6; solvent = $D_2O/(CD_3)_2SO$ (4:1, v/v); temperature 295 K; approximate pH 5.9 ± 0.3.

Proton	K_a (M^{-1})	$\Delta\delta_{max}$ (ppm)	$\Delta\delta_{obs}$ (ppm)
P2β	20.9	0.367	0.063
P3β	14.8	0.285	0.037
F5β	28.0	0.187	0.040
F8β(1)	22.2	0.213	0.038
F8β(2)	24.8	0.229	0.045
P2γ	16.2	0.398	0.055
P3γ	15.0	0.274	0.035
P2δ	18.3	0.300	0.046
P3δ	15.7	0.362	0.048
F5δ	25.0	0.341	0.066
P7δ	17.4	0.342	0.050
F8δ	20.1	0.432	0.071
F5ε	24.0	0.395	0.075
F8ε	22.5	0.444	0.080

Average K_a=20.4 ($\pm$ 4.2) M^{-1}

Table 7.5 The association constant, K_a, for bradykinin-TGG complexation and the chemical shift change on complexation, $\Delta\delta_{max}$, calculated using equation (2.9). $\Delta\delta_{obs}$ values are the observed chemical shift change at peptide to tannin molar ratio 1:6; solvent = $D_2O/(CD_3)_2SO$ (4:1, v/v); temperature 295 K; approximate pH 5.9 ± 0.3.

Proton	K_a (M^{-1})	$\Delta\delta_{max}$ (ppm)	$\Delta\delta_{obs}$ (ppm)
P3α	3.5	0.427	0.018
F5α	3.0	0.536	0.020
F8α	3.7	0.469	0.021
P2β	3.6	0.951	0.041
P3β	3.9	0.645	0.030
F5β	7.8	0.346	0.031
P7β	3.7	0.888	0.041
F8β(1)	4.4	0.578	0.031
F8β(2)	5.3	0.568	0.036
P3γ	2.8	0.771	0.027
R1δ	2.6	0.655	0.022
P2δ	3.5	0.784	0.033
P3δ	6.9	0.508	0.040
R9δ	3.2	0.765	0.030
F5ε	7.3	0.516	0.043
F8ε	5.7	0.664	0.045

Average K_a=4.4 ($\pm$ 1.6) M^{-1}

Table 7.6 The association constant, K_a, for bradykinin-Procyanidin B-2 complexation and the chemical shift change on complexation, $\Delta\delta_{max}$, calculated using equation (2.9). $\Delta\delta_{obs}$ values are the observed chemical shift change at peptide to tannin molar ratio 1:6; solvent = $D_2O/(CD_3)_2SO$ (4:1, v/v); temperature 295 K; approximate pH 5.9 ± 0.3..

Proton	K_a (M^{-1})	$\Delta\delta_{max}$ (ppm)	$\Delta\delta_{obs}$ (ppm)
P3α	07.3	0.139	0.012
F5α	14.4	0.082	0.013
S6α	13.5	0.105	0.015
F8α	07.5	0.140	0.012
P2β	04.5	0.319	0.023
P3β	04.5	0.354	0.019
F5β	13.9	0.122	0.018
F8β(1)	07.9	0.186	0.017
F8β(2)	11.1	0.141	0.017
P2δ	04.9	0.399	0.023
F5δ	06.1	0.307	0.022
F8δ	06.6	0.288	0.022
R9δ	05.4	0.260	0.017
F5ε	07.1	0.288	0.023
F8ε	07.2	0.282	0.025

Average K_a=8.1 ($\pm$ 3.4) M^{-1}

Table 7.7 The association constant, K_a, for bradykinin (1-5)-PGG complexation and the chemical shift change on complexation, $\Delta\delta_{max}$, calculated using equation (2.9). $\Delta\delta_{obs}$ values are the observed chemical shift change at peptide to tannin molar ratio 1:6; solvent = $D_2O/(CD_3)_2SO$ (4:1, v/v); temperature 295 K; approximate pH 5.9 ± 0.3.

Proton	K_a (M^{-1})	$\Delta\delta_{max}$ (ppm)	$\Delta\delta_{obs}$ (ppm)
F5δ	25.6	0.235	0.047
F5ε	21.1	0.389	0.066
F5ζ	22.1	0.411	0.073

Average K_a=23.0 ($\pm$ 2.4) M^{-1}

Table 7.8 The association constant, K_a, for desArg^9-bradykinin-PGG complexation and the chemical shift change on complexation, $\Delta\delta_{max}$, calculated using equation (2.9). $\Delta\delta_{obs}$ values are the observed chemical shift change at peptide to tannin molar ratio 1:6; solvent = $D_2O/(CD_3)_2SO$ (4:1, v/v); temperature 295 K; approximate pH 5.9 ± 0.3..

Proton	K_a (M^{-1})	$\Delta\delta_{max}$ (ppm)	$\Delta\delta_{obs}$ (ppm)
F5β	28.1	0.308	0.065
P7β	25.9	0.368	0.073
P2δ	16.1	0.530	0.072
P7δ	19.8	0.457	0.073
F5ε	32.0	0.493	0.116
F8ε	37.3	0.430	0.113

Average K_a=26.5 ($\pm$ 7.8) M^{-1}

Table 7.9 The association constant, K_a, for desArg[1]-bradykinin-PGG complexation and the chemical shift change on complexation, $\Delta\delta_{max}$, calculated using equation (2.9). $\Delta\delta_{obs}$ values are the observed chemical shift change at peptide to tannin molar ratio 1:6; solvent = $D_2O/(CD_3)_2SO$ (4:1, v/v); temperature 295 K; approximate pH 5.9 ± 0.3.

Proton	K_a (M^{-1})	$\Delta\delta_{max}$ (ppm)	$\Delta\delta_{obs}$ (ppm)
F5β	38.5	0.194	0.053
F8β(1)	34.0	0.204	0.050
F8β(2)	28.5	0.295	0.064
F5δ	34.3	0.401	0.099
P7δ	25.7	0.340	0.068
F8δ	29.3	0.480	0.106
F5ε	30.9	0.514	0.118
F8ε	30.2	0.542	0.123

Average K_a=31.4 ($\pm$ 4.0) M^{-1}

Table 7.10 Comparison of association constants (K_a) in $D_2O/(CD_3)_2SO$ (4:1, v/v) and precipitation threshold in H_2O at 295 K for the complexation of bradykinin and its analogues with tannins. The standard deviation presented with K_a values indicates the range of the calculated K_a values, rather than calculational error. The starting concentration of peptide solutions was 2.0 mM in all studies.

System	K_a (M^{-1}) $\pm \sigma_{n-1}$ (M^{-1})	Onset of precipitation in H_2O (Peptide : tannin)	Comments
BK-B-2	8.1 ± 3.4	[a]1: 4.00	Redissolved on heating
BK-TGG	4.4 ± 1.6	1: 0.35	”
BK-TeGG	20.5 ± 4.2	1: 0.25	”
BK-PGG	34.9 ± 6.4	1: 0.10	”
BK(1-5)-PGG	[b]23.0 ± 2.4	$\approx$1: 0.10	,,
desArg[9]-BK/PGG	26.5 ± 7.8	$\approx$1: 0.10	,,
desArg[1]-BK/PGG	31.4 ± 4.0	$\approx$1: 0.10	,,

[a] Value may not be very accurate, colour of procyanidin B-2 prevented accurate assessment;

[b] The K_a value does not represent the overall association constant because many of the protons were found to be exchange broadened and therefore K_a determination was not possible.
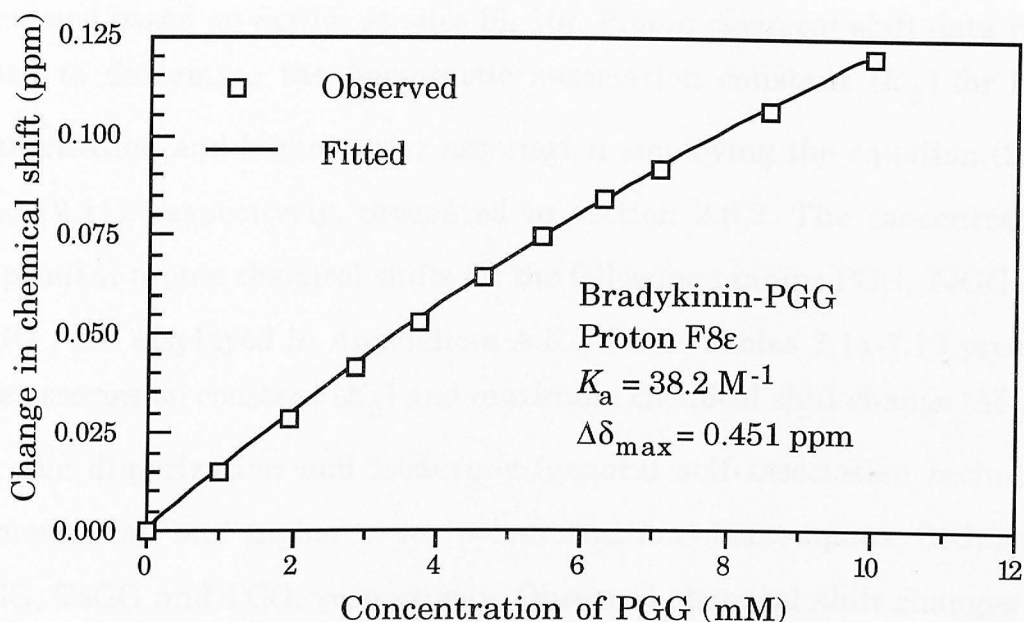
Fig. 7.11 Comparison of observed and calculated (fitted) chemical shift differences (δ_{free}-$\delta_{peptide/tannin}$) of the peptide proton resonance for various peptide-tannin titration experiments with increasing concentration of tannin in $D_2O/(CD_3)_2SO$ (4:1, v/v) at 295 K.

7.9 Self-association of tannins

During the titration of peptides with tannin in $D_2O/(CD_3)_2SO_2$ (4:1 v/v), it was observed that many of the proton resonances of tannins, especially those of PGG, TeGG and TGG moved upfield with increasing concentration of tannins. This indicated that in the bradykinin-tannin systems there was not only bradykinin-tannin interactions but also tannin-tannin interactions. So, for the proper evaluation of the bradykinin-tannin complexation process it was judged necessary to assess the self-association of the tannins.

250 MHz ^1H NMR spectroscopy was employed to monitor the changes in chemical shifts for proton resonances of tannins with increasing concentration of tannins (see section 2.8). The proton resonances were

assigned based on earlier studies [6, 10]. Proton chemical shift data were used to determine the homotactic association constant (K_a) for both dimerization and higher order association employing the equation (2.10) and (2.11), respectively, presented in section 2.8.2. The concentration dependent proton chemical shifts for the following tannins PGG, TeGG and TGG , are displayed in Appendices A.5.1-A.5.3. Tables 7.11-7.13 present the association constant (K_a) and maximum chemical shift change ($\Delta\delta_{max}$) for the dimerization and isodesmic (general self-association including dimerization and higher order polymerization) least-square fittings of PGG, TeGG and TGG, respectively. Observed chemical shift changes for H1 (proton attached to C-1 of glucose core) of PGG alone and during titration with bradykinin are compared in Fig 7.12a, b. Error in exprimental data is exemplified in Fig. 7.13 which compares the observed and calculated changes in chemical shifts with increasing concentration of tannin.

Table 7.11 Self-association of PGG in $D_2O/(CD_3)_2SO$ (4:1, v/v) at 295 K.

Dimerization model

Proton	K_a (M^{-1})	$\Delta\delta_{max}$ (ppm)	$\Delta\delta_{obs}$ (ppm)
Glc H-1	20.8	0.385	0.106
Glc H-3	21.2	0.330	0.095
Gall-6	20.2	0.243	0.068

Average K_a = 20.7 ($\pm$ 0.5) M^{-1}

Isodesmic Model

Proton	K_a (M^{-1})	$\Delta\delta_{max}$ (ppm)	$\Delta\delta_{obs}$ (ppm)
Glc H-1	27.4	0.274	0.106
Glc H-3	29.3	0.231	0.095
Gall-6	27.8	0.170	0.068

Average K_a = 28.2 ($\pm$ 1.0) M^{-1}

Table 7.12 Self-association of TeGG in $D_2O/(CD_3)_2SO$ (4:1, v/v) at 295 K.

Dimerization Model

Proton	K_a (M-1)	$\Delta\delta_{max}$ (ppm)	$\Delta\delta_{obs}$ (ppm)
Glc H-1	3.4	0.265	0.020
Glc H-3	4.8	0.137	0.014
Gall-6	4.7	0.398	0.042

Average K_a = 4.3 (± 0.8) M^{-1}

Isodesmic Model

Proton	K_a (M-1)	$\Delta\delta_{max}$ (ppm)	$\Delta\delta_{obs}$ (ppm)
Glc H-1	2.5	0.337	0.020
Glc H-3	3.7	0.157	0.014
Gall-6	7.1	0.263	0.042

Average K_a = 4.4 (± 2.4) M^{-1}

Table 7.13 Self-association of TGG in $D_2O/(CD_3)_2SO$ (4:1, v/v) at 295 K.

Dimerization Model

Proton	K_a (M-1)	$\Delta\delta_{max}$ (ppm)	$\Delta\delta_{obs}$ (ppm)
Gall-1	4.5	0.241	0.029
Gall-3	4.5	0.168	0.020
Gall-6	5.3	0.243	0.041

Average K_a = 4.8 (± 0.5) M^{-1}

Fig. 7.13 (contd.).

Isodesmic Model

Proton	K_a (M-1)	$\Delta\delta_{max}$ (ppm)	$\Delta\delta_{obs}$ (ppm)
Gall-1	6.9	0.157	0.029
Gall-3	7.0	0.107	0.020
Gall-6	7.9	0.200	0.041

Average K_a = 7.3 ($\pm$ 0.6) M^{-1}

Table 7.14 Comparison of dimerisation and self-association constants of tannins in $D_2O/(CD_3)_2SO$ (4:1, v/v) at 295 K.

Tannin	K_a (M^{-1})	
	Dimer model	Isodesmic model
PGG	20.7 $\pm$ 0.5	28.2 $\pm$ 1.0
TeGG	04.3 $\pm$ 0.8	04.4 $\pm$ 2.4
TGG	04.8 $\pm$ 0.5	07.3 $\pm$ 0.6

(a)

(b)
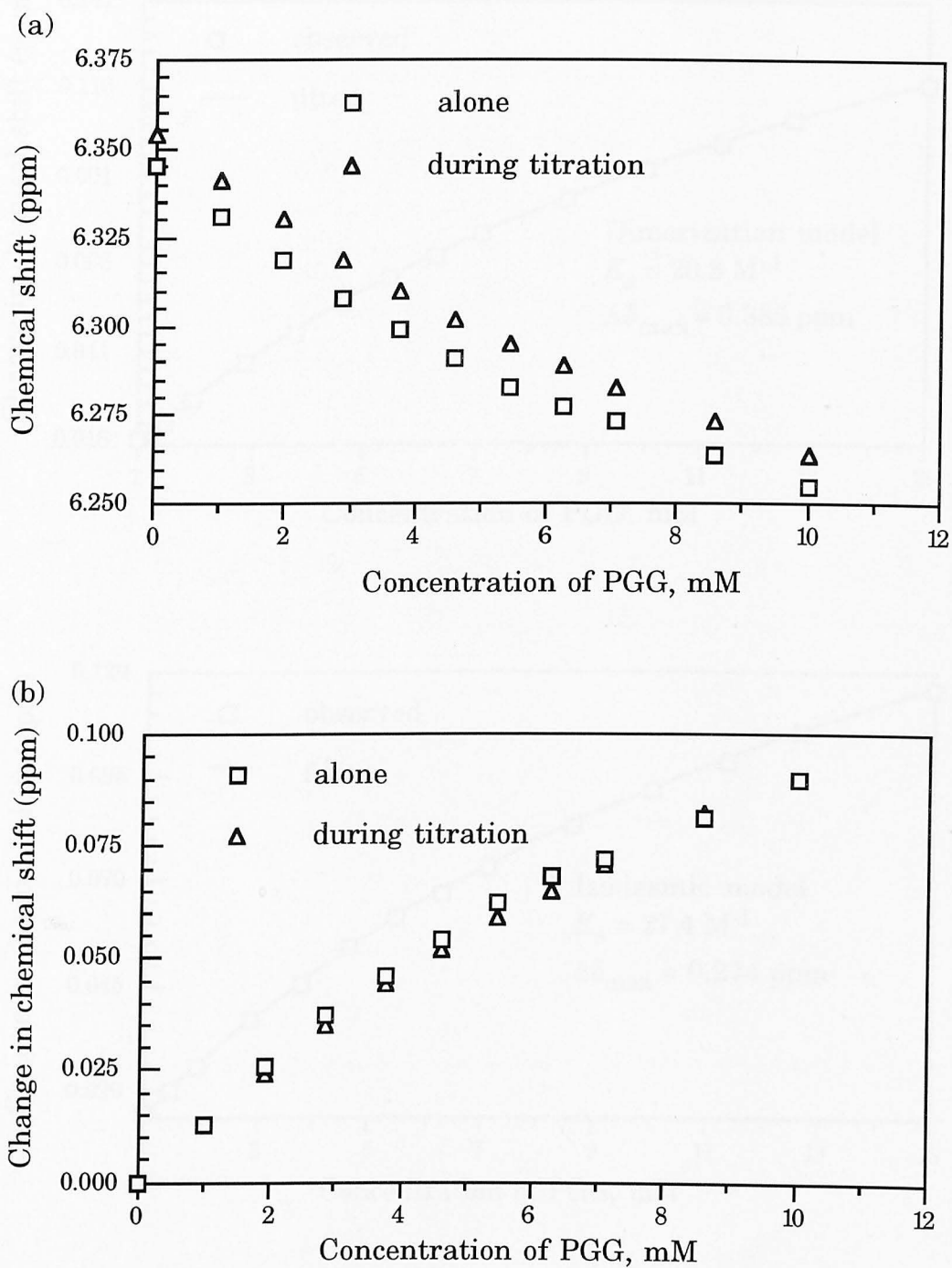
Fig 7.12 Observed chemical shift changes for H-1 proton (attached to C-1 of glucose core) resonance of PGG alone and during titration with bradykinin in $D_2O/(CD_3)_2SO$ (4:1, v/v) at 295 K. (a) Chemical shift values and (b) change in chemical shift.

206
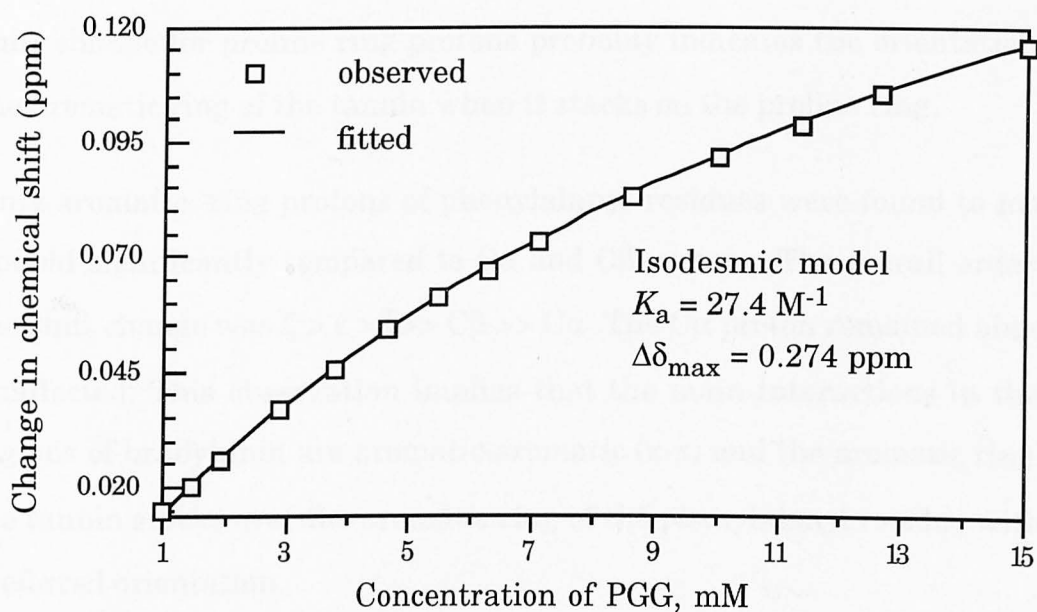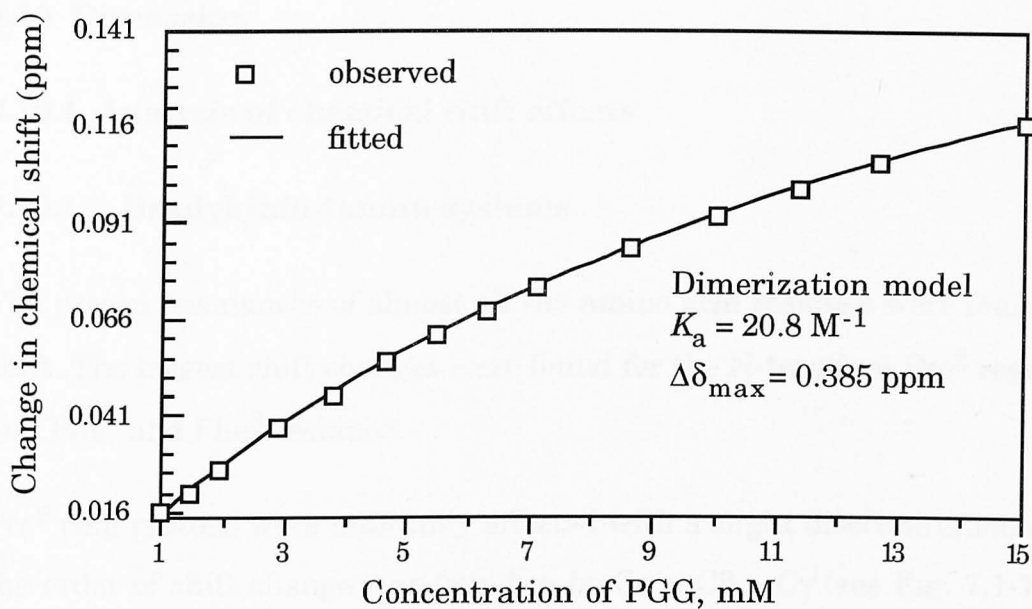
Fig. 7.13 Comparison of the observed chemical shift changes for H-1 proton (attached to C-1 of glucose core) resonance of PGG and those obtained by fitting the same data by the dimerization and isodesmic models. Solvent $D_2O/(CD_3)_2SO$ (4:1, v/v); temperature 295 K. The changes in chemical shifts are the differences of chemical shift between the calculated shift of monomer and that observed at experimental concentration.

207

7.10 Discussion

7.10.1 Analysis of chemical shift effects

7.10.1.1 Bradykinin-tannin systems

The proton resonances of almost all the amino acid residues were found to shift. The largest shift changes were found for the N-terminal Pro^2 residue and Phe^5 and Phe^8 residues.

Pro^2 ring protons were uniformly affected with a slight discrimination and the order of shift change was found to be Cα > Cβ > Cγ (see Fig. 7.1-7.3). The upfield shift change indicates the influence of aromatic ring current effects induced by the aromatic rings of tannin molecules. The order of shift change for proline ring protons probably indicates the orientation of the aromatic ring of the tannin when it stacks on the proline ring.

Only aromatic ring protons of phenylalanyl residues were found to move upfield significantly compared to Cα and Cβ protons. The overall order of the shift change was ζ > ε > δ >> Cβ >> Cα .The Cα proton remained almost unaffected. This observation implies that the main interactions in these regions of bradykinin are aromatic-aromatic (π-π) and the aromatic ring of the tannin stacks over the aromatic ring of the phenylalanyl residue with a preferred orientation.

The patterns of chemical shift changes observed for bradykinin with PGG, TeGG and TGG were similar, although there was some difference in the absolute magnitude of the shift changes. The magnitude of shift change was dependent on the number of galloyl groups attached to the glucopyranose ring i.e. the order of the magnitude was: PGG > TeGG > TGG. Another interesting difference was found for the change in chemical shift for the Arg$^9\alpha$ proton. For bradykinin-PGG and bradykinin-TeGG the

208

the $Arg^9\alpha$ proton resonances were found to move downfield whereas for the bradykinin-TGG and bradykinin-B-2 systems the change was upfield although small. However, since $Arg\alpha$ protons are prone to pH changes, so the changes in the chemical shifts could be due to slight change in pH on the addition of tannins.

One point which should be stressed is that the bradykinin-tannin complexation process was conducted in $D_2O/(CD_3)_2SO$ (4:1, v/v) and was monitored by one-dimensional ^1H NMR spectroscopy. Due to the exchange of amide protons by D of deuteriated water, it was not possible to observe the change in chemical shift, if any, for these protons. The regions of the $C\gamma$ proton resonances of all residues and $C\beta$ proton resonances of Arg residues were severely crowded and the situation was worsened by overlapping with tannin protons in the one-dimensional spectra. Thus it was impossible to measure the chemical shifts for these proton resonances. Close examination of the stack plot of one-dimensional spectra recorded during bradykinin-tannin titration revealed that $C\gamma$ protons of Arg residues moved upfield significantly (see Fig. 7.14). So it was not possible to assess directly the overall influence of the Arg residues on binding of bradykinin to tannin. However, this limitation was compensated by studying the complexation of bradykinin analogues such as desArg^1-bradykinin (Arg^1 deleted), desArg^9-bradykinin (Arg^9 deleted) and bradykinin (1-5) (first five residues of full length bradykinin) with PGG. These systems provided indirect evidence for the influence of Arg residues on the binding of bradykinin with tannin.
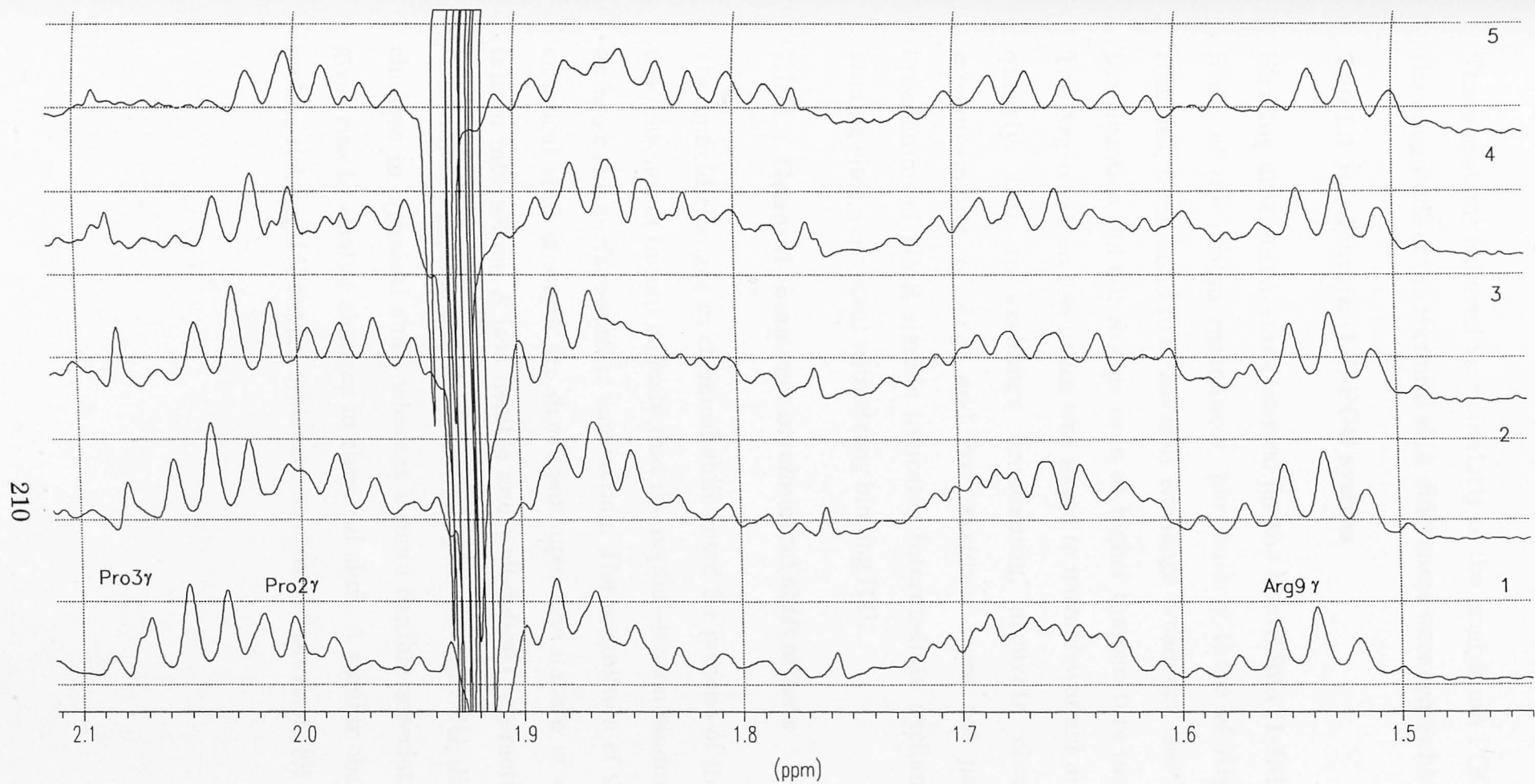
Fig. 7.14 Stack plot of one-dimensional ^{1}H NMR spectra of bradykinin (Cγ proton region), recorded during the titration of PGG into bradykinin in D$_2$O/(CD$_3$)$_2$SO (4:1 v/v) at 295 K. Numbered spectra (1-5) correspond to spectra of solutions resulting from the addition of 0, 20, 40, 60, and 100 µl of 60 mM PGG to 600 µl, 2 mM solution of bradykinin.

7.10.1.2 desArg^9/desArg^1-bradykinin-PGG systems

These systems behaved very similarly to the bradykinin-PGG system but the magnitude of the chemical shift differences were somewhat smaller.

7.10.1.3 Bradykinin (1-5)-PGG system

Striking differences were observed for the bradykinin (1-5)-PGG system. Some of the proton resonances, particularly those of Arg^1 and Pro^2 residues, were found to be severely exchange broadened (see Fig. 7.8) and the situation did not change even at higher temperature (around 70°C). The Arg$^1\alpha$ proton resonance was found to move downfield and saturated quickly. Due to exchange broadening, accurate chemical shift measurements of Arg^1 and Pro^2 residues were not possible. The broadening of NMR signals indicates intermediate exchange between binding sites, consistent with strong binding [11].

7.10.1.4 General comments on chemical shift effects

The upfield changes in chemical shift noted for protons of the peptide in the presence of tannin indicate that the peptide-tannin binding occurs *via* an aromatic surface-surface interaction. The magnitude of the observed chemical shift changes are dependent upon the nature of the peptide-tannin interaction. A less flexible and well-defined interaction, such as that between peptide and the larger polyphenols e.g. PGG, displays large changes in chemical shift, whereas a more flexible association e.g. B-2 gives rise to smaller changes in chemical shift. A similar observation for proline-rich peptide-tannin systems was observed previosly [6].

7.10.2 Analysis of K_a values determined from the peptide-tannin titration data

The chemical shift data allowed the association constants to be determined. The K_a values were averaged to give overall K_a values for bradykinin-tannin complexation (see Table 7.10). The average K_a values for desArg^9-bradykinin-PGG and desArg^1-bradykinin-PGG systems should be considered as an approximate overall K_a value, because many of the chemical shift data were too small and K_a values determined from those data were excluded from the averaging.

The bradykinin (1-5)-PGG system should be treated as a special case because it behaved strangely compared to native bradykinin. Only K_a values determined from chemical shift changes of aromatic protons were included in the average. Arg^1 and Pro^2 proton resonances were broadened and other non-aromatic shift data were not reliable due to overlapping by PGG protons. If intermediate exchange is considered as an indicator of strong binding, then it should be admitted that bradykinin (1-5)-PGG is a complicated system where one end of the peptide binds strongly and the other end binds moderately to tannins. The overall balance is probably towards the stronger binding. Examination of molecular models also supports this view. The unstructured random coil of bradykinin (1-5) can easily bridge two adjacent galloyl ester groups. Thus this minimum structural feature is probably responsible for stronger binding, which is evident from exchange broadening.

Tannins bind bradykinin with different affinities. The average K_a values for bradykinin-tannin systems can be used to place the tannins in order of their binding effectiveness to bradykinin PGG > TeGG > B-2 ≥ TGG. Analysis of the results reinforces the existing view that the galloyl function

of hydrolysable tannins alone is not responsible for the strength of binding to a substrate but that the tannin molecule as a whole provides the specific substrate binding properties [6, 10, 12].

Precipitation studies of bradykinin-tannin complexation (see Table 7.1) also suggest a similar ranking order of hydrolysable tannins in order of their binding effectiveness towards bradykinin PGG > TeGG > TGG. Recent protein-tannin complexation and precipitation studies such as the reversible complexation of tannins with BSA, haemoglobin and caffeine [4, 13-16] and non-competetive inhibition of β-glucosidase activity by polyphenols [4] supports this ranking order. A more recent study of peptide-tannin complexatiion study [6] presented a different view that TGG binds proline rich peptides more effectively than PGG, on the ground that TGG is sterically much accessible to proline rich proteins than PGG. It was argued that TGG is more flexible and sterically unhindered compared to PGG which is sterically crowded. However, no evidence was obtained from the present study that TGG binds bradykinin stronger than PGG. One point should be stressed here that the work described in reference [6] has used peptides that lack any phenylalanyl residues and has a different composition of solvent ($D_2O/(CD_3)_2SO$ (9:1 v/v)) compared to the present work which could be the reason for differential behaviour of TGG.

Analysis of K_a values (Tables 7.3-7.9) suggests that the magnitude of K_a values obtained from aromatic proton shifts is generally larger than that obtained from other protons of the same peptide. This was found true for all the systems investigated.

7.10.3 Modes of bradykinin-tannin binding

A number of pieces of evidence presented, namely, the formation of precipitate when PGG was added to the solution of bradykinin, change in chemical shift during the titration of bradykinin with tannin in $D_2O/(CD_3)_2SO$, and finally the observation of bradykinin-tannin precipitates at the end of the titration study (after a few days of storage) indicate that tannins bind bradykinin. It would be now appropriate to examine the modes of bradykinin-tannin binding.

The main features of bradykinin are that it has three proline residues, two phenylalanyl residues and two terminal arginine residues. Both proline and the aromatic ring of the phenylalanyl residue are open, flat and, obviously, hydrophobic in nature and thus are ideal binding sites for hydrophobic compounds. In addition the long hydrocarbon chain of arginine residues provides further hydrophobicity. The situation is made further attractive by the presence of potential hydrogen-bond-donating groups such as the proline peptide bond and the guanidino groups containing delocalized π-electrons at the terminus.

The chemical shift data and association constant results presented above demonstrate that the principal modes of binding between bradykinin and tannins are via proline-galloyl ester and aromatic-galloyl ester interaction driven by hydrophobic association which may then be stabilized by hydrogen bond formation. Upfield changes in chemical shift for both the protons of proline residues and aromatic rings of phenylalanyl residues are consistent with the prediction made above. Although it was not possible to obtain any direct evidence from bradykinin-tannin titration data of the influence of the arginine group (due to limitations of one-dimensional spectra), but the fact that bradykinin analogues, which lack either of the

214

terminal arginine groups, showed lower binding affinity for tannins, is indirect evidence that arginine groups also take part in binding.

Although the largest chemical shift changes were observed for Pro2, Phe5 and Phe8 proton resonances, Pro3 and Pro7 proton resonances (specially Cβ protons) were also found to move significantly. This effect could be due to cooperative interactions through multidentate ligands (PGG, TeGG and TGG). Interestingly, in case of the bradykinin-B-2 system no preferential chemical shift change for any particular residues were observed, rather a uniform change in all residues was observed. This is consistent with the size, shape and denticity of the procyanidin B-2. The magnitude of shift change for bradykinin in bradykinin-B-2 system was so small (≈ 0.02 ppm) that treatment of data and analysis of results should be considered with extreme care.

The prediction that the proline-aromatic hydrophobic interaction is stabilized by hydrogen-bond-formation is supported by experimental evidence [8, 16, 17]. It has been shown that the tertiary amide (present in proline) interacts more strongly with the zwitterionic groups and is poorly solvated by water, thus requiring breaking of fewer hydrogen bonds compared to secondary amide groups. Furthermore, the carbonyl function becomes electron rich (*i.e.* a hydrogen bond acceptor) by withdrawing electrons from the methylene substituent via the tertiary amide.

An upfield change in chemical shift for the aromatic proton resonances of phenylalanyl residues indicates that there are interactions between aromatic rings of Phe residues and galloyl groups of tannins. The (π-π) nature of this interaction can be understood from recent experimental and energy calculation evidence. It has been demonstrated that extensive π-overlap occurs when one of the π-systems is polarized by the presence of heteroatoms. The phenolic rings of tannins are polarized: the phenolic

oxygen becomes becomes π-deficient by donating electrons and the rest of the aromatic ring correspondingly becomes π-rich (Fig.7.15) [18-21]. From the work described in referencecs [18-21] a model can be visualized for the π-π interactions present in the tannin-peptide binding. Stacking of galloyl functions over the aromatic ring of the peptides is indicated by the upfield shift change of the latter protons. In a stacked structure the π-deficient (acceptor) region of the tannin galloyl group probably lies above the plane of the π-rich (donor) region of the Phe π-system (aromatic ring of phenylalanyl residue). Thus a neutral aromatic ring can bind a polarized π-system. This model is consistent with the chemical shift effects observed for the Phe aromatic protons ($\zeta > \varepsilon > \delta$ probably indicates the preferred orientation) (see Fig. 7.5).

The electron rich phenolic nucleus can act as a hydrogen bond acceptor when it interacts with hydrogen bond donor groups like -NH- and -NHC(NH)-NH$_2$ (guanidino) groups. This is evidenced by simple energy calculations [22]. This phenomenon could explain why arginine groups have a role to play in stabilizing bradykinin-tannin complexes.
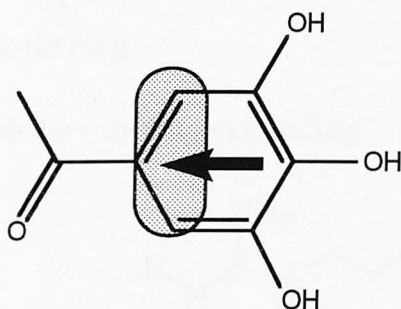
Fig. 7.15 Polarization of galloyl function (shaded area indicates π-rich region).

From the experimental evidence extracted from the present study and arguments placed in this section, the principal modes of bradykinin-tannin binding are summarized in Fig. 7.16.

(a) *Prolyl residues* - prolyl-galloyl interaction

R

(b) *Phenylalanyl residue* - π-π interaction

OH

Possible
hydrogen bond

π-rich region

O-H

Phenolic oxygen
(π-poor)

(ζ) H

H (ε)   H (δ)

Phe aromatic ring

H—

Phe aromatic ring
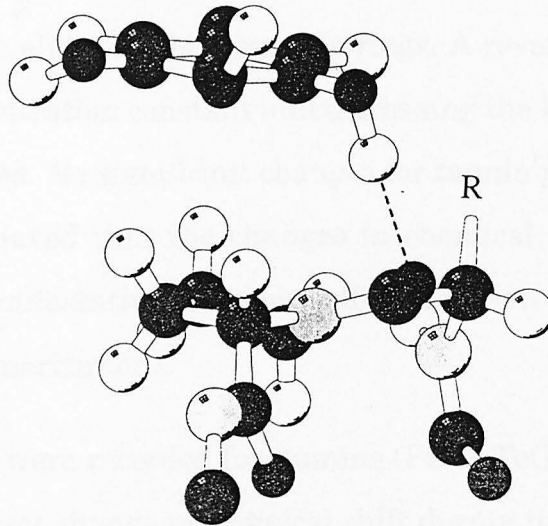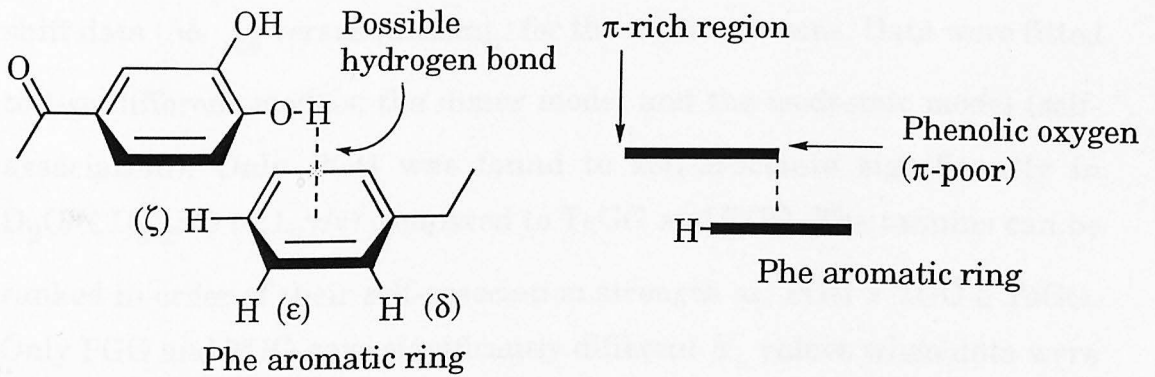
(c) *Arginyl residue* - hydrogen bonding

NH$_2$

H   N

N
H

H

HO

HO

HO

O
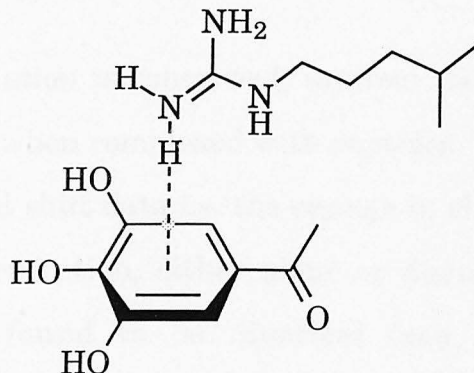
Fig. 7.16 Possible main modes of complexation of tannins with the proline rich peptide - bradykinin. Figure (a) taken from reference [8].

7.10.4 Self-association of tannins

Large changes in chemical shift for tannin protons were initially thought be due to the effect of Phe aromatic rings. A reverse titration keeping the tannin concentration constant and increasing the bradykinin concentration was attempted. No significant changes for tannin protons were observed. It was now believed that the changes in chemical shift for tannin protons were the manifestation of some self-association (dimerization or higher order of polymerization).

Experiments were recorded for tannins (PGG, TeGG and TGG; B-2 did not show significant change in chemical shift during titration with bradykinin) where concentrations of tannins were gradually increased. Association constants for homotactic association (K_a) were determined using chemical shift data ($\Delta\delta_{i,\,obs}$ versus $[\text{tannin}]_i$) for the tannin protons. Data were fitted to two different models: the dimer model and the isodesmic model (self-association). Only PGG was found to self-associate significantly in $D_2O/(CD_3)_2SO$ (4:1, v/v) compared to TeGG and TGG. The tannins can be ranked in order of their self-association strength as: PGG > TGG ≥ TeGG. Only PGG and TGG gave significantly different K_a values when data were fitted to two different models. It seems possible that PGG and TGG remain in solution as dimers or higher order polymers.

As far as the self-association is concerned, tannins behaved strikingly similarly either alone or when complexed with peptides. This is evidenced by experimental chemical shift data i.e. the change in chemical shift as a function of tannin concentration, either alone or during titration with peptides, which were found to be identical (see Fig. 7.12). The experimental results imply that the peptide-tannin complexation process does not affect the self-association of tannins. This could provide a useful clue to how the tannins precipitate peptides in solution (see next section).

7.10.5 Model for complexation and precipitation of tannin by bradykinin

Extensive NMR study in aqueous media suggests that bradykinin is in rapid equilibrium among many conformers and does not show any persistent structural features such as β-turns or internal hydrogen bonding [23]. On the other hand bradykinin in DMSO assumes a rigid structure with β-bends at both termini and is stabilized by electrostatic interaction between the two terminal Arg residues, which come closer together as a consequence of folding [24]. Examination of NMR data of bradykinin in $D_2O/(CD_3)_2SO$ (4:1, v/v) suggests that there is no significant deviation of conformation compared to that in D_2O (Tables 7.15 and 7.16). Bradykinin remains conformationally flexible, extended and no internal hydrogen bonds are formed ($\Delta\delta/\Delta T$ values are $\approx$ 4.5-7.5 ppbK^{-1}).

Analysis of ROESY spectra implies that bradykinin does not change its conformation on going from free peptide to complexation with tannins. No apparent change in ROE (or NOE) intensity was observed during complexation with equimolar tannins. With equimolar PGG no intermolecular NOE was observed. It should be borne in mind that in a solvent like $D_2O/(CD_3)_2SO$ (4:1, v/v) (improved solvation of both solutes) and at a temperature of 295K, the absence of intermolecular NOEs is not very surprising. The combined implication of these findings could be that bradykinin remains extended when complexed with tannins and the complexation process is non-specific. The driving force is the nonselective association of aromatic nuclei of the tannins with hydrophobic groups (Pro and Phe (π-π interaction)) on bradykinin followed by hydrogen bonding reinforcing this initial complexation.

The analysis of chemical shift changes for the three proline residues shows that only Pro^2 protons were affected uniformly. The magnitude of the shift

change for the other two proline residues was almost half compared to that for Pro[2]. This indicates selectivity of binding sites. In other words the Pro[2] residue is a discrete binding site on bradykinin for tannins. As far as the phenyl residues are concerned, aromatic-aromatic interactions need geometrical requirements and are directional [22]. The magnitudes of shift changes and corresponding K_a values imply that aromatic-aromatic interactions between Phe residues and galloyl functions of tannins are quite selective. The overall association process between bradykinin and tannins, however, is probably a balance between selective and random processes, either could dominate the association process depending on the composition of solvents. The nature and quality of data available is not sufficient to make a definitive comment.

Table 7.15 Chemical shifts and coupling constants of amide protons in bradykinin in different solvents. Chemical shifts are relative to TSP. Data for D_2O and DMSO are taken from references [23] and [24], respectively.

Residue	Chemical shift (ppm)			$^3J_{HN\alpha}$ (Hz)		
	D_2O	$D_2O/$ DMSO (4:1, v/v)	DMSO	D_2O	$D_2O/$ DMSO (4:1,v/v)	DMSO
	294 K pH 4.7	295 K pH 5.9	298 K	294 K pH 4.7	295 K pH 5.9	298 K
Gly[4]	8.42	8.41	8.53	5.8	5.7	uc
Phe[5]	8.03	8.08	8.10	6.7	6.9	7.3
Ser[6]	8.15	8.21	8.33	7.7	7.3	5.5
Phe[8]	8.01	8.00	7.85	7.1	8.1	8.6
Arg[9]	7.72	7.70	7.34	7.5	7.6	6.1

uc = unequally coupled.

Analysis of the stoichiometry of bradykinin-tannin precipitation threshold values in water (Table 7.1) indicates that the effectiveness of precipitation

depends on multiplicity of galloyl functions in the tannin molecule and the same is true for self-association of tannins. The presence of DMSO in the medium (water) provides better solvation for both tannin and the bradykinin-tannin complex and delays the precipitation process, *i.e.* a higher amount of tannin is required to precipitate a given amount of peptide. The experimental results suggest that in $D_2O/(CD_3)_2SO$ (4:1, v/v) heterotactic association between peptide and tannin is stronger (eg. K_a for bradykinin-PGG = 34.9 M^{-1}) than homotactic association for tannin itself (eg. K_a for PGG = 28.2 M^{-1}, calculated from isodesmic model). The results also suggest that tannins remain self-associated when complexed with peptides.

Table 7.16 Temperature coefficients, $\Delta\delta/\Delta T$ and average coupling constants of amide proton in bradykinin in different solvents. Data for DMSO are taken from reference [24].

Residue	Amide $\Delta\delta/\Delta T$ (ppb K^{-1})		$^3J_{HN\alpha}$ (Hz)	
	$D_2O/DMSO$ (4:1, v/v)	DMSO	$D_2O/DMSO$ (4:1, v/v)	DMSO
Gly^4	7.5	1.7	-	-
Phe^5	6.1	0.3	7.1	7.3
Ser^6	7.2	5.8	6.9	5.5
Phe^8	6.6	3.9	7.8	8.6
Arg^9	4.5	1.6	7.5	6.1

The process of precipitation now can be visualized as the aggregation of tighter bradykinin-tannin complexes mediated by weaker association of multidentate (galloyl functions) tannin. The stronger is the latter kind of association, the more 'forward' is the precipitation. The different

interactions taking part in the complexation and precipitation of tannin by bradykinin are illustrated in Fig. 7.17.
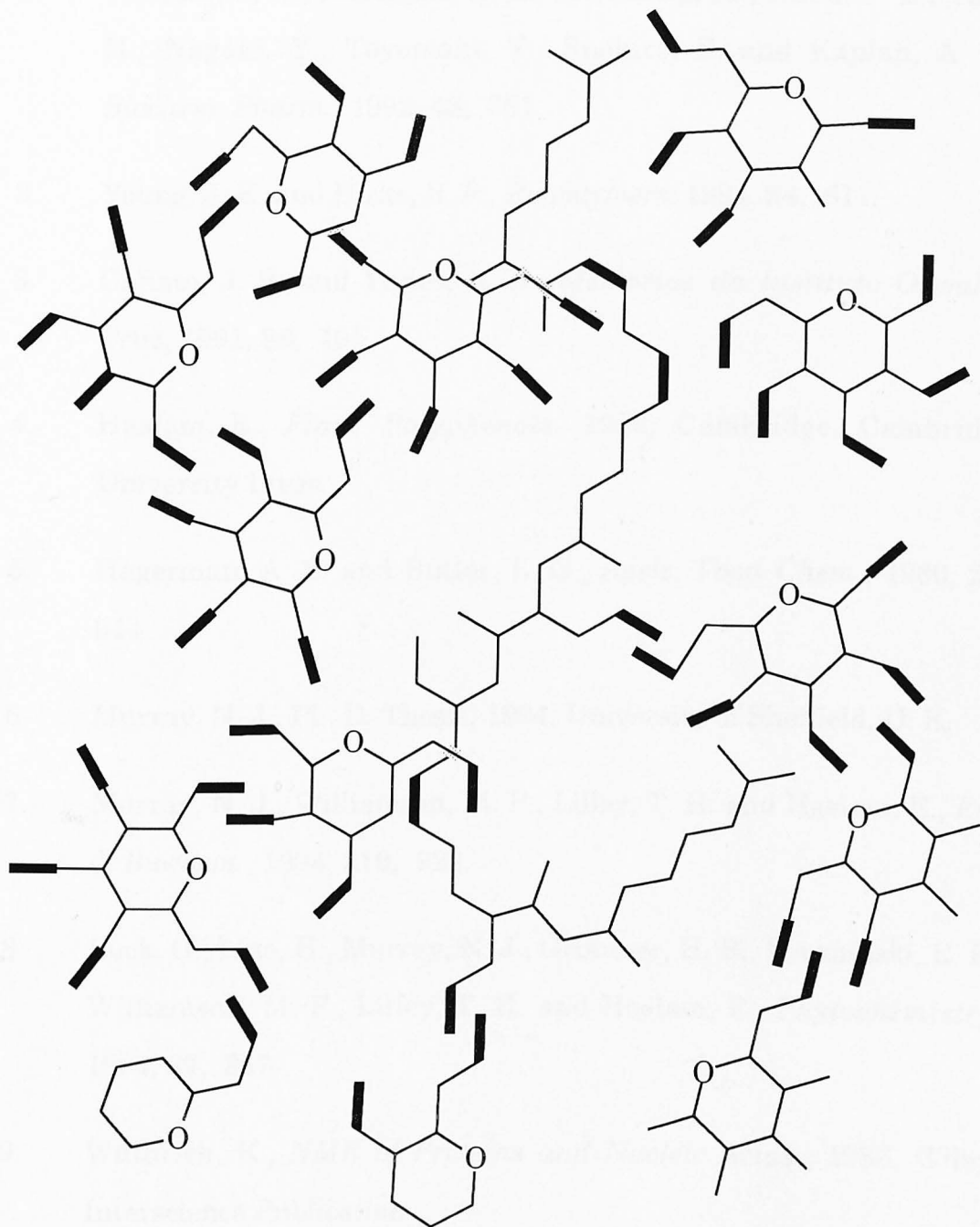
Fig 7.17 Schematic illustration of tannin-tannin and tannin-peptide complexation during precipitation of soluble complexes in $D_2O/(CD_3)_2SO$ (4:1 v/v). For simplicity only one strand of bradykinin is shown. Solid bars represent hydrophobic ring faces, either proline or aromatic. [Simplistic two-dimensional view of three-dimensional concept.]

References

1. Nishikawa, K., Reddigari, S. R., Silverberg, M., Kuna, P. B., Yago, H., Nagaki, Y., Toyomaki, Y., Suehiro, S. and Kaplan, A. P., *Biochem. Pharm.*, 1992, **43**, 361.

2. Young, J. K. and Hicks, R. P., *Biopolymers*, 1994, **34**, 611.

3. Calixto, J. B. and Yunes, R. A., *Memorias do Instituto Oswaldo Cruz*, 1991, **86**, 195.

4. Haslam, E., *Plant Polyphenols*. 1989, Cambridge, Cambridge University Press.

5. Hagerman, A. E. and Butler, L. G., *Agric. Food Chem.*, 1980, **28**, 944.

6. Murray, N. J., Ph. D. Thesis, 1994, University of Sheffield, U. K.

7. Murray, N. J., Williamson, M. P., Lilley, T. H. and Haslam, E., *Ew. J. Biochem* , 1994, **219**, 923.

8. Luck, G., Liao, H., Murray, N. J., Grimmer, H. R., Warminski, E. E., Williamson, M. P., Lilley, T. H. and Haslam, E., *Phytochemistry*, 1994, **37**, 357.

9. Wüthrich, K., *NMR of Proteins and Nucleic Acids.*, 1986, Wiley-Interscience Publication.

10. Cai, Y., Ph. D. Thesis, 1989, University of Sheffield, U. K.

11. Feeney, J., Batchelor, J. G., Albrand, J. P. and Roberts, G. C. K., *J. Magn. Reson.*, 1979, **33**, 519.

12. Martin, R., Ph. D. Thesis, 1986, University of Sheffield, U. K.

13. Hagerman, A. E. and Butler, L. G., *J. Biol. Chem.*, 1981, **256**, 4494.

14. McManus, J. P., Davis, K. G., Beart, J. E., Gaffney, S. H., Lilley, T. H. and Haslam, E., *J. Chem. Soc. Perkin Trans. 2*, 1985, 1429.

15. Cai, Y., Gaffney, S. H., Lilley, T. H., Magnolato, D., Martin, R., Spencer, C. M. and Haslam, E., *J. Chem. Soc. Perkin Trans. 2*, 1990, 2197.

16. Fernandez, J. and Lilley, T. H., *J. Chem. Soc. Faraday Trans.*, 1992, **88**, 2503.

17. Wolfenden, R., *Science*, 1983, **222**, 1087.

18. Smithrud, D. B. and Dietrich, F., *J. am. Chem. Soc.*, 1990, **112**, 339.

19. Hunter, C. A. and Sanders, J. K. M., *J. Am. Chem. Soc.*, 1990, **112**, 5525.

20. Hunter, C. A., Singh, J. and Thornton, J. M., *J. Mol. Biol.*, 1991, **218**, 837.

21. Hunter, C. A., *Angew. Chem. Intl. Ed. Engl.*, 1993, **32**, 1584.

22. Hunter, C. A., *Chem. Soc. Rev.*, 1994, 101.

23. Denys, L., Bothner-By, A. A., Fisher, G. H. and Ryan, J. W., *Biochemistry*, 1982, **21**, 6531.

24. Mirmira, S. R., Durani, S., Srivastava, S. and Phadke, R. S., *Mag. Reson. Chem.*, 1990, **28**, 587.

CHAPTER EIGHT

CONCLUDING REMARKS

8.1 Structure of procyanidins

The structure of procyanidin B-2 and its decaacetate was fully elucidated. Initial structures were based on earlier knowedge [1-6] of the compounds. The combined and systematic use of two-dimensional homo- and heteronuclear shift correlation spectroscopy allowed complete ^{1}H and ^{13}C assignments of the natural procyanidin B-2 and its decaacetate derivative. From the HMBC spectra the interflavan connectivity has been unequivocally established as C4→C8, for the first time.

Spectral data reported previously [1, 2] are in good agreement with the ^{1}H and ^{13}C NMR data and molecular modelling results presented in this thesis. The conformation of the pyran rings of the (-)epicatechin units of the procyanidin dimer were established as C2 sofa. Speculations and hypotheses put forward by earlier workers [3-6] are confirmed.

8.2 Tannin-caffeine complexation

Studies of tannin-caffeine complexation reported earlier [7] were extended to investigate the effect of solvent composition on the complexation processes. The solvent composition has an enormous effect on the complexation of caffeine with tannins. For caffeine-PGG complexation an eight times decrease in the binding was obtained when the solvent was switched from D_2O to D_2O/CD_3OD (1:1 v/v). No significant change in chemical shift for any protons of tannins was observed during titration of caffeine with tannins with increasing concentrations of tannins in

225

D_2O/CD_3OD (1:1 v/v). This implies that tannins do not self-associate in D_2O/CD_3OD (1:1 v/v). On the other hand tannins strongly self-associate in D_2O [7, 8].

The upfield chemical shift change for the protons of caffeine during the caffeine-tannin titration and the overall weakening of the association between caffeine and tannins in the presence of the hydrophobic solvent methanol re-inforce the view that caffeine-tannin association predominantly occurs *via* hydrophobic interactions. The role of hydrogen bonding is probably secondary.

8.3 Calixarene-caffeine/proline peptide complexation

The synthetic polyphenols calix[4]pyrogallolarene and calix[4]resorcin-arene were found to form significantly stable complexes in CD_3OD. Caffeine and a small prolyl peptide behaved more or less similarly. The five-membered ring of caffeine and the proline group of the peptide were found to enter the calixarene crater indicating successful molecular recognition. Interactions in methanol, if realised in aqueous media, should be highly relevant to what occurs in biological systems.

8.4 Bradykinin-tannin complexation

^{1}H NMR chemical shifts of bradykinin in ($H_2O/(CD_3)_2SO$, 4:1 v/v) were completely assigned by the combined use of TOCSY and ROESY experiments. Values of the chemical shift temperature coefficients (ppb.K^{-1}, ≈ 7.0) indicate that the bradykinin molecule remained extended, *i.e.* no internal hydrogen bonding is present.

Chemical shift data indicate that the tannins PGG, TeGG, TGG and procyanidin B-2 associate with the hormone peptide bradykinin at binding sites comprised of the residues proline (including the intervening peptide

bond), phenylalanine and arginine. Precipitation of bradykinin by tannin from aqueous media (H_2O or (D_2O/(CD_3)$_2$SO, 4:1 v/v) confirm that the bradykinin-tannin association is occuring. The peptide chemical shift changes suggest that a proline residue (proline[2] in the case of bradykinin) which is followed by another proline residue in the sequence is the preferred tannin binding site. Thus the chemical shift of protons associated with the proline[2] residue were perturbed most compared to the other proline residues. Phenyl aromatic ring protons were affected significantly. Arginine groups also took part in the complexing process which is evident from the fact that the absence of arginine residues from either termini reduces the binding strength.

The chemical shift data for protons of bradykinin and its analogues obtained from peptide-tannin titration experiments enabled the association constants for the peptide-tannin interactions to be determined. Comparison of the overall average association constants for the various peptide-tannin experiments provides the following rank of tannin binding effectiveness: PGG > TeGG >> TGG ≈ B-2.

The upfield changes in chemical shift noted for protons of the peptide in the presence of tannin indicate that the peptide-tannin binding occurs by an aromatic surface-surface interaction. The interaction is dominated by hydrophobic association but hydrogen bonding may take place to stabilize the complexes. The magnitude of the observed chemical shift changes are dependent upon the nature of the peptide-tannin interaction. A less flexible and well-defined interaction, such as that between peptide and the larger polyphenols e.g. PGG, displays large changes in chemical shift, whereas a more flexible association e.g. B-2 gives rise to smaller changes in chemical shift.

Analysis of the change in chemical shift for protons of the tannin species both in the presence and absence of peptides indicates that the tannin molecules are self-associated when bound to the peptides.

The formation of precipitates with tannins having multiple aromatic surfaces at very low peptide: tannin mole ratio from water and also the formation of precipitate during titration experiments at higher mole ratios and their subsequent dissolution at elevated temperature suggest that precipitation of the peptide-tannin complexes arises from non-covalent cross-linking. Peptide-tannin and tannin-tannin intermolecular crosslinking and subsequent precipitation is promoted by the multidentate and flexible nature of both the peptide and the tannin molecules.

No evidence was obtained to show that the peptide underwent significant changes from a random coil conformation upon complexation with tannins. Although the most significant proton chemical shift changes in the bradykinin were associated with each of the three proline residues and the two phenylalanyl groups, suggesting that these amino acid side chains were participating preferentially in the complexation with tannin, it is not thought probable that there is a specific mode of binding between the tannin and peptide substrates. Rather the driving force is visualised as the relatively unselective association of the aromatic nuclei of the tannin with hydrophobic groups on the nonapeptide followed by secondary hydrogen bonding re-inforcing this initial complexation.

Clearly natural polyphenols such as PGG possess the property of precipitating and/or sequestering bioactive peptides such as bradykinin and its derivatives *in vitro*. It would be now of considerable interest to ascertain if and how tannins modify *in vivo* physiological actions of bradykinin.

8.5 Tannin-protein precipitation

The phenomenon of tannin-protein precipitation has been known about for centuries, e.g. Sir Humphrey Davy described his observations [9] on isinglass and tannin extracts in 1803. Leather making, another example of tannin-protein complexation and/or precipitation, is a craft of great antiquity which has over the years achieved a very high degree of technical development. Plant extracts (vegetable tannins) were employed exclusively to tan hides and skins to make leather for well over 1000 years. History dictated that the impact of science and the new technologies on vegetable tannage should be small. Emil Fischer, Karl Freudenberg and Paul Karrer made some characteristically brilliant and definitive studies of the chemistry of vegetable tannins in the early years of this century (around 1920's) but by the 1940's this area was untidy, neglected and quite unfashionable. Interests reawakened in the 1960's as the importance of vegetable tannins or plant polyphenols to a host of questions in biology, agriculture and the food industries, and medicine was realised. The structure, biosynthesis and chemical properties of tannins are now well understood. Studies of their physical properties – particularly as they relate to various intermolecular complexation phenomena – have now also begun to take shape and the role of tannins in the reactions, such as occur with collagen in the formation of leathers, is now beginning to be understood at the molecular level.

It is now both timely and strategically appropriate that this fundamental scientific knowledge should be deployed in the technology of leather manufacture using natural vegetable tannins, or as they are better defined, plant polyphenols.

It has long been thought that the biological as well as the industrial aspects of tannins may be primarily attributed to their propensity to bind

to and, in some cases, precipitate certain substrates, e.g. proteins. It was hoped that studies of homogeneous tannins with single proteins or peptides would illuminate these important aspects of the action of tannins. As tannin-protein precipitation has already been studied in some detail [10], for the purpose of the present study important and relevant knowledge from that study was extracted and only few highly relevant experiments were performed as a matter of demonstration. The findings were as below.

The aggregation of tannin-proten complexes, thereby producing precipitation, can be dramatically altered by conditions mainly affecting the protein component. The ease with which aggregation is affected is primarily linked to the charged nature of the protein i.e. to electrostatic attractions or repulsions. These effects are most readily seen in the pH dependence of precipitation. Here, the overall charge of certain proteins can be increased to such a level that precipitation is completely prevented by the inhibition of aggregation induced by coulombic repulsions.

At pH levels before drastic curtailment of precipitation occurred, it was noticed that more polyphenol was being incorporated into the precipitate. This increase in polyphenol 'uptake' may well be caused by expansion of the protein tertiary structure brought about by these acidic pH's. The seemingly paradoxical increase in polyphenolic complexation accompanied by a decrease in precipitation seems to reflect the dominance of the relative change in intercomplex coulombic repulsions over that of the forces responsible for complex aggregation. Generally, precipitation is primarily controlled by a balance between the strength and ability of the polyphenol to complex with proteins and the counteracting Coulombic repulsions between the complexes thus formed. In other words complexation may well occur but the 'freedom' to aggregate determines

whether precipitation occurs. The hydrophobic effect, which is thought to be the primary driving force for polyphenol-protein complexation and especially for aggregation of the polyphenol-protein complexes, may be effectively counteracted by electrostatic forces.

That the tannin-protein interaction has been described as primarily arising from the hydrophobic effect does not necessarily mean that additional forces may not be involved. It has been suggested that the selectivity shown in particular systems may come about by the supplementation of the hydrophobic effect by a complementary 'local' network of hydrogen bonding. The balance between these two types of non-covalent binding forces depends upon the nature of both participating components. However, it is also suggested that selectivity and overall strength of binding primarily occurs through the flexibility of the protein component. It is this feature of the protein's conformational properties that is enhanced by a high proline content as opposed to the imino acid itself acting as a specific binding site.

It would appear that tannin-protein complexation is indeed a general surface phenomenon which involves relatively simple 'ligand' binding processes. Once enough ligands have been attached to the protein and when the critical stoichiometry is exceeded, precipitation ensues. If the initial binding to the protein is relatively weak, precipitation levels will be low and it is unlikely that the critical stoichiometry will be significantly exceeded, thereby resulting in the precipitate having an invariant stoichiometry. Conversely, if binding is strong (such as is brought about by the flexibility of the protein component which may result in encapsulation of the polyphenol) the critical stoichiometry can be exceeded and variable stoichiometry may be observed.

General tannin-protein precipitation thus provided a macroscopic picture of the tannin-protein complexation. The behaviour of tannin itself in the system and the microscopic tannin and protein binding sites were not possible to positively ascertain. Now it might not be very unrealistic to assume that the behaviour of tannin in tannin-peptide systems described in the earlier section (and in chapter 7) should prevail in the tannin-protein precipitation processes. If so, then the overall picture of tannin-protein complexation and precipitation may be visualized as processes that occur *via* non-covalent forces and the tannin-protein and tannin-tannin intermolecular cross-linking and subsequent precipitation is promoted by the multidentate and flexible nature of both proteins and tannin molecules. The principal binding sites on proteins and tannins are proline residues and galloyl/aromatic rings, respectively.

References

1.   Thompson, R. S., Jacques, D., Haslam, E. and Tanner, R. J. N., *J. Chem. Soc. Perkin Trans. 1*, 1972, 1387.

2.   Porter, L. J., Newman, R. H., Foo, L. Y. and Wong, H., *J. Chem. Soc. Perkin Trans. 1*, 1982, 1217.

3.   Weinges, K., Marx, H. -D. and Goritz, K., *Chem. Ber.*, 1970, **103**, 2336.

4.   Jurd, L. and Lundin, R., *Tetrahedron*, 1968, **24**, 2653.

5.   Fletcher, A. C., Porter, L. J., Haslam, E. and Gupta, R. K., *J. Chem. Soc. Perkin Trans. 1*, 1977, 1628.

6. du Preez, I. C., Rowan, A. C., Roux, D. G. and Feeny, J., *J. Chem. Soc. Chem. Commun.*, 1971, 315.

7. Cai, Y., 1989, Ph. D. Thesis, University of Sheffield, U. K.

8. Martin, R., 1988, Ph. D. Thesis, University of Sheffield, U. K.

9. Davy, H., in *Incunabula of Tannin Chemistry (from Phil. Trans. 1803),* M. Nierenstein and E. Arnold, Editors, 1932, London, p. 116.

10. Warminski, E. E., 1992, Ph. D. Thesis, University of Sheffield, U. K.

APPENDICES

Appendix A.1 Tannin-protein precipitation data

A.1.1 PGG-Gelatin precipitation in 10 mM acetate buffer, pH 5.4, 293-295 K. The initial concentration of PGG was 10 µM.

Initial concentra -tion of gelatin (µM)	Absorbance at λ_1 (215 nm)	Absorbance at λ_2 (280 nm)	% Relative absorbance	PGG in the precipitate (µM)	Gelatin in the precipitate (µM)	Mole ratio in the precipitate
0.000	0.983	0.432	00.00	0.000	0.000	-
0.040	0.740	0.324	24.83	2.667	0.033	80.82
0.121	0.500	0.207	51.92	5.374	0.097	55.40
0.201	0.359	0.130	69.84	7.175	0.150	47.83
0.281	0.386	0.116	73.09	7.492	0.181	41.39
0.362	0.422	0.108	74.94	7.689	0.219	35.11
0.442	0.487	0.105	75.64	7.759	0.242	32.06
0.523	0.551	0.104	75.87	7.785	0.269	28.94
0.603	0.634	0.107	75.17	7.721	0.288	26.81
0.683	0.701	0.105	75.64	7.789	0.307	25.37
0.764	0.822	0.115	73.32	7.525	0.317	23.73
0.844	0.910	0.114	73.55	7.595	0.321	23.66
0.925	1.041	0.108	74.94	7.769	0.281	27.65
1.005	1.104	0.121	71.93	7.441	0.340	21.89
1.085	1.114	0.093	78.42	8.145	0.367	22.19

A.1.2 PGG-BSA system

A.1.2.1 PGG-BSA precipitation in 10 mM acetate buffer, pH 5.4, 293-295 K. The initial concentration of PGG was 10 µM.

Initial concentra -tion of BSA µM	Absorbance at λ_1 (215 nm)	Absorbance at λ_2 (280 nm)	% Relative absorbance	PGG in the precipitate (µM)	BSA in the precipitate (µM)	Mole ratio in the precipitate
0.000	0.880	0.384	00.00	0.000	00.000	-
0.048	0.912	0.388	-	0.032	0.017	01.88
0.096	0.848	0.360	7.22	0.768	0.065	11.82
0.144	0.748	0.314	19.07	1.985	0.106	18.73
0.192	0.704	0.292	24.74	2.572	0.145	17.74
0.240	0.714	0.267	31.19	3.319	0.106	31.31
0.288	0.683	0.261	32.73	3.454	0.176	19.63
0.336	0.632	0.239	38.40	4.032	0.226	17.92
0.384	0.631	0.228	41.24	4.353	0.242	17.99
0.432	0.647	0.227	41.50	4.404	0.266	16.56
0.480	0.687	0.226	41.75	4.486	0.259	17.32
0.720	0.772	0.201	48.20	5.333	0.313	17.04
0.816	0.872	0.200	48.45	5.495	0.276	19.91
0.912	0.898	0.197	49.28	5.517	0.329	16.77
1.008	0.991	0.201	48.20	5.620	0.315	17.85

A.1.3.2 PGG-BSA precipitation in 10 mM acetate buffer, pH 4.0, 293-295 K. The initial concentration of PGG was 10 μM.

Initial concentra -tion of BSA μM	Absorbance at λ_1 (215 nm)	Absorbance at λ_2 (280 nm)	% Relative absorbance	PGG in the precipitate (μM)	BSA in the precipitate (μM)	Mole ratio in the precipitate
0.000	0.959	0.417	00.00	0.000	0.000	-
0.048	0.886	0.394	5.516	0.530	0.083	6.39
0.096	0.899	0.382	08.39	0.890	0.060	14.83
0.144	0.957	0.402	03.59	0.420	0.087	4.83
0.192	0.998	0.390	06.48	0.825	0.014	58.93
0.240	1.013	0.389	06.72	0.878	0.032	27.43
0.288	1.043	0.374	10.31	1.349	-	-
0.336	1.015	0.350	16.07	1.982	-	-
0.384	1.098	0.393	05.55	0.904	0.043	21.02
0.432	1.122	0.391	06.23	0.999	0.041	24.37
0.480	1.151	0.388	06.95	1.131	0.026	43.50
0.720	1.310	0.396	05.04	1.164	0.019	61.26
0.816	1.368	0.396	05.04	1.259	0.013	96.84
0.912	1.445	0.403	03.36	1.187	0.002	-
1.008	1.465	0.398	04.56	1.361	0.043	31.65

A.1.2.4 PGG-PVP precipitation in 50 mM NaCl(aq) solution at 293-295 K. The initial concentration of PGG was 10 μM.

Initial concentra -tion of PVP μM	Absorbance at λ_1 (215 nm)	Absorbance at λ_2 (280 nm)	% Relative absorbance at λ_2 (280 nm)	PGG in the precipitate (μM)	PVP in the precipitate (μM)	Mole ratio in the precipitate
0.000	0.948	0.419	00.00	0.000	0.000	-
0.332	0.648	0.282	32.70	3.337	-	-
0.664	0.471	0.201	52.03	5.310	0.521	10.19
0.996	0.244	0.100	76.13	7.770	0.842	9.23
1.328	0.144	0.050	88.07	8.988	1.060	8.48
1.660	0.126	0.032	92.36	9.428	1.196	8.60
1.992	0.160	0.040	90.45	9.235	1.390	6.64
2.324	0.269	0.071	83.06	8.483	1.386	6.12
3.320	0.585	0.156	62.77	6.422	1.311	4.90
4.150	1.085	0.300	28.40	2.928	0.633	4.63
4.980	1.328	0.357	14.80	1.549	0.476	3.25
5.810	1.449	0.368	12.17	1.288	0.474	2.72
6.640	1.617	0.388	07.40	0.811	0.241	3.37
8.300	1.805	0.393	06.21	0.702	0.372	1.89
9.960	2.010	0.396	5.49	0.644	0.316	2.04

Appendix A.2 Caffeine-tannin titration data

A.2.1 Proton assignments (ppm) for caffeine and PGG (incomplete) from the titration of PGG into caffeine. Aliquots (0-160 µl) of 60 mM PGG in D_2O/CD_3OD (1:1, v/v) were titrated into 600 µl 2 mM caffeine dissolved in the same solvent to give PGG concentrations of 0-12.63 mM at the mole ratios indicated in the table. The titration was followed by one-dimensional ^1H NMR experiments, recorded at 295 K. Chemical shifts are given relative to external TSP in the same solvent ± 0.001 ppm.

PGG added (µl)	[PGG] (mM)	[caffeine] (mM)	mole ratio [PGG]/ [Caff.]	H8	Me7	Me3	Me1
0	0.00	2.00	0.0	7.916	3.968	3.538	3.355
10	0.98	1.97	0.5	7.897	3.957	3.528	3.345
20	1.94	1.94	1.0	7.880	3.946	3.519	3.336
30	2.86	1.91	1.5	7.865	3.935	3.510	3.327
40	3.75	1.88	2.0	7.850	3.925	3.502	3.319
50	4.62	1.85	2.5	7.837	3.916	3.494	3.311
60	5.46	1.82	3.0	7.824	3.908	3.487	3.305
70	6.27	1.80	3.5	7.812	3.900	3.480	3.297
80	7.06	1.77	4.0	7.801	3.893	3.474	3.292
90	7.83	1.74	4.5	7.792	3.887	3.469	3.286
100	8.57	1.71	5.0	7.783	3.880	3.463	3.281
120	10.00	1.67	6.0	7.765	3.869	3.453	3.271
140	11.35	1.62	7.0	7.750	3.858	3.445	3.263
160	12.63	1.58	8.0	7.737	3.850	3.437	3.255

Glucose C1	Glucose C3	Galloyl C1	Galloyl C2	Galloyl C3	Galloyl C4	Galloyl C6
-	-	-	-	-	-	-
6.244	5.921	7.060	6.974	6.911	6.979	7.090
6.245	5.922	7.062	6.975	6.912	6.981	7.090
6.246	5.922	7.063	6.975	6.912	6.981	7.090
6.246	5.922	7.063	6.975	6.912	6.981	7.091
6.246	5.921	7.064	6.976	6.912	6.982	7.091
6.245	5.921	7.065	6.976	6.913	6.982	7.091
6.245	5.921	7.065	6.976	6.913	6.983	7.091
6.245	5.921	7.066	6.976	6.914	6.983	7.091
6.245	5.921	7.067	6.976	6.914	6.984	7.091
6.245	5.920	7.067	6.976	6.914	6.984	7.091
6.244	5.920	7.068	6.977	6.915	6.985	7.092
6.244	5.919	7.069	6.977	6.915	6.986	7.092
6.244	5.919	7.070	6.977	6.916	6.986	7.092

A.2.2 Proton assignments (ppm) for caffeine from the titration of TeGG into caffeine. Aliquots (0-100 µl) of 60 mM TeGG in D_2O/CD_3OD (1:1, v/v) were titrated into 600 µl 2 mM caffeine dissolved in the same solvent to give TeGG concentrations of 0-8.57 mM at the mole ratios indicated in the table. The titration was followed by one-dimensional ^1H NMR experiments, recorded at 295 K. Chemical shifts are given relative to external TSP in the same solvent ± 0.001 ppm.

TeGG added (µl)	[TeGG] (mM)	[caffeine] (mM)	mole ratio [TeGG]/ [Caff.]	H8	Me7	Me3	Me1
0	0.00	2.00	0.0	7.916	3.968	3.539	3.356
10	0.98	1.97	0.5	7.900	3.959	3.529	3.347
20	1.94	1.94	1.0	7.885	3.948	3.521	3.339
30	2.86	1.91	1.5	7.872	3.939	3.513	3.332
40	3.75	1.88	2.0	7.859	3.931	3.506	3.325
50	4.62	1.85	2.5	7.846	3.923	3.499	3.317
60	5.46	1.82	3.0	7.835	3.915	3.492	3.311
70	6.27	1.80	3.5	7.826	3.909	3.486	-
80	7.06	1.77	4.0	7.815	3.902	3.480	3.301
90	7.83	1.74	4.5	7.807	3.897	3.476	3.297
100	8.57	1.71	5.0	7.797	3.892	3.471	3.292

A.2.3 Proton assignments (ppm) for caffeine from the titration of TGG into caffeine. Aliquots (0-150 µl) of 60 mM TGG in D_2O/CD_3OD (1:1, v/v) were titrated into 600 µl 2 mM caffeine dissolved in the same solvent to give TGG concentrations of 0- 12.00 mM at the mole ratios indicated in the table. The titration was followed by one-dimensional ^1H NMR experiments, recorded at 295 K. Chemical shifts are given relative to external TSP in the same solvent ± 0.001 ppm.

TGG added (µl)	[TGG] (mM)	[caffeine] (mM)	mole ratio [TGG]/ [Caff.]	H8	Me7	Me3	Me1
0	0.00	2.00	0.0	7.916	3.968	3.538	3.355
10	0.98	1.97	0.5	7.905	3.961	3.532	3.350
20	1.94	1.94	1.0	7.895	3.955	3.525	3.344
30	2.86	1.91	1.5	7.885	3.949	3.519	3.339
40	3.75	1.88	2.0	7.877	3.943	3.514	3.335
50	4.62	1.85	2.5	7.868	3.936	3.508	3.329
60	5.46	1.82	3.0	7.859	3.931	3.503	3.325
70	6.27	1.80	3.5	7.853	3.926	3.498	3.321
80	7.06	1.77	4.0	7.846	3.922	3.494	3.317
90	7.83	1.74	4.5	7.839	3.917	3.489	-
110	9.30	1.69	5.5	7.827	3.908	3.482	-
130	10.68	1.64	6.5	7.816	3.901	3.474	3.301
150	12.00	1.60	7.5	7.806	3.894	3.468	3.295

237

A.2.4 Proton assignments (ppm) for caffeine from the titration of DGG into caffeine. Aliquots (0-160 μl) of 60 mM DGG in D_2O/CD_3OD (1:1, v/v) were titrated into 600 μl 2 mM caffeine dissolved in the same solvent to give DGG concentrations of 0-12.63 mM at the mole ratios indicated in the table. The titration was followed by one-dimensional ^{1}H NMR experiments, recorded at 295 K. Chemical shifts are given relative to external TSP in the same solvent ± 0.001 ppm.

DGG added (μl)	[DGG] (mM)	[caffeine] (mM)	mole ratio [DGG]/ [Caff.]	H8	Me7	Me3	Me1
0	0.00	2.00	0.0	7.916	3.969	3.539	3.356
10	0.98	1.97	0.5	7.911	3.966	3.535	3.353
20	1.94	1.94	1.0	7.907	3.963	3.532	3.350
30	2.86	1.91	1.5	7.903	3.961	3.539	3.348
40	3.75	1.88	2.0	7.899	3.958	3.526	3.345
50	4.62	1.85	2.5	7.895	3.955	3.523	3.343
60	5.46	1.82	3.0	7.892	3.953	3.521	3.341
70	6.27	1.80	3.5	7.888	3.951	3.518	3.339
80	7.06	1.77	4.0	7.885	3.949	3.516	3.337
90	7.83	1.74	4.5	7.882	3.947	3.513	3.335
100	8.57	1.71	5.0	7.879	3.945	3.511	3.333
120	10.00	1.67	6.0	7.873	3.941	3.507	3.330
140	11.35	1.62	7.0	7.868	3.938	3.503	3.326
160	12.63	1.58	8.0	7.863	3.935	3.499	3.323

A.2.5 Proton assignments (ppm) for caffeine from the titration of DGAG into caffeine. Aliquots (0-100 μl) of 60 mM DGAG in D_2O/CD_3OD (1:1, v/v) were titrated into 600 μl 2 mM caffeine dissolved in the same solvent to give DGAG concentrations of 0-8.57 mM at the mole ratios indicated in the table. The titration was followed by one-dimensional ^{1}H NMR experiments, recorded at 295 K. Chemical shifts are given relative to external TSP in the same solvent ± 0.001 ppm.

DGAG added (μl)	[DGAG] (mM)	[caffeine] (mM)	mole ratio [DGAG]/ [Caff.]	H8	Me7	Me3	Me1
0	0.00	2.00	0.0	7.917	3.968	3.539	3.356
10	0.98	1.97	0.5	7.913	3.966	3.536	3.353
20	1.94	1.94	1.0	7.909	3.963	3.533	3.351
30	2.86	1.91	1.5	7.905	3.961	3.530	3.348
40	3.75	1.88	2.0	7.902	3.959	3.527	3.346
50	4.62	1.85	2.5	7.898	3.956	3.524	3.344
60	5.46	1.82	3.0	7.893	3.953	3.521	3.341
70	6.27	1.80	3.5	7.890	3.951	3.519	3.339
80	7.06	1.77	4.0	7.887	3.949	3.516	3.337
90	7.83	1.74	4.5	7.884	3.947	3.514	3.335
100	8.57	1.71	5.0	7.881	3.945	3.512	3.333

A.2.6 Proton assignments (ppm) for caffeine from the titration of MeG into caffeine. Aliquots (0-200 µl) of 60 mM MeG in D_2O/CD_3OD (1:1, v/v) were titrated into 600 µl 2 mM caffeine dissolved in the same solvent to give MeG concentrations of 0-15.00 mM at the mole ratios indicated in the table. The titration was followed by one-dimensional ^1H NMR experiments, recorded at 295 K. Chemical shifts are given relative to external TSP in the same solvent ± 0.001 ppm.

MeG added (µl)	[MeG] (mM)	[caffeine] (mM)	mole ratio [MeG]/ [Caff.]	H8	Me7	Me3	Me1
0	0.00	2.00	0	7.916	3.969	3.539	3.356
20	1.94	1.94	1	7.912	3.966	3.536	3.353
40	3.75	1.88	2	7.907	3.963	3.532	3.350
60	5.46	1.82	3	7.903	3.961	3.529	3.348
80	7.06	1.76	4	7.899	3.958	3.526	3.345
100	8.57	1.71	5	7.895	3.956	3.524	3.343
120	10.00	1.67	6	7.892	3.954	3.521	3.341
140	11.35	1.62	7	7.889	3.951	3.519	3.338
160	12.63	1.58	8	7.886	3.950	3.516	3.337
180	13.85	1.54	9	7.884	3.948	3.514	3.335
200	15.00	1.50	10	7.880	3.946	3.512	3.333

A.2.7 Proton assignments (ppm) for caffeine from the titration of epicatechin into caffeine. Aliquots (0-180 µl) of 60 mM epicatechin in D_2O/CD_3OD (1:1, v/v) were titrated into 600 µl 2 mM caffeine dissolved in the same solvent to give epicatechin concentrations of 0-13.85 mM at the mole ratios indicated in the table. The titration was followed by one-dimensional ^1H NMR experiments, recorded at 295 K. Chemical shifts are given relative to external TSP in the same solvent ± 0.001 ppm.

epicat. added (µl)	[epicat.] (mM)	[caffeine] (mM)	mole ratio [epicat.]/ [Caff.]	H8	Me7	Me3	Me1
0	0.00	2.00	0.0	7.916	3.969	3.539	3.356
10	0.98	1.97	0.5	7.914	3.967	3.537	3.354
20	1.94	1.94	1.0	7.911	3.964	3.536	3.353
30	2.86	1.91	1.5	7.909	3.964	3.534	3.352
40	3.75	1.88	2.0	7.907	3.962	3.533	3.350
50	4.62	1.85	2.5	7.905	3.960	3.531	3.349
60	5.46	1.82	3.0	7.903	3.959	3.530	3.347
70	6.27	1.80	3.5	7.901	3.957	3.529	3.346
80	7.06	1.77	4.0	7.899	3.956	3.527	3.345
100	8.57	1.71	5.0	7.896	3.953	3.525	3.343
120	10.00	1.67	6.0	7.893	3.951	3.522	3.340
140	11.35	1.62	7.0	7.889	3.948	3.520	3.338
160	12.63	1.58	8.0	7.887	3.946	3.519	3.337
180	13.85	1.54	9.0	7.884	3.944	3.516	3.334

A.2.8 Proton assignments (ppm) for caffeine from the titration of EGCG into caffeine. Aliquots (0-160 µl) of 60 mM EGCG in D_2O/CD_3OD (1:1, v/v) were titrated into 600 µl 2 mM caffeine dissolved in the same solvent to give EGCG concentrations of 0-12.63 mM at the mole ratios indicated in the table. The titration was followed by one-dimensional ^1H NMR experiments, recorded at 295 K. Chemical shifts are given relative to external TSP in the same solvent ± 0.001 ppm.

EGCG added (µl)	[EGCG] (mM)	[caffeine] (mM)	mole ratio [EGCG]/ [Caff.]	H8	Me7	Me3	Me1
0	0.00	2.00	0.0	7.916	3.969	3.539	3.356
10	0.98	1.97	0.5	7.907	3.963	3.535	3.352
20	1.94	1.94	1.0	7.898	3.958	3.531	3.349
30	2.86	1.91	1.5	7.889	3.953	3.527	3.345
40	3.75	1.88	2.0	7.882	3.948	3.524	3.342
50	4.62	1.85	2.5	7.874	3.943	3.520	3.339
60	5.46	1.82	3.0	7.867	3.939	3.517	3.336
70	6.27	1.80	3.5	7.859	3.935	3.514	3.333
80	7.06	1.77	4.0	7.853	3.930	3.511	3.330
90	7.83	1.74	4.5	7.846	3.926	3.508	3.328
100	8.57	1.71	5.0	7.841	3.923	3.505	3.325
120	10.00	1.67	6.0	7.828	3.916	3.500	3.320
140	11.35	1.62	7.0	7.817	3.909	3.495	3.316
160	12.63	1.58	8.0	7.807	3.903	3.491	3.311

A.2.9 Proton assignments (ppm) for caffeine from the titration of A-2 into caffeine. Aliquots (0-160 µl) of 60 mM A-2 in D_2O/CD_3OD (1:1, v/v) were titrated into 600 µl 2 mM caffeine dissolved in the same solvent to give A-2 concentrations of 0-12.63 mM at the mole ratios indicated in the table. The titration was followed by one-dimensional ^1H NMR experiments, recorded at 295 K. Chemical shifts are given relative to external TSP in the same solvent ± 0.001 ppm.

A-2 added (µl)	[A-2] (mM)	[caffeine] (mM)	mole ratio [A-2]/ [Caff.]	H8	Me7	Me3	Me1
0	0.00	2.00	0.0	7.916	3.969	3.539	3.356
10	0.98	1.97	0.5	7.909	3.965	3.537	3.354
20	1.94	1.94	1.0	7.902	3.962	3.535	3.352
30	2.86	1.91	1.5	7.896	3.959	3.534	3.351
40	3.75	1.88	2.0	7.890	3.955	3.532	3.349
50	4.62	1.85	2.5	7.884	3.952	3.530	3.347
60	5.46	1.82	3.0	7.878	3.949	3.528	3.345
70	6.27	1.80	3.5	7.873	3.946	3.526	3.344
80	7.06	1.77	4.0	7.867	3.943	3.525	3.342
90	7.83	1.74	4.5	7.862	3.941	3.523	3.340
100	8.57	1.71	5.0	7.857	3.938	3.522	3.339
120	10.00	1.67	6.0	7.848	3.933	3.519	3.336
140	11.35	1.62	7.0	7.839	3.929	3.517	3.334
160	12.63	1.58	8.0	7.831	3.925	3.514	3.332

A.2.10 Proton assignments (ppm) for caffeine from the titration of B-2 into caffeine. Aliquots (0-160 μl) of 60 mM B-2 in D_2O/CD_3OD (1:1, v/v) were titrated into 600 μl 2 mM caffeine dissolved in the same solvent to give B-2 concentrations of 0-12.63 mM at the mole ratios indicated in the table. The titration was followed by one-dimensional ^1H NMR experiments, recorded at 295 K. Chemical shifts are given relative to external TSP in the same solvent ± 0.001 ppm.

B-2 added (μl)	[B-2] (mM)	[caffeine] (mM)	mole ratio [B-2]/ [Caff.]	H8	Me7	Me3	Me1
0	0.00	2.00	0.0	7.916	3.969	3.539	3.356
10	0.98	1.97	0.5	7.912	3.967	3.537	3.354
20	1.94	1.94	1.0	7.908	3.964	3.535	3.353
30	2.86	1.91	1.5	7.904	3.962	3.533	3.351
40	3.75	1.88	2.0	7.900	3.960	3.531	3.350
50	4.62	1.85	2.5	7.897	3.958	3.530	3.348
60	5.46	1.82	3.0	7.893	3.956	3.528	3.347
70	6.27	1.80	3.5	7.889	3.954	3.527	3.346
80	7.06	1.77	4.0	7.886	3.952	3.525	3.344
90	7.83	1.74	4.5	7.883	3.950	3.524	3.343
100	8.57	1.71	5.0	7.880	3.948	3.522	3.342
120	10.00	1.67	6.0	7.874	3.945	3.519	3.340
140	11.35	1.62	7.0	7.869	3.942	3.517	3.338
160	12.63	1.58	8.0	7.862	3.939	3.514	3.336

A.2.11 Proton assignments (ppm) for caffeine from the titration of B-3 into caffeine. Aliquots (0-160 μl) of 60 mM B-3 in D_2O/CD_3OD (1:1, bv/v) were titrated into 600 μl 2 mM caffeine dissolved in the same solvent to give B-3 concentrations of 0-12.63 mM at the mole ratios indicated in the table. The titration was followed by one-dimensional ^1H NMR experiments, recorded at 295 K. Chemical shifts are given relative to external TSP in the same solvent ± 0.001 ppm.

B-3 added (μl)	[B-3] (mM)	[caffeine] (mM)	mole ratio [B-3]/ [Caff.]	H8	Me7	Me3	Me1
0	0.00	2.00	0.0	7.917	3.969	3.539	3.356
10	0.98	1.97	0.5	7.911	3.965	3.536	3.354
20	1.94	1.94	1.0	7.905	3.962	3.533	3.351
30	2.86	1.91	1.5	7.900	3.959	3.531	3.349
40	3.75	1.88	2.0	7.895	3.956	3.528	3.347
50	4.62	1.85	2.5	7.891	3.953	3.526	3.345
60	5.46	1.82	3.0	7.886	3.949	3.523	3.342
70	6.27	1.80	3.5	7.882	3.947	3.521	3.341
80	7.06	1.77	4.0	7.878	3.944	3.519	3.339
90	7.83	1.74	4.5	7.874	3.942	3.517	3.337
100	8.57	1.71	5.0	7.870	3.939	3.514	3.335
120	10.00	1.67	6.0	7.863	3.935	3.511	3.332
140	11.35	1.62	7.0	7.857	3.931	3.508	3.329
160	12.63	1.58	8.0	7.850	3.926	3.504	3.326

A.2.12 Proton assignments (ppm) for caffeine from the titration of B-4 into caffeine. Aliquots (0-160 μl) of 60 mM B-4 in D_2O/CD_3OD (1:1, v/v) were titrated into 600 μl 2 mM caffeine dissolved in the same solvent to give B-4 concentrations of 0-12.63 mM at the mole ratios indicated in the table. The titration was followed by one-dimensional ^{1}H NMR experiments, recorded at 295 K. Chemical shifts are given relative to external TSP in the same solvent ± 0.001 ppm.

B-4 added (μl)	[B-4] (mM)	[caffeine] (mM)	mole ratio [B-4]/ [Caff.]	H8	Me7	Me3	Me1
0	0.00	2.00	0.0	7.917	3.969	3.539	3.356
10	0.98	1.97	0.5	7.910	3.964	3.536	3.353
20	1.94	1.94	1.0	7.904	3.961	3.533	3.351
30	2.86	1.91	1.5	7.899	3.957	3.530	3.348
40	3.75	1.88	2.0	7.893	3.954	3.528	3.346
50	4.62	1.85	2.5	7.888	3.951	3.524	3.344
60	5.46	1.82	3.0	7.883	3.947	3.522	3.341
70	6.27	1.80	3.5	7.879	3.944	3.520	3.339
80	7.06	1.77	4.0	7.874	3.941	3.517	3.337
90	7.83	1.74	4.5	7.870	3.938	3.515	3.335
100	8.57	1.71	5.0	7.866	3.936	3.513	3.334
120	10.00	1.67	6.0	7.859	3.931	3.509	3.330
140	11.35	1.62	7.0	7.851	3.926	3.505	3.327
160	12.63	1.58	8.0	7.845	3.922	3.502	3.324

Appendix A.3 Caffeine-calixarene titration data

A.3.1 Proton assignments (ppm) for caffeine from the titration of calix[4]resorcinarene (C[4]RA) into caffeine. Aliquots (0-250 μl) of 20 mM calix[4]resorcinarene in CD_3OD were titrated into 500 μl 2 mM caffeine dissolved in the same solvent to give calix[4]resorcinarene concentrations of 0-6.67 mM at the mole ratios indicated in the table. Stock solution of calix[4]resorcinarene was prepared by dissolving the compound in 2 mM caffeine solution. The titration was followed by one-dimensional ^{1}H NMR experiments, recorded at 295 K. Chemical shifts are given relative to external TSP in the same solvent ± 0.001 ppm.

C[4]RA added (μl)	[C[4]RA] (mM)	[caffeine] (mM)	mole ratio [C[4]RA]/ [Caff.]	H8	Me7	Me3	Me1
0	0.00	2.00	0.0	7.857	3.966	3.526	3.344
25	0.95	,,	0.5	7.847	3.957	3.525	3.344
50	1.82	,,	0.9	7.839	3.948	3.525	3.343
75	2.61	,,	1.3	7.831	3.941	3.524	3.343
100	3.33	,,	1.7	7.824	3.933	3.524	3.343
125	4.00	,,	2.0	7.817	3.926	3.524	3.343
150	4.62	,,	2.3	7.811	3.921	3.523	3.343
175	5.19	,,	2.6	7.805	3.915	3.523	3.342
200	5.71	,,	2.9	7.800	3.910	3.523	3.342
225	6.21	,,	3.1	7.795	3.905	3.523	3.342
250	6.67	,,	3.3	7.790	3.900	3.522	3.342

A.3.2 Proton assignments (ppm) for caffeine from the titration of calix[4]pyrogallolarene (C[4]PA) into caffeine. Aliquots (0-250 μl) of 20 mM calix[4]pyrogallolarene in CD_3OD were titrated into 500 μl 2 mM caffeine dissolved in the same solvent to give calix[4]resorcinarene concentrations of 0-6.67 mM at the mole ratios indicated in the table. Stock solution of calix[4]pyrogallolarene was prepared by dissolving the compound in 2 mM caffeine solution. The titration was followed by one-dimensional ^{1}H NMR experiments, recorded at 295 K. Chemical shifts are given relative to external TSP in the same solvent ± 0.001 ppm.

C[4]PA added (μl)	[C[4]PA] (mM)	[caffeine] (mM)	mole ratio [C[4]PA]/ [Caff.]	H8	Me7	Me3	Me1
0	0.00	2.00	0.0	7.857	3.966	3.526	3.344
25	0.95	,,	0.5	7.843	3.951	3.525	3.344
50	1.82	,,	0.9	7.829	3.936	3.524	3.343
75	2.61	,,	1.3	7.816	3.924	3.524	3.343
100	3.33	,,	1.7	7.805	3.912	3.524	3.342
125	4.00	,,	2.0	7.794	3.901	3.523	3.343
150	4.62	,,	2.3	7.784	3.891	3.523	3.342
175	5.19	,,	2.6	7.775	3.882	3.522	3.342
200	5.71	,,	2.9	7.766	3.873	3.522	3.342
225	6.21	,,	3.1	7.758	3.865	3.522	3.342
250	6.67	,,	3.3	7.751	3.858	3.522	3.342

A.3.3 Proton assignments (ppm) for N-Ac-Pro-Gly-NH$_2$ that were used to obtain association constants (K_a) from the titration of calix[4]resorcinarene (C[4]RA) into N-Ac-Pro-Gly-NH$_2$ (Pro-Gly). Aliquots (0-360 µl) of 30 mM calix[4]resorcinarene in CD$_3$OD were titrated into 600 µl 2 mM N-Ac-Pro-Gly-NH$_2$ dissolved in the same solvent to give calix[4]resorcinarene concentrations of 0-11.25 mM at the mole ratios indicated in the table. Stock solution of calix[4]resorcinarene was prepared by dissolving the compound in 2 mM N-Ac-Pro-Gly-NH$_2$ solution. The titration was followed by one-dimensional ^{1}H NMR experiments, recorded at 295 K. Chemical shifts are given relative to external TSP in the same solvent ± 0.001 ppm.

C[4]RA added (µl)	[C[4]RA] (mM)	[Pro-Gly] (mM)	mole ratio [C[4]RA]/ [Pro-Gly]	Pα	Pδ1	Gα1	Me
0	0.00	2.00	0.0	4.301	3.615	3.725	2.098
10	0.49	,,	0.2	4.296	3.601	3.724	2.094
20	0.97	,,	0.5	4.289	3.587	3.724	2.090
30	1.43	,,	0.7	4.283	3.574	3.723	2.086
40	1.88	,,	0.9	4.278	3.564	3.723	2.084
50	2.31	,,	1.2	4.272	3.548	3.721	2.079
70	3.13	,,	1.6	-	3.526	3.721	2.072
90	3.91	,,	2.0	4.252	3.505	3.720	2.066
110	4.65	,,	2.3	-	3.484	3.718	2.060
160	6.32	,,	3.2	4.223	3.456	3.716	2.048
210	7.78	,,	3.9	4.206	3.419	3.714	2.037
260	9.07	,,	4.5	4.191	3.370	3.712	2.028
360	11.25	,,	5.6	4.166	3.310	3.709	2.013

A.3.4 Proton assignments (ppm) for N-Ac-Pro-Gly-NH$_2$ that were used to obtain association constants (K_a) from the titration of calix[4]pyrogallolarene (C[4]PA) into N-Ac-Pro-Gly-NH$_2$ (Pro-Gly). Aliquots (0- 300 µl) of 20 mM calix[4]pyrogallolarene in CD$_3$OD were titrated into 600 µl 2 mM N-Ac-Pro-Gly-NH$_2$ dissolved in the same solvent to give calix[4]pyrogallolarene concentrations of 0-10.00 mM at the mole ratios indicated in the table. Stock solution of calix[4]pyrogallolarene was prepared by dissolving the compound in 2 mM N-Ac-Pro-Gly-NH$_2$ solution. The titration was followed by one-dimensional ^{1}H NMR experiments, recorded at 295 K. Chemical shifts are given relative to external TSP in the same solvent ± 0.001 ppm.

C[4]PA added (µl)	[C[4]PA] (mM)	[Pro-Gly] (mM)	mole ratio [C[4]PA]/ [Pro-Gly]	Pα	Pδ1	Gα1	Me
0	0.00	2.00	0.0	4.304	3.599	3.726	2.097
10	0.49	,,	0.2	4.276	3.578	3.724	2.088
20	0.97	,,	0.5	4.269	3.565	3.724	2.080
30	1.43	,,	0.7	4.253	3.512	3.722	2.072
40	1.88	,,	0.9	4.236	3.481	3.721	2.064
50	2.31	,,	1.2	4.220	3.467	3.720	2.056
60	2.73	,,	1.4	4.206	3.420	3.719	2.049
80	3.53	,,	1.8	4.179	3.367	3.717	2.036
100	4.29	,,	2.1	4.156	3.339	3.715	2.025
160	5.32	,,	3.2	4.104	3.216	3.712	1.999
200	7.50	,,	3.8	4.075	3.158	3.710	1.985
260	9.07	,,	4.5	4.039	3.086	3.708	1.967
300	10.00	,,	5.0	4.019	3.046	3.706	1.957

Appendix A.4 Bradykinin-tannin complexation data

A.4.1 Proton assignments (ppm) for bradykinin (BK) that were used to obtain association constants (K_a) from the titration of PGG into bradykinin. Aliquots (0- 120 µl) of 60 mM PGG in $D_2O/(CD_3)_2SO$ (4:1,v/v) were titrated into 600 µl 2 mM bradykinin dissolved in the same solvent to give PGG concentrations of 0-10.00 mM at the mole ratios indicated in the table. The titration was followed by one-dimensional ^1H NMR experiments, recorded at 295 K. Chemical shifts are given relative to external TSP in the same solvent ± 0.001 ppm.

PGG added (µl)	[PGG] (mM)	[BK] (mM)	mole ratio [PGG]/[BK]	R1δ	P2β	P2γ	P2δ
0	0.00	2.00	0.0	3.12	2.429	2.004	3.476
10	0.98	1.97	0.5	3.1182	2.416	1.994	3.467
20	1.94	1.94	1.0	3.117	2.405	1.983	3.460
30	2.86	1.90	1.5	3.1148	2.394	1.974	3.452
40	3.75	1.88	2.0	3.1132	2.384	1.964	3.446
50	4.62	1.85	2.5	3.1113	2.374	1.957	3.439
60	5.45	1.82	3.0	3.1092	2.366	1.949	3.433
70	6.27	1.79	3.5	3.1077	2.357		3.427
80	7.06	1.76	4.0	3.1074	2.348		3.422
100	8.57	1.71	5.0	3.1061	2.336		3.414
120	10.00	1.67	6.0		2.324		3.406

P3α	P3β	P3γ	P3δ	G4α1	G4α2	F5α	F5β
4.414	2.295	2.051	3.677	3.926	3.835	4.573	3.037
4.411	2.288	2.045	3.669	3.925	3.834	4.570	3.030
4.408	2.283	2.040	3.661	3.924	3.834	4.569	3.023
4.405	2.277	2.034	3.652	3.923	3.833	4.567	3.016
4.403	2.272	2.029	3.647	3.922	3.832	4.565	3.011
4.400	2.267	2.024	3.640	3.922	3.832	4.563	3.005
4.398	2.262	2.019	3.634	3.921	3.831	4.561	3.000
4.396	2.258	2.015	3.629	3.920	3.831	4.559	2.995
4.393	2.252	2.010	3.622	3.919	3.830	4.557	2.992
4.390	2.245	2.004	3.612	3.918	3.830	4.556	2.985
4.387	2.239	1.997	3.603	3.917	3.829	4.554	2.978

F5δ	F5ε	S6α	S6β	P7α	P7β	P7δ	F8α
7.224	7.322	4.670	3.739	4.312	2.143	3.585	4.611
7.211	7.308	4.667	3.738	4.309	2.133	3.577	4.609
7.200	7.295	4.664	3.737	4.307	2.126	3.569	4.607
7.188	7.281	4.661	3.736	4.305	2.118	3.561	4.604
7.178	7.269	4.658	3.735	4.303	2.111	3.554	4.602
7.169	7.259	4.656	3.734	4.300	2.104	3.548	4.600
7.160	7.248	4.654	3.733	4.298	2.099	3.541	4.598
7.152	7.239	4.652	3.732	4.296	2.094	3.536	4.596
7.146	7.233	4.650	3.731	4.295	2.088	3.530	4.595
7.133	7.217	4.646	3.730	4.291	2.075	3.523	4.592
7.122	7.203	4.644	3.729	4.289	2.069	3.514	4.590

F8β1	F8β2	F8δ	F8ε	R9α	R9γ	R9δ	
3.228	2.921	7.269	7.365	4.127	1.537	3.171	
3.222	2.914	7.256	7.351	4.128	1.535	3.166	
3.217	2.907	7.245	7.337	4.130	1.533	3.162	
3.211	2.900	7.233	7.324	4.130	1.530	3.158	
3.206	2.894	7.223	7.312	4.131	1.529	3.154	
3.202	2.889	7.214	7.301	4.132	1.527	3.151	
3.197	2.883	7.205	7.291	4.132	1.525	3.148	
3.194	2.878	7.198	7.281	4.133	1.523	3.144	
3.190	2.875	7.191	7.274	4.133	1.522	3.141	
3.185	2.868	7.177	7.259	4.134	1.519	3.136	
3.179	2.861	7.166	7.245	4.135	1.518	3.131	

A.4.2 Proton assignments (ppm) for bradykinin (BK) that were used to obtain association constants (K_a) from the titration of TeGG into bradykinin. Aliquots (0- 120 μl) of 60 mM TeGG in $D_2O/(CD_3)_2SO$ (4:1, v/v) were titrared into 600 μl 2 mM bradykinin dissolved in the same solvent to give TeGG concentrations of 0-10.00 mM at the mole ratios indicated in the table. The titration was followed by one-dimensional ^1H NMR experiments, recorded at 295 K. Chemical shifts are given relative to external TSP in the same solvent ± 0.001 ppm.

TeGG added (μl)	[TeGG] (mM)	[BK] (mM)	mole ratio [TeGG]/[BK]	R1δ	P2β	P2γ	P2δ
0	0.00	2.00	0.0	3.122	2.428	2.003	3.475
10	0.98	1.97	0.5	3.120	2.421	1.997	3.470
20	1.94	1.94	1.0	3.118	2.415	1.992	3.465
30	2.86	1.90	1.5	3.117	2.408	1.986	3.460
40	3.75	1.88	2.0	3.115	2.404	1.980	3.456
50	4.62	1.85	2.5	3.114	2.397	1.976	3.451
60	5.45	1.82	3.0	3.113	2.391	1.971	3.448
70	6.27	1.79	3.5	3.112	2.386	1.967	3.445
80	7.06	1.76	4.0	3.111	2.382	1.963	3.442
100	8.57	1.71	5.0	3.109	2.373	1.955	3.435
120	10.00	1.67	6.0	3.107	2.365	1.948	3.429

P3α	P3β	P3γ	P3δ	G4α1	G4α2	F5α	F5β
4.413	2.294	2.051	3.678	3.926	3.833	4.573	3.037
4.411	2.290	2.048	3.672	3.925	3.832	4.571	3.032
4.409	2.286	2.044	3.668	3.925	3.831	4.569	3.027
4.407	2.283	2.041	3.663	3.924	3.831	4.567	3.023
4.405	2.280	2.038	3.659	3.924	3.830	4.566	3.020
4.403	2.276	2.034	3.654	3.922	3.829	4.564	3.016
4.402	2.273	2.031	3.650	3.922	3.829	4.562	3.013
4.400	2.270	2.028	3.647	3.921	3.829	4.561	3.010
4.399	2.267	2.025	3.643	3.920	3.828	4.560	3.007
4.396	2.262	2.021	3.636	3.919	3.828	4.557	3.002
4.393	2.257	2.016	3.630	3.919	3.827	4.555	2.996

F5δ	F5ε	S6α	S6β	P7α	P7β	P7δ	F8α
7.226	7.324	4.671	3.741	4.313	2.141	3.587	4.611
7.218	7.315	4.669	3.740	4.311	2.135	3.582	4.609
7.211	7.307	4.665	3.739	4.309	2.130	3.576	4.607
7.204	7.299	4.663	3.738	4.307	2.125	3.571	4.605
7.198	7.292	4.661	3.738	4.306	2.121	3.567	4.603
7.192	7.285	4.658	3.736	4.304	2.116	3.561	4.601
7.185	7.279	4.657	3.736	4.302	2.111	3.558	4.600
7.181	7.274	4.655	3.735	4.301	2.108	3.554	4.599
7.177	7.269	4.654	3.735	4.300	2.104	3.550	4.597
7.167	7.258	4.651	3.733	4.298	2.097	3.543	4.595
7.159	7.249	4.648	3.732	4.296	2.092	3.537	4.592

F8β1	F8β2	F8δ	F8ε	R9γ	R9δ
3.231	2.918	7.270	7.367	1.539	3.172
3.227	2.913	7.262	7.358	1.537	3.169
3.223	2.908	7.254	7.349	1.536	3.166
3.219	2.903	7.247	7.341	1.534	3.163
3.216	2.899	7.240	7.333	1.533	3.160
3.212	2.895	7.234	7.326	1.531	3.157
3.209	2.892	7.227	7.319	1.530	3.155
3.206	2.889	7.223	7.313	1.529	3.153
3.203	2.886	7.218	7.309	1.528	3.152
3.198	2.880	7.208	7.297	1.526	3.148
3.193	2.873	7.198	7.286	1.524	3.144

A.4.3 Proton assignments (ppm) for bradykinin (BK) that were used to obtain association constants (K_a) from the titration of TGG into bradykinin. Aliquots (0- 160 μl) of 60 mM TGG in $D_2O/(CD_3)_2SO$ (4:1, v/v) were titrated into 600 μl 2 mM bradykinin dissolved in the same solvent to give TGG concentrations of 0-12.63 mM at the mole ratios indicated in the table. The titration was followed by one-dimensional ^{1}H NMR experiments, recorded at 295 K. Chemical shifts are given relative to external TSP in the same solvent ± 0.001 ppm.

TGG added (μl)	[TGG] (mM)	[BK] (mM)	mole ratio [TGG]/ [BK]	R1δ	P2β	P2γ	P2δ
0	0.00	2.00	0.0	3.123	2.427	2.004	3.474
10	0.98	1.97	0.5	3.122	2.424	2.001	3.472
20	1.94	1.94	1.0	3.120	2.421	1.997	3.469
40	3.75	1.88	2.0	3.116	2.415	1.993	3.464
60	5.45	1.82	3.0	3.114	2.409	1.988	3.460
80	7.06	1.76	4.0	3.112	2.402	1.984	3.455
100	8.57	1.71	5.0	3.109	2.398	1.980	3.451
120	10.00	1.67	6.0	3.107	2.393	1.976	3.447
140	11.35	1.62	7.0	3.104	2.389		3.444
160	12.63	1.58	8.0	3.102	2.385		3.441

P3α	P3β	P3γ	P3δ	G4α1	G4α2	F5α	F5β
4.412	2.293	2.051	3.678	3.925	3.833	4.573	3.037
4.411	2.291	2.049	3.675	3.924	3.832	4.572	3.034
4.409	2.288	2.047	3.671	3.923	3.831	4.570	3.031
4.407	2.284	2.043	3.666	3.922	3.829	4.567	3.027
4.405	2.280	2.040	3.660	3.920	3.828	4.565	3.023
4.402	2.276	2.037	3.655	3.919	3.826	4.562	3.019
4.400	2.273	2.034	3.651	3.918	3.825	4.560	3.016
4.398	2.269	2.030	3.646	3.916	3.823	4.558	3.012
4.396	2.266	2.027	3.642	3.914	3.821	4.555	3.009
4.394	2.263	2.024	3.638	3.913	3.820	4.553	3.006

F5δ	F5ε	P7α	P7β	F8α	F8β1	F8β2	F8δ
7.226	7.324	4.314	2.140	4.611	3.232	2.918	7.271
7.223	7.321	4.312	2.137	4.609	3.229	2.915	7.267
7.219	7.317	4.310	2.134	4.608	3.227	2.912	7.263
7.215	7.311	4.307	2.128	4.605	3.222	2.906	7.256
7.208	7.305	4.305	2.123	4.602	3.218	2.903	7.250
7.201	7.299	4.302	2.117	4.599	3.214	2.898	7.244
7.198	7.295	4.299	2.113	4.597	3.211	2.894	7.239
7.193	7.290	4.297	2.109	4.594	3.207	2.890	7.234
7.186	7.285	4.294	2.103	4.592	3.204	2.886	
7.184	7.281	4.293	2.099	4.590	3.201	2.882	

F8ε	R9α	R9γ	R9δ
7.368	4.117	1.539	3.172
7.364	4.118	1.538	3.170
7.360	4.118	1.536	3.167
7.354	4.119	1.534	3.163
7.348	4.120	1.532	3.159
7.342	4.121	1.529	3.155
7.337	4.122	1.528	3.152
7.333	4.124	1.525	3.148
7.327	4.124	1.523	3.145
7.323	4.124	1.521	3.142

A.4.4 Proton assignments (ppm) for bradykinin (BK) that were used to obtain association constants (K_a) from the titration of B-2 into bradykinin. Aliquots (0- 160 µl) of 60 mM B-2 in $D_2O/(CD_3)_2SO$ (4:1, v/v) were titrated into 600 µl 2 mM bradykinin dissolved in the same solvent to give B-2 concentrations of 0-12.63 mM at the mole ratios indicated in the table. The titration was followed by one-dimensional ^1H NMR experiments, recorded at 295 K. Chemical shifts are given relative to external TSP in the same solvent ± 0.001 ppm.

B-2 added (µl)	[B-2] (mM)	[BK] (mM)	mole ratio [B-2]/[BK]	R1δ	P2β	P2γ	P3α
0	0.00	2.00	0.0	3.111	2.428	2.003	4.413
10	0.98	1.97	0.5	3.110	2.427	2.002	4.414
20	1.94	1.94	1.0	3.109	2.424	1.999	4.411
40	3.75	1.88	2.0	3.108	2.421	1.996	4.409
60	5.45	1.82	3.0	3.107	2.419	1.995	4.408
80	7.06	1.76	4.0	3.107	2.415	1.992	4.406
100	8.57	1.71	5.0	3.106	2.413	1.989	4.405
120	10.00	1.67	6.0	3.104	2.410		4.404
140	11.35	1.62	7.0	3.104	2.407		4.402
160	12.63	1.58	8.0	3.103	2.405		4.401

P3β	P3γ	P3δ	G4α1	G4α2	F5α	F5β	F5δ
2.293	2.051	3.677	3.926	3.833	4.573	3.037	7.226
2.292	2.050	3.675	3.925	3.832	4.572	3.035	7.224
2.290	2.048	3.673	3.924	3.831	4.571	3.034	7.222
2.288	2.046	3.670	3.922	3.830	4.569	3.031	7.219
2.285	2.042	3.667	3.922	3.829	4.567	3.028	7.216
2.283	2.040	3.664	3.920	3.827	4.566	3.026	7.214
2.281	2.038	3.662	3.919	3.826	4.564	3.024	7.211
2.279	2.036	3.659	3.918	3.825	4.563	3.022	7.208
2.276	2.034	3.657	3.916	3.824	4.562	3.021	7.206
2.274	2.033	3.655	3.916	3.823	4.561	3.019	7.204

F5ε	S6α	S6β	P7α	P7β	P7δ	F8α	F8β1
7.324	4.671	3.741	4.313	2.140	3.579	4.611	3.231
7.322	4.670	3.740	4.312	2.139	3.578	4.610	3.230
7.320	4.668	3.739	4.311	2.137	3.576	4.609	3.228
7.317	4.666	3.738	4.309	2.133	3.573	4.607	3.226
7.314	4.664	3.737	4.308	2.130	3.570	4.606	3.224
7.311	4.662	3.736	4.306	2.127	3.566	4.604	3.221
7.308	4.660	3.734	4.304	2.124	3.564	4.603	3.220
7.305	4.659	3.733	4.303	2.123	3.563	4.602	3.218
7.302	4.657	3.732	4.302	2.120	3.560	4.600	3.216
7.301	4.656	3.731	4.301	2.118	3.559	4.599	3.214

F8β2	F8δ	F8ε	R9α	R9γ	R9δ
2.919	7.270	7.367	4.117	1.539	3.171
2.917	7.268	7.365	4.117	1.538	3.170
2.915	7.267	7.363	4.118	1.537	3.169
2.913	7.263	7.360	4.118	1.535	3.167
2.911	7.261	7.357	4.119	1.534	3.164
2.909	7.258	7.354	4.120	1.533	3.162
2.906	7.255	7.351	4.120	1.532	3.160
2.905	7.253	7.348	4.121	1.531	3.158
2.903	7.250	7.346	4.122	1.530	3.156
2.902	7.248	7.344	4.123	1.529	3.155

A.4.5 Proton assignments (ppm) for bradykinin(1-5) (BK(1-5)) that were used to obtain association constants (K_a) from the titration of PGG into bradykinin. Aliquots (0- 120 μl) of 60 mM PGG in $D_2O/(CD_3)_2SO$ (4:1, v/v) were titrated into 600 μl 2 mM bradykinin(1-5) dissolved in the same solvent to give PGG concentrations of 0-10.00 mM at the mole ratios indicated in the table. The titration was followed by one-dimensional ^{1}H NMR experiments, recorded at 295 K. Chemical shifts are given relative to external TSP in the same solvent ± 0.001 ppm.

PGG added (μl)	[PGG] ·(mM)	[BK(1-5)] (mM)	mole ratio [PGG]/ [BK(1-5)]	R1α	R1δ	P2β	P2γ
0	0.00	2.00	0.0	4.217	3.190	2.411	2.055
10	0.98	1.97	0.5	4.261	3.190	2.404	2.051
20	1.94	1.94	1.0	4.277	3.188	2.396	2.046
30	2.86	1.90	1.5	4.286	3.186	2.387	2.041
40	3.75	1.88	2.0	4.285	3.184	2.381	2.038
50	4.62	1.85	2.5	4.288	3.183	2.373	2.034
60	5.45	1.82	3.0	4.294	3.181	2.367	2.030
70	6.27	1.79	3.5	4.294	3.180	2.360	2.026
80	7.06	1.76	4.0	4.295	3.178	2.353	2.023
100	8.57	1.71	5.0	4.300	3.176	2.342	2.017
120	10.00	1.67	6.0	4.302	3.174	2.331	2.011

P2δ	P3α	P3β	P3γ	P3δ	G4α1	G4α2	F5α
3.835	4.368	2.286	2.097	3.459	4.002	3.647	4.414
3.826	4.361	2.282	2.095	3.448	4.003	3.645	4.412
3.824	4.368	2.277	2.091	3.439	4.002	3.643	4.409
3.822	4.368	2.273	2.087	3.431	4.002	3.642	4.407
3.813	4.368	2.269	2.084	3.422	4.002	3.641	4.402
3.806	4.367	2.266	2.081	3.418	4.001	3.640	4.402
3.800	4.367	2.263	2.077	3.411	4.001	3.639	4.401
3.796	4.362	2.260	2.074	3.405	4.001	3.639	4.401
3.795	4.359	2.256	2.071	3.400	4.000	3.639	4.401
3.783	4.357	2.250	2.066	3.391	3.999	3.638	4.401
3.781	4.353	2.244	2.061	3.386	3.998	3.637	4.401

F5β1	F5β2	F5δ	F5ε	F5ζ
3.157	2.928	7.222	7.344	7.285
3.155	2.921	7.217	7.337	7.277
3.153	2.916	7.211	7.330	7.269
3.152	2.912	7.206	7.323	7.261
3.150	2.909	7.202	7.317	7.255
3.149	2.906	7.198	7.311	7.248
3.147	2.903	7.194	7.305	7.242
3.145	2.901	7.190	7.300	7.236
3.144	2.899	7.187	7.295	7.231
3.142	2.895	7.181	7.286	7.221
3.140	2.891	7.175	7.278	7.212

A.4.6 Proton assignments (ppm) for desArg^9-bradykinin (dR^{9}BK) that were used to obtain association constants (K_a) from the titration of PGG into bradykinin. Aliquots (0-120 µl) of 60 mM PGG in $D_2O/(CD_3)_2SO$ (4:1, v/v) were titrated into 600 µl 2 mM desArg^9-bradykinin dissolved in the same solvent to give PGG concentrations of 0- 10.00 mM at the mole ratios indicated in the table. The titration was followed by one-dimensional ^{1}H NMR experiments, recorded at 295 K. Chemical shifts are given relative to external TSP in the same solvent ± 0.001 ppm.

PGG added (µl)	[PGG] (mM)	[dR^{9}BK] (mM)	mole ratio [PGG]/ [dR^{9}BK]	R1γ	R1δ	P2β	P2δ
0	0.00	2.00	0.0	1.686	3.117	2.413	3.449
10	0.98	1.97	0.5	1.683	3.115	2.403	3.441
20	1.94	1.94	1.0	1.682	3.114	2.396	3.435
30	2.86	1.90	1.5	1.679	3.112	2.380	3.426
40	3.75	1.88	2.0	1.678	3.111	2.371	3.420
50	4.62	1.85	2.5	1.676	3.109	2.361	3.413
60	5.45	1.82	3.0	1.673	3.107	2.352	3.407
70	6.27	1.79	3.5	1.671	3.106	2.343	3.401
80	7.06	1.76	4.0	1.670	3.105	2.336	3.396
100	8.57	1.71	5.0	1.666	3.102	2.321	3.386
120	10.00	1.67	6.0	1.664	3.100	2.310	3.378

P3α	P3β	P3γ	G4α1	G4α2	F5α	F5β	F5δ
4.390	2.287	2.067	3.977	3.773	4.427	3.019	3.449
4.388	2.280	2.061	3.976	3.772	4.423	3.011	3.441
4.387	2.275	2.057	3.976	3.772	4.420	3.005	3.435
4.387	2.269	2.051	3.974	3.771	4.419	2.997	3.426
4.381	2.264	2.047	3.973	3.771	4.418	2.991	3.420
4.378	2.259	2.042	3.973	3.771	4.419	2.985	3.413
4.376	2.254	2.037	3.972	3.769	4.419	2.979	3.407
4.373	2.249	2.031	3.971	3.769	4.419	2.974	3.401
4.371	2.245	2.028	3.970	3.769	4.419	2.969	3.396
4.367	2.236	2.018	3.969	3.767	4.418	2.961	3.386
4.364	2.230	2.011	3.968	3.767	4.419	2.954	3.378

F5ε	S6α	S6β	P7α	P7β	P7δ	F8α	F8β1
7.324	4.649	3.738	4.337	2.121	3.584	4.571	3.183
7.310	4.646	3.737	4.336	2.113	3.575	4.569	3.180
7.295	4.644	3.737	4.335	2.105	3.569	4.567	3.177
7.285	4.641	3.735	4.333	2.097	3.560	4.564	3.174
7.274	4.639	3.734	4.331	2.090	3.553	4.563	3.171
7.264	4.637	3.733	4.330	2.083	3.547	4.561	3.169
7.254	4.635	3.732	4.328	2.077	3.540	4.559	3.167
7.244	4.632	3.731	4.327	2.071	3.534	4.557	3.164
7.236	4.631	3.731	4.325	2.066	3.529	4.556	3.163
7.221	4.627	3.728	4.323	2.056	3.519	4.552	3.159
7.208	4.625	3.727	4.321	2.048	3.511	4.551	3.157

F8β2	F8δ	F8ε
2.954	3.584	7.349
2.950	3.575	7.336
2.947	3.569	7.320
2.942	3.560	7.311
2.939	3.553	7.300
2.936	3.547	7.290
2.933	3.540	7.280
2.930	3.534	7.271
2.928	3.529	7.263
2.923	3.519	7.249
2.919	3.511	7.236

A.4.7 Proton assignments (ppm) for desArg^1-bradykinin (dR^{1}BK) that were used to obtain association constants (K_a) from the titration of PGG into bradykinin. Aliquots (0-120 µl) of 60 mM PGG in $D_2O/(CD_3)_2SO$ (4:1, v/v) were titrated into 600 µl 2 mM desArg^1-bradykinin dissolved in the same solvent to give PGG concentrations of 0- 10.00 mM at the mole ratios indicated in the table. The titration was followed by one-dimensional ^{1}H NMR experiments, recorded at 295 K. Chemical shifts are given relative to external TSP in the same solvent ± 0.001 ppm.

PGG added (µl)	[PGG] (mM)	[dR^{1}BK] (mM)	mole ratio [PGG]/ [dR^{1}BK]	P3β	P3γ	P3δ	G4α1
0	0.00	2.00	0.0	2.324	2.903	3.703	3.933
10	0.98	1.97	0.5	2.317	2.895	3.702	3.932
20	1.94	1.94	1.0	2.310	2.888	3.700	3.931
30	2.86	1.90	1.5	2.304	2.881	3.700	3.930
40	3.75	1.88	2.0	2.298	2.875	3.698	3.930
50	4.62	1.85	2.5	2.292	2.869	3.698	3.930
60	5.45	1.82	3.0	2.286	2.864	3.697	3.929
70	6.27	1.79	3.5	2.281	2.860	3.698	3.929
80	7.06	1.76	4.0	2.275	2.855	3.696	3.928
100	8.57	1.71	5.0	2.266	2.847	3.695	3.927
120	10.00	1.67	6.0	2.257	2.839	3.695	3.926

G4α2	F5α	F5β	F5δ	F5ε	S6α	S6β	P7α
3.832	4.591	3.056	7.217	7.323	4.690	3.759	4.346
3.833	4.589	3.049	7.204	7.308	4.687	3.757	4.343
3.833	4.586	3.043	7.193	7.295	4.684	3.756	4.340
3.832	4.584	3.038	7.183	7.283	4.681	3.755	4.338
3.832	4.582	3.034	7.173	7.272	4.679	3.754	4.336
3.831	4.580	3.029	7.164	7.261	4.676	3.753	4.334
3.830	4.577	3.024	7.156	7.252	4.674	3.752	4.332
3.831	4.577	3.021	7.149	7.243	4.672	3.751	4.331
3.830	4.574	3.016	7.141	7.234	4.670	3.750	4.328
3.829	4.571	3.010	7.129	7.219	4.666	3.749	4.325
3.828	4.568	3.004	7.117	7.205	4.663	3.748	4.322

P7β	P7δ	F8α	F8β1	F8β2	F8δ	F8ε	R9α
2.139	3.614	4.644	3.244	2.903	7.263	7.376	4.144
2.128	3.605	4.641	3.238	2.895	7.250	7.361	4.145
2.121	3.598	4.639	3.232	2.888	7.239	7.348	4.146
2.112	3.591	4.637	3.227	2.881	7.228	7.335	4.147
2.105	3.585	4.635	3.222	2.875	7.218	7.323	4.148
2.099	3.580	4.632	3.218	2.869	7.208	7.312	4.149
2.092	3.574	4.630	3.214	2.864	7.199	7.302	4.149
2.087	3.569	4.629	3.211	2.860	7.192	7.293	4.150
2.081	3.564	4.626	3.207	2.855	7.184	7.284	4.150
2.071	3.555	4.623	3.200	2.847	7.170	7.268	4.152
2.066	3.546	4.620	3.194	2.839	7.157	7.254	4.153

R9γ	R9δ
1.535	3.152
1.533	3.147
1.531	3.144
1.529	3.140
1.527	3.136
1.525	3.133
1.524	3.130
1.523	3.128
1.521	3.125
1.518	3.119
1.516	3.114

Appendix A.5 Self-association of tannins

A.5.1 Proton assignments (ppm) for PGG that were used to obtain homotactic association constants (K_a) (dimerization or higher order polymerization). PGG was dissolved in $D_2O/(CD_3)_2SO$ (4:1, v/v) and was stepwise diluted to give the concentrations indicated in the table. The dilution was followed by one-dimensional ^1H NMR experiments, recorded at 295 K. Chemical shifts are given relative to external TSP in the same solvent $\pm$ 0.001 ppm.

[PGG]	Glc H1	Glc H3	Gall1	Gall2	Gall3	Gall4	Gall6
15.00	6.240	5.897	7.103	6.944	6.977	7.056	7.026
12.63	6.250	5.906	7.105	6.945	6.980	7.063	7.028
11.35	6.257	5.911	7.106	6.947	6.981	7.068	7.030
10.00	6.264	5.918	7.108	6.948	6.983	7.072	7.031
8.57	6.273	5.925	7.109	6.949	6.985	7.077	7.032
7.06	6.283	5.934	7.111	6.950	6.987	7.083	7.035
6.27	6.289	5.938	7.111	6.951	6.989	7.087	7.035
5.46	6.295	5.944	7.113	6.952	6.990	7.091	7.037
4.62	6.302	5.950	7.114	6.953	6.991	7.095	7.038
3.75	6.310	5.957	7.115	6.954	6.993	7.100	7.039
2.86	6.319	5.964	7.116	6.955	6.995	7.106	7.041
1.94	6.330	5.973	7.117	6.957	6.998	7.112	7.043
1.46	6.336	5.979	7.118	6.958	6.999	7.117	7.043
0.98	6.341	5.985	7.119	6.958	7.000	7.120	7.044

A.5.2 Proton assignments (ppm) for TeGG that were used to obtain homotactic association constants (K_a) (dimerization or higher order polymerization). TeGG was dissolved in $D_2O/(CD_3)_2SO$ (4:1, v/v) and was step wise diluted to give the concentrations indicated in the table. The dilution was followed by one-dimensional ^1H NMR experiments, recorded at 295 K. Chemical shifts are given relative to external TSP in the same solvent $\pm$ 0.001 ppm.

[TeGG}	Glc H1	Glc H3	Gall1	Gall2	Gall3	Gall6
15.00	6.187	5.661	7.053	7.159	7.099	7.002
12.63	6.190	5.663	7.056	7.165	7.101	7.004
11.35	6.192	5.664	7.057	7.168	7.102	7.005
10.00	6.194	5.665	7.059	7.172	7.104	7.006
8.57	6.196	5.667	7.061	7.176	7.105	7.007
7.06	6.199	5.668	7.063	7.181	7.106	7.009
6.27	6.199	5.669	7.064	7.183	7.107	7.010
5.46	6.201	5.671	7.065	7.185	7.108	7.010
4.62	6.202	5.671	7.066	7.188	7.109	7.011
3.75	6.204	5.672	7.068	7.191	7.110	7.012
2.86	6.205	5.673	7.069	7.194	7.110	7.012
1.94	6.206	5.674	7.070	7.197	7.111	7.013
1.46	6.207	5.674	7.071	7.198	7.112	7.014
0.98	6.208	5.675	7.071	7.200	7.112	7.014

A.5.3 Proton assignments (ppm) for TGG that were used to obtain homotactic association constants (K_a) (dimerization or higher order polymerization). TGG was dissolved in $D_2O/(CD_3)_2SO$ (4:1, v/v) and was step wise diluted give the concentrations indicated in the table. The dilution was followed by one-dimensional ^{1}H NMR experiments, recorded at 295 K. Chemical shifts are given relative to external TSP in the same solvent ± 0.001 ppm.

[TGG}	Glc H1	Glc H3	Gal11	Gal13	Gal16
19.09	5.878	5.309	7.173	7.235	7.116
17.14	5.879	5.309	7.175	7.236	7.119
15.00	5.880	5.310	7.179	7.239	7.123
13.85	5.880	5.310	7.180	7.240	7.125
12.63	5.881	5.310	7.182	7.241	7.128
11.35	5.882	5.311	7.184	7.242	7.131
10.00	5.883	5.312	7.186	7.244	7.134
8.57	5.884	5.313	7.189	7.246	7.137
7.06	5.885	5.313	7.191	7.247	7.141
5.46	5.887	5.314	7.194	7.249	7.145
3.75	5.888	5.314	7.197	7.251	7.149
2.86	5.889	5.315	7.198	7.252	7.152
1.94	5.889	5.315	7.201	7.254	7.155
0.98	5.890	5.316	7.202	7.255	7.157